68-8131

KATZ-MASSON, Jose, 1944-

THE RELATIVISTIC SCHRÖDINGER EQUATION AND ITS APPLICATION TO PSEUDOSCALAR MESON BARYON SCATTERING IN A BROKEN SU(3) SYMMETRY MODEL.

University of Illinois, Ph.D., 1967
Physics, nuclear

University Microfilms, Inc., Ann Arbor, Michigan

# THE RELATIVISTIC SCHRODINGER EQUATION AND ITS APPLICATION TO PSEUDOSCALAR MESON BARYON SCATTERING IN A BROKEN SU(3) SYMMETRY MODEL

BY

JOSE KATZ-MASSON
B.S., University of Illinois, 1963
M.S., University of Illinois, 1964

THESIS

Submitted in partial fulfillment of the requirements
for the degree of Doctor of Philosophy in Physics
in the Graduate College of the
University of Illinois, 1967

Urbana, Illinois

# UNIVERSITY OF ILLINOIS

## THE GRADUATE COLLEGE

September 1967

I HEREBY RECOMMEND THAT THE THESIS PREPARED UNDER MY SUPERVISION BY JOSE KATZ-MASSON

ENTITLED THE RELATIVISTIC SCHRÖDINGER EQUATION AND ITS APPLICATION TO PSEUDOSCALAR MESON BARYON SCATTERING IN A BROKEN SU(3) SYMMETRY MODEL

BE ACCEPTED IN PARTIAL FULFILLMENT OF THE REQUIREMENTS FOR THE DEGREE OF DOCTOR OF PHILOSOPHY IN PHYSICS

J. W. Wyld, Jr.
In Charge of Thesis

G M Almy
Head of Department

Recommendation concurred in†

G. Arnol
David C. Sutton
Mary E. Hohn
D G Ravenhall

Committee on Final Examination†

† Required for doctor's degree but not for master's

D517

# ACKNOWLEDGMENTS

Now that his studies at the University of Illinois have come to an end, the author wishes to express his sincere gratitude to all those under whom he has studied in the Physics and Mathematics Departments, and in particular to Professors H. W. Wyld, Jr., D. G. Ravenhall, and R. Haag of the Physics Department and F. Hohn of the Mathematics Department.

He is especially indebted to his advisor Professor H. W. Wyld, Jr. for suggesting the problem on which this thesis is based and for his advice, encouragement, example, and interest as an advisor and teacher.

The author would like to thank Professor G. M. Almy for his kindness and interest throughout the author's entire period of university study.

He wishes to acknowledge support for this work from the National Science Foundation and the Office of Naval Research.

The author would like to thank his wife, Janet, for help and encouragement.

Also he wishes to thank all his friends for discussions and encouragement.

Last, but not least, the author wishes to thank his parents for their advice and encouragement which have meant a great deal to him.

TABLE OF CONTENTS

Page

Page

Page

# I. INTRODUCTION

## A. General Remarks

This thesis will deal with dynamical calculations of scattering amplitudes for multichannel problems. In these calculations we should ideally employ the principles of relativistic invariance; unitarity; analyticity or causality; and crossing symmetry. In dynamical calculations the first three principles are usually taken into account exactly. The last one is generally ignored. It is hoped that once the masses and widths of the particles which are exchanged in producing the forces are given, analyticity, unitarity, and single particle exchange forces will then define a calculational program from which phase shifts can be obtained. However, this program has not been completely successful.

The usual methods used in calculating scattering amplitudes include the N/D method and its various approximations, the Bethe-Salpeter equation, the Blankenbecler-Sugar equation, the equivalent energy dependent potential method, and the strip approximation. We will briefly discuss all of these methods to examine their advantages and disadvantages. In these discussions it will become clear that there is certainly a need for other calculational techniques.

Our calculational method consists of solving a multichannel relativistic Schrödinger equation. Starting from the usual decomposition of the Hamiltonian $H = H_o+V$, we obtain the integral equation for the T matrix $T = V+VGT$, where V is the input potential and $G = \frac{1}{\sqrt{s} - Ho+i\varepsilon}$,

where $\sqrt{s}$ is the total energy of the system and $H_o$ is the free Hamiltonian.

In order to make use of this equation in dynamical calculations we must make sure that relativistic invariance, unitarity, and analyticity or causality are satisfied. In order to satisfy the first principle we use the relativistic expressions for the particle energies in $H_o$. It can then be shown that relativistic invariance is satisfied. Bakamjian and Thomas (1953) and also Fongand Sucher (1963) have addressed themselves to this problem. The proof reduces to explicitly exhibiting a set of generators of the Poincare group with the usual Lie algebra relations which yield a covariant S matrix. We shall discuss this further in Chapter III. Two particle unitarity also follows directly as discussed in Chapter III. The problem of the causality properties of the equation is a more difficult one. This problem was solved by Coester (1965). He showed that such an equation obeys the principle of macrocausality which states that the behavior of a system of particles will not be affected by other particles at a great distance from the system.

Since the principles of relativistic invariance, unitarity, and analyticity or causality are satisfied it follows that the relativistic Schrödinger equation is an acceptable technique to be used in dynamical calculations. Perhaps it may be a better method than other techniques based on the N/D method since it includes iterations of the potential.

B. Description of Thesis

The main consideration of this thesis will be to apply the relativistic Schrödinger equation to the multichannel scattering problem of pseudoscalar meson baryon scattering in the four lowest partial waves using broken SU(3) symmetry. Also we will compare our results with other calculations where possible. In addition a brief discussion of the other calculational methods will be given to compare the relativistic Schrödinger equation with the other techniques. In Appendix A we give the SU(3) calculations and results which were used in the computation of the potentials. The notation used in computing the momentum dependence of the potentials is given in Appendix B. A brief discussion of the helicity formalism follows in Appendix C. Appendix D deals with the momentum dependence of the potentials used in our calculations, computed as discussed in Chapter III.

## II. DETERMINATION OF SCATTERING AMPLITUDES

### A. The N/D Method and Approximations Thereto

The method which is most commonly used in dynamical calculations is the N/D method. In this method one writes the amplitude T as

$$T = N D^{-1}, \tag{2.1}$$

where N and D are both matrices, N containing all left-hand and D all right-hand singularities. Using these properties of N and D together with the unitarity condition, we obtain the following system of integral equations to be solved, denoting the right-hand cut by RHC:

$$N(s) = B(s) + \frac{1}{\pi} \int_{RHC} ds' \left[ B(s') - \frac{s-s_o}{s'-s_o} B(s) \right] \frac{\rho(s') N(s')}{s'-s} \tag{2.2}$$

and

$$D(s) = 1 - \frac{s-s_o}{\pi} \int_{RHC} \frac{ds'}{(s'-s)(s'-s_o)} \rho(s') N(s'), \tag{2.3}$$

where B(s) is some input, usually taken to be a single particle exchange graph, $\rho(s)$ is a phase space factor and $s_o$ is the subtraction point. We can then show that the T matrix so computed is automatically a symmetric matrix if the input force matrix B is symmetric, and also is independent of the subtraction point . There are several advantages to the N/D method. Among these are the manifest relativistic invariance, unitarity, and analyticity of the scattering amplitude, which follow by construction. Also we need to know only the on

shell potential B(s); and, therefore, do not need a prescription for how to go off shell.

Chief among the disadvantages of this method is that one can add poles in D which are zeroes in T, since the dispersion relation for T is then not altered. These are the well known CDD ambiguities (Castillejo, Dalitz, Dyson, 1956). This is only a reminder that in dispersion theory the original system of equations which must be solved to obtain the scattering amplitude is nonlinear. Since the dispersion relations reflect only general properties such as relativistic invariance, unitarity, and causality, they give no details as to the specific mechanism of interaction. The N/D method is nothing more than a technique used to linearize such a system.

In practical calculations it is customary to drop the CDD poles. In so doing one must assume analyticity in the complex angular momentum plane. One then shows the nonexistance of CDD poles by studying the behavior of the scattering amplitude for large angular momenta and analytically continuing to lower values (Jones, 1965).

Another disadvantage is that in certain calculations (usually those involving particles with non-zero spin) the N/D method leads to a non-Fredholm system of integral equations. One must then use an arbitrary cutoff parameter to convert it into a Fredholm system. This is because the Feynman diagram corresponding to high-spin single particle exchange is highly divergent. In addition the input potential $B(\dot{s})$ is not iterated in the N/D method. We shall also mention that there is the question of what should be the kinematic

structure of the partial wave amplitude, which is written as N/D, as discussed by Martin and Uretsky (1963).

Next we will discuss some approximations to the N/D method. A very frequently used simplification of the N/D method is the determinantal approximation. This is written as

$$N(s) = B(s) \tag{2.4}$$

and

$$D(s) = 1 - \frac{s-s_o}{\pi} \int_{RHC} ds' \frac{1}{(s'-s)(s'-s_o)} \rho(s') B(s'). \tag{2.5}$$

This approximation method, although it does have the advantage of being simpler, carries all of the disadvantages of the N/D method. A further disadvantage is that the scattering amplitude T(s) is no longer independent of the subtraction point. Also it is no longer symmetric in a multichannel scattering problem, even when a symmetric input is used. Furthermore Luming (1964) has shown by direct calculation for a soluble case that the determinantal method often gives a poor approximation to the N/D method. Different suggestions have been made to modify the determinantal method in order to avoid the unsymmetrical nature of the scattering amplitude. One such suggestion, due to Bjorken (1960), is to write

$$T = \frac{1}{2} [BD^{-1} + (D^{-1})^T B]. \tag{2.6}$$

Another approximation to the N/D method is the pole approximation, which consists of representing the left hand cut by poles, chosen in the nearby part of the left hand cut in such a way as to obtain the maximum contribution to the force. The residues of the poles are determined by matching the amplitude obtained from the poles with the amplitude obtained from fixed energy dispersion relations at some convenient point. This method insures a symmetric scattering matrix, which is an advantage over the determinantal approximation.

Let us close this section by remarking that the proof of the validity of the N/D method for a multichannel problem is not as simple as for the single channel case, since the existance of the determinant of D does not necessarily imply the existance of D itself. Recently Hartle and Taylor (1967) have succeeded in giving a formal proof of the multichannel N/D method.

## B. The Bethe-Salpeter Equation

Consider the formal sum shown in Figure 2-1 . This sum can be written in the form of an integral equation as shown in Figure 2-2 and is the Bethe-Salpeter equation in the ladder approximation (Bethe and Salpeter, 1951). It is written in symbols as

$$F(p,q) = V_F(p,q) + i\int \frac{d^4k}{(2\pi)^4} V_F(p,k)\,G(P,k)\,F(k,q)\,, \qquad (2.7)$$

Fig. 2-1. Formal sum for a two particle scattering amplitude.

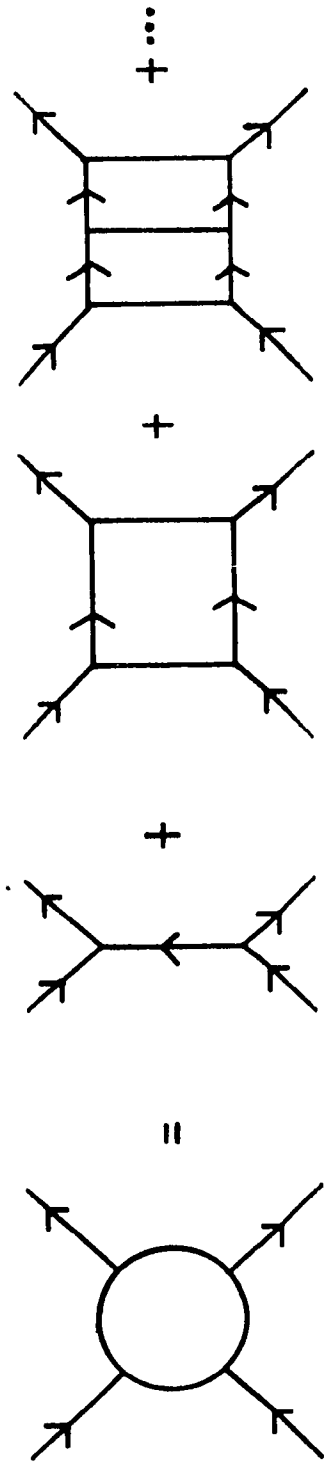

Fig. 2-2. Bethe-Salpèter equation in the ladder approximation. The total energy momentum of the system is denoted by P, and p, k, and q denote the relative energy momentum in the initial, intermediate, and final states respectively.

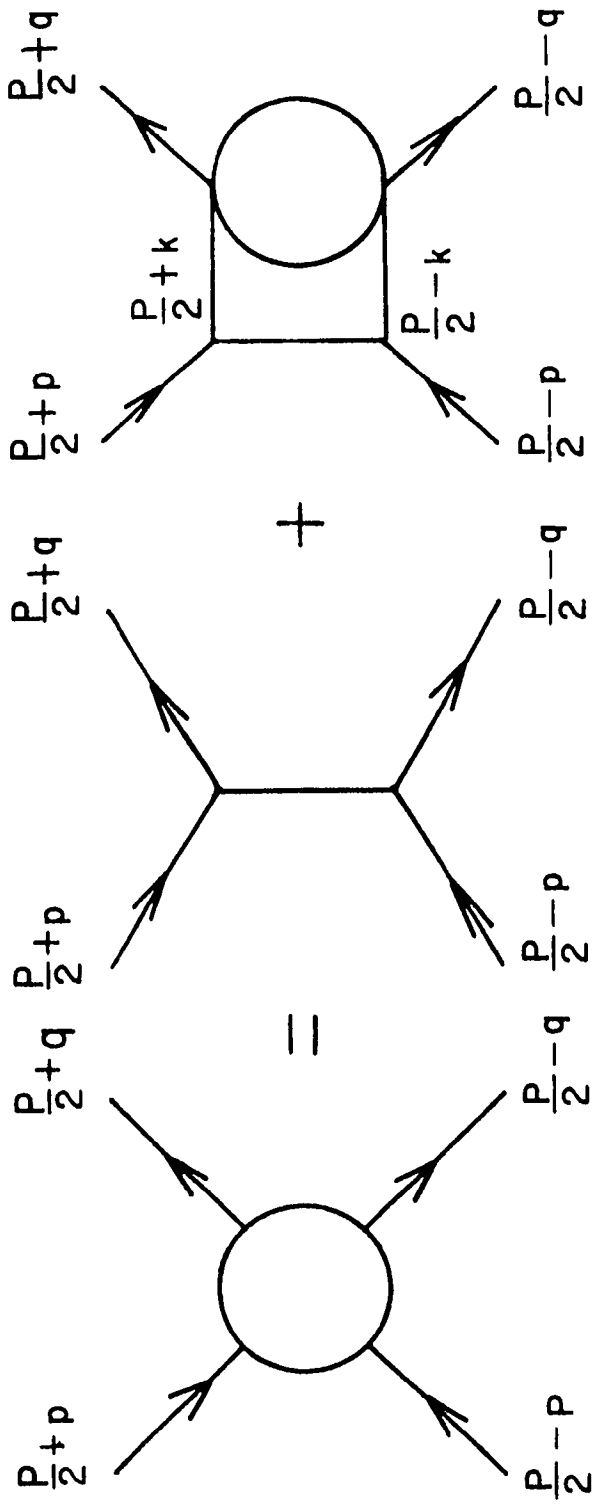
P/2+q
P/2−q
P/2+k
P/2−k
P/2+p
P/2−p
+
P/2+q
P/2−q
P/2+p
P/2−p
=
P/2+q
P/2−q
P/2+p
P/2−p

where

$$S_{fi} = \delta_{fi} - (2\pi)^4 i\delta^4(P_f - P_i) \frac{1}{\sqrt{16E_1E_2E_3E_4}} F_{fi}, \tag{2.8}$$

and where G(P,k) stands for the product of propagators corresponding to the particles in the intermediate state, and $V_F$ for the sum of all two particle irreducible graphs. In the case of spinless particles and ignoring self energy graphs we may write

$$G(P,k) = \frac{1}{\left[\left(\frac{P}{2} + k\right)^2 + m_1^2\right]\left[\left(\frac{P}{2} - k\right)^2 + m_2^2\right]}, \tag{2.9}$$

where the masses of the corresponding particles are denoted by $m_1$ and $m_2$.

Among the advantages of the equation are the manifest relativistic invariance, analyticity, and unitarity of the scattering amplitude. A further advantage is that this equation includes iterations of the potential.

An important practical disadvantage is that this equation involves after angular momentum decomposition a two dimensional integral equation which is difficult to solve numerically. Also the equation contains a relative energy variable and overlapping singularities which affect the compactness proof.(1) A further disadvantage is that the two particle unitarity is satisfied only below the three particle production threshold. This is because the

---

1. Compactness of the kernel is a necessary condition for the solution of an integral equation by matrix inversion. To prove compactness we must perform a Wick rotation which cannot be rigorously justified.

Bethe-Salpeter equation contains terms corresponding to graphs, such as the ones shown in Figure 2-3 . These are the graphs responsible for the extra relative energy variable and the overlapping singularities which affect the compactness proof. The Bethe-Salpeter equation is a two particle equation, and these higher intermediate states do not really belong in it. It is, therefore, natural to eliminate such graphs. Next we will consider the Blankenbecler-Sugar equation.

## C. The Blankenbecler-Sugar Equation

### 1. "Derivation" by using the Landau-Cutkosky's Rules and Discussion

Starting with the Bethe-Salpeter equation we can now convert it into a one dimensional integral equation as was done by Blankenbecler and Sugar (1966). We shall for simplicity consider the case of scalar particles. We start with the Bethe-Salpeter equation

$$F(p,q) = V_F(p,q) + i\int \frac{d^4k}{(2\pi)^4} V_F(p,k)\ G(P,k)\ F(k,q)\,, \qquad (2.10)$$

and then reduce it to a three dimensional integral equation by replacing the product of propagators by a function which is not singular except when both particles are on the mass shell, as in accordance with the Landau-Cutkosky rules (Landau (1959), Cutkosky (1960)). We then reconstruct G(P,k) from the discontinuity across the two particle cut by means of a dispersion relation

Fig. 2-3. Examples of multiparticle intermediate states included in the Bethe-Salpeter equation.

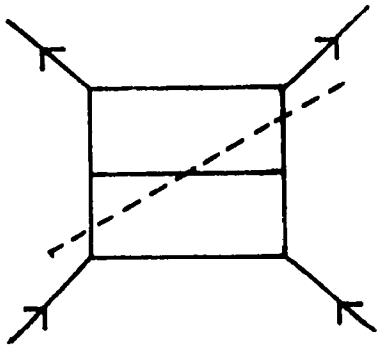

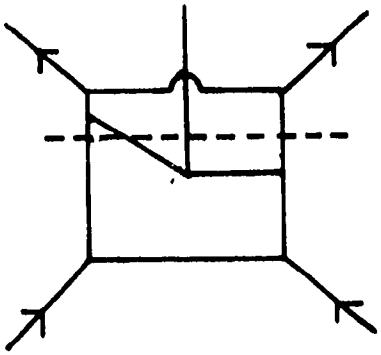

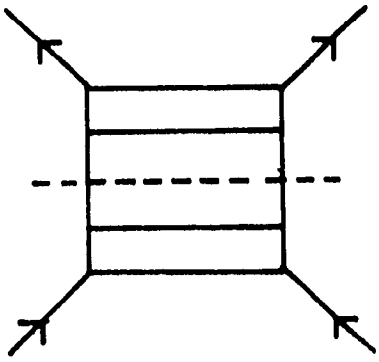

$$G(P,k) = \frac{1}{2\pi i}\int_{s_o}^{\infty} \frac{ds'}{s'-s}\,\tilde{G}(P',k) + f(k), \qquad (2.11)$$

where $s = -P^2$, $s_o$ is the lowest threshold, and

$$\tilde{G}(P',k) = (2\pi_1)^2\delta^{(4)}(p_1'^2 + m_1^2)\;\delta^{(4)}(p_2'^2 + m_2^2)\;\theta(p_{10})\theta(p_{20}). \qquad (2.12)$$

With the choice of Lorentz frame given by $p_i' = \frac{P}{2} + \varepsilon_i k_i$, where

$\varepsilon_i = \begin{cases} +1 & i=1 \\ -1 & i=2 \end{cases}$, we obtain

$$\tilde{G}(P',k) = (2\pi i)^2\,\delta^{(4)}\left(\left(\frac{P}{2}+k\right)^2 + m_1^2\right)\delta^{(4)}\left(\left(\frac{P}{2}-k\right)^2 + m_2^2\right)\theta\left(\frac{P_o}{2}+k_o\right)$$
$$\theta\left(\frac{P_o}{2}-k_o\right). \qquad (2.13)$$

Of course, we could in principle choose a different Lorentz frame to evaluate the dispersion integral (2.11). For example, if we choose

$$p_1 = k$$
$$p_2 = P-k\ .$$

We then obtain

$$\tilde{G}(P',k) = (2\pi i)^2\,\delta^{(4)}(k^2+m_1^2)\;\delta^{(4)}((P-k)^2+m_2^2)\;\theta(k_o)\;\theta(P_o-k_o). \qquad (2.14)$$

Substituting the expression given for $\tilde{G}(P,k)$ in equation (2.12) into equation (2.11) we obtain

$$G(P,k) = 2\pi i \int_{s_o}^{\infty} \frac{ds'}{s'-s} \theta\left(\frac{P'_o}{2} + k_o\right)\theta\left(\frac{P'_o}{2} - k_o\right) \delta^{(4)}\left[-\frac{1}{4}s' - \sqrt{s'}\, k_o + \vec{k}^2 - k_o^2 + m_1^2\right]$$

$$\delta^{(4)}\left[-\frac{1}{4}s' + \sqrt{s'}\, k_o + \vec{k}^2 - k_o^2 + m_2^2\right] . \qquad (2.15)$$

Defining

$$E_1 = \sqrt{k^2+m_1^2} \ ,$$

$$E_2 = \sqrt{k^2+m_2^2} \ ,$$

and assuming without loss of generality that $E_1 \geq E_2$ we obtain, upon making use of the $\theta$ functions,

$$k_o > 0 \text{ and } k_o^2 < \frac{m_1^2 - m_2^2}{4} . \qquad (2.16)$$

Upon performing the integral in equation (2.15) with the above restrictions we obtain

$$G(P,k) = 1\pi \left(\frac{E_1 + E_2}{(E_1+E_2)^2 - s}\right) \frac{1}{E_1 E_2} \delta \left[k_o - \frac{1}{2}(E_1 - E_2)\right], \qquad (2.17)$$

where we have assumed $f(k)=0$.

If instead we make use of the expression for $\tilde{G}(P,k)$ given in equation (2.13) we obtain, upon substituting in equation (2.11);

$$G(P,k) = 2\pi i \int_{s_o}^{\infty} \frac{ds'}{s'-s} \delta^{(4)}[k^2 + m_1^2] \ \delta^{(4)}[(P'-k)^2 + m_2^2] \ \theta(k_o) \ \theta(P'_o - k_o),$$

(2.18)

and thus

$$G(P,k) = i\pi\left(\frac{E_1+E_2}{(E_1+E_2)^2-s}\right)\frac{1}{E_1E_2}\ \delta\left[k_o - \sqrt{k^2+m_1^2}\right], \qquad (2.19)$$

where we have assumed $f(k) = 0$.

We have assumed that the function $f(k)$ is zero so that it can be neglected. (Actually the real assumption is not that $f(k) = 0$, but rather that $\int V_F(P,k)\ f(k)\ F(k,q) = 0$). Nothing is known about this integral since this would require solving the Bethe-Salpeter equation. The results vary according to the Lorentz frame in which we assume this function is zero. Thus we will have obtained the Blankenbecler-Sugar equation which will also vary according to the Lorentz frame in which we perform the reduction. We note that

$$\frac{E_1+E_2}{(E_1+E_2)^2-s} = \frac{1}{2}\left[-\frac{1}{\sqrt{s}-E_1-E_2}+\frac{1}{\sqrt{s}+E_1+E_2}\right]. \qquad (2.20)$$

By substituting the expression for $G(P,k)$ into the Bethe-Salpeter equation, we then obtain

$$F(p,q) = V_F(p,q) + \frac{1}{4}\int\frac{d^3k}{(2\pi)^3}V_F(p,k)\left[\frac{1}{\sqrt{s}-E_1-E_2}-\frac{1}{\sqrt{s}+E_1+E_2}\right]$$

$$\frac{1}{E_1E_2}\ F(k,q), \qquad (2.21)$$

which is the Blankenbecler-Sugar equation.

2. Another "Derivation" of the Equation

To illustrate more clearly the ambiguities in the procedure used to obtain the Blankenbecler-Sugar equation, we will give another derivation of the equation. Again we start from the Bethe-Salpeter equation for spinless particles:

$$F(p,q) = V_F(p,q) + i\int \frac{d^4k}{(2\pi)^4} V_F(p,k)\ G(P,k)\ F(k,q), \tag{2.22}$$

where

$$G(P,k) = \frac{1}{\left[\left(\frac{P}{2}+k\right)^2 + m_1^2\right]\left[\left(\frac{P}{2}-k\right)^2 + m_2^2\right]}, \tag{2.23}$$

provided we ignore self energy terms.

We shall now perform the three dimensional reduction by neglecting retardation effects. In the case of equal masses this is clear. We merely set $p_o = k_o = 0$ in $V_F$. For unequal masses we shall do this by setting

$$\begin{aligned} {}_o &= E_1 - \frac{\sqrt{s}}{2} = E_1 - \frac{1}{2}(E_1 + \omega_1) = \frac{1}{2}(E_1 - \omega_1), \\ k_o &= E_2 - \frac{\sqrt{s}}{2} = E_2 - \frac{1}{2}(E_2 + \omega_2) = \frac{1}{2}(E_2 - \omega_2). \end{aligned} \tag{2.24}$$

We then see that the right hand side of equation (2.22) is independent of $p_o$. Therefore, $F(p',q)$ is independent of $p_o$. We can do the integration in (2.22) by closing the contour in the upper half plane. We obtain

$$i\int \frac{d^4k}{(2\pi)^4} V_F(p,k)\ G(P,k)\ F(k,q) = i\int \frac{d^3k}{(2\pi)^3} V_F(p,k)\ F(k,q) \int \frac{dk_o}{2\pi} G(P,k). \tag{2.25}$$

Using our expression for $G(P,k)$, we then obtain

$$\int \frac{dk_o}{2\pi} G(P,k) = i \left[ \frac{-1}{\sqrt{s} - E_1 - E_2} + \frac{1}{\sqrt{s} + E_1 + E_2} \right] \frac{1}{4} \frac{1}{E_1 E_2}, \tag{2.26}$$

which yields

$$F(p,q) = V_F(p,q) + \frac{1}{4} \int \frac{d^3k}{(2\pi)^3} V_F(p,k) \left[ \frac{1}{\sqrt{s} - E_1 - E_2} - \frac{1}{\sqrt{s} + E_1 + E_2} \right] \frac{1}{E_1 E_2} F(k,q). \tag{2.27}$$

We observe that the equation has become the Blankenbecler-Sugar equation. The above derivation illustrates more clearly the true nature of the assumptions used in obtaining the equation and its ambiguous nature.

## D. The Equivalent Potential Approach

This method for computing scattering amplitudes was suggested by Balazs (1964) as a generalization of a technique due to Charap and Fubini (1959, 1960). In this method we assume as the potential an energy dependent superposition of Yukawa potentials, which is used in a nonrelativistic Schrödinger equation to obtain the scattering amplitude. Such a potential is assumed because the scattering amplitude computed from it satisfies the Mandelstam representation

(Blankenbecler et al, 1960). Among the advantages of this method are unitarity of the scattering amplitude and that the Mandelstam representation is satisfied by construction. A strong disadvantage is that the nonrelativistic Schrödinger equation, which in this method is used to enforce unitarity, clearly has no physical significance in the relativistic region. Further disadvantages are that this method leads to divergent potentials in many cases of physical interest, and it requires in principle the solution of a nonlinear system of integral equation to obtain the potential. Moreover, CDD ambiguities (as we have discussed in connection with the N/D method) are also present in this method.

## E. The Strip Approximation

This technique consists in approximating the non-zero parts of the double spectral functions in the Mandelstam representation by strips. The dispersion theory system of integral equations so obtained can then be solved by using the N/D method. Chew (1963) proposed a scheme based on the strip approximation usually referred to as the new strip approximation. In this scheme one uses Regge pole expressions in calculating the discontinuties of the scattering amplitude in the crossed channels. The strip approximation method has the advantage of incorporating crossing symmetry and Regge behavior of the exchanged particles if so desired. Among the disadvantages we may mention the CDD ambiguities as already discussed with the N/D method. Also the input potential is not iterated.

Another disadvantage is that the strip width is an arbitrary parameter to be fixed only phenomenologically (it takes the role played by an arbitrary cutoff parameter in other calculations).

# III. RELATIVISTIC SCHRÖDINGER EQUATION

## A. Two Particle Unitarity of the Equation

Suppose we consider two particle scattering as shown in Figure 3-1. Starting from

$$S_{fi} = \delta_{fi} - (2\pi)^4 i\, \delta^{(4)}(P_f - P_i) \sqrt{\frac{m_b\, m_d}{4a_o b_o c_o d_o}}\, \mathcal{M}_{fi}, \tag{3.1}$$

and defining

$$\mathcal{M}_{fi} = -\frac{4\pi \sqrt{(a_o+b_o)(c_o+d_o)}}{\sqrt{m_b\, m_d}}\, T_{fi}\,, \tag{3.2}$$

we obtain for the differential cross section:

$$\frac{d\sigma}{d\Omega} = \frac{q_2}{q_1} |T|^2, \tag{3.3}$$

where $q_2$ and $q_1$ denote the magnitude of the momenta in the center of mass frame in the final and initial states, respectively. Expanding we obtain

$$T = \sum_J (2J+1)\, d^J_{\lambda\mu}(\theta)\; T^J, \tag{3.4}$$

where

$$\lambda = \lambda a - \lambda b;\ \mu = \lambda c - \lambda d.$$

The two particle unitarity condition reads

$$i(\mathcal{M}_{ij} - \mathcal{M}^*_{ij}) = (2\pi)^4 \sum_k \mathcal{M}_{ik} \left(\frac{m_e\, m_f}{8e_o f_o}\right) \mathcal{M}^*_{jk}\, \delta^{(4)}(p_j - p_k), \tag{3.5}$$

Fig. 3-1. Scattering of arbitrary spin particles. The helicity of particle j is denoted by $\lambda_j$ and the magnitude of the momentum in the initial or final state is denoted by $q_1$ or $q_2$ respectively.

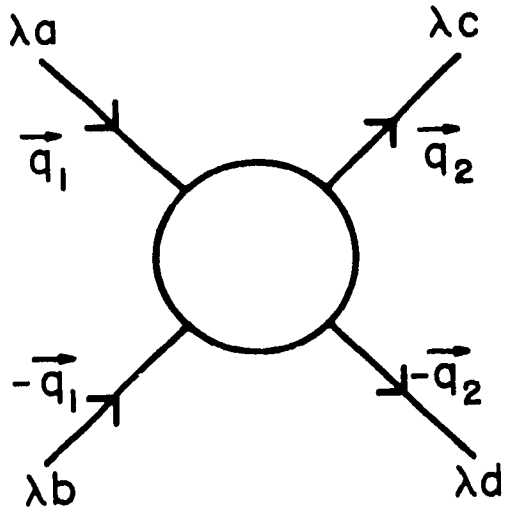
λa
λc
$\vec{q}_1$
$\vec{q}_2$
$-\vec{q}_1$
$-\vec{q}_2$
λb
λd

where the masses and energies of the particles in the intermediate state are denoted by $m_e$, $m_f$, $e_o$ and $f_o$ respectively. Using equation (3.2) this becomes

$$\text{Im } T^J_{\lambda c\lambda d;\ \lambda a\lambda b} = \sum_{ef} T^J_{\lambda c\lambda d;\ \lambda e\lambda f}\ q_{ef}\ T^{*J}_{\lambda e\lambda f;\ \lambda a\lambda b'} \tag{3.7}$$

where $q_{ef}$ denotes the momentum of either particle in the two particle channel ef in the center of mass frame.

In matrix notation we can rewrite the above equation in the form

$$\text{Im } T^J = T^J\ q\ T^{J+}. \tag{3.8}$$

Time reversal invariance implies that

$$T^J_{\lambda c\lambda d;\ \lambda a\lambda b} = T^J_{\lambda a\lambda b;\ \lambda c\lambda d'} \tag{3.9}$$

and thus we obtain

$$\text{Im } T^J = \frac{1}{2i}\ (T^J - T^{J+}), \tag{3.10}$$

where we have used (3.9). Defining

$$T'^J = \sqrt{q_2}\ T^J \sqrt{q_1}\ , \tag{3.11}$$

we obtain

$$\frac{1}{T^{\dagger\prime J}} - \frac{1}{T'^J} = 2i\ . \tag{3.12}$$

Let

$$\frac{1}{T^{i,J}} = \frac{1}{K^{i,J}} - i, \tag{3.13}$$

then

$$\frac{1}{K^{\dagger,J}} - \frac{1}{K^{i,J}} = 0.$$

That is

$$K^{i,J} = K^{\dagger,J}. \tag{3.14}$$

Since $T^{i,J}$ is symmetric, so is $K^{i,J}$. Equation (3.14) indicates $K^{i,J}$ is real.

The relativistic Schrödinger equation can then be written as

$$T^{i,J}(q_2,q_1) = V^{i,J}(q_2,q_1) - \frac{1}{\pi}\int V^{i,J}(q_2,q)\,\frac{d(E_q+\omega_q)}{\sqrt{s}-E_q-\omega_q+i\varepsilon}\,T^{i,J}(q,q_1), \tag{3.15}$$

where $\sqrt{s}$, $E_q$ and $\omega_q$ are the total energies of the system and of the particles in the intermediate state, respectively. On shell we have

$$\sqrt{s} = E_{q_1}+\omega_{q_1} = E_{q_2}+\omega_{q_2}\ . \tag{3.16}$$

However, this is not true off shell.

It is now clear that the above equation obeys two particle unitarity. In fact, using

$$\frac{1}{\sqrt{s}-E_q-\omega_q+i\varepsilon} = P\,\frac{1}{\sqrt{s}-E_q-\omega_q} - i\pi\,\delta(\sqrt{s}-E_q-\omega_q), \tag{3.17}$$

where P denotes the principal value, we obtain

$$T'^{J}(q_2,q_1) = V'^{J}(q_2,q_1)[1+ iT'^{J}(q_1,q_1)] - P\frac{1}{\pi}\int V'^{J}(q_2,q)\frac{d(E_q+\omega_q)}{\sqrt{s}-E_q-\omega_q}\times$$

$$T'^{J}(q,q_1). \qquad (3.18)$$

By defining

$$K'^{J}(q_2,q_1) = T'^{J}(q_2,q_1)[1+ iT'^{J}(q_1,q_1)]^{-1}, \qquad (3.19)$$

we obtain

$$K'^{J}(q_2,q_1) = V'^{J}(q_2,q_1) - P\frac{1}{\pi}\int V'^{J}(q_2,q)\frac{d(E_q+\omega_q)}{\sqrt{s}-E_q-\omega_q}K'^{J}(q,q_1). \qquad (3.20)$$

$K'^{J}$ is the so-called K' matrix as discussed by Dalitz and Tuan (1960).

From equation (3.20) we now see that K' is real and symmetric provided V' is real and symmetric. Moreover, equation (3.19) can be rewritten as

$$\frac{1}{T'^{J}} = \frac{1}{K'^{J}} - i$$

which is relation (3.13) and also the statement of two particle unitarity.

Equation (3.15) can be written in terms of $F^{J}$ and $V_F^{J}$ defined by

$$- 8\pi \sqrt{(a_o + b_o)(c_o + d_o)}\ T^J = F^J,$$

$$- 8\pi \sqrt{(a_o + b_o)(c_o + d_o)}\ V^J = V_F^J, \tag{3.21}$$

as

$$F^J(q_2,q_1) = V_F^J(q_2,q_1) + \frac{1}{\pi} \int V_F^J(q_2,q) \frac{d(E_q + \omega_q)}{\sqrt{s} - E_q - \omega_q + i\varepsilon} \frac{1}{E_q \omega_q} F^J(q,q_1),$$

or (3.22)

$$F(q_2,q_1) = V_F(q_2,q_1) + \frac{1}{4} \int \frac{d^3q}{(2\pi)^3} V_F(q_2,q) \frac{1}{\sqrt{s} - E_q - \omega_q + i\varepsilon} \frac{1}{E_q \omega_q} F(q,q_1),$$

(3.23)

before we carry out the angular decomposition.

## B. Comparison with the Blankenbecler-Sugar Equation

We recall the Blankenbecler-Sugar equation

$$F(q_2,q_1) = V_F(q_2,q_1) + \frac{1}{4} \int \frac{d^3q}{(2\pi)^3} V_F(q_2,q) \left[ \frac{1}{\sqrt{s} - E_q - \omega_q + i\varepsilon} - \right.$$

$$\left. \frac{1}{\sqrt{s} + E_q + \omega_q + i\varepsilon} \right] \frac{1}{E_q \omega_q} F(q,q_1) . \tag{3.24}$$

By similar arguments as we have given in Chapter III section A, this equation obeys two particle unitarity. Moreover, this equation is nothing more than Schrödinger's equation with relativistic expressions for the particle energies and an extra term corresponding to the energy

denominator $\frac{1}{\sqrt{s}+E_q+\omega_q}$. The corresponding potential function in the Blankenbecler-Sugar equation is computed according to the recipe of replacing relative energies by their on shell value.

We now have a procedure for finding the potential, once the corresponding potential for the Bethe-Salpeter equation is known, but we can also carry out the reduction in any other frame. The result is then a different procedure for finding the potential. Also we can see that the term involving the energy denominator corresponds to a six particle intermediate state, as shown in Figure 3-2. By our approximations these higher order intermediate states do not really belong in this two particle equation. Thus it is reasonable to drop this term. The resulting equation is the relativistic Schrödinger equation which we have briefly discussed in Chapter III, section A. In our calculations, however, we are still left with the question of what input potential to use in the equation.

## C. Choice of Potential

Usual dynamical calculations of scattering amplitudes use single particle exchanges as the input or "potential." If we assume that the force is given by computing some particular Feynman diagram, we still have an ambiguity in how to go off shell, since the Schrödinger equation is a one dimensional off shell equation after carrying out the angular momentum decomposition. In the choice of potential we must assume that when the particles are on shell it reduces to the

Fig. 3-2. Example of a six particle intermediate state included in the Blankenbecler-Sugar equation.

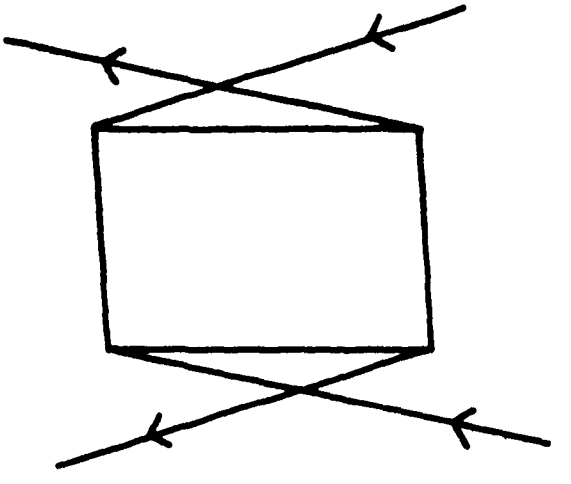

value obtained by computing the corresponding Feynman diagram according to the usual rules.

In our calculations we compute the "potential" by assuming the particles involved are on the mass shell and by treating initial and final particles symmetrically. The results of these calculations for the cases considered are given in Appendices A and D

## D. Formal Discussion of the Equation

In part A we have discussed the two particle unitarity property of the relativistic Schrödinger equation. We will now discuss its relativistic and casual properties. To do this we first introduce the usual generators of the Poincaré group with their commutation relations and an alternative set usually referred to as the center of mass set.

### 1. Generators of Lorentz Transformations

We first introduce the four components of the momentum four vector $P_\mu$ ($\mu = 1,2,3,4$; $P_4 = iH$) representing translations in space time and the six components of the antisymmetric tensor $M_{\mu\nu}$ representing rotations in space time. They obey the commutation relations:

$$[P_\mu, P_\nu] = 0$$

$$[M_{\mu\nu}, P_\lambda] = i[P_\nu \delta_{\mu\lambda} - P_\mu \delta_{\nu\lambda}], \quad \text{and} \tag{3.25}$$

$$[M_{\mu\nu}, M_{\lambda\sigma}] = i[M_{\nu\sigma}\delta_{\mu\lambda} - M_{\nu\lambda}\delta_{\mu\sigma} + M_{\mu\lambda}\delta_{\nu\sigma} - M_{\mu\sigma}\delta_{\nu\lambda}],$$

where

$$\mu,\nu = 1,2,3,4.$$

The operator $U(a,\Lambda)$ corresponding to an infinitesimal Lorentz transformation may be written as:

$$u(a,\Lambda) = 1 + \frac{1}{2}\,\epsilon_{\mu\nu}M_{\mu\nu} - ia_{\mu}P_{\mu}, \tag{3.26}$$

where $a_{\mu\nu}$ and $\epsilon_{\mu\nu}$ are such that $x'_{\mu} = a_{\mu\nu}x_{\nu} + a_{\mu}$, and $a_{\mu\nu} = \delta_{\mu\nu} + \epsilon_{\mu\nu}$. It is convenient to separate the components of $M_{\mu\nu}$ into the generators $J_i$ of pure rotations about the i axis in three space and the generators $K_i$ of pure Lorentz transformations along the i axis by

$$J_{\imath} = \frac{1}{2}\,\epsilon_{ij}k\,M_{j}k \quad \text{and}$$
$$K_i = -iM_i4, \tag{3.27}$$

where

$$\imath,j,k = 1,2,3.$$

Expressing the commutation relations in terms of $P_{\imath}$, $J_i$, $K_i$ and H, i=1,2,3, we obtain:

$$[P_{\imath},P_j] = 0, \quad [P_i,H] = 0, \quad [P_i,J_j] = \imath\epsilon_{\imath jk}P_k,$$

$$[J_i,H] = 0, \quad [J_{\imath},J_j] = \imath\epsilon_{\imath jk}J_k, \; [J_i,K_j] = i\epsilon_{ijk}K_k, \tag{3.28}$$

$$[K_i,P_j] = i\delta_{ij}H, \; [K_{\imath},H] = \imath P_i, \text{ and } [K_i,K_j] = -i\epsilon_{ijk}J_k.$$

The center of mass set consists of operators $\vec{p}$, h, $\vec{j}$, $\vec{x}$ defined by

$$\vec{P} = \vec{p},$$

$$H = \sqrt{\vec{p}^2 + h^2}$$

$$\vec{J} = \vec{x} \times \vec{p} + \vec{j}, \text{ and} \tag{3.29}$$

$$\vec{K} = \frac{1}{2} (\vec{x} H + H\vec{x}) - \frac{\vec{j} \times \vec{p}}{j + H} .$$

They satisfy the commutation relations:

$$[p_i, p_j] = 0, \quad [p_i, x_j] = -i\delta_{ij}, \quad [p_i, j_k] = 0,$$

$$[x_i, x_j] = 0, \quad [x_i, J_k] = 0, \quad [x_i, h] = 0, \tag{3.30}$$

$$[p_i, h] = 0, \quad [j_i, j_j] = i\epsilon_{ijk} J_k, \text{ and } [j_i, h] = 0.$$

The Hilbert space of physical states can now be written as a direct product:

$$\mathcal{H} = S \times L^{(2)},$$

where $L^{(2)}$ is the Hilbert space of square integrable functions of the total momentum $\vec{p}$; S is spanned by basis vectors which are eigenvectors of $h, \vec{j}^2$ and $\eta_3$ where $\eta$ is anything else needed to define the basis. That is, other quantum numbers. A representation $u(a,\Lambda)$ of the Lorentz group induces in S a representation $U(R)$ of the three dimensional rotation group with generators $\vec{j}$ and in addition a representation of the mass operator h.

We shall next direct our attention to two particle states, of masses $m_1$ and $m_2$. For simplicity we shall neglect spin. In the absence of interactions and using a subscript "o" to distinguish operators referring to the free system, we may write for the generators

$$\begin{aligned} \vec{P}_o &= \sum_{i=1}^{2} \vec{p}_i \ , \\ H_o &= \sum_{i=1}^{2} h_i \ , \\ \vec{J}_o &= \sum_{i=1}^{2} \vec{x}_i \times \vec{p}_i , \quad \text{and} \\ \vec{K}_o &= \frac{1}{2} \sum_{i=1}^{2} (\vec{x}_i h_i + h_i \vec{x}_i). \end{aligned} \tag{3.31}$$

Denoting the four vector $(\vec{P}_o, H_o)$ by $\tilde{P}_o$ and introducing $h_o$ and the relative moment $\vec{k}$ by

$$\begin{aligned} H_o &= \sqrt{\vec{p}_o^{\,2} + h_o^2} \quad \text{and} \\ \vec{k}_i &= \frac{1}{2} \sum_{\mu}' \beta^{-1}(\tilde{p}_o)_{i\mu} (p_1 - p_2)_\mu \ , \end{aligned} \tag{3.32}$$

where

$$\begin{aligned} \beta_{ik}(\tilde{P}) &= \delta_{ik} + \frac{P_{oi} P_{ok}}{h_o} (h_o + H_o), \\ \beta_{4\mu} &= -i \frac{P_{o\mu}}{h_o} \ , \qquad \begin{matrix} i,k = 1,2,3, \\ \mu = 1,2,3,4, \end{matrix} \end{aligned} \tag{3.33}$$

is designed so that

$$\beta(\tilde{P})(\vec{o},h_o) = (\vec{P}_o,H_o).$$

The center of mass generators of the Poincaré group for the two non-interacting particles may be explicitly represented by

$$\begin{aligned}
\vec{P}_o &= \vec{p}_o, \\
h_o &= \sqrt{\vec{k}^2+m_1^2} + \sqrt{\vec{k}^2+m_2^2}, \\
\vec{j}_o &= -\frac{1}{i}\vec{k}\times\vec{\nabla}_k, \quad \text{and} \\
\vec{x}_o &= i\frac{\partial}{\partial\vec{p}_o}.
\end{aligned} \tag{3.34}$$

An interaction is defined by letting $h_o \to h_o+v$ and leaving the other generators unaltered. Then we find

$$H_o \to H = \sqrt{\vec{p}_o^2+h^2} \tag{3.35}$$

where

$$h = \sqrt{\vec{k}^2+m_1^2} + \sqrt{\vec{k}^2+m_2^2} + v,$$

and v is a rotationally invariant function

## 2. Existence of Möller Operators, Lorentz Invariance and Causality

In this section we shall briefly review the Lorentz invariance of the relativistic Schrödinger equation, its causal properties, and the general conditions which v must satisfy in order to clearly define the scattering problem.

We start by recalling the usual definition of the Möller operators

$$\Omega_{\pm}(h,h_o) = \operatorname*{slim}_{t\to\pm\infty} e^{iht}\, e^{-iho t},$$

and (3.36)

$$\Omega_{\pm}(h_o,h) = \operatorname*{slim}_{t\to\pm\infty} e^{iho t}\, e^{-iht},$$

where 's denotes the strong limit. For a discussion of scattering theory see Branig and Haag (1959). We can now make the following statements for suitable potentials v.

The scattering problem is well defined. That is if both $\Omega_{\pm}(h,h_o)$ and $\Omega_{\pm}(h_o,h)$ exist, then the strong limits $\Omega_{\pm}(H,H_o)$ and $\Omega_{\pm}(H_o,H)$ exist also and

$$\Omega_{\pm}(H,H_o) = \Omega_{\pm}(h,h_o),\ \Omega_{\pm}(H_o,H) = \Omega_{\pm}(h_o,h). \tag{3.37}$$

The existance of the Möller operators has been proven under sufficient conditions on the potential v set forth by Haag (1959), Kureda (1959), and Kato (1963). These conditions can be summarized in the statement that the potential v be of trace class. That is, it can be written as sums of products of Schmidt class operators. (A Schmidt class operator is one which has a finite trace norm).

The equation is relativistically invariant. That is we can explicitly exhibit a unitary representation of the Poincare group in the Hilbert space of physical states such that the resultant S matrix is covariant. This point has been fully discussed by Fong and Sucher (1963). We shall briefly review it.

They have defined unitary operators corresponding to a Poincare transformation $(a,\Lambda)$ by

$$U_+ \quad (a,\Lambda)\ \Psi^{(+)}_{\vec{q}_1,\vec{q}_2} = N\ \Psi^{(+)}_{L\vec{q}_1,L\vec{q}_2}$$

and (3.38)

$$U_- \quad (a,\Lambda)\ \Psi^{(-)}_{\vec{q}_1,\vec{q}_2} = N\ \Psi^{(-)}_{L\vec{q}_1,L\vec{q}_2},$$

where $\Psi^{(+)}_{\vec{q}_1,\vec{q}_2}$ ($\Psi^{(-)}_{\vec{q}_1,\vec{q}_2}$) denotes the Heisenberg state corresponding to a final (initial) two particle state configuration characterized by momenta $\vec{q}_1$ and $\vec{q}_2$, and $L\vec{q}_1$ and $L\vec{q}_2$ denote the Lorentz transform by $(a,\Lambda)$ of $\vec{q}_1$ and $\vec{q}_2$ respectively. The normalization factor N is chosen to make $U_+$ and $U_-$ unitary. Using the normalization:

$$\langle \vec{q}_1',\vec{q}_2' \mid \vec{q}_1,\vec{q}_2\rangle = \delta^{(3)}(\vec{q}_1' - \vec{q}_1)\ \delta^{(3)}(\vec{q}_2' - \vec{q}_2), \tag{3.39}$$

it follows that

$$N = \sqrt{\frac{E_{L\vec{q}_1}\ E_{L\vec{q}_2}}{E_{\vec{q}_1}\ E_{\vec{q}_2}}}\ , \tag{3.40}$$

where the E's denote the corresponding energies.

Since

$$\Psi^{(\pm)}_{\vec{q}_1\vec{q}_2} = \Omega^{(\pm)}|\vec{q}_1,\vec{q}_2\rangle, \tag{3.41}$$

where $|\vec{q}_1,\vec{q}_2\rangle$ denotes the two particle state in the absence of interactions, it follows that in the absence of bound states

$$U_{\pm}(a,\Lambda) = \Omega^{(\pm)} u_o(a,\Lambda)\, \Omega^{\dagger(\pm)}, \tag{3.42}$$

where $U_o(a,\Lambda)$ is a unitary representation of the Poincare group in the Hilbert space formed by considering direct sums of tensor products of single particle states. If there are bound states, we write

$$U_{\pm}(a,\Lambda) = U_{\pm b}(a,\Lambda) + U_{\pm c}(a,\Lambda), \tag{3.43}$$

where $U_{\pm c}(a,\Lambda)$ refers to the continuum part of the spectrum as we have already discussed, and $U_{\pm b}(a,\Lambda)$ is the restriction of $U_{\pm}(a,\Lambda)$ to the bound state subspace.

Clearly the operators $U_+(a,\Lambda)$ and $U_-(a,\Lambda)$ obey the commutation relations of the Poincare group, because they are similarity transforms of the operators $U_o(a,\Lambda)$. The condition necessary for the covariance of the S matrix,

$$[S, U_o(a,\Lambda)] = 0, \tag{3.44}$$

is then

$$\Omega_+ U_o(a,\Lambda)\Omega_+^{\dagger} = \Omega_- U_o(a,\Lambda)\Omega_-^{\dagger}. \tag{3.45}$$

Thus out of all the possible class of generators of Lorentz transformations which may be adjoined to $\vec{P}_o$, $\vec{J}_o$, H, only an equivalence class of them yields a covariant S matrix.(1) Therefore, stipulating the Hamiltonian $H = \sqrt{\vec{p}_o^2 + h^2}$ does in fact yield a covariant S matrix as shown by Fong and Sucher. In addition they show that this is the more general Hamiltonian which should be considered from the viewpoint of scattering theory. If a two body covariant S matrix is the S matrix of some direct interaction theory, there always exists a Hamiltonian of the type $H = \sqrt{p_o^2 + h^2}$ which yields the same S matrix.(2)

The equation is macrocausal. By this we mean that when the two particles are at a great distance from each other, they have virtually no effect upon each other. In local quantum field theory, however, one has strict microcausality, since one assumes that observables commute with each other at space like distances for each space-time point.

The requirement of macrocausality, formulated as a strong limit is

$$\operatorname{slim}_{|a|\to\infty} \exp(ip'a)\, S \exp(-ip'a) = S' \otimes S'', \tag{3.48}$$

where p' is the total momentum of a subsystem of particles. Note that in the above equation, we have used a strong limit. The above condition has sometimes been formulated in the literature as a weak limit

---

(1) The equivalence class we refer to is that corresponding to the set of Hamiltonians which produce the same S matrix.

(2) R. Fong and J. Sucher, J. Math Phys. 5, 465 (1963).

(Wichmann and Chricton, 1963). The strong limit follows from the weak one, since the S matrix is unitary. Coester proved equation (3.48) under the condition that v is of trace class. His proof is essentially a simple application of Cauchy Schwartz inequality.

# IV. PRACTICAL CONSIDERATIONS

## A. Numerical Analysis

We start with the relativistic multichannel Schrödinger equation for scattering states:

$$K'(q_2,q_1) = V'(q_2,q_1) - \frac{P}{\pi}\int_{\Delta_m}^{\infty} V'(q_2,q)\,\frac{d(E_q+\omega_q)}{\sqrt{s}-E_q-\omega_q}\,K'(q,q_1), \qquad (4.1)$$

where $K'$ and $V'$ are matrices, $\dfrac{d(E_q+\omega_q)}{\sqrt{s}-E_q-\omega_q}$ is a diagonal matrix in channel space, and $\Delta_m$ is the lowest threshold. In order to solve this integral equation numerically, we first map the infinite interval onto the finite interval $[0,1]$. To do this we make the transformations

$$(E_q+\omega_q)_i = \frac{\alpha\, x_i}{1-x_i} + \Delta_i$$

and (4.2)

$$\sqrt{s} = \frac{\alpha\, z_i}{1-z_i} + \Delta_i,$$

where the threshold for the corresponding channel i is $\Delta_i$, and where $\alpha$ is a scale factor chosen to make the integrand peak around the middle of the interval of integration. This is to obtain maximum numerical accuracy.

We then obtain

$$K'(x,z) = V'(x,z) - \frac{P}{\pi}\int_0^1 V'(x,x')\,\frac{dx'}{z-x'}\,\frac{1-z}{1-x'}\,K'(x',z). \qquad (4.3)$$

To take care of the singularity, we write

$$\int_0^1 V'(x,x') \frac{dx'}{z-x'} \frac{1-z}{1-x'} K'(x',z) = \int_0^1 \left[ V'(x,x') \frac{dx'}{z-x'} \frac{1-z}{1-x'} - V'(x,z) \frac{dx'}{z-x'} \right]$$

$$K'(x',z) + V'(x,z) \int_0^1 \frac{dx'}{z-x'} K'(x',z) \ . \tag{4.4}$$

Then,

$$K'(x,z) = V'(x,z) \left[ 1 - \frac{1}{\pi} \int_0^1 \frac{dx'}{z-x'} K'(x',z) \right] + \frac{1}{\pi} \int_0^1 \left[ V'(x,x') \frac{dx'}{z-x'} \frac{1-z}{1-x'} \right.$$

$$\left. - V'(x,z) \frac{dx'}{z-x'} \right] K'(x',z) \ . \tag{4.5}$$

We define

$$u'(x,z) = K'(x,z) \left[ 1 - \frac{1}{\pi} \int_0^1 \frac{dx'}{z-x'} K'(x',z) \right]^{-1} \ . \tag{4.6}$$

Then we obtain

$$u'(x,z) = V'(x,z) - \frac{1}{\pi} \int_0^1 \left[ V'(x,x') \frac{dx'}{z-x'} \frac{1-z}{1-x'} - V'(x,z) \frac{dx'}{z-x'} \right] u'(x',z). \tag{4.7}$$

This equation can now easily be solved by standard techniques. After solving equation (4.7) we then obtain $K'$ by inverting equation (4.6). That is, by using

$$K'(x,z) = u'(x,z)\left[1 + \frac{1}{\pi}\int_0^1 \frac{dx'}{z-x'} u'(x',z)\right]^{-1} . \qquad (4.8)$$

To compute

$$\int_0^1 \frac{dx'}{z-x'} u'(x',z), \qquad (4.9)$$

we again take care of the singularity by writing

$$\int_0^1 \frac{dx'}{z-x'} u'(x',z) = \int_0^1 \frac{dx'}{z-x'} [u'(x',z) - u'(z,z)] - \log\left(\frac{1-z}{z}\right) u'(z,z). \qquad (4.10)$$

In order to solve the integral equation (4.7) we approximate the integral by a sum, and then solve the system of linear equations so obtained for the unknown function $u'(x,z)$. In approximating the integral by a sum we use the technique of Gaussian quadratures. We can then use few terms in the sum. Thus the matrices we have to invert in solving the system of linear equations for the unknown function $u'$ can be solved on most computers.

In the technique of Gaussian quadratures the abscissas and weights are preassigned in an optimal way to obtain a polynomial fit of degree 2n-1, when we use n points. This technique is fully discussed in any standard numerical analysis textbook, such as Hildebrand (1958) or Kopal (1961).

We give equation (4.7) with the integral approximated by a sum and all matrix indices:

$$u'(x_j^{(i)},z_\ell) = V'(x_j^{(i)},z_\ell) - \sum_{rm} A_r^{(m)}[V'(x_j^{(i)},x_r^{(m)}) \frac{1-z_r}{1-x_r^{(m)}} -$$

$$V'(x_j^{(i)},z_r)] \frac{u'(x_r^{(m)},z_\ell)}{z_r - x_r^{(m)}} , \qquad (4.11)$$

where the corresponding Gaussian weights are denoted by $A_r^{(m)}$. Superscripts stand for the preassigned Gaussian abscissas; subscripts stand for the corresponding channel indices.

Once we solve for $u'(x_j^{(i)},z_\ell)$ we then obtain $u'(x_i,z_\ell)$ by again using equation (4.11). The quantity $u'(x_i,z_\ell)$ is $u'$ with the momenta of the incoming and outgoing particles both on the mass shell. We then use equation (4.6) to obtain $K'(x_j,z_\ell)$. In computing the integral (4.9) appearing in equation (4.6) we also use the technique of Gaussian quadratures.

A computer program was written for the IBM 7094 computer to accomplish this procedure. In our numerical calculations sufficient accuracy was obtained with the use of approximately ten Gaussian quadrature points, with a value of the scale factor of about 0.5 BeV.

To check the validity of our programs, we used this technique to solve a nonrelativistic multichannel Schrödinger equation in momentum space for a Yukawa potential in a broken SU(3) symmetry model. This equation had an energy dependent reduced mass to take some account of relativistic kinematics. This problem was first solved by Wyld (1967) who wrote the multichannel Schrödinger differential equations directly in position space.[1] The results obtained by

---

1. His model is further discussed in Chapter V, where we compare his results with those obtained by solving the relativistic Schrödinger equation, to take full account of the relativistic kinematics.

solving the equations in momentum space agreed with those of Wyld who used position space.

In the case of bound states, the inhomogeneous term in equation (4.1) is not present. The solution of the equation is then reduced to finding its energy eigenvalues $\sqrt{s}$ or what is equivalent to finding the eigenvalues $z_r$ since these are related by equation (4.2).

We must then find the eigenvalues of the equation

$$K'(x,z) = -\frac{1}{\pi}\int_0^1 V'(x,x')\,\frac{dx'}{z-x'}\,\frac{1-z}{1-x'}\,K'(x',z)\ . \qquad (4.12)$$

Upon writing the above equation as a sum, all indices included, we obtain

$$K'(x_j^{(i)},z_\ell) = -\frac{1}{\pi}\sum_{rm} A_r^{(m)}\,V'(x_j^{(i)},x_r^{(m)})\ \frac{1-z_r}{1-x_r^{(m)}}\ \frac{K'(x_r^{(m)},z_\ell)}{z_r-x_r^{(m)}}, \qquad (4.13)$$

where the corresponding Gaussian weights are denoted by $A_r^{(m)}$ and superscripts stand for the preassigned Gaussian abscissas; subscripts stand for the corresponding channel indices. The eigenvalues $z_r$ of the above equation are then obtained by finding the zeroes of the corresponding determinant function. In other words we compute the values $z_r$ so that

$$\det\left[\delta_{im}\delta_{jr} + \frac{1}{\pi}\ A_r^{(m)}\,V'(x_j^{(i)},x_r^{(m)})\ \frac{1-z_r}{1-x_r^{(m)}}\ \frac{1}{z_r-x_r^{(m)}}\right] = 0. \qquad (4.14)$$

In cases where we solve the Blankenbecler-Sugar equation for scattering states, we start from the equation

$$K'(q_2,q_1) = V'(q_2,q_1) - \frac{P}{\pi}\int_{\Delta_m}^{\infty} V'(q_2,q)\left[\frac{d(E_q+\omega_q)}{\sqrt{s}-E_q-\omega_q} - \frac{d(E_q+\omega_q)}{\sqrt{s}+E_q+\omega_q}\right]K'(q,q_1), \tag{4.15}$$

where both $\frac{d(E_q+\omega_q)}{\sqrt{s}-E_q-\omega_q}$ and $\frac{d(E_q+\omega_q)}{\sqrt{s}+E_q+\omega_q}$ are diagonal matrices in channel space and $\Delta_m$ is the lowest threshold.

In the bound state case the above equation can be written in the form

$$K'(q_2,q_1) = -\frac{1}{\pi}\int_{\Delta_m}^{\infty} V'(q_2,\bar{q})\left[\frac{d(E_q+\omega_q)}{\sqrt{s}-E_q-\omega_q} - \frac{d(E_q+\omega_q)}{\sqrt{s}+E_q+\omega_q}\right] K'(q,q_1). \tag{4.16}$$

We solve these integral equations by making transformation (4.2) and proceeding in the same way as before.

In cases where we solve any of the above equations with a cutoff matrix function $F_{ij}(q)$ we modify the original kernel of these integral equations by multiplying by this matrix function. We then solve these equations by making transformation (4.2) and proceeding as before. As an example of a cutoff matrix function $F_{ij}(q)$ we use

$$F_{ij}(q) = \delta_{ij} e^{-[(E_q+\omega_q-\Delta)_j]^2/\lambda^2}, \tag{4.17}$$

where $\lambda$ is properly chosen and $\Delta_j$ is the threshold for the $j^{th}$ channel.

In cases where we solve the relativistic Schrödinger equation or the Blankenbecler-Sugar equation with a cutoff parameter $\lambda$ we make the transformations

$$(E_q + \omega_q)_i = (\lambda - \Delta_i)x_i + \Delta_i$$

and (4.18)

$$\sqrt{s}_i = (\lambda - \Delta_i)z_i + \Delta_i$$

and proceed as we have already discussed.

B. Justification of Numerical Analysis

With no loss of generality let us consider equation (4.1). The same reasoning can be applied to the other cases. We write this equation in symbolic form as

$$T = V + VG_oT, \tag{4.19}$$

where

$$G_o = \frac{1}{\sqrt{s} - H_o} .$$

Basic to our treatment is the existance of the Schmidt norm defined by

$$\tau(s) = ||VG_o||^2 = \mathrm{Tr}[(VG_o)^\dagger (VG_o)] . \tag{4.20}$$

That is, writing (4.20) in full[2]

---

2. Defining the Schmidt norm in this manner we avoid the inessential complications due to the pole at $\sqrt{s} = E_q + \omega_q$.

$$\tau(s) = \int dp \int dq \left| \frac{V'(p,q) - V'(q,q)}{\sqrt{s} - E_q - \omega_q} \left( \frac{q}{E_q} + \frac{q}{\omega_q} \right) \right|^2 < \infty \ . \qquad (4.21)$$

This is based on the theorem which states that a completely continuous operator W can be uniformly approximated by a finite rank operator U .[3],[4] (This theorem is shown, for example, in Riesz and Nagy (1955)). In symbols, if W is completely continuous there exists a finite rank operator U such that

$$|W - U| < \epsilon \qquad (4.22)$$

for any given $\epsilon > o$. We write

$$VG_o \equiv W = U + Z \qquad (4.23)$$

where U is of finite rank. Using (4.22) we see that $|Z| < \epsilon$. Then we write

$$T = V + VG_o T = V + (U+Z)T = V + UT + ZT, \qquad (4.24)$$

and see that

$$T(1-Z) = V + UT. \qquad (4.25)$$

---

3. An operator W is called completely continuous if it maps weakly converging sequences onto strongly converging ones. The existance of the Schmidt norm is a sufficient, but not a necessary condition for the complete continuity of the operator W. In the theory of integral equations, operators of finite Schmidt norm are called Fredholm.

4. An operator U is said to be of finite rank if its range is of finite dimension. It is easily shown as for example in Rickart (1960) that an operator U of finite rank r can be written in the form $Ux = \sum_{i=1}^{r} f_i(x) u_i$, where the $u_i$'s are linearly independent vectors, the fi's are linear functionals, and x denotes any vector in the domain of U .

Defining the resolvent of Z by

$$(1 - Z)^{-1} = 1 + R_Z , \tag{4.26}$$

we obtain

$$T = (1 + R_Z)(V + UT) . \tag{4.27}$$

Defining

$$\tilde{V} = (1 + R_Z)V$$

$$\text{and} \tag{4.28}$$

$$\tilde{U} = (1 + R_Z)U$$

we then obtain

$$T = \tilde{V} + \tilde{U}T . \tag{4.29}$$

The solution to (4.29) is then seen to approach the desired solution since $|Z| < \epsilon$ by (4.22).

# V. INTRODUCTORY REMARKS, NOTATION, AND S WAVE RESULTS

## A. Introductory Remarks

In this and the remaining chapters we will discuss numerical results obtained by solving the multichannel relativistic Schrödinger equation in the case of pseudoscalar meson baryon scattering in a broken SU(3) symmetry model and in the four lowest partial waves. Also we will compare our results with those of other calculations where possible. We use the potentials obtained from single particle exchange processes computed using the usual Feynman rules and extrapolated off shell following the procedure discussed in Chapter III, Part C It is worthwhile to emphasize that extrapolating the potential off shell is certainly not a unique process and is one of the most serious disadvantages of our calculational procedure. However, we would hope that the qualitative features of the model be roughly independent of the way we extrapolate the potential off shell. This has been the case in our calculations. In calculating the potentials we use interaction Lagrangians obtained by assuming SU(3) invariance so as to obtain relations between otherwise unrelated coupling constants. However, we break the symmetry in the sense that we use actual experimental masses for both the exchanged particles and also the incoming or outgoing particles. The crossing coefficients so obtained are given in Appendix A, where we also discuss in detail the procedure followed in obtaining them. The momentum dependence of the potentials is given in Appendix D. The assumptions of our model can best be illustrated through a brief discussion of earlier approaches to the problem.

The technique which has been most widely used in the theoretical investigation of pion nucleon scattering is the N/D method and its approximations. In order to take some account of inelastic channels, many of these calculations have made use of the multichannel N/D method or the Frye-Warnock equations (1963).[1] Generally these two methods are not equivalent. Bander, Coulter, and Shaw (1965) have considered a simple model and have shown that the results obtained by using multichannel N/D equations do not in general agree with those obtained using the Frye-Warnock equations when there are bound states present.

Among the calculations which have made use of the N/D equations we may mention the calculations performed by Martin and Wali (1963; 1964).[2] Their method of calculation consisted in using Bjorken's determinantal approximation to the multichannel N/D equations. The forces were approximated by considering the contributions due to allowed single particle exchange processes. The interaction Lagrangians were obtained by assuming SU(3) invariance. In M.W. 1 they considered the problem of P wave pseudoscalar meson-baryon scattering for all states such that $J = \frac{3}{2}$ with only the contribution due to baryon exchange as the input potential. In M.W. 2 they considered the four lowest partial waves and the contribution due to the other possible single particle exchanges. Also we will mention

---

1. Single channel N/D equations with an inelasticity parameter are usually referred to as Frye-Warnock equations.

2. Hereafter referred to as M.W. 1 and M.W. 2 respectively.

the calculations of Coulter and Shaw (1966). They solved the Frye-Warnock equations for pion nucleon scattering in cases such that $J \leq 3/2$. The inelasticity parameter was taken from experiment and for the input potential they considered the contribution due to $\rho$, N, and N* exchange. More recently the multichannel N/D equations for pseudoscalar meson baryon scattering were also considered by Brehm and Kane (1966) who solved them using an approximation procedure first suggested by Pagels (1965).

Dispersion relation methods have also been used in studying pion nucleon scattering problems. One such technique, used by Donnachie, Hamilton, and Lea (1964) and also Donnachie and Hamilton (1965) was to write dispersion relations for $f_{\ell\pm}/k^{2\ell}$ where $f_{\ell\pm}$ is the scattering amplitude and k the momentum.[3] The factor $k^{2\ell}$ was introduced to suppress the contributions of short range forces. The contribution of the nearby singularities was obtained by evaluating the long range part of $\rho$, N, N*, and $\pi$-$\pi$ I = 0, J = 0 exchange. Experimental data was used to evaluate the contribution of these processes. The contribution of the distant singularities was approximated by poles. The S wave problem was not considered by these authors since short range forces are then expected to provide an important contribution which cannot be neglected.

Pseudoscalar meson baryon scattering has also been treated recently within the framework of the Schrödinger equation by Wyld as we have briefly discussed in Chapter IV. He addressed himself to the

3. Hereafter referred to as D.H.L. and D.H. respectively.

S wave problem and considered a multichannel Yukawa potential in a broken SU(3) symmetry model as the input potential. To take some account of the relativistic kinematics he used an energy dependent reduced mass. In the next section we will compare his results with those obtained in our model, taking full account of the relativistic kinematics and actual experimental particle masses. His calculation was repeated within the framework of the multichannel N/D equations by Brehm (1966), who solved these equations using Pagel's method. Due to kinematical complications he could address himself only to the pion nucleon scattering case. His results remotely agreed with those of Wyld, but there is certainly not a quantitative agreement. Also the Argand diagrams given by Brehm were in violent disagreement with experimental evidence.

The effective potential method due to Balazs was used recently by Finkelstein (1966) in the problem of meson nucleon scattering. The advantages and disadvantages of this technique have already been discussed in Chapter II. Another practical disadvantage was that he could not address himself to all possible states since he encountered divergent potentials in all those cases for which $J = \ell - \frac{1}{2}$. Also he considered a one channel problem and completely neglected inelastic effects. The main success of his model was, however, that the scattering length corresponding to the $S_{11}$ state was positive, in agreement with experiment.[4] This was in contrast

4. We shall use the notation $L_{2I,2J}$ to denote a state of orbital angular momentum L , isospin I, and total angular momentum J. We shall occassionally also use the symbol $L_J$ to denote any isospin state with orbital angular momentum L and the total angular momentum J.

to calculations based on the N/D method, even after taking account of inelasticity. As an example we may consider the calculations of Coulter and Shaw, which predicted a negative scattering length unless a CDD pole in the solution to the N/D equations was introduced.

## B. Notation

We start with the multichannel relativistic Schrödinger equation for scattering states

$$K'(q_2,q_1) = V'(q_2,q_1) - \frac{1}{\pi} P \int V'(q_2,q) \frac{d(E_q + \omega_q)}{\sqrt{s} - E_q - \omega_q} K'(q,q_1), \quad (5.1)$$

or with the Blankenbecler-Sugar equation for scattering states

$$K'(q_2,q_1) = V'(q_2,q_1) - \frac{1}{\pi} P \int V'(q_2,q) \left[ \frac{d(E_q + \omega_q)}{\sqrt{s} + E_q + \omega_q} - \frac{d(E_q + \omega_q)}{\sqrt{s} + E_q + \omega_q} \right] K'(q,q_1), \quad (5.2)$$

where K' is the K' matrix and V' is the input potential matrix. In the bound state case the inhomogeneous term is not present and the above system of integral equations reduces to an eigenvalue equation for the energy $\sqrt{s}$.

For scattering states once we find K' we then find its eigenvalues and eigenvectors, denoted by $\tan \delta_\alpha$ and $v_{i\alpha}$ respectively.[5]

---

5. This section follows rather closely the discussion given by Wyld (1967).

The $\delta_\alpha$ are the eigenphases, the multichannel generalization of phase shifts. The T' matrix, which is the T matrix with a kinematical factor removed is then

$$T'_{j1} = \left(\frac{K'}{1-iK'}\right)_{ji} = \sum_\alpha v_{i\alpha}\, v_{j\alpha}\, e^{i\delta_\alpha} \sin\delta_\alpha. \tag{5.3}$$

From this we obtain the cross section

$$\sigma_{j1} = \frac{4\pi}{k_1^2}\,(2J+1)\,|T'_{ji}|^2, \tag{5.4}$$

where i refers to the initial and j to the final state.

We give our results by discussing several kinds of graphs. To keep the size of this thesis manageable we will in general only exhibit explicitly graphs corresponding to the case of pion nucleon scattering. The other cases will also be discussed but usually no graphical illustration will be presented. First we have Argand diagrams such as Figure 5-1 of the real versus the imaginary part of the scattering amplitude

$$2kf = 2e^{i\delta_\alpha}\sin\delta_\alpha = 2T'_{1i} \tag{5.5}$$

as a function of energy. Here $\delta = \delta_r + i\delta_i$ is the complex phase shift in some specified channel, $\delta_r$ and $\delta_i$ denote its real and imaginary parts, and 2kf is twice a diagonal element of the T' matrix. Unitarity limits 2kf to the interior of a circle with unit radius about the point i. If only one channel is open so that the scattering is elastic, 2kf lies on the unit circle; if two or more channels are open so that the

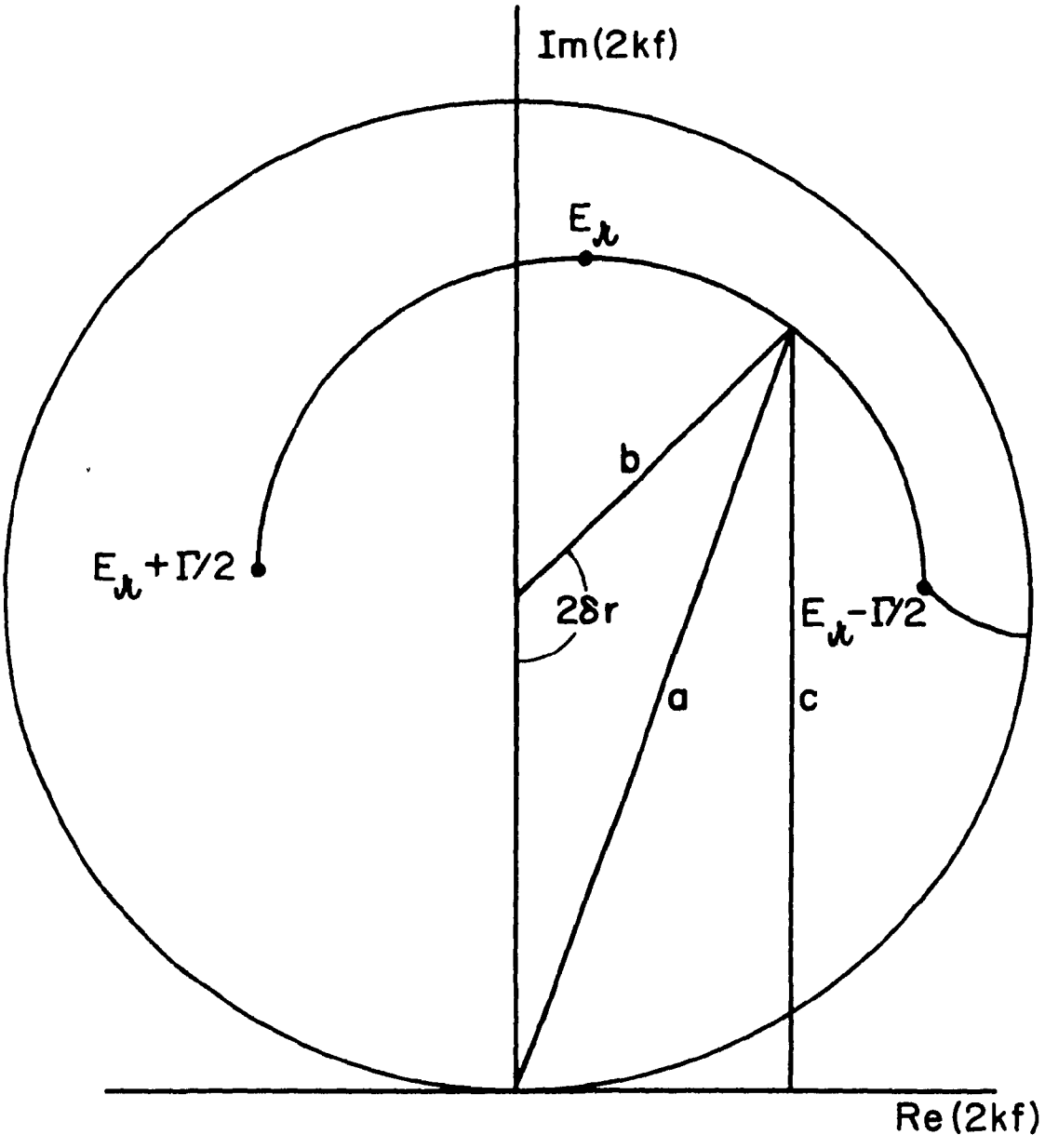


FIG. 5-1 ARGAND DIAGRAM.

scattering is inelastic, 2kf lies inside the unit circle. The scattering cross section $\sigma_s$, the reaction cross section $\sigma_r$, and the total cross section $\sigma_t$ are given by

$$\sigma_s = \frac{4\pi}{k_i^2}(2J+1)|a|^2,$$

$$\sigma_r = \frac{4\pi}{k_i^2}(2J+1)(1-|b|^2), \text{ and} \qquad (5.6)$$

$$\sigma_t = \frac{2\pi}{k_i^2}(2J+1)|c|,$$

with a, b, and c as in Figure 5-1.

There are various ways of defining a resonance. In case of a single channel problem we have the condition that the (real) phase shift increases through $90^\circ$. This corresponds to the amplitude 2kf traversing the top of the unitarity circle in Figure 5-1 in a counterclockwise direction. In case of a multichannel problem, if a resonance can be represented by a Breit Wigner term plus a constant complex background term, the Argand diagram of 2kf will be semicircular in a counterclockwise sense.[6] The energy at the top of the semicircle is the resonance energy $E_r$; the energies at the edges of the semicircle are $E_r \pm \frac{\Gamma}{2}$, where $\Gamma$ is the width of the resonance. Another possible condition for a resonance in a multichannel problem is that one of

---

6. A simple proof that this follows from causality was given by Wigner (1955). Wigner's proof applies to elastic resonances but the anticlockwise condition is also true in the presence of inelastic channels. Dalitz (1963) gave a more rigorous discussion which is appropriate to the general case.

the (necessarily real) eigenphases $\delta_\alpha$ goes through $90^\circ$. The resonance energy $E_r'$ would then be the energy at which this occurs.[7] Both $E_r$ and $E_r'$ are generally different, but relatively close. The experimentalists give the resonance energy as the energy of the peak in a mass distribution. A related, although somewhat shifted peak is also obtained in a scattering cross section.

Unless otherwise stated we use the following values for the coupling constants and the F/D ratio:

$$\frac{g_{\pi N}^2}{4\pi} = 14.6,$$

$$F/D = 0.33, \tag{5.7}$$

$$\frac{g_{\rho\pi\pi}\, g_{\rho NN}}{4\pi} = 1,$$

and

$$\frac{g_{N^*\pi N}^2}{4\pi} = 22.6/\text{Bev}^2.$$

Based on universality (Sakurai, 1966) we could use somewhat larger values for the product $\frac{g_{\rho\pi\pi}\, g_{\rho NN}}{4\pi}$. Also the experimental value of the F/D ratio is somewhat uncertain at present. Similarly we could also use slightly different values for the other coupling constants. However, our results are not very sensitive to such variations. We believe this is one of the main advantages of our model.

## C. S Wave Results

### 1. Experimental Situation

Experimental results concerning S wave pion nucleon scattering in the cases $I = 3/2$, $Y = 1$ ($S_{31}$) and $I = \frac{1}{2}$, $Y = 1$ ($S_{11}$) are given

7. We define the resonance energy $E_r'$ as the energy at which the eigenphase crosses $90^\circ$. The width of the resonance is defined by $\frac{\Gamma}{2} = 57.3 \times (d\omega/d\delta)$.

in Figures 5-2 and 5-3 respectively. In Figure 5-2 we present Argand diagrams obtained by Bareyre et al.(1965) and Donnachie et al. (1964) in the case of $S_{31}$. In Figure 5-3 we present Argand diagrams as obtained by Bareyre et al. and Bransden et al. (1965) in the case of $S_{11}$. Analysis of Figure 5-2 shows the interesting behavior of $S_{31}$ wave. It starts off as a repulsive wave and continues as such to about 1400 MeV (center of mass energy). The Argand diagram then shows a loop above this repulsive background. The analysis of Figure 5-3 shows the behavior of the $S_{11}$ wave. A strong cusp is seen at the $\eta$ production threshold. The Argand diagram then displays a circular shape. This is the behavior which establishes the existence of the $N^*_{\frac{1}{2}}(1570)$ resonance. Also the Argand diagram of Figure 5-3 seems to show some evidence for a higher $S_{11}$ resonance at a center of mass energy of approximately 1700 MeV.

## 2. Review of Wyld's Calculations

It is clear from the analysis of the Argand diagrams, as shown in Figures 5-2 and 5-3, that in attempting to explain the behavior of the S wave scattering amplitude, we must take account of inelasticity. Wyld did this using a broken SU(3) symmetric Yukawa potential with an energy dependent reduced mass. The use of a Yukawa potential can be justified as the nonrelativistic limit of a vector exchange process. It is clear that his model could not account for the existence of an $S_{31}$ resonance, since the crossing coefficients for this case yield a repulsive potential. However, he accounted for the $N^*_{\frac{1}{2}}(1570)$

Fig. 5-2. The experimental Argand diagram for the $S_{31}$ $\pi N$ scattering amplitude. The numbers are center of mass energies in MeV. The solid curve gives the results of Bareyre et al. The dashed curve gives the results of Donnachie et al.

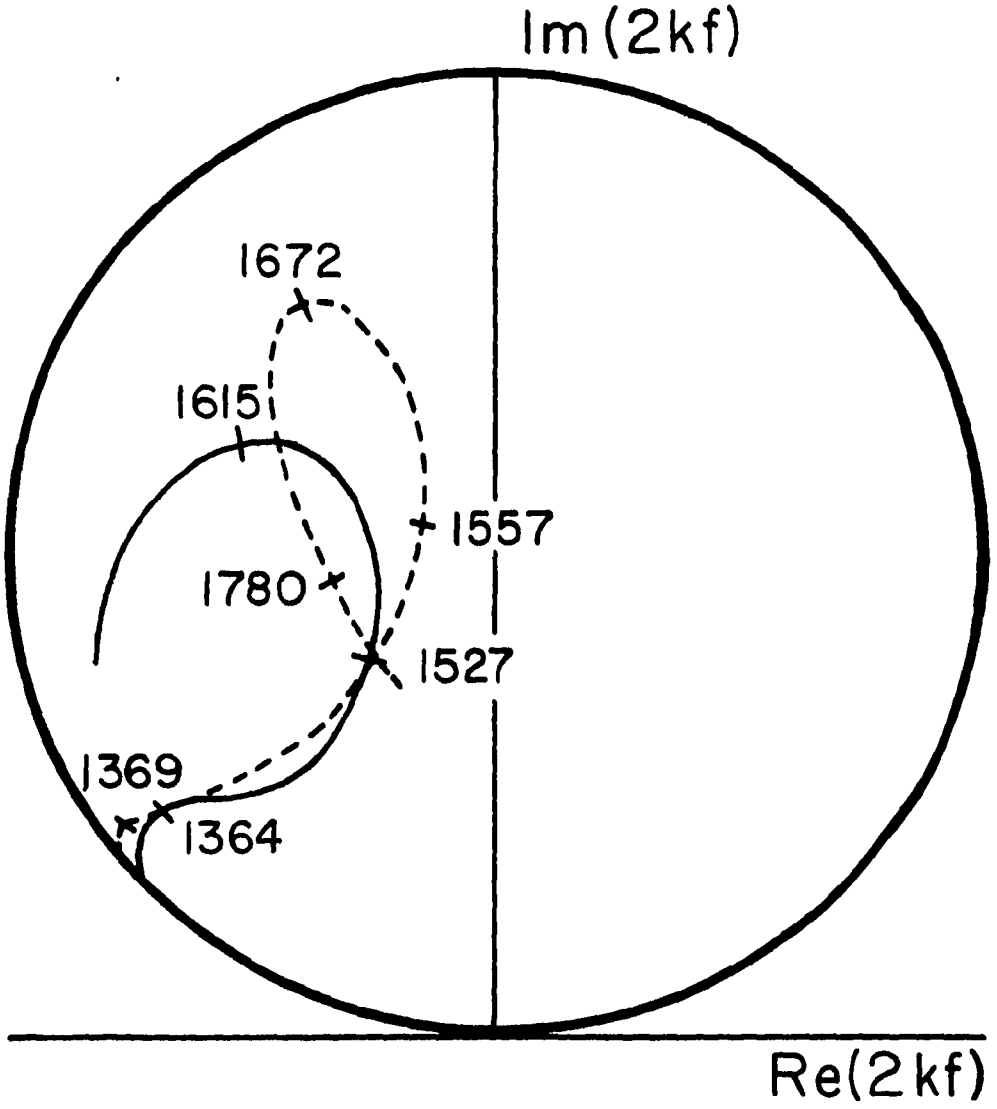
Im(2kf)
1672
1615
1557
1780
1527
1369
1364
Re(2kf)
Bareyre et al
Donnachie et al

Fig. 5-3. The experimental Argand diagram for the $S_{11}$ $\pi N$ scattering amplitude. The solid curve gives the results of Baryere et al. The dashed and dot-dash curves give the two solutions obtained by Bransden et al.

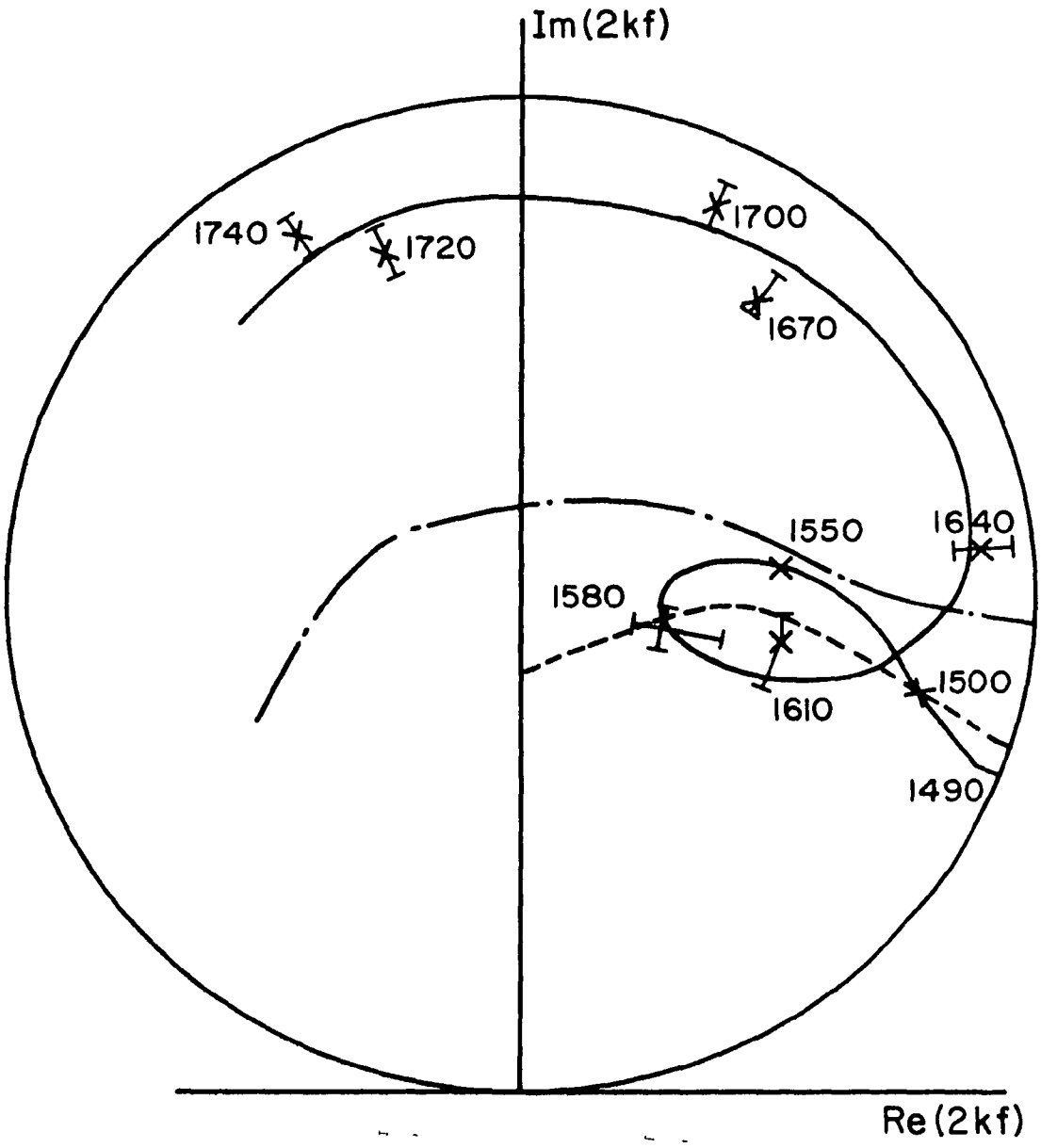
Im(2kf)
1740
1720
1700
1670
1550
1640
1580
1610
1500
1490
Re(2kf)

and interpreted it as a bound state in the KΣ channel. His model also accounted for the $Y_0^*$ (1405), $Y_0^*$ (1670), and predicted a $\Xi_{\frac{1}{2}}^*$ (1615). No $Y_1^*$ resonance appeared in this model. In Figures 5-4 and 5-5 we show (in dotted lines) the eigenphases and Argand diagram respectively corresponding to the $S_{11}$ partial wave amplitude as obtained by Wyld.

## 3. Electric ($\gamma_\mu$) Vector Exchange Contribution to the Driving Force

### a. The $S_{11}$ Partial Amplitude

In our calculations we first consider as our input potential the $\gamma_\mu$ contribution of the vector exchange process as shown in Appendix A, Figure A-1. First we compute the space part of this potential as we have discussed in Appendix D. We then note that using this input potential equation (5.1) becomes a non-Fredholm system of coupled integral equations.

Upon further analysis we observe that this is due to the presence of the factor $a_o + b_o + c_o + d_o$ in equations D.3 and D.4 in Appendix D. We then recall that only the on shell potential is known, and its extrapolation off shell is arbitrary. Since this factor is twice the energy ($2\sqrt{s}$) when the particles are on shell, we can then make the replacement $a_o + b_o + c_o + d_o \rightarrow 2\sqrt{s}$. With this replacement, equation (5.1) becomes a Fredholm system of coupled integral equations. In this manner we avoid the introduction of an arbitrary cutoff parameter at this point.

We recall that in the calculations performed by Wyld, he used for the coupling constant a value of $\frac{g_{\rho\pi\pi}\, g_{\rho NN}}{4\pi} = 0.91$ in most

Fig. 5-4. Eigenphases for the $I = \frac{1}{2}$, $Y = +1$, $S_{\frac{1}{2}}$ state. The solid curves give the eigenphases obtained considering only the contribution from the $\gamma_\mu$ part of the vector exchange process to the input potential. The dashed curves give the eigenphases obtained by Wyld. Both of these calculations used $\frac{g_{\rho\pi\pi}\, g_{\rho NN}}{4\pi} = 0.91$.

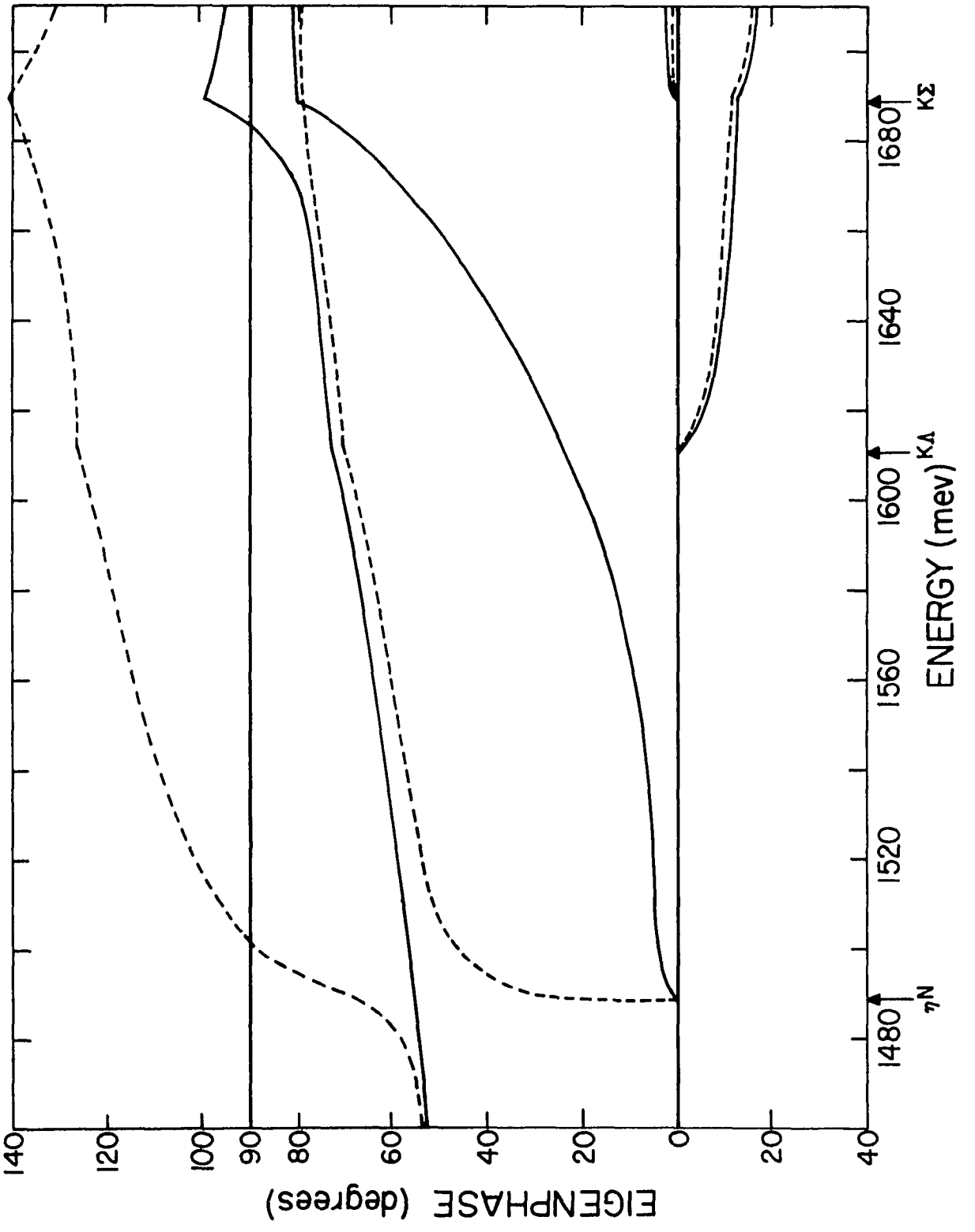
EIGENPHASE (degrees)
140
120
100
90
80
60
40
20
0
20
40
ENERGY (mev)
1480
1520
1560
1600
1640
1680
$\eta N$
$K\Lambda$
$K\Sigma$

Fig. 5-5. Argand diagrams for $\pi N$ scattering in the $I = \frac{1}{2}$, $Y = +1$, $S_{\frac{1}{2}}$ state. The solid curve gives the Argand diagram obtained following the procedure discussed in Figure 5-4. The dashed curve gives the Argand diagram obtained by Wyld. Both of these calculations used $\frac{g_{\rho\pi\pi}\, g_{\rho NN}}{4\pi} = 0.91$.

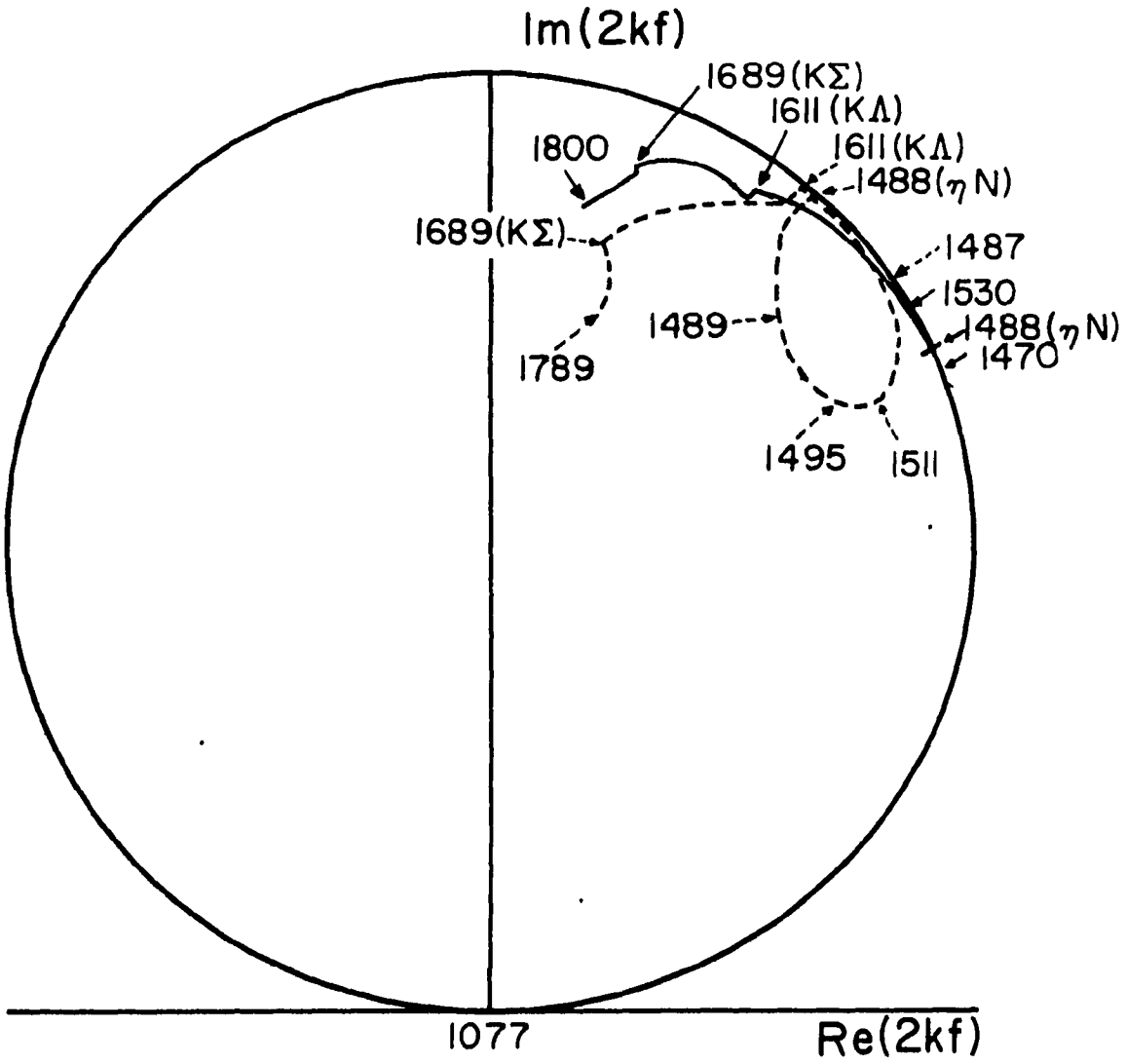
Im(2kf)
1689(KΣ)
1611(KΛ)
1800
1611(KΛ)
1488(ηN)
1689(KΣ)
1487
1530
1489
1488(ηN)
1789
1470
1495
1511
1077
Re(2kf)

cases. We use this value to analyze what happens in his model when the full relativistic kinematics and breaking of the SU(3) symmetry are introduced. The results of these calculations are shown in Figures 5-4 and 5-5. The first of these shows the eigenphases for both his results (in dotted lines) and ours (in solid lines) for the $S_{11}$ wave. Figure 5-5 compares the Argand diagrams obtained in both calculations. Analyzing Figure 5-4 we observe that the results of both calculations certainly show qualitative agreement. However, for the same value of the coupling constant, our model predicts the $N^*_{\frac{1}{2}}$ resonance to appear at an energy of 1679 MeV in contrast to Wyld's value of approximately 1501 MeV. Also analysis of the Argand diagram of Figure 5-5 shows that the Argand diagram corresponding to this model resembles experiment less than the one obtained by Wyld.

Clearly we can move the position of the resonance down in energy by increasing the value of the coupling constant $\frac{g_{\rho\pi\pi}\, g_{\rho NN}}{4\pi}$. By increasing its value to 1.0, we lower the position of the resonance from 1679 MeV to 1673 MeV. If we further increase the value of the coupling constant to 1.25, we note that the position of the resonance moves down to an energy of 1535 MeV. Thus our results are consistent with those of Wyld. However, inclusion of the relativistic kinematics in the way we have discussed seems to make the potential weaker, since we need a larger value of the coupling constant than the one in Wyld's model to position the resonance at about the right experimental energy. Both models seem to agree in the sense that they only account for one resonance in the $S_{11}$ partial wave amplitude. Thus these models do not

account for $N^*_{\frac{1}{2}}$ (1700) which seems to be present in the Argand diagram of Figure 5-3.

b. Other Isospin States

If we next consider the other isospin states, we again note that the resonances obtained from this model appear at a larger value of the energy than those in Wyld's model. However, both results qualitatively agree. For example, in Wyld's model and in the case I = 0, Y = 0 the coupling constant $\frac{g_{\rho\pi\pi}\, g_{\rho NN}}{4\pi} = 0.91$ used for the other states is too large; it led to a bound state. With a coupling constant of 0.56 the bound state disappeared, and the eigenphase crossed $90^\circ$ at 1409 MeV. With a coupling constant of 0.91 the bound state corresponded to the $Y^*_o$ (1405), and Wyld observed that the eigenphase also crossed $270^\circ$ at an energy of 1630 MeV. In our model when the coupling constant is 0.91 we observe a bound state corresponding to the $Y^*_o$, similar to his conclusions. However, no higher resonance is observed. With a coupling constant of 0.56 we observe a $Y^*_o$ at an energy of 1704 MeV. Again by increasing the coupling constant, we can produce the $Y^*_o$ at the right value of the energy (1405 MeV). Similar conclusions are made with the other states. In summary, full inclusion of the relativistic kinematics seems to weaken the potential, but the qualitative behavior agrees with that investigated by Wyld.

If we next consider the $S_{31}$ resonance, it is clear that the $\gamma_\mu$ contribution of the vector exchange process cannot account for this resonance. This is so, since this contribution of the vector exchange

process yields a repulsive potential, which can be seen by observing the signs of the crossing coefficients in Appendix A.

4. Other Contributions to the Driving Force

a. Vector, Baryon, and Decuplet Exchange Contributions

In addition to vector exchange, we can also have baryon and decuplet exchanges. Moreover, the contribution of the $\sigma_{\mu\nu}$ term in the vector exchange process (which vanishes in the nonrelativistic limit) must also be included in the relativistic calculation. Addition of these terms clearly makes the potential divergent. We can no longer convert equation (5.1) into a Fredholm system of couped integral equations by making the replacement $a_o + b_o + c_o + d_o \rightarrow 2\sqrt{s}$.

However, another way of converting this system of integral equations into a Fredholm system is to introduce a cutoff parameter. By so doing and then analyzing the relative strengths and signs of the forces corresponding to the different exchanges, we see the vector exchange process yields a moderately attractive force. The baryon exchange process produces an extremely attractive force. The decuplet exchange process yields a repulsive force which tends to compensate the strong attraction due to the baryon exchange proces. The net result is a very attractive force.

However, the agreement with experiment now worsens. If we assume that the cutoff must be larger than the $K\Sigma$ threshold (since this is the most massive channel which contributes to the $I = \frac{1}{2}$, $Y = 1$ state) we observe that it is impossible to adjust the cutoff in order to

produce the $S_{11}$ resonance above the $\pi N$ threshold, The $S_{11}$ resonance now moves down into a bound state of negative energy. Therefore, trying to make a more elaborate calculation of the S wave resonances does not improve the results obtained by considering the $\gamma_\mu$ part of the vector exchange contribution and making the replacement $a_o + b_o + c_o + d_o \rightarrow 2\sqrt{s}$ to compute the potential matrix.

Next we consider the $S_{31}$ resonance. Due to the signs of the crossing coefficients in the potential matrix, we cannot account for this resonance in the same way as we have accounted for the $S_{11}$ resonance. Again if we consider the full contribution due to vector exchange (both $\gamma_\mu$ and $\sigma_{\mu\nu}$ couplings), baryon, and decuplet exchange , we observe that the strength of the potential is increased, and we can still not account for the $S_{31}$ resonance.

b. The $S_{31}$ and $S_{11}$ Partial Wave Amplitudes in the Cook-Lee Model

To construct a model that might explain the behavior of the $S_{31}$ wave, we turn to the Cook-Lee model (Cook and Lee, 1962). The basic idea of this model is the assumption that a large contribution to the force in pion nucleon scattering is due to one pion exchange coupling to the $\rho N$ channel. Also the elastic channel contribution is neglected by merely setting it equal to zero. The obvious extension to our case is to assume that the main contribution to the force in pseudoscalar meson baryon scattering is due to single pseudoscalar meson coupling to the vector baryon channels. Also the elastic channel contributions are neglected by setting them equal to zero. Again due

to divergences we must use a cutoff to perform these calculations. In the case of the $S_{31}$ partial wave amplitude we must then solve a six channel problem. This is so because although four SU(3) channels contribute to this process ($\pi N$, $K\Sigma$, $\rho N$, and $K^*\Sigma$) both $\rho N$ and $K^*\Sigma$ can be an S or D wave state for a pseudoscalar meson baryon system in an S wave state.

We then note that for a proper choice of the cutoff parameter, we can obtain the $S_{31}$ resonance at the correct experimental energy. In Figure 5-6 we see the eigenphases obtained with a cutoff of 8.7 BeV and a coupling constant value of $\frac{g_{\rho\pi\pi}\, g_{\rho NN}}{4\pi} = 5.4$.[8] We note that the $\pi N$ eigenphase crosses $90^\circ$ at about 1784 MeV. However, the corresponding Argand diagram does not show the initial repulsive loop and the resonating background which can be observed in Figure 5-2. In fact the curve in the Argand diagram starts counterclockwise and remains so as the energy is increased and traces a semicircular shaped loop near the top of the unitarity circle corresponding to the $S_{31}$ resonance.

An obvious way of trying to obtain a repulsive background would be to consider the contribution of the $\gamma_\mu$ part of the vector exchange process in the elastic channels (rather than setting these elements of the potential matrix equal to zero). This is so since this part of the vector exchange process yields a repulsive contribution.

---

8. This is the value of the cutoff which is necessary to produce the $N^*_{3/2}(1236)$ at the correct experimental energy, considering only the energy independent baryon exchange force.

Fig. 5-6. Eigenphases for the $I = \frac{3}{2}$, $Y = +1$, $S_{\frac{1}{2}}$ state in the Cook-Lee model for the coupling constant $\frac{g_{\rho\pi\pi}{}^{\frac{1}{2}} g_{\pi NN}}{4\pi} = 5.4$. A cutoff value of 8.7 BeV is used in this calculation.

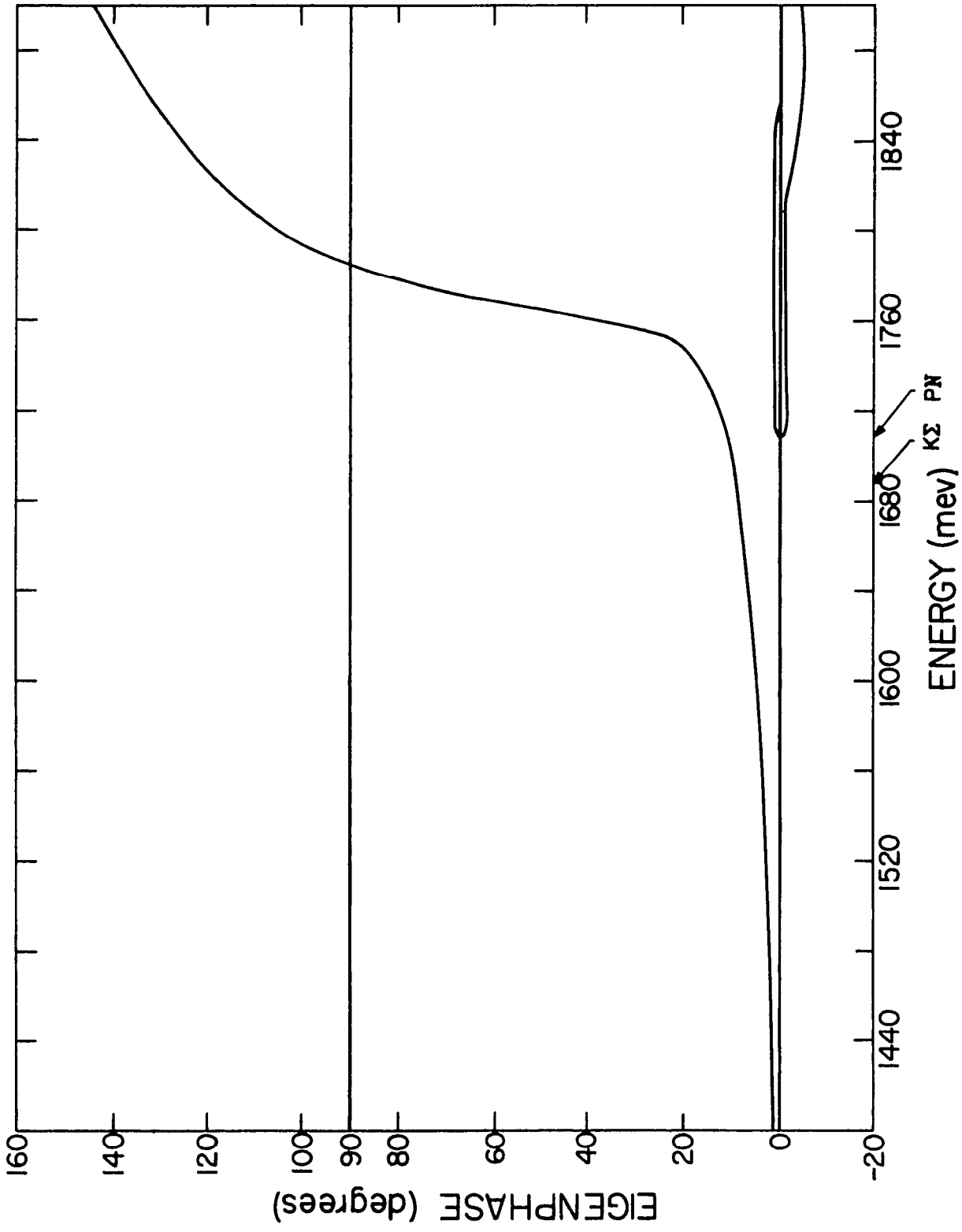
EIGENPHASE (degrees)
160
140
120
100
90
80
60
40
20
0
-20
1440
1520
1600
1680
1760
1840
ENERGY (mev)
KΣ PN

If we do this, we then observe that the corresponding Argand diagram does start off repulsive as it should. However, the corresponding curve moves around the unitarity circle in a clockwise direction, and then flips, starts to move counterclockwise, and then goes through a resonance. Analysis of the Argand diagram also shows that the corresponding curve leaves the unitarity circle at an energy larger than the experimental energy for which this happens. This is in disagreement with the experimental results shown in Figure 5-2.

To try to increase the attraction and to provide an opportunity for the curve in the Argand diagram to leave the unitarity circle at a lower energy, we then include the contribution due to the inelastic pseudoscalar meson decuplet channels. To compute the main contribution to this force, we consider the single vector exchange contribution with both the $\gamma_\mu$ and $\sigma_{\mu\nu}$ couplings. This idea is analagous to the Cook-Lee idea. The VBB* coupling is treated in accordance with the Stodolsky-Sakurai model (1962). Since in addition to the elastic and vector baryon channels, we are also considering the contribution of the pseudoscalar meson decuplet channels, it follows that we now have seven SU(3) channels ($\pi N$, $K\Sigma$, $\rho N$, $K^*\Sigma$, $\pi N^*$, $KY^*$, and $\eta N^*$). Since there are two linearly independent amplitudes for the vector meson baryon channels, we must solve a nine channel problem. As expected, inclusion of the pseudoscalar meson decuplet channels increases the attraction. However, only a slight increase in the attraction is observed. This is presumably so because the pseudoscalar meson decuplet channels are in a D wave state when the

pseudoscalar meson baryon channels are in an S wave state. Thus, no better agreement with the experimental Argand diagram is obtained.

We can also use the Cook-Lee model to study the $S_{11}$ partial wave amplitude. We then assume the main contribution to the driving force is obtained by considering inelastic coupling to the vector baryon channels via pseudoscalar meson exchange. We must solve a twelve channel problem, since there are eight SU(3) channels which contribute ($\pi N$, $\eta N$, $K\Lambda$, $K\Sigma$, $\rho N$, $\varphi_0 N$, $K^*\Lambda$, and $K^*\Sigma$), and there are two linearly independent amplitudes for the vector baryon channels which must be considered.

However, the corresponding Argand diagram still does not resemble the experimental one. The Argand diagram now displays a semicircular shaped loop near the top of the unitarity circle similar to the one seen in the experimental $S_{11}$ Argand diagram shown in Figure 5-3 and which corresponds to $N^*_{\frac{1}{2}}(1700)$. However, there is no circular loop just above the $\eta N$ threshold which is also present in that figure and corresponds to $N^*_{\frac{1}{2}}(1570)$.

We conclude this chapter on the behavior of S waves by noting that this has always been a notoriously difficult problem. The main reason for this is that short range forces are expected to play an important role in the study of S waves. Not much is known about these forces and thus there is no general way of including them. We recall this was precisely the reason due to which Donnachie et al. did not consider the S wave problem in their calculations.

# VI. P WAVE RESULTS

## A. Experimental Situation

Analyses of the experimental P wave amplitudes show the existence of the well-known baryon octet of spin parity $\frac{1}{2}+$ consisting of N(939), $\Lambda$(1115), $\Sigma$(1193), and $\Xi$(1318). In addition there seems to be some experimental evidence for the existence of another $\frac{1}{2}+$ resonance at an energy of about 1400 MeV. This is the so-called $N^*_{\frac{1}{2}}(1400)$. This resonance has not yet been seen in total cross section measurements or bubble chamber pictures. However, the phase shift analysis of Roper (1965) seems to indicate that the real part of the $P_{11}$ phase shift starts out at $180^\circ$. It then decreases at low energy and reaches a minimum of about $178^\circ$ at a center of mass energy of about 1160 MeV. It then increases and becomes $180^\circ$ at about 1225 MeV and $270^\circ$ at about 1400 MeV.

At present there are no likely SU(3) partners for this resonance. From SU(3) arguments (considering only the lowest irreducible representations) $N^*_{\frac{1}{2}}(1400)$ could be part of an octet (8) or an adjoint ten dimensional irreducible representation of SU(3) $(\overline{10})$. If we assume the validity of the quark model, then we would expect this resonance to be a bound state of three quarks (with L = 0). Thus it must be a member of an octet, decuplet, or singlet. Since we know that its isospin and hypercharge are $I = \frac{1}{2}$ and $Y = 1$ respectively, it then follows that the quark model implies that it must be a member of an octet. However, Brehm and Kane have recently suggested (based on dynamical calculations which they performed) that the $N^*_{\frac{1}{2}}(1400)$ might

be a member of a $\overline{10}$ and not an 8. If this is true, it would definitely invalidate all of the conclusions based on the quark model.

P wave analyses also show the existence of an SU(3) decuplet of spin parity $3/2^+$ resonances consisting of $N^*_{3/2}(1236)$, $Y^*_1(1385)$, $\Xi^*(1529)$, and $\Omega^-(1675)$. We should recall that after SU(3) became prominent, it was the discovery of the $\Omega^-(1675)$ at an energy in accordance with the mass formula of Gellmann (1962) and Okubo (1962) which clarified the validity of SU(3) as a dynamical group for strong interaction symmetries.

B. Results of Other Calculations

No discussion of the P waves would be complete without mentioning the Chew-Low model (Chew and Low, 1956) and the bootstrap hypothesis. This hypothesis assumes that all particles are composite systems bound by forces arising from the exchange of the particles themselves. This idea was first suggested by Chew and Low from their consideration of a reciprocal self-sustaining mechanism for the N and N* and was later generalized. Their calculation made use of unitarity as the basis for the dynamics. The static approximation was employed. This required a cutoff to avoid divergence difficulties. Improved calculations of the N and N* bootstrap have been made by Frautschi and Walecka (1960), Abers and Zemach (1963), and Ball and Wong (1964). These calculations were based on a many pole approximation in the N/D technique. The main result of these calculations was that the N and N* reciprocal bootstrap hypothesis is qualitatively successful.

However, the bootstrap hypothesis is very stringent. It cannot be formulated independently of dynamical equations whose validity must be assumed. Also it is not clear that a different set of dynamical equations would yield the same solutions. A weaker version of this hypothesis is the traditional one in which the effects of certain selected graphs are examined in a dynamical model. Calculations based on this version make use of input masses and coupling constants taken from experiment rather than determining them by identification with the output masses and coupling constants. Our calculations are based on this view point.

We next review the P wave results of some other calculations which are based on this weaker version. The calculations of Coulter and Shaw yielded results which agree reasonably well with the experimental low energy phase shifts except for the $P_{11}$ partial wave amplitudes. To fit this $P_{11}$ phase shift they needed to add a CDD pole corresponding to the nucleon state to the solutions of the Frye-Warnock equations. The N* appeared in their model with a width somewhat larger than the experimental value even after including inelastic effects. These effects reduced the N* width from 235 MeV to 195 MeV. This is to be compared with the experimental width of 120 MeV.

The results of the calculations of D.H.L. and D.H. generally agreed with experiment. However, SU(3) was not incorporated in their calculations and thus they only considered the case of pion nucleon scattering. Analysis of their P wave results showed the existence of

the N* resonance at an energy of roughly 1370 MeV. This is to be compared with the experimental energy of 1236 MeV.

Next we consider the results of Martin and Wali and Brehm and Kane . In their calculations SU(3) symmetry was taken into account in contrast to the calculations of Coulter and Shaw and Donnachie et al., which did not incorporate SU(3) symmetry. In M.W.1 the authors concluded that within the framework of Bjorken's determinantal approximation to the broken SU(3) multichannel N/D equations and considering only the baryon exchange force, it was possible to account for the SU(3) decuplet of 3/2+ resonances. Their results are briefly summarized in column 4 of table 6-1. In M.W. 2 they considered other single particle exchange contributions to the driving force , a cutoff was introduced to avoid divergences, and exact SU(3) symmetry was assumed. That is, average masses were used for both the exchanged and the incoming or outgoing particles. Therefore, they could not speak meaningfully of resonance positions and widths in their model. Their results indicated the existence of a $P_{\frac{1}{2}}$ baryon octet and a $P_{3/2}$ decuplet. Thus their model did not account for any higher $P_{\frac{1}{2}}$ resonances.

Brehm and Kane considered the problem of pseudoscalar meson baryon scattering in a perfect SU(3) symmetry model. They solved the multichannel N/D equations making use of Pagel's method. For the input potential they considered the contribution due to the elastic pseudoscalar meson baryon channels and the inelastic scalar meson baryon channels. The elastic channel forces were assumed to arise from the baryon and decuplet exchanges. The inelastic channel forces

Table 6-1. Summary of results for the 3/2+ decuplet. Particle masses and widths are given in MeV. The mass of particle i is denoted by $M_i$. Branching ratios for the decays $Y^* \rightarrow \Lambda\pi$ and $Y^* \rightarrow \Sigma\pi$ are denoted by $\Gamma(\Lambda\pi)$ and $\Gamma(\Sigma\pi)$ respectively. The values of the cutoff (in BeV) used in those calculations which made use of it are given (in parenthesis) in the first row. The energy dependent baryon exchange process (for a coupling constant of $\frac{g^2_{\pi NN}}{4\pi} = 38$) is denoted by $B(\sqrt{s})$. Vector exchange, energy independent baryon exchange, and decuplet exchange are denoted by V, B, and B* respectively. The terms B$\ell$&S and G.C.F. are used as abbreviations for the Blackenbecler-Sugar equation with a cutoff and the Blackenbecler-Sugar equation with a Gaussian cutoff matrix function respectively.

| | | Exp | m.w. | B($\sqrt{s}$) | B(8.7) | B(9.3) | B(10.0) | Bl. & S. (3.2) | Bl. & S. GCF(1.63) | VBB* (1.88) | VBB* (1.90) | VBB* (2.00) |
|---|---|---|---|---|---|---|---|---|---|---|---|---|
| $N^*$ | MASS | 1236 | 1388 | 1236 | 1238 | 1180 | 1125 | 1236 | 1238 | 1231 | 1197 | 1153 |
| | WIDTH | 120 | 146 | 176 | 167 | 69 | 23 | 170 | 208 | 260 | 199 | 69 |
| $Y^*$ | MASS | 1385 | 1605 | 1444 | 1492 | 1440 | 1385 | 1464 | 1425 | 1400 | 1390 | 1305 |
| | WIDTH | 35 | NOT GIVEN | 83 | 137 | 81 | 48 | 111 | 83 | 95 | 92 | 14 |
| | $\Gamma(\Lambda\pi)$ | 91% | 94% | 99% | 99% | 99% | 99% | 99% | 94% | 99% | 99% | 100% |
| | $\Gamma(\Sigma\pi)$ | 9% | 6% | 1% | 1% | 1% | 1% | 1% | 6% | 1% | 1% | 0% |
| $\Xi^*$ | MASS | 1529 | 1749 | 1629 | 1720 | 1678 | 1624 | 1674 | 1620 | MISSING | | 1680 |
| | WIDTH | 7.3 | 11.5 | 30 | 129 | 76 | 26 | 90 | 35 | | | 10 |
| $\Omega^-$ | MASS | 1675 | 1872 | 1801 | MISSING | 2130 | 1924 | 1859 | 1714 | (MISSING) REQUIRES A CUT OFF OF 2.10 Bev TO JUST APPEAR AT A RESONANCE ENERGY OF 1897 Mev | | |
| | BOUND STATE? | YES | NO | YES | | NO | NO | NO | YES | | | |
| | RESONANCE? | NO | YES | NO | | EIGENPHASE GOES THROUGH 90° SLOWLY | YES | YES | NO | | | |
| $M_{N^*} - M_{Y^*}$ | | 149 | 217 | 208 | 254 | 260 | 260 | 228 | 187 | 169 | 193 | 152 |
| $M_{Y^*} - M_{\Xi^*}$ | | 144 | 144 | 185 | 228 | 238 | 238 | 210 | 177 | — | — | 375 |
| $M_{\Xi^*} - M_{\Omega^-}$ | | 146 | 123 | 172 | — | 452 | 300 | 185 | 112 | — | — | — |

were assumed to arise from pseudoscalar meson exchange. The conclusion was that decuplet exchange alone was sufficient to produce a resonant $\overline{10}$ when it gives a bound nucleon.octet. Therefore, the $N^*_{\frac{1}{2}}(1400)$ appeared in their model as a member of a $\overline{10}$ in contrast to quark model predictions of its inclusion in an octet of resonances. Based on their idea we have analyzed the predictions of our model when we consider the $\overline{10}$ representation.

C. The 3/2+ Decuplet

1. Energy Dependent Baryon Exchange Contribution to the Driving Force

We first consider a calculation similar in principle to the one discussed in M.W, 1. That is, we start by assuming the existence of baryons and mesons as members of SU(3) octets. However, actual physical masses are employed. We then consider the contribution to the force from baryon exchange in pseudoscalar meson baryon scattering and ask whether it is possible to produce the 3/2+ decuplet as a dynamical consequence. We differ from M.W.1 in that we use the multichannel relativistic Schrödinger equation as our dynamical equation. Of course calculations of this type cannot be expected to predict exact locations and widths of resonances, since they are known to be sensitive to many dynamical effects which are not fully understood.

Study of the space part of the baryon exchange process shows that if we make use of this process as an input potential in the multichannel relativistic Schrödinger equation, a non-Fredholm system of coupled integral equations for the scattering amplitude is obtained.

Upon further analysis we can see this system of linear integral equations can be converted into a Fredholm system by making the replacement $a_o + b_o + c_o + d_o \rightarrow 2\sqrt{s}$ in equations D.3 and D.4 in Appendix D. This is the same replacement which we made when we considered the contribution to S wave scattering from the $\gamma_\mu$ part of the vector exchange process. It is possible in principle since all that is assumed to be known is the on shell potential.

i) I = 3/2, Y = 1 state.

In this part of the calculation we assume the F/D ratio is given and equal to 0.33. The coupling constant $\frac{g^2_{\pi N}}{4\pi}$ is taken as a variable parameter, to be adjusted to produce the N* at the correct experimental position. We then find that we must use a value of $\frac{g^2_{\pi N}}{4\pi}$ 38.0 in order to obtain the N* at the correct energy. Plots of the eigenphase and cross section for this case are given in Figures 6-1 and 6-2. The experimental N* phase shift as taken from Behrends et al. (1967) is shown in Figure 6-3. Study of Figure 6-1 shows that the N* width is then about 176 MeV in comparison with the experimental width of about 120 MeV. Our results for this case and the other isospin states are summarized in column 5 of table 6-1.

ii) Other Isospin States.

If we consider the other isospin states, we note that Y*, $\Xi^*$, and $\Omega^-$ appear at energies in agreement with the experimental values. They appear at energies of 1444, 1629, and 1801 MeV in our calculations and at energies of 1385, 1529, and 1675 MeV in experiments.

Fig. 6-1. Eigenphase for the I = 3/2, Y = +1, $P_{3/2}$ state for the coupling constant $\frac{g^2_{\pi NN}}{4\pi} = 38$. Only the contribution from the energy dependent baryon exchange process to the input potential is considered.

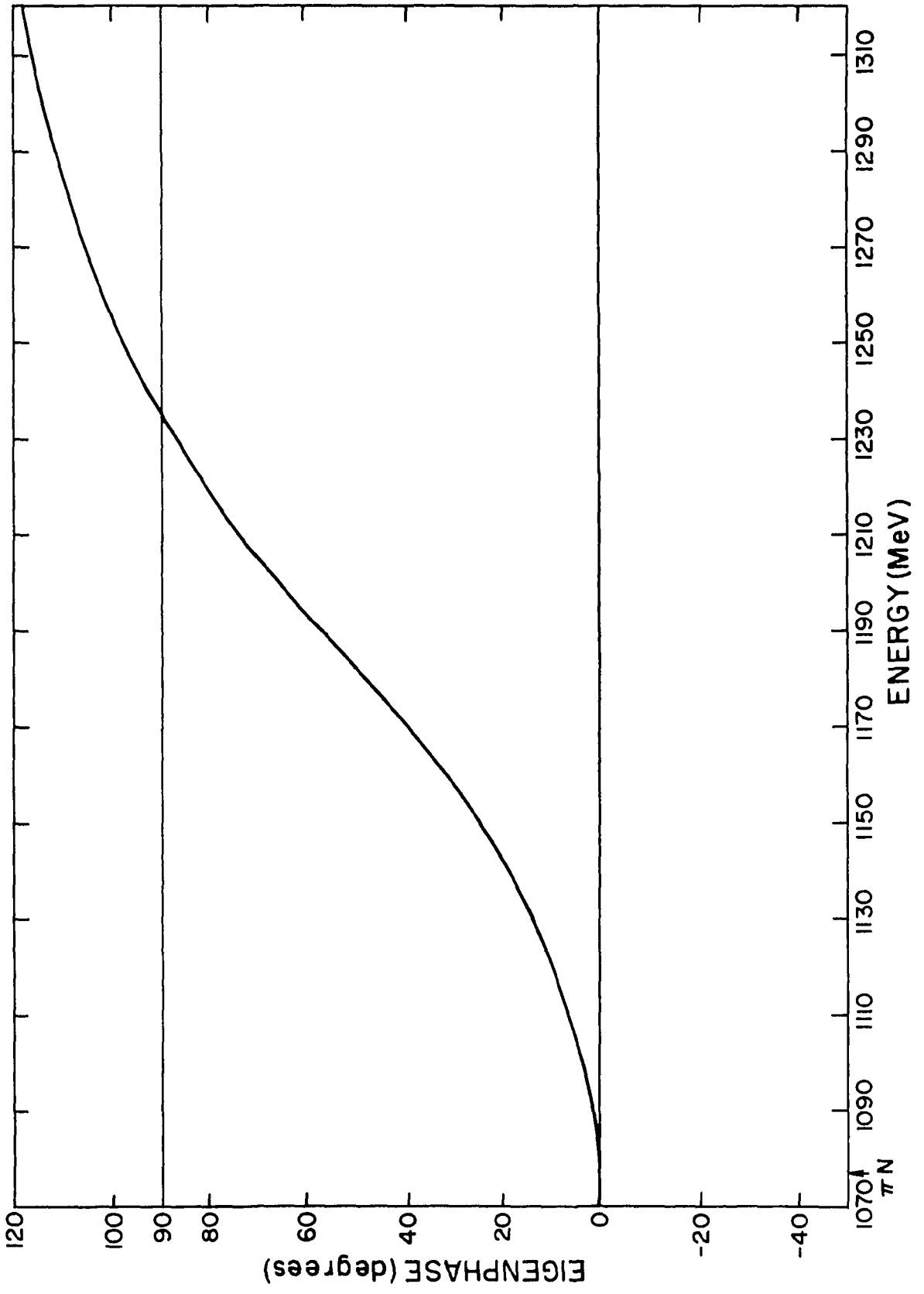
EIGENPHASE (degrees)
120
100
90
80
60
40
20
0
-20
-40
1070
1090
1110
1130
1150
1170
1190
1210
1230
1250
1270
1290
1310
ENERGY (MeV)
πN

Fig. 6-2. The cross section for $\pi N$ scattering in the I = 3/2, Y = +1, $P_{3/2}$ state for the coupling constant $\frac{g^2_{\pi NN}}{4\pi} = 38$. Only the contribution from the energy dependent baryon exchange process to the input potential is considered.

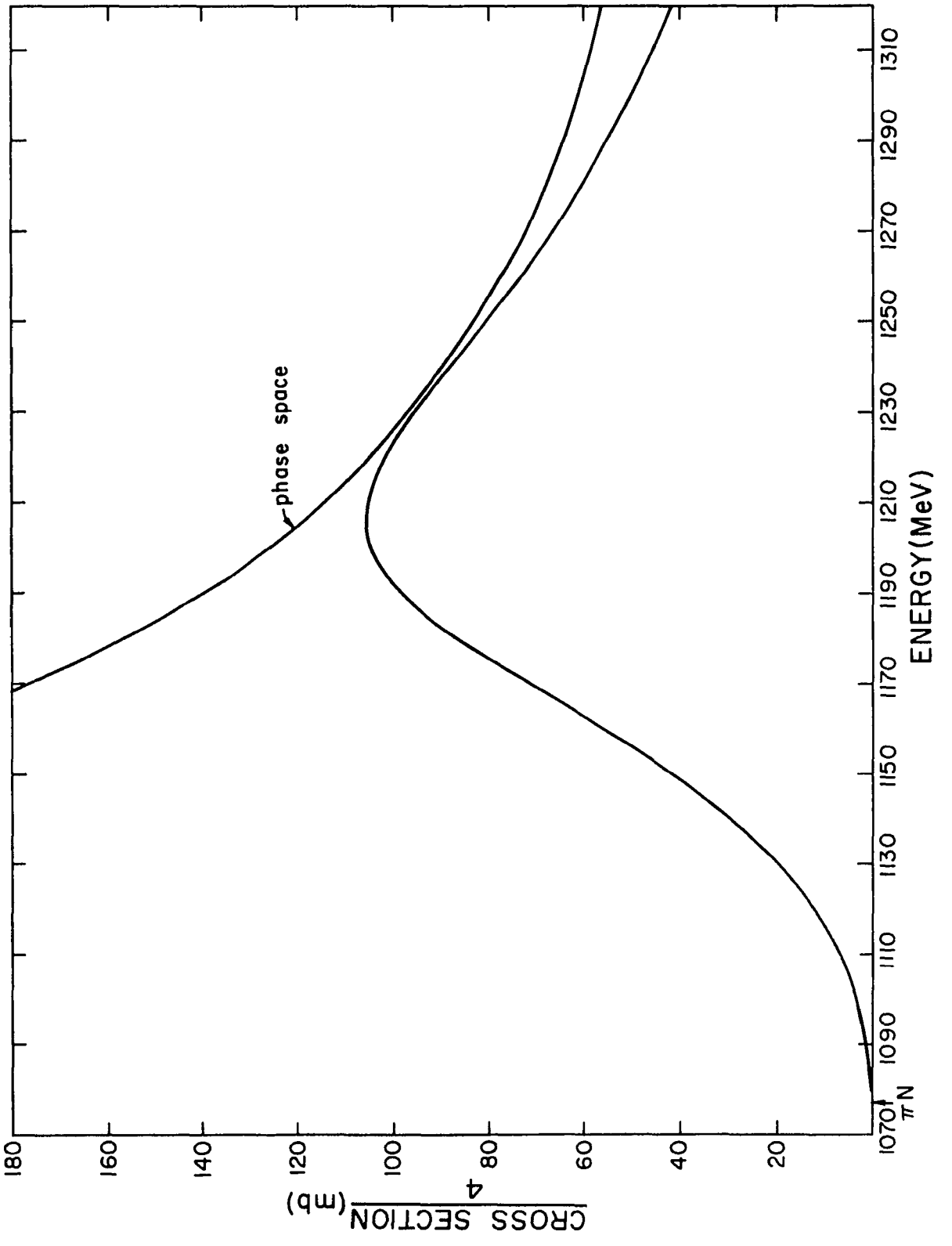
CROSS SECTION / 4 (mb)
180
160
140
120
100
80
60
40
20
phase space
1070
1090
1110
1130
1150
1170
1190
1210
1230
1250
1270
1290
1310
ENERGY(MeV)
πN

Fig. 6-3. Experimental phase shift for the I = 3/2, Y = +1, $P_{3/2}$ state, as given by Behrends et al.

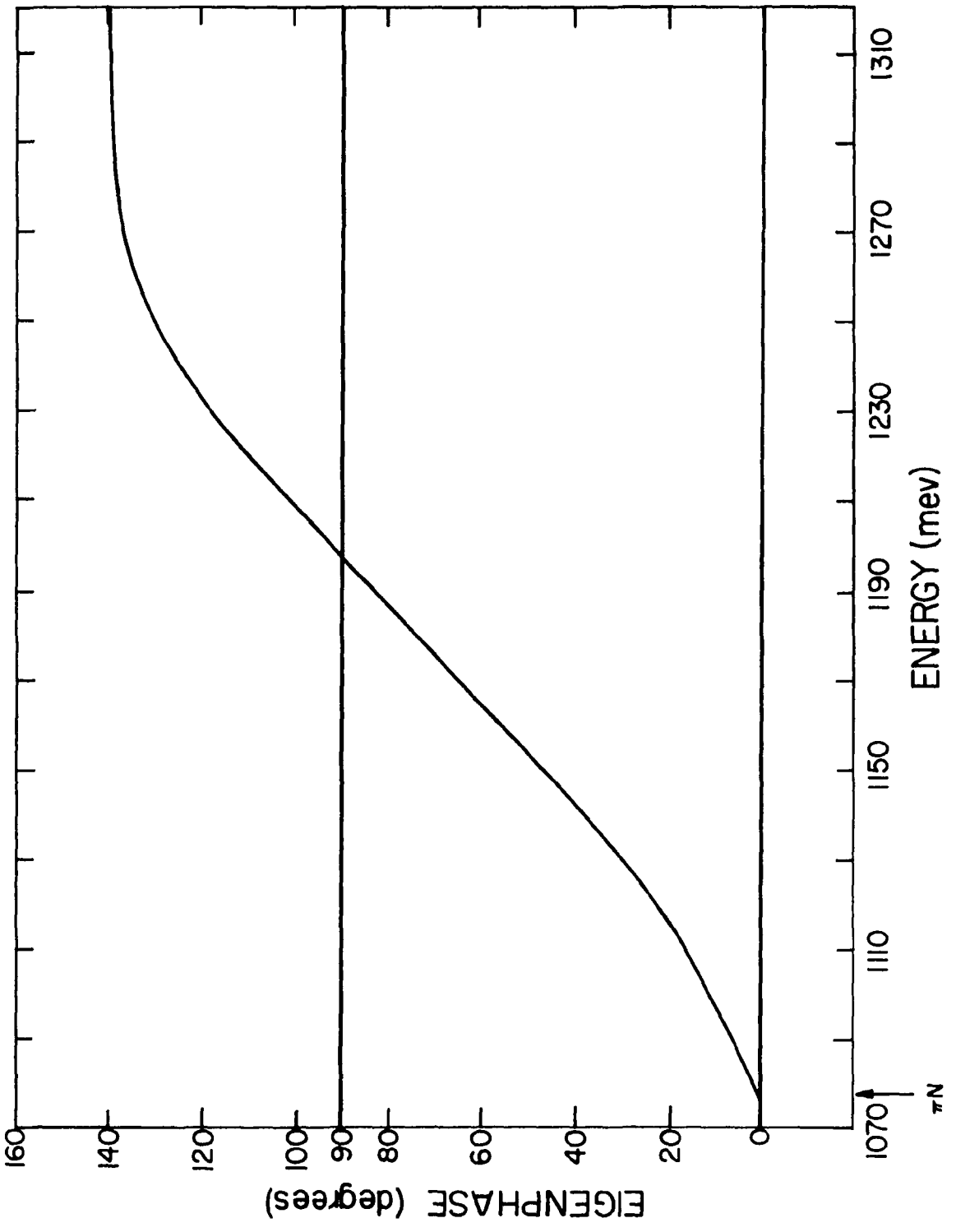
EIGENPHASE (degrees)
160
140
120
100
90
80
60
40
20
0
1070
1110
1150
1190
1230
1270
1310
ENERGY (mev)
$\pi^+ N$

The $\Omega^-$ appears in this model as a bound state. This in in agreement with experiment, since the $\bar{K}\Xi$ threshold (1814 MeV) is above the $\Omega^-$ mass (1675 MeV). This contrasts with the calculations given in M.W. 1, in which the $\Omega^-$ appeared as a resonance in the I = 0, Y = -2 state with an energy of 1872 MeV. In Figure 6-4 we show the behavior of the determinant whose zero must be computed in order to find the bound state position of the $\Omega$ as a function of energy. This is an example of a typical bound state calculation. In addition the widths of the Y* and the $\Xi$* are predicted to be about 83 and 30 MeV respectively. The experimental widths are about 35 and 8 MeV respectively. Even though these widths are larger than the experimentally observed values, they arenot very sensitive to the F/D ratio. In this way our results differ from those given in M.W. 1, in which a small change in the F/D ratio yielded large changes in the resonance positions and widths. Also it is encouraging that the width ordering as obtained from this model is in agreement with experimental observations.

iii) Equal Spacing Rule.

Since members of an SU(3) decuplet obey the relation I = Y/2 + 1, the Gellmann Okubo mass formula predicts an equal spacing between consecutive members of the decuplet

$$M_{Y^*} - M_{N^*} = M_{\Xi^*} - M_{Y^*} = M_{\Omega^-} - M_{\Xi^*}. \qquad (6.1)$$

This is in agreement with experiment. The validity of the Gellmann Okubo mass formula is remarkable since it relates space time properties

Fig. 6-4. Determinant whose zero must be computed to find the bound state position of $\Omega^-$ for the coupling constant $\frac{g^2_{\pi NN}}{4\pi} = 38$. Only the contribution from the energy dependent baryon exchange process to the input potential is considered.

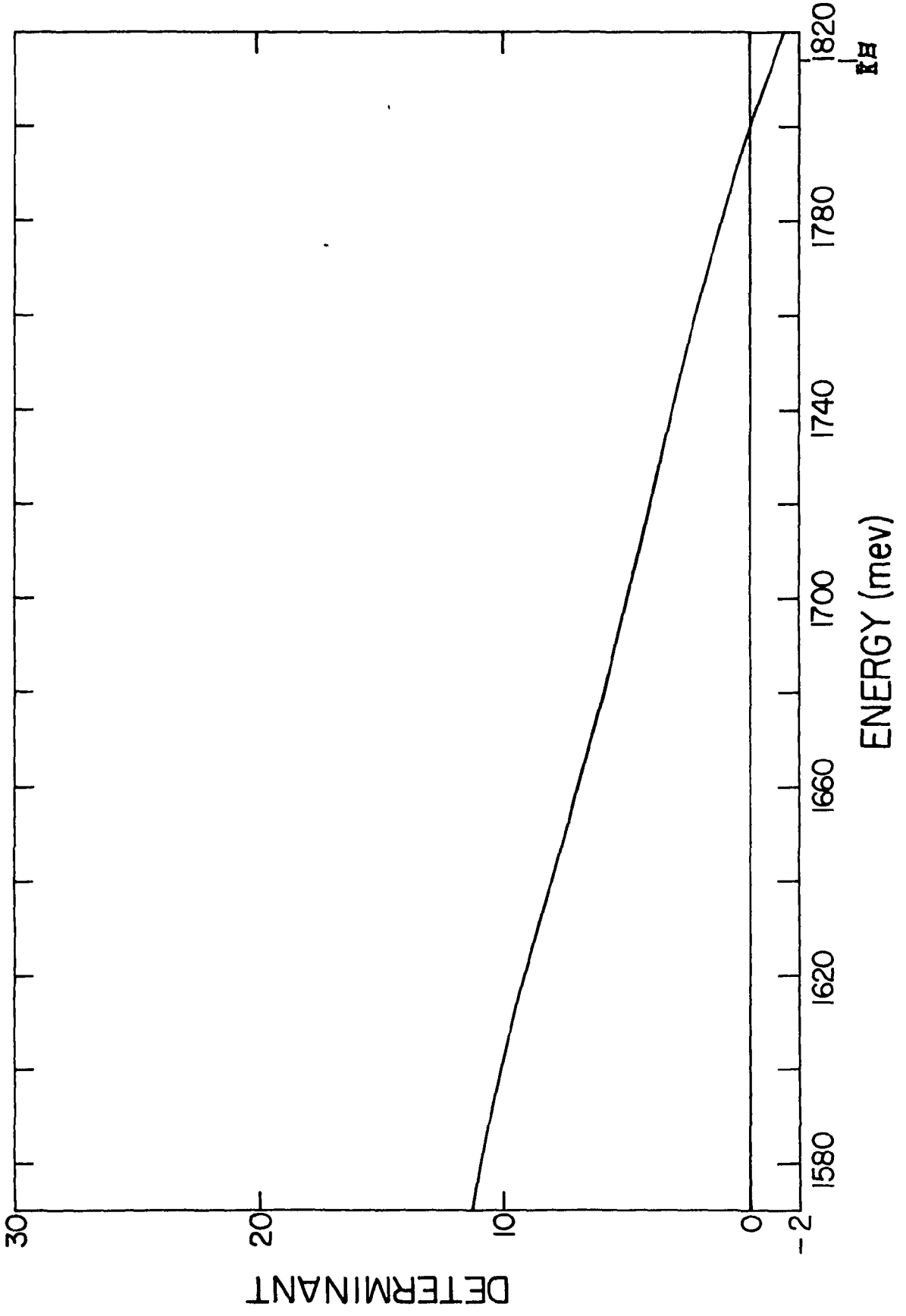
DETERMINANT
30
20
10
0
-2
1580
1620
1660
1700
1740
1780
1820
ENERGY (mev)

of a physical system (mass) to its internal symmetry properties, (isospin and hypercharge). Its validity is even more surprising when the assumptions used in deriving this relation are considered.

The validity of a Lagrangian field theory is assumed. We then write

$$H = H_o + H_{int}, \tag{6.2}$$

where $H_o$ is the free Hamiltonian and $H_{int}$ is the interaction which is responsible for the symmetry breaking. $H_{int}$ can be expanded

$$H_{int} = \sum_{(i)} H^{(i)}_{int}\ (0,0,0), \tag{6.3}$$

where $H^{(i)}_{int(000)}$ denotes the $I = I_z = Y = 0$ component of irreducible SU(3) operators $H^{(i)}_{int(II_zY)}$ which transform according to the $i^{th}$ irreducible representation of SU(3). (Only this component must be considered due to isospin and hypercharge conservation). Mass corrections are then obtained as power series in the interaction Hamiltonian $H_{int}$. The first assumption used in deriving the Gellmann Okubo mass formula is the validity of the first order perturbation theory so that the interaction Hamiltonian $H_{int}$ (also known as the mass operator responsible for the SU(3) breaking) transforms in the same way as the mass differences $\delta m$ due to the SU(3) breaking. We can then write

$$\delta m = \sum_i \delta m^{(i)}_{(0,0,0)}. \tag{6.4}$$

The second main assumption is that only one term must be included in the above sum. This term is $\delta m^{(8)}_{(000)}$. From these assumptions the Gellmann Okubo mass formula then follows in the usual way.

It is worthwhile to ask to what extent the equal mass spacing rule is a consequence of dynamical calculations. The results given in M.W. 1 were

$$\begin{aligned} M_{Y^*} - M_{N^*} &= 217 \text{ MeV}, \\ M_{\Xi^*} - M_{Y^*} &= 144 \text{ MeV, and} \\ M_{\Omega^-} - M_{\Xi^*} &= 123 \text{ MeV}. \end{aligned} \tag{6.5}$$

This is to be compared with the experimental values

$$\begin{aligned} M_{Y^*} - M_{N^*} &= 149 \text{ MeV}, \\ M_{\Xi^*} - M_{Y^*} &= 144 \text{ MeV, and} \\ M_{\Omega^-} - M_{\Xi^*} &= 146 \text{ MeV}. \end{aligned} \tag{6.6}$$

The baryon exchange process computed using the replacement $a_o + b_o + c_o + d_o \rightarrow 2\sqrt{s}$ yields

$$\begin{aligned} M_{Y^*} - M_{N^*} &= 208 \text{ MeV}, \\ M_{\Xi^*} - M_{Y^*} &= 185 \text{ MeV, and} \\ M_{\Omega^-} - M_{\Xi^*} &= 172 \text{ MeV}. \end{aligned} \tag{6.7}$$

It is thus apparent that the discrepancy from the equal mass spacing rule is slightly smaller in this model than in the model given in M.W. 1. However, it is surprising that both models seem to predict

masses in rough agreement with the equal spacing rule. One of the assumptions used in the derivation of the Gellmann Okubo mass formula is the validity of first order perturbation theory. However, in models of the kind discussed by M. W. and in this thesis, first order perturbation theory should clearly not be valid since terms corresponding to higher order corrections are also taken into account. This is precisely one of the arguments which can be given against models of this kind, since the Gellmann Okubo mass formula is extremely well satisfied experimentally. In later sections of this thesis we shall observe that some of our calculations satisfy the Gellmann Okubo mass formula better than others. However, we observe no general rule as to when the equal spacing rule is satisfied or when there is a large disagreement from it.

iv) Y* Branching Ratios.

The decay of the Y* allowed by energy, $I_z$, $I^2$, and Y conservation are

$Y^* \rightarrow \Lambda\pi$

and $Y^* \rightarrow \Sigma\pi$.

On the basis of pure unitary symmetry we would expect

$$\Gamma(\Lambda\pi) = \frac{\text{Rate}(Y^* \rightarrow \Lambda\pi)}{\text{Rate}(Y^* \rightarrow \Sigma\pi) + \text{Rate}(Y^* \rightarrow \Lambda\pi)} = \frac{\left(\frac{1}{\sqrt{2}}\right)^2}{\left(\frac{1}{\sqrt{3}}\right)^2 + \left(\frac{1}{\sqrt{2}}\right)^2} = \frac{3}{5} = 60\%, \tag{6.8}$$

where $\Gamma(\Lambda\pi)$ denotes the branching ratio for the decay of Y* into the $\Lambda\pi$ channel, and where $\frac{1}{\sqrt{2}}$ and $\frac{1}{\sqrt{3}}$ are the corresponding isoscalar factors for the two processes. The above result is in disagreement with the experimental value of about 91%.

Usually to obtain agreement with experiment, kinematical corrections are then supplied. Thus we write

$$\Gamma(\Lambda\pi) = \frac{3}{5} \times (\text{phase factor}) = \frac{3}{5} \frac{p_{\Lambda}^{3}}{p_{\Sigma}^{3}} \simeq 90\%. \qquad (6.9)$$

In the above, $P_{\Lambda}$ and $P_{\Sigma}$ are defined as the momenta in the center of mass frame of the $\Lambda\pi$ and $\Sigma\pi$ channels respectively. They appear cubed since the threshold behavior for P waves is $p^{2\ell+1}$ where $\ell=1$. Very good agreement with experiment is now obtained.

However, it is certainly worthwhile to ask the extent to which branching ratios are a consequence of dynamical calculations. In the case of the Y* we find $\Gamma(\Lambda\pi) = 99\%$. This is compared to the experimental result of about 91% and the result given in M.W. 1 (94%). Thus we note that Y* as obtained in these dynamical models decays mainly into the $\Lambda\pi$ channel. We observe that the branching ratio for the decay $Y^* \rightarrow \Lambda\pi (Y^* \rightarrow \Sigma\pi)$ is larger (smaller) in these dynamical models than the branching ratio obtained using SU(3) and phase space arguments. This discrepancy can be understood since in these models both the $\Lambda\pi$ and $\Sigma\pi$ channels are no longer members of a pure SU(3) decuplet, as is assumed to obtain expressions (6.8) and (6.9). In fact the $\Lambda\pi$ and $\Sigma\pi$ channels in these dynamical models are mixtures of many irreducible

SU(3) representations, of which the decuplet representation is just one of the many representations which contribute.

2. Energy Independent Baryon Exchange Contribution to the Driving Force.

a. Solving the Multichannel Relativistic Schrödinger Equation with a Cutoff Parameter.

In an earlier section of this chapter we discussed the 3/2+ decuplet by considering the baryon exchange force as the input potential and making the replacement $a_o + b_o + c_o + d_o \rightarrow 2\sqrt{s}$. We recall this was done to obtain a Fredholm system of coupled linear integral equations.

In this part of the calculation we choose a different approach. Instead of making this replacement, we will make the system of integral equations Fredholm by introducing a cutoff parameter. The coupling constant $\frac{g^2_{\pi N}}{4\pi}$ and the F/D ratio are held fixed at their experimental values (14.6 and 0.33 respectively).

i) I = 3/2, Y = 1 state.

We assume the cutoff to be an arbitrary parameter chosen to fix the N* at the correct experimental energy. This requires a cutoff of 8.7 BeV. The corresponding eigenphase for this state is shown in Figure 6-5. Analysis of that figure shows that for a cutoff of 8.7 BeV, the N* appears at the correct experimental position with a width of about 167 MeV. Figure 6-5 also shows eigenphases for cutoff values of 9.3 and 10 BeV. For a cutoff value of 9.3 BeV the N* appears at an energy of 1180 MeV with a width of about 69 MeV. For a

Fig. 6-5. Eigenphases for the I = 3/2, Y = +1, $P_{3/2}$ state for the coupling constant $\frac{g^2_{\pi NN}}{4\pi} = 14.6$. Only the contribution from the energy independent baryon exchange process to the input potential is considered. The solid curve gives the eigenphase for a cutoff of 8.7 BeV. The dashed curve gives the eigenphase for a cutoff of 9.3 BeV. The dot-dash curve gives the eigenphase for a cutoff of 10 BeV.

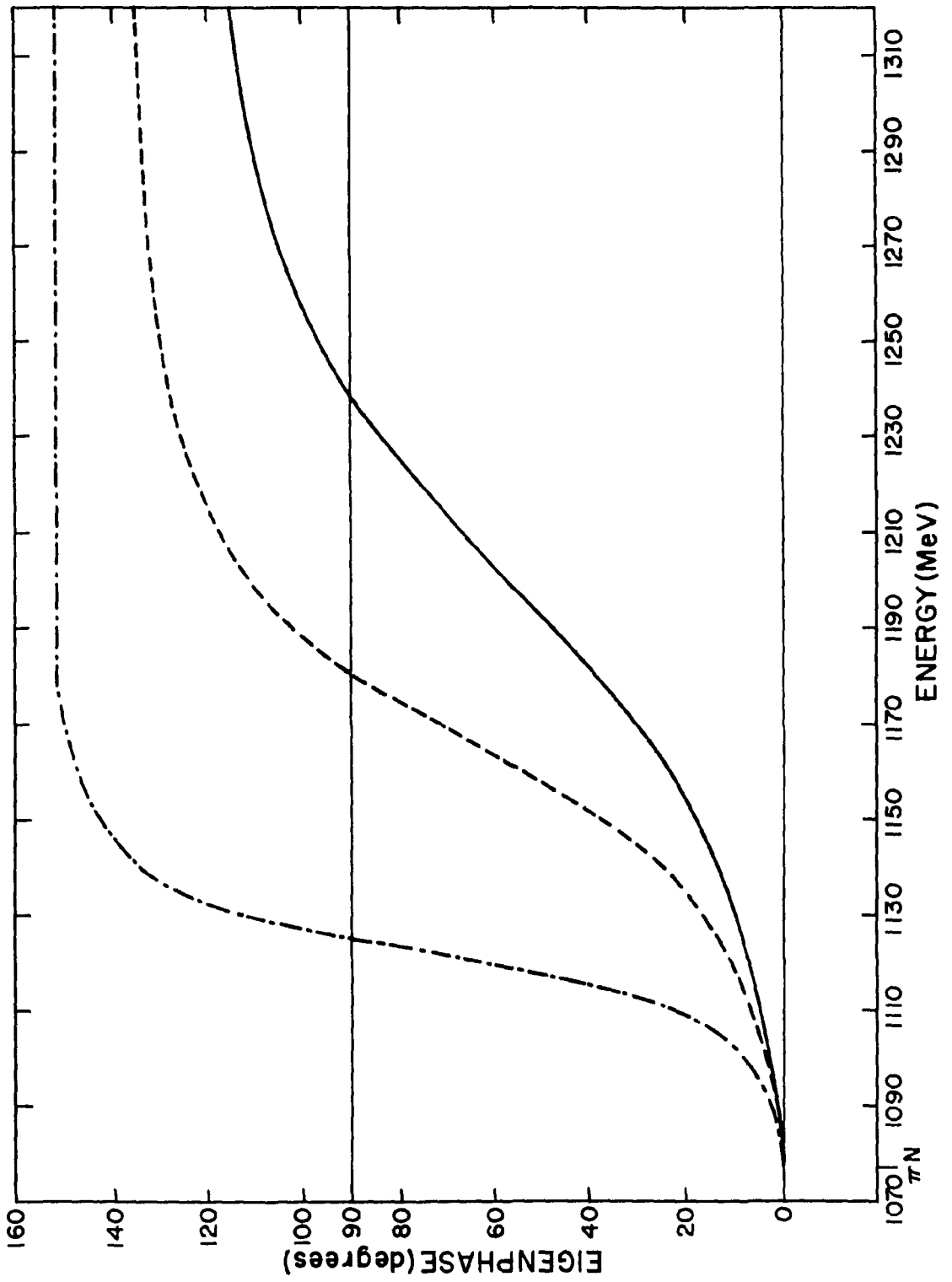
ENERGY (MeV)
1070
1090
1110
1130
1150
1170
1190
1210
1230
1250
1270
1290
1310
πN
EIGENPHASE (degrees)
0
20
40
60
80
90
100
120
140
160

cutoff value of 10 BeV the N* appears at an energy of 1125 MeV with a width of about 23 MeV. In columns 6, 7, and 8 of table 5-1 we summarize our results for cutoffs of 8.7, 9.3 and 10 BeV, both for the N* and the other isospin states.

ii) Other Isospin States.

We first consider the other isospin states obtained by using a cutoff of 8.7 BeV, the one required to produce the N* at its experimental energy. For this value we observe that both the Y* and the $\Xi^*$ appear at energies of 1492 and 1629 respectively. Their respective widths are about 137 and 129 MeV. However, the $\Omega^-$ does not appear with this cutoff parameter. In Figure 6-6 we show the eigenphases for the I = 0, Y = -2 state, both for this value of the cutoff parameter and also for cutoffs of 9.3 and 10 BeV.

In order to investigate the behavior of the $\Omega^-$, we increase the cutoff until the eigenphase corresponding to the I = 0, Y = -2 state crosses $90^\circ$. This requires a cutoff of 9.3 BeV. The eigenphase crosses $90^\circ$ at an energy of 2130 MeV, but does it so slowly that we cannot call this a resonance. With this cutoff parameter the Y* and the $\Xi^*$ appear at energies of 1440 and 1678 MeV respectively. Their respective widths are 81 and 76 MeV. For this value of the cutoff parameter we observe that the width of the N* (69 MeV) becomes smaller than both the widths of the Y* (81 MeV) and the $\Xi^*$ (76 MeV) which contradicts the experiments.

If we further increase the cutoff parameter to 10 BeV, the Y* now appears at its experimental energy (1385 MeV). The $\Xi^*$ and the

Fig. 6-6. Eigenphases for the I = 0, Y = -2, $P_{3/2}$ state for the coupling constant $\frac{g^2_{\pi NN}}{4\pi} = 14.6$. Only the contribution from the energy independent baryon exchange process to the input potential is considered. The solid curve gives the eigenphase for a cutoff of 8.7 BeV. The dashed curve gives the eigenphase for a cutoff of 9.3 BeV. The dot-dash curve gives the eigenphase for a cutoff of 10 BeV.

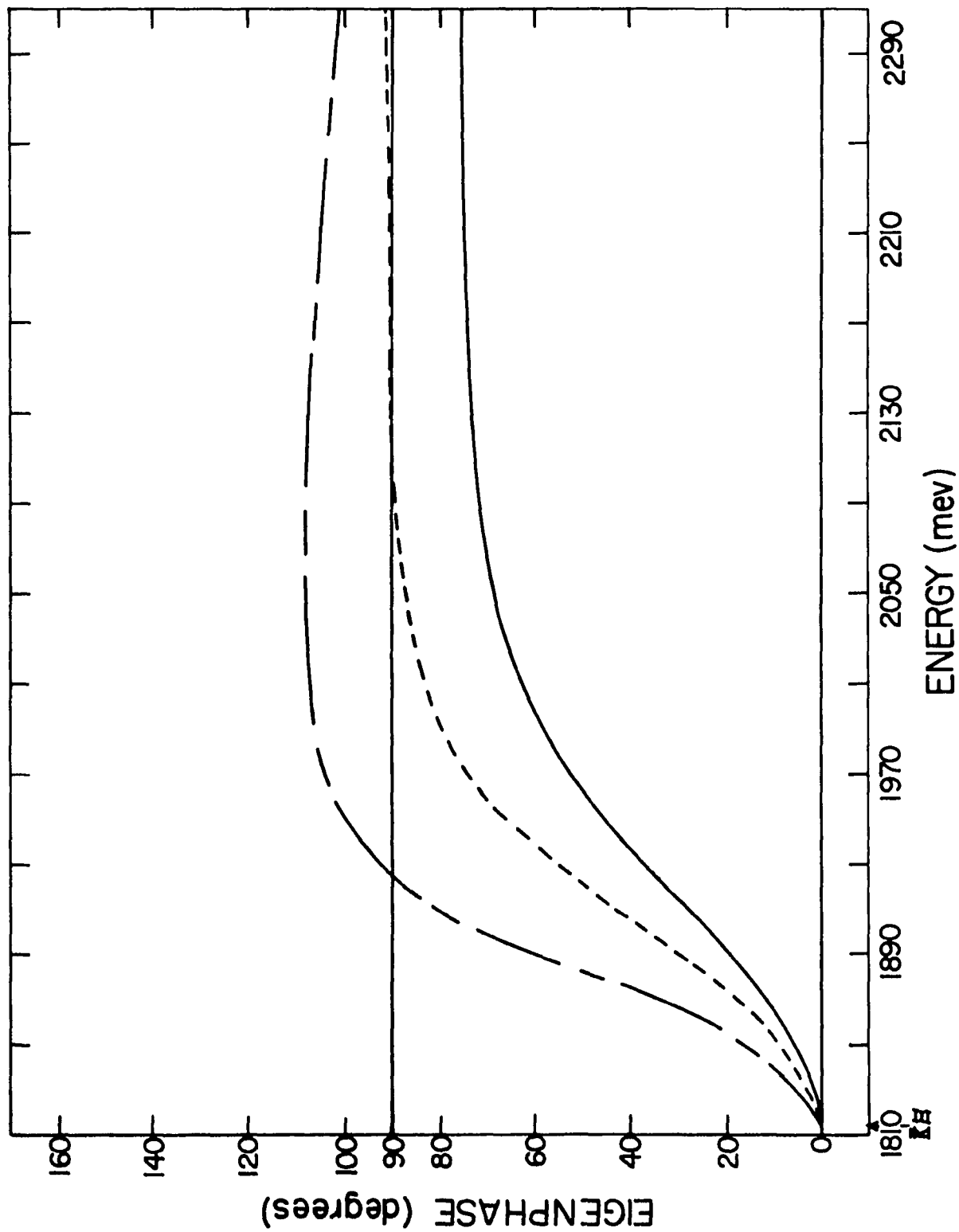
EIGENPHASE (degrees)
160
140
120
100
90
80
60
40
20
0
1810
1890
1970
2050
2130
2210
2290
ENERGY (mev)

$\Omega^-$ now appears at energies of 1624 and 1924 MeV respectively. The widths of the Y* and the ≡* are now 48 and 26 respectively. However, the N* width is still smaller than the width of the other members of the decuplet.

iii) Equal Spacing Rule.

Table 6-1 shows that for a cutoff of 8.7 BeV the mass differences between consecutive numbers of the decuplet which appear with this value of the cutoff agree with the equal spacing rule to about 12%. For a cutoff value of 9.3 BeV the mass differences between the $\Omega^-$ and the ≡* is about 1.7 larger than it should be to satisfy the equal spacing rule. This is not surprising since for this cutoff parameter, the eigenphase for the I = 0, Y = -2 state reaches $90^\circ$ very slowly. Thus we should not identify the reaching of $90^\circ$ with the existence of a resonance.

We observe that for a cutoff of 10 BeV, the equal spacing rule is satisfied more closely than for a cutoff of 9.3 BeV. However there is still a discrepancy from this rule.

The reason for which the equal spacing rule seems to be better satisfied with this cutoff than with a cutoff of 9.3 BeV is probably that the eigenphase for the I = 0, Y = -2 state clearly shows the existance of a resonance corresponding to the $\Omega^-$ for a cutoff of 10 BeV, while such is not the case for a cutoff of 9.3 BeV.

iv) Y* Branching Ratios.

The introduction of a cutoff parameter does not seem to affect the predicted branching ratios for the Y* decay. For cutoffs

of 8.7, 9.3 and 10 BeV, the model predicts the Y* decays mainly into the $\Lambda\pi$ channel (99%) with only a small fraction decaying into the $\Sigma\pi$ channel (1%). This is in rough agreement with the experimental evidence as previously discussed.

b. Solving the Multichannel Relativistic Schrödinger Equation with a Gaussian Cutoff Matrix Function

In this section we discuss a different cutoff procedure and its effect upon the solutions to the relativistic Schrödinger equation for the case discussed in part a. Rather than introducing a straight cutoff parameter, we introduce a Gaussian cutoff matrix function

$F_{ij}(q)$ by

$$F_{ij}(q) = \delta_{ij} e^{-[(E_q+\omega_q-\Delta)_j]^2/\lambda^2} \tag{6.10}$$

where i and j are channel indices, $\Delta_j$ is the threshold for the $j^{th}$ channel, and $\lambda$ is chosen to obtain the N* at the correct experimental energy.

To obtain the N* at the observed experimental energy, we need a value of $\lambda$ = 6.14 BeV. In Figure 6-7 we show the corresponding eigenphase. Analysis of this figure shows that with this choice of the cutoff the N* appears with a width of about 146 MeV and agrees with its experimental value.

We next consider the other isospin states, keeping the cutoff $\lambda$ fixed at 6.14 BeV. We observe that they appear at larger values of the energy and with a larger width than we had obtained by solving the

Fig. 6-7. Eigenphase for the I = 3/2, Y = +1, $P_{3/2}$ state for the coupling constant $\frac{g^2_{\pi NN}}{4\pi} = 14.6$. Only the contribution from the energy independent baryon exchange process to the input potential is considered. The eigenphase is obtained solving the relativistic Schrödinger equation with a Gaussian cutoff matrix function for $\lambda = 6.14$ BeV. (We use the same definition of $\lambda$ as in equation 6.13.)

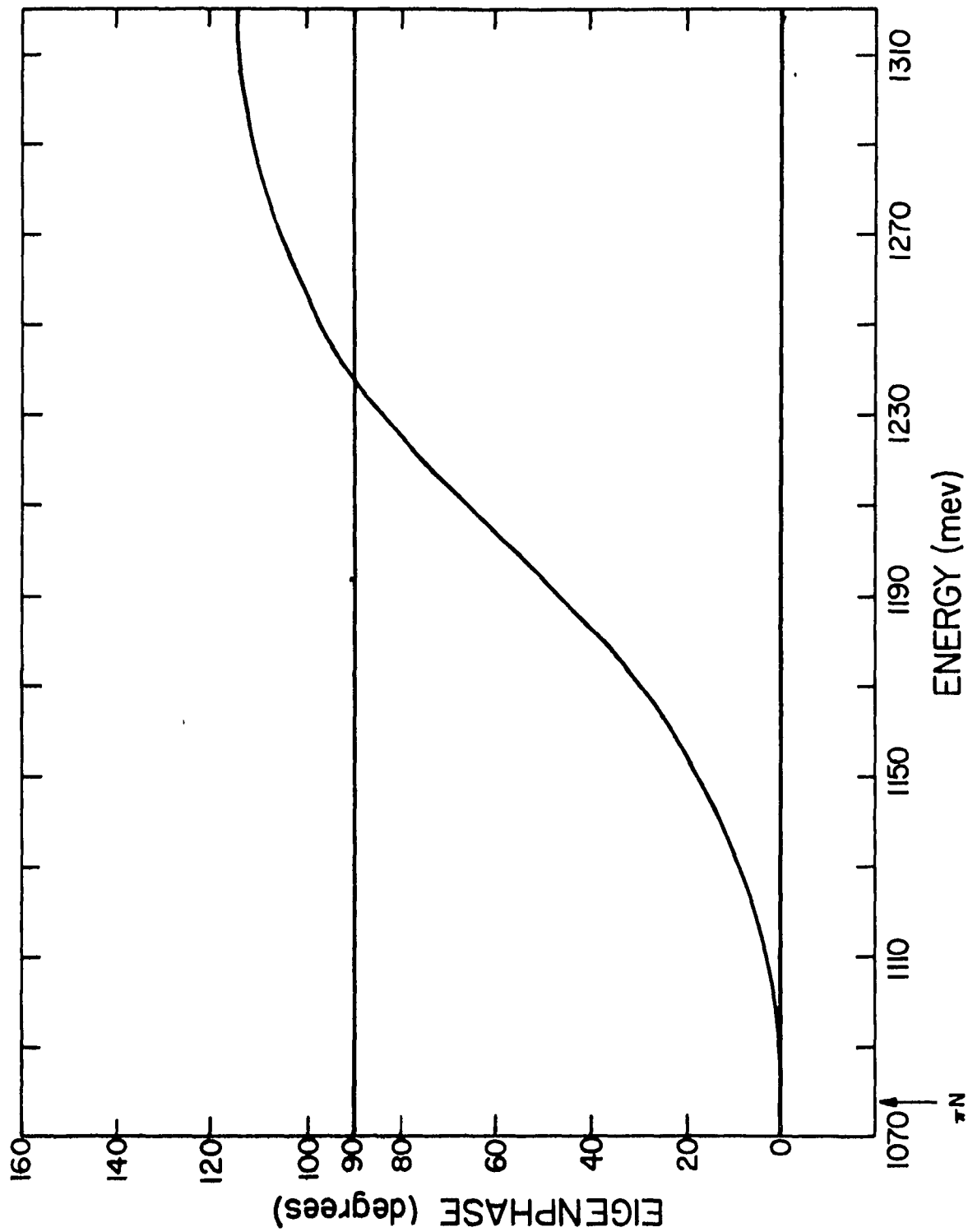
EIGENPHASE (degrees)
160
140
120
100
90
80
60
40
20
0
1070
1110
1150
1190
1230
1270
1310
ENERGY (mev)
π-N

relativistic Schrödinger equation with a straight cutoff parameter. For example the Y* now appears at an energy of 1675 MeV and its width is about 280 MeV. Thus we note that the Y* width so obtained is larger than the N* width. However, its branching ratios into the $\Lambda\pi$ and $\Sigma\pi$ channels are the same as we had obtained by using a straight cutoff.

Thus we see that cutting off the integrals in this fashion yields similar qualitative results. However, the exact numerical results change. We also reiterate that the introduction of a Gaussian cutoff matrix function yields an N* of a width which agrees closely with the experimental width. However, this is not the case for the other isospin states.

c. Solving the Multichannel Blankenbecler-Sugar Equation with a Cutoff Parameter

In this section we solve the Blankenbecler-Sugar equation with a cutoff with the input potential discussed in part a. We introduce a cutoff parameter to convert the coupled system of linear integral equations for the scattering amplitude into a Fredholm system.

i) $I = 3/2$, $Y = 1$ state.

Again we choose the cutoff to produce the N* at the correct experimental energy. The presence of the extra energy denominator $-\frac{1}{\sqrt{s}+E_q+\omega_q}$ in the Blankenbecler-Sugar equation makes the potential more attractive than it would be if it were used as an input potential in the relativistic Schrödinger equation. Thus we expect the cutoff required to produce the N* at the correct experimental position is smaller than the cutoff needed in solving the relativistic Schrödinger equation for the same case. In fact, this is what happens. To produce

the N* at the observed experimental energy we now use a cutoff parameter of 3.2 BeV. The corresponding eigenphase is shown in Figure 6-8. Our results for this state and for the other states are given in column 9 of table 6-1. Study of Figure 6-8 shows that the N* resonance now appears with a width of about 170 MeV. This is about the same width we had obtained when we solved the relativistic Schrödinger equation for this case with a cutoff of 8.7 BeV.

ii) Other Isospin States.

If we consider the other isospin states we note that Y*, ≡*, and $\Omega^-$ now appear at energies of 1464, 1674, and 1859 MeV. The corresponding widths for the Y* and the ≡* states are 111 and 90 MeV respectively. We note that in this case the N* width obtained by solving the Blankenbecler-Sugar equation with a cutoff of 3.2 BeV is about the same as the N* width obtained by solving the relativistic Schrödinger equation with a cutoff of 8.7 BeV. The widths for the other members of the decuplet are somewhat smaller.

We also note that the eigenphase corresponding to the I = 0, Y = -2 state ($\Omega^-$) goes through $90^o$ at an energy of 1859 MeV. Thus the $\Omega^-$ appears in this model as a resonance.. We recall when the relativistic Schrödinger equation is solved for this state with a cutoff of 8.7 BeV, an attractive scattering amplitude is obtained. However, no resonance is observed corresponding to the $\Omega^-$, unless the cutoff parameter is increased. There is no simple reason why this should be the case.

Fig. 6-8. Eigenphase for the I = 3/2, Y = +1, $P_{3/2}$ state for the coupling constant $\frac{g^2_{\pi NN}}{4\pi} = 14.6$. Only the contribution from the energy independent baryon exchange process to the input potential is considered. The eigenphase is obtained solving the Blankenbecler-Sugar equation with a cutoff of 3.2 BeV.

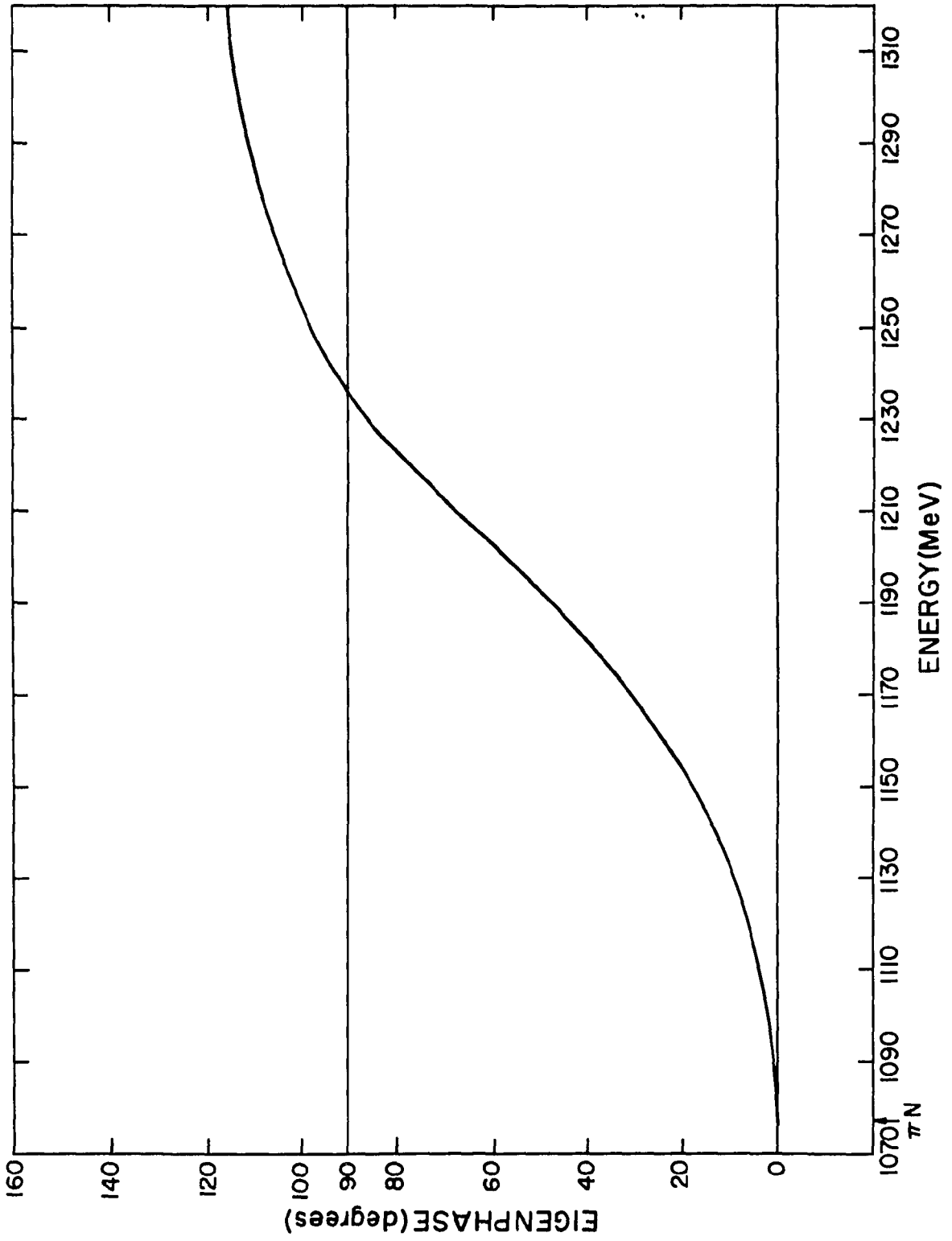
EIGENPHASE (degrees)
160
140
120
100
90
80
60
40
20
0
1070
1090
1110
1130
1150
1170
1190
1210
1230
1250
1270
1290
1310
ENERGY (MeV)
π N

iii) Equal Spacing Rule.

Table 6-1 shows that the equal spacing rule is satisfied in this model to about 12%.

iv) Y* Branching Ratios.

The model predicts Y* decays mainly into the $\Lambda\pi$ channel with a branching ratio of about 99%. Thus only a small fraction of the Y*'s decay into the $\Sigma\pi$ channel (1%). This is the same result as we have obtained in solving the relativistic Schrödinger equation.

d. Solving the Multichannel Blankenbecler-Sugar Equation with a Gaussian Cutoff Matrix Function

We discuss the effects of a Gaussian cutoff matrix function on the solutions to the Blankenbecler-Sugar equation for the case discussed in part c. This function is of the same form as the one introduced in part b. in the discussion of the relativistic Schrödinger equation. That is, we introduce a Gaussian cutoff function

$F_{ij}(q)$ by

$$F_{ij}(q) = e^{-[(E_q+\omega_q-\Delta)_j]^2/\lambda^2}, \qquad (6.11)$$

where the notation is as before.

We choose $\lambda$ to produce the N* at the correct experimental position. This requires $\lambda$ = 1.63 BeV. Our results for this and other states are summarized in column 10 of table 6.1. In Figure 6-9 we

Fig. 6-9. Eigenphase for the $I = 3/2$, $Y = +1$, $P_{3/2}$ state for the coupling constant $\frac{g^2_{\pi NN}}{4\pi} = 14.6$. Only the contribution from the energy independent baryon exchange process to the input potential is considered. The eigenphase is obtained solving the Blankenbecler-Sugar equation with a Gaussian cutoff matrix function for $\lambda = 1.63$ BeV. (We use the same definition of $\lambda$ as in equation 6.13.)

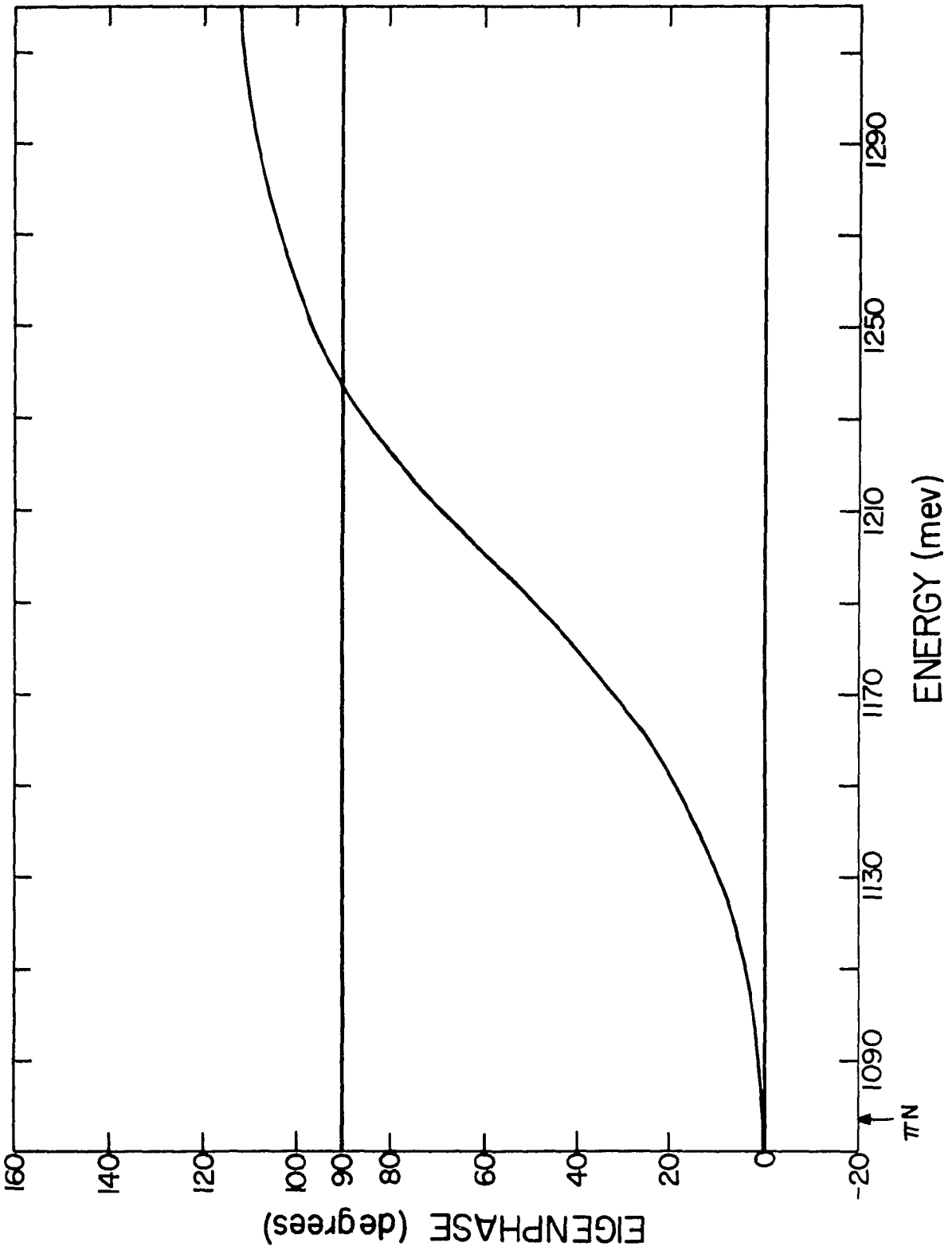
EIGENPHASE (degrees)
160
140
120
100
90
80
60
40
20
0
-20
1090
πN
1130
1170
1210
1250
1290
ENERGY (mev)

show the eigenphase corresponding to the N* resonance, obtained by using $\lambda$ = 1.63 BeV. Analysis of that figure indicates the N* now appears at the correct experimental energy with a width of about 200 MeV, which is somewhat larger than the experimental value.

Considering the other isospin states, we observe that Y*, $\Xi$*, and $\Omega^-$ now appear at energies of 1425, 1602, and 1714 MeV respectively. The widths of Y* and $\Xi$* are 83 and 35 MeV respectively. We see that even though the N* width is somewhat larger than the one obtained in solving the relativistic Schrödinger equation with the same input potential, the widths for Y* and $\Xi$* are definitely much smaller. This is probably due to the introduction of a cutoff matrix function, which introduces some channel dependence. With a straight cutoff parameter in the energy variable, no such dependence is introduced.

It is interesting that the $\Omega^-$ appears in this model as a bound state in agreement with the experimental situation. We note that only one other of our previous calculations has yielded the $\Omega^-$ as a bound state. This was the calculation in which we solved the relativistic Schrödinger equation with an energy dependent potential due to baryon exchange.

The equal spacing rule is also roughly satisfied in this model as can be seen from table 6-1.

Finally we remark that the Y* branching ratios as obtained from this model also agree with experiment. The obtained values are $\Gamma(\Lambda\pi)$ = 94% and $\Gamma(\Sigma\pi)$ = 6%. These are precisely the same values given in M.W. 1.

3. Vector, Baryon, and Decuplet Exchange Contributions to the Driving Force

a. Solving the Multichannel Relativistic Schrödinger Equation with a Cutoff Parameter

Here we will reinvestigate the 3/2+ decuplet by considering the contrubition due to baryon, vector, and decuplet exchange to the input potential. For the vector exchange process we include both the electric and magnetic VBB coupling. It is clear that the coupled system of linear integral equations for the scattering amplitude which we obtain is a non-Fredholm system. This is due to the large spins of the vector mesons and the decuplet, which are 1 and 3/2 respectively. Therefore, the corresponding potential functions diverge for large values of the momenta. To convert this system of linear integral equations into a Fredholm system, we introduce a cutoff parameter.

i) $I = 3/2$, $Y = 1$ State.

We choose the cutoff parameter to obtain the N* at the correct experimental energy. This requires a cutoff of 1.88 BeV. In Figure 6-10 the eigenphases for cutoffs of 1.88, 1.90, 2, and 2.1 BeV are shown. Analysis of this figure shows that for a cutoff of 1.88 the N* appears at the experimentally observed energy, but its width is 260 MeV, which is larger than the experimental value. For cutoff values of 1.90, 2.0, and 2.1 BeV the N* appears at energies of 1197, 1153, and 1110 MeV respectively. The N* width as obtained for each of these values of the cutoff is 199, 69, and 10 MeV respectively. Our

Fig. 6-10. Eigenphases for the I = 3/2, Y = +1, $P_{3/2}$ state for the coupling constants $\frac{g^2_{\pi NN}}{4\pi} = 14.6$, $\frac{g_{\rho\pi\pi}\, g_{\rho NN}}{4\pi} = 1$, and $\frac{g^2_{N^*N\pi}}{4\pi} = 22.6$ $BeV^{-2}$. The contributions from vector, baryon, and decuplet exchange to the input potential are considered. The eigenphases for cutoffs of 1.88, 1.90, 2.0, and 2.1 BeV are given by the dashed, solid, two sized dashed, and dot-dash curves respectively.

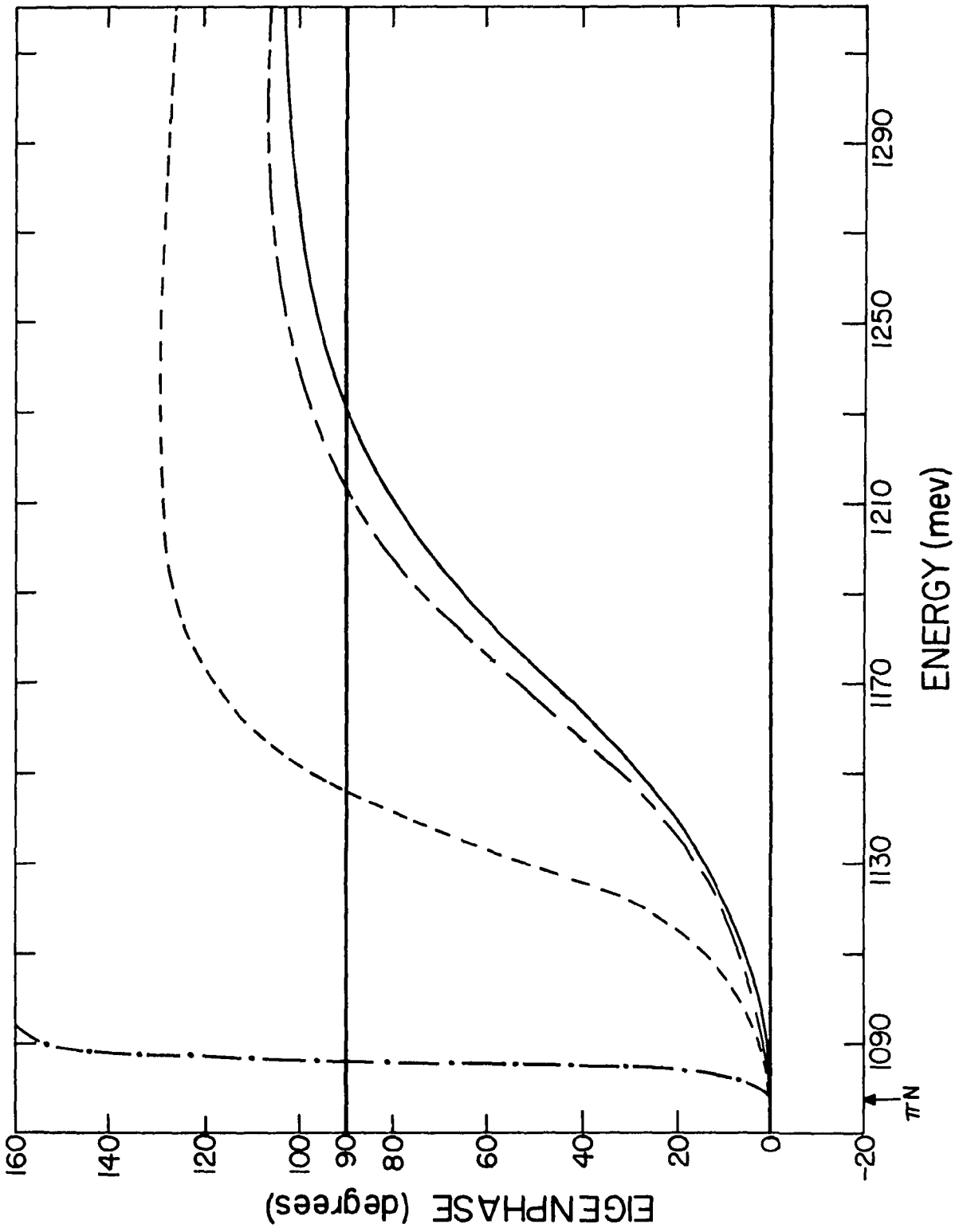
EIGENPHASE (degrees)
160
140
120
100
90
80
60
40
20
0
-20
1090
1130
1170
1210
1250
1290
ENERGY (mev)
πN

results, both for the N* and the other isospin states, are summarized in columns 11, 12, and 13 of table 6-1 for cutoff values of 1.88, 1.9, and 2 BeV respectively.

We will now compare the results obtained by considering the contribution to the input potential from baryon, vector, and decuplet exchange with the results obtained by considering only the baryon exchange contribution. The cutoff necessary to produce the N* at its experimentally observed value decreases by a factor of about 4.6. In fact the cutoff decreases from about 8.7 BeV to about 1.88 BeV. This is encouraging, since we no longer need a large cutoff to produce the N*.

The model now becomes much more cutoff dependent. For example, changing the cutoff parameter from 1.90 to 2.0 BeV changes the N* width from about 200 MeV to about 70 MeV. This is not surprising and is due to the large momentum dependence introduced by the decuplet exchange and the anomalous part of the vector exchange. However, we again emphasize that the qualitative features of the model are unaffected by the addition of these exchanges.

Analysis of the effect due to each of these exchanges shows that the main contribution to the force is due to baryon and decuplet exchange. The contribution due to vector exchange is small. Consideration of the $I = 3/2$, $Y = 1$ state shows that both the baryon and decuplet exchange produce an attractive force. Vector exchange yields a slightly repulsive force. The net effect is consequently attractive.

ii) Other Isospin States

Consideration of the other isospin states shows the following features. For a cutoff of 1.88 BeV, the Y* appears at an energy of 1400 MeV, with a width of about 95 MeV. However, both the $\Xi^*$ and the $\Omega^-$ do not appear. Increasing the cutoff further, we observe that for a cutoff of 1.9 BeV the Y* moves down to 1390 MeV, and its width decreases to about 92 MeV. However, the $\Xi^*$ and the $\Omega^-$ still do not appear. Increasing the cutoff further, we note that for a cutoff of 2 BeV the Y* appears at an energy of 1305 MeV, with a width of 1+ MeV. The $\Xi^*$ is now also present at an energy of 1680 MeV and with a width of about 10 MeV. The $\Omega^-$ is still absent. In order to produce the $\Omega^-$ we must increase the cutoff further . For a cutoff of 2.1 BeV the $\Omega^-$ now appears as a narrow resonance at an energy of 1897 MeV. However, the other members of the decuplet now appear with small widths. For example, the N* appears with a width of about 10 MeV. The eigenphases corresponding to the Y*, $\Xi^*$, and $\Omega^-$ states are shown in Figures 6-11, 6-12, and 6-13 respectively for the different values of the cutoff parameter.

iii) Equal Spacing Rule.

For a cutoff parameter of 2 BeV, for example, we obtain

$$M_{Y^*} - M_{N^*} = 152 \text{ MeV}$$

and (6.12)

$$M_{\Xi^*} - M_{Y^*} = 375 \text{ MeV}.$$

Fig. 6-11. Eigenphases for the I = 1, Y = 0, $P_{3/2}$ state for the coupling constants $\frac{g^2_{\pi NN}}{4\pi} = 14.6$, $\frac{g_{\rho\pi\pi}\, g_{\rho NN}}{4\pi} = 1$, and $\frac{g^2_{N^*N\pi}}{4\pi} = 22.6$ $BeV^{-2}$. The contributions from vector, baryon, and decuplet exchange to the input potential are considered. The eigenphases for cutoffs of 1.9 and 2 BeV are given by the solid and dashed curves respectively.

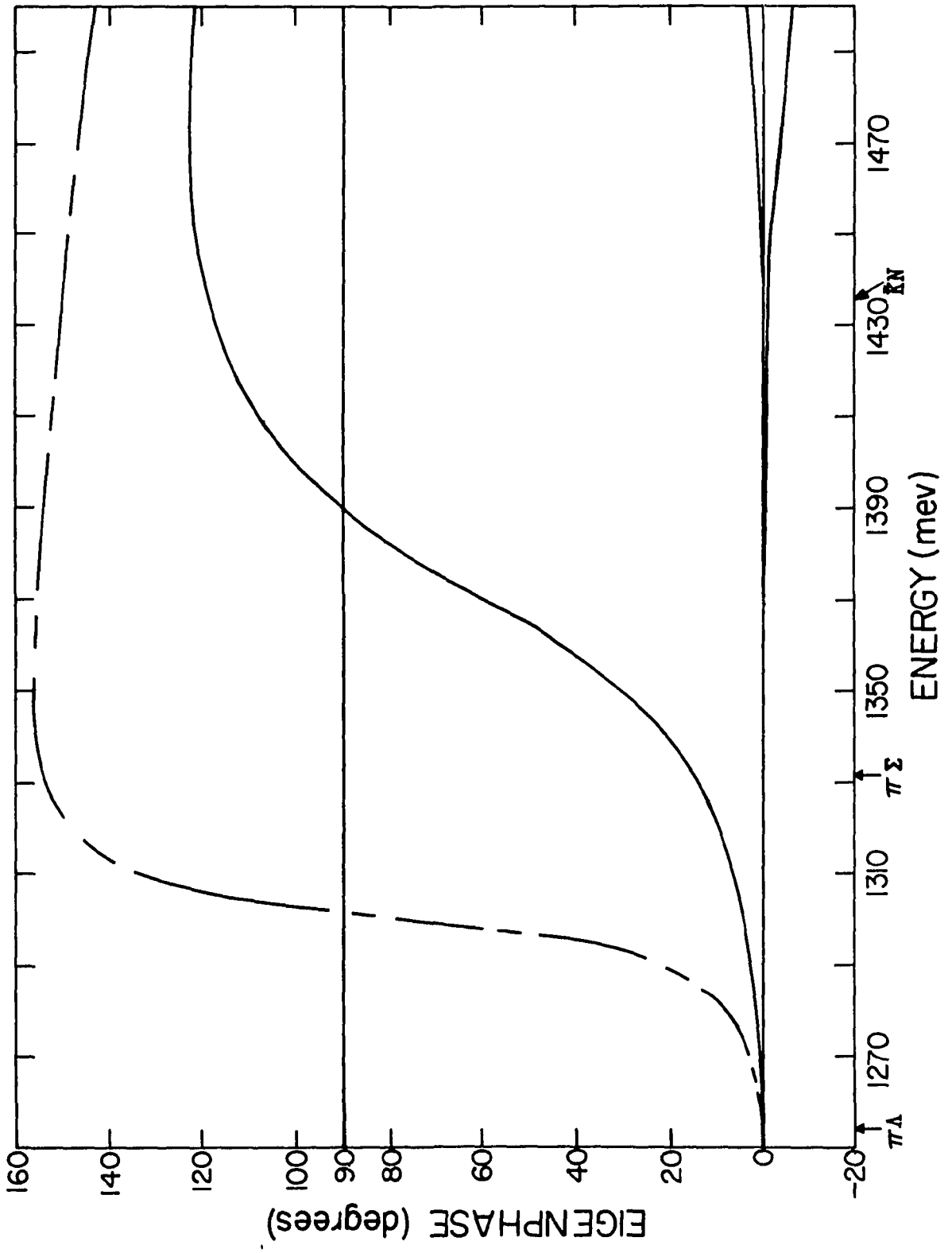
EIGENPHASE (degrees)
160
140
120
100
90
80
60
40
20
0
-20
ENERGY (mev)
1270
1310
1350
1390
1430
1470
πΛ
πΣ
KN

Fig. 6-12. Eigenphases for the I = 1/2, Y = -1, $P_{3/2}$ state for the coupling constants $\frac{g^2_{\pi NN}}{4\pi} = 14.6$, $\frac{g_{\rho\pi\pi}\, g_{\rho NN}}{4\pi} = 1$, and $\frac{g^2_{N^*N\pi}}{4\pi} = 22.6$ $BeV^{-2}$. The contributions from vector, baryon, and decuplet exchange to the input potential are considered. The eigenphases for cutoffs of 1.9 and 2 BeV are given by the solid and dashed curves respectively.

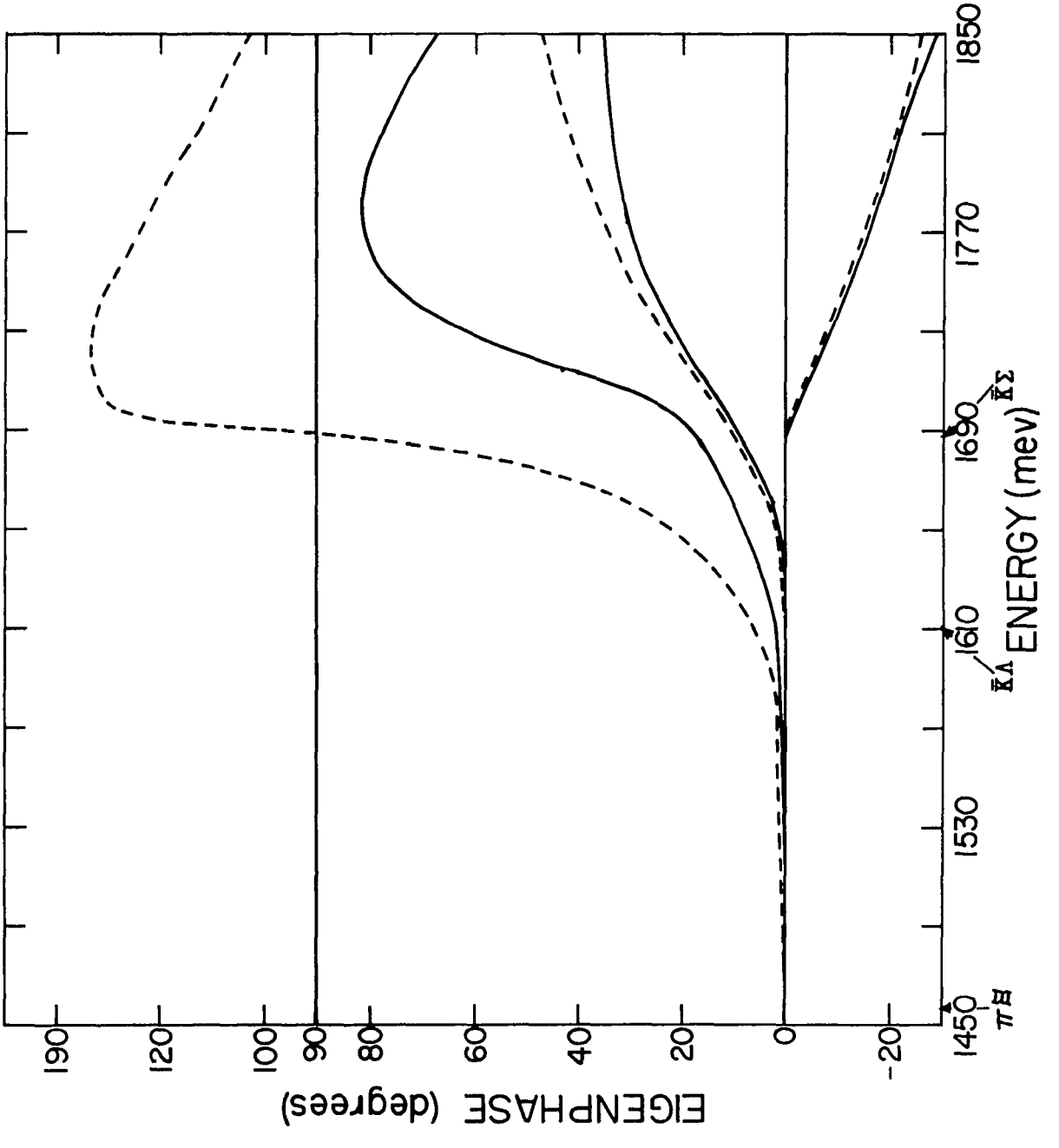
EIGENPHASE (degrees)
190
120
100
90
80
60
40
20
0
-20
1450
1530
1610
1690
1770
1850
ENERGY (mev)
πΞ
ΛK̄
ΣK̄

Fig. 6-13. Eigenphases for the I = 0, Y = -2, $P_{3/2}$ state for the coupling constants $\frac{g^2_{\pi NN}}{4\pi} = 14.6$, $\frac{g_{\rho\pi\pi}\, g_{\rho NN}}{4\pi} = 1$, and $\frac{g^2_{N^*N\pi}}{4\pi} = 22.6$ $BeV^{-2}$. The contributions from vector, baryon, and decuplet exchange to the input potential are considered. The eigenphases for cutoffs of 2.0 and 2.1 BeV are given by the solid and dashed curves respectively.

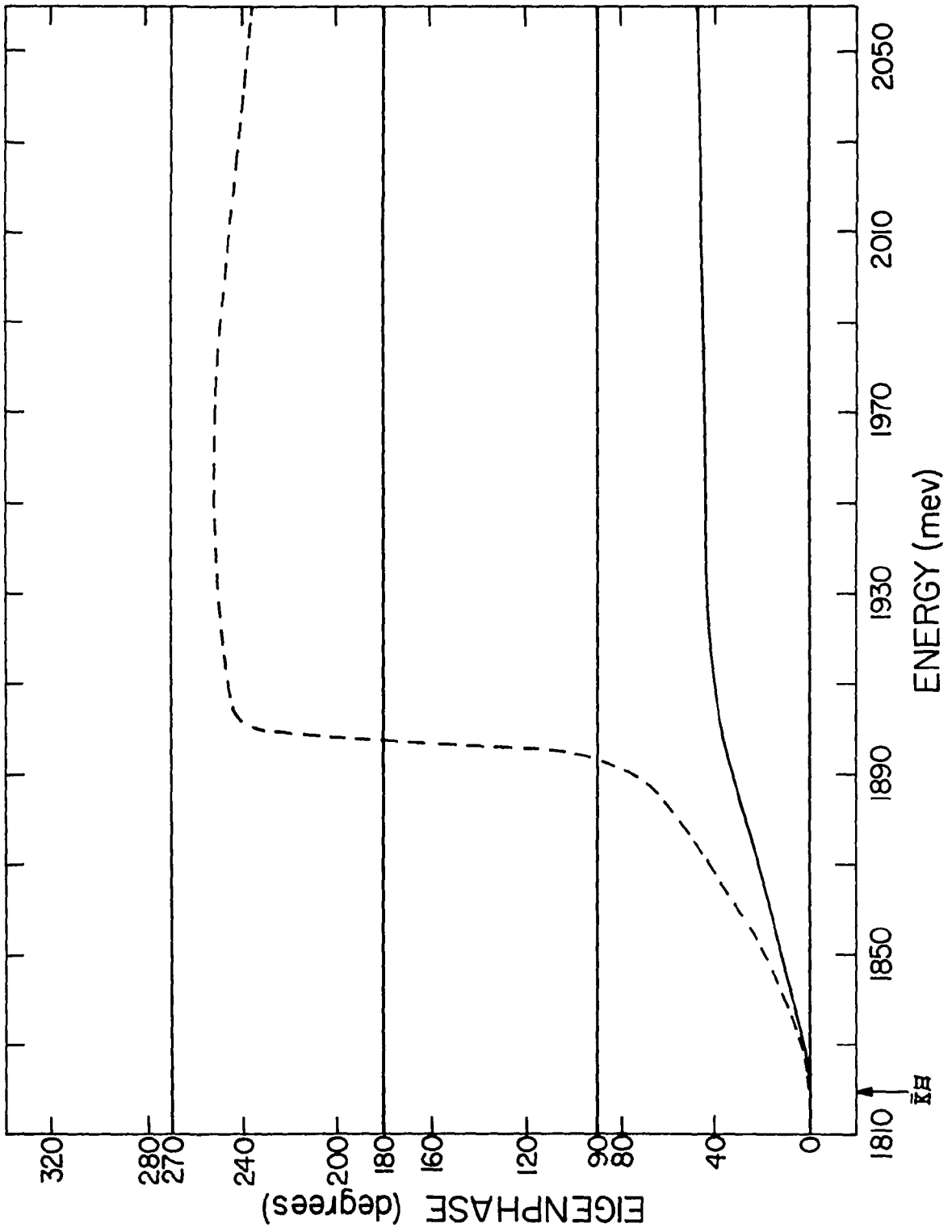
EIGENPHASE (degrees)
320
280
270
240
200
180
160
120
90
80
40
0
ENERGY (mev)
1810
1850
1890
1930
1970
2010
2050

The above quantities seem to indicate that the equal spacing rule is violated by a factor of about 2.5. Thus it seems that the addition of the vector and decuplet exchange increases the disagreement with the equal spacing rule. Martin and Wali claimed that addition of more exchanges would improve the validity of the equal spacing rule. Our results seem to disagree with this assertion.

iv) Y* Branching Ratios.

For a cutoff value of 1.88 BeV the corresponding Y* branching ratios are $\Gamma(\Lambda\pi) = 99\%$ and $\Gamma(\Sigma\pi) = 1\%$. Increasing the cutoff to 1.9 BeV, the branching ratios remain about the same. For a cutoff of 2 BeV the Y* appears at an energy of 1308 MeV. That is, it appears below the $\Sigma\pi$ threshold. Thus for this value of the cutoff, the model predicts the Y* to be a pure $\Lambda\pi$ resonance, and thus it can only decay into the $\Lambda\pi$ channel.

In concluding this section on the Y* branching ratios, we indicate that all the models for the 3/2+ decuplet which we have discussed in this thesis seem to give very similar results for the Y* decay branching ratios. Addition of more exchanges does not seem to alter the branching ratios obtained by considering only the baryon exchange force.

b. Solving the Multichannel Blankenbecler-Sugar Equation with a Gaussian Cutoff Matrix Function

We recall that consideration of the baryon exchange force in the Blankenbecler-Sugar equation with a Gaussian cutoff matrix

function yields a 3/2+ decuplet with no missing members. In addition the $\Omega^-$ appears as a bound state.

In this section we will investigate the results of adding both the vector and decuplet exchange to the baryon exchange force in the input potential. We fix $\lambda$ to obtain the N* at the correct experimental energy. We observe that this requires $\lambda$ = 0.60 BeV. Thus the addition of vector and decuplet exchanges to the baryon exchange force causes $\lambda$ to decrease from 3.2 BeV to 0.60 BeV. However, our results are made worse. For example, the N* now appears with an extremely large width (about 668 MeV). The corresponding eigenphase is shown in Figure 6-14.

D. The 1/2+ Resonances

1. The Baryon Octet

Here we will consider the P wave amplitudes corresponding to total angular momentum J = $\frac{1}{2}$. As discussed in Section A, we expect to observe an octet of bound states corresponding to the baryon octet. Our results for different values of the cutoff parameter are summarized in table 6-2.

Analysis of this table shows that for a cutoff of 1.88 BeV, the nucleon appears as a bound state at an energy of 810 MeV. The experimentally observed energy for the nucleon is 939 MeV. We recall that this was the value of the cutoff required to produce the N* at the correct experimental energy. Thus choosing the cutoff to produce the N* at the observed experimental energy, also produces the nucleon near

Fig. 6-14. Eigenphase for the I = 3/2, Y = +1, $P_{3/2}$ state for the coupling constants $\frac{g^2_{\pi NN}}{4\pi} = 14.6$, $\frac{g_{\rho\pi\pi}\, g_{\rho NN}}{4\pi} = 1$, and $\frac{g^2_{N^*N\pi}}{4\pi} = 22.6$ $BeV^{-2}$. The contributions from vector, baryon, and decuplet exchange to the input potential are considered. The eigenphase is obtained solving the Blankenbecler-Sugar equation with a Gaussian cutoff matrix function for $\lambda = 0.60$ BeV. (We use the same definition of $\lambda$ as in equation 6.13.)

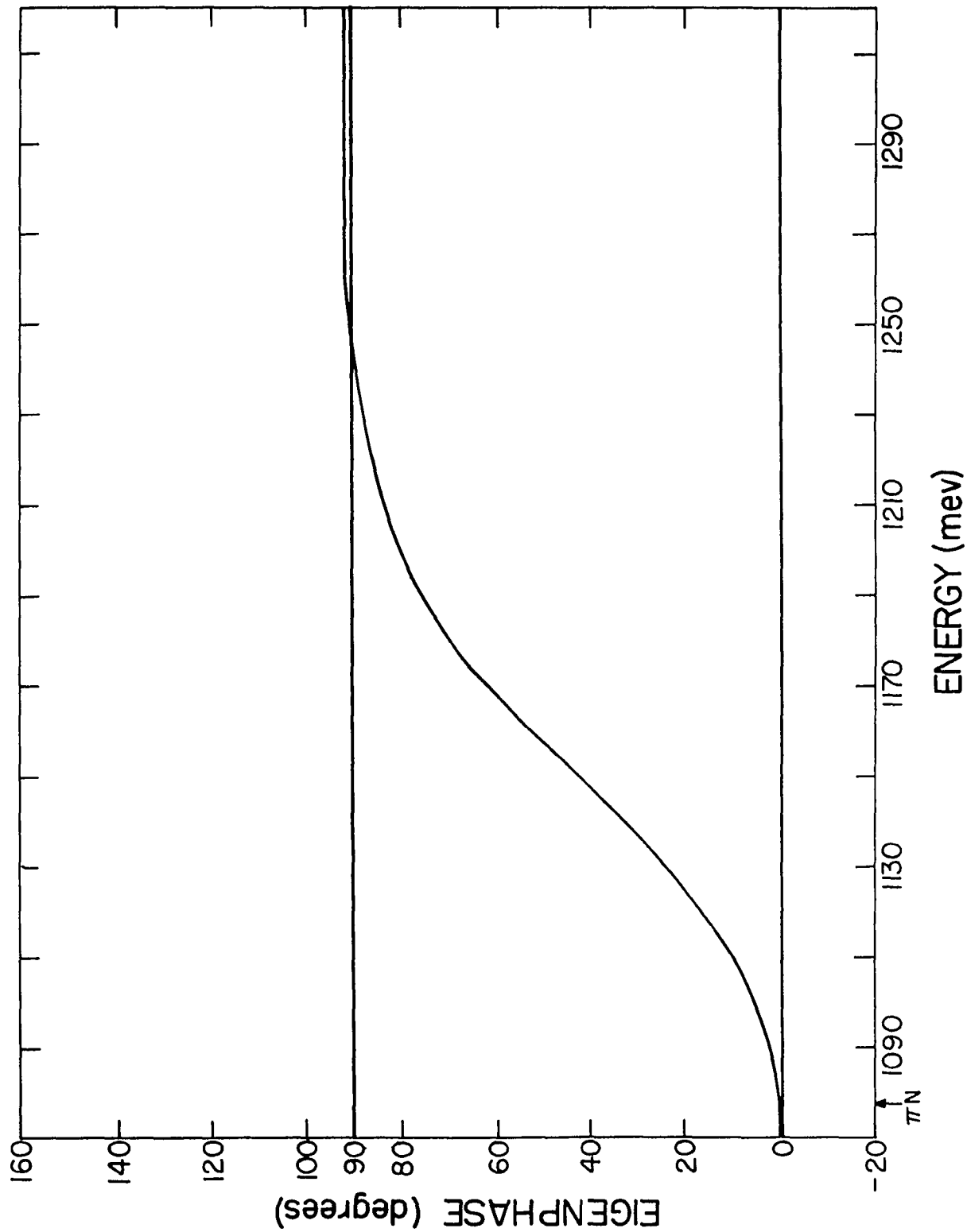
EIGENPHASE (degrees)
160
140
120
100
90
80
60
40
20
0
-20
1090
1130
1170
1210
1250
1290
ENERGY (mev)
πN

Table 6-2. Summary of results for the $\frac{1}{2}+$ baryon octet. The mass (in MeV) of particle i is denoted by $M_i$. Column 2 gives the experimental masses. Columns 3 to 6 give the results obtained for the same coupling constants and exchanges as in the preceding figure for cutoff values of 1.88, 1.89, 1.9, and 2 BeV, respectively.

| | EXP. | 1.88 | 1.89 | 1.90 | 2.0 |
|---|---|---|---|---|---|
| $N$ | 939 | 810 | 795 | 745 | 513 |
| $\Lambda$ | 1115 | 1329 | 1323 | 1313 | 1148 |
| $\Sigma$ | 1193 | 1627 | 1624 | 1621 | 1595 |
| $\Xi$ | 1318 | 1758 | 1755 | 1730 | 1715 |
| $\frac{M_N + M_\Xi}{2}$ | 1129 | 1284 | 1275 | 1238 | 1114 |
| $\frac{3M_\Lambda + M_\Sigma}{4}$ | 1135 | 1403 | 1398 | 1390 | 1260 |

the correct experimental energy. This is in agreement with the Chew Low reciprocal bootstrap hypothesis. By further increasing the cutoff, we note that for cutoffs of 1.89, 1.9, and 2 BeV, the nucleon appears at energies of 795, 745, and 513 MeV respectively.

Analysis of the contributions to the force from vector, baryon, and decuplet exchange shows that both the vector and decuplet exchange contributions are attractive. The baryon exchange process yields a repulsive force. The main contribution to the force is from the decuplet exchange. Both vector and baryon exchange yield somewhat smaller contributions. The net effect is an attractive force.

ii) Other Isospin States.

Considering the other members of the baryon octet, we observe that for a cutoff of 1.88 BeV, the $\Lambda$, $\Sigma$, and $\equiv$ appear at energies of 1329, 1627, and 1758 MeV respectively. Their experimentally observed energies are 1115, 1193, and 1318 MeV respectively. For a cutoff of 1.89 they appear at energies of 1323, 1624, and 1755 MeV respectively. By increasing the cutoff to 1.9 BeV, they now appear at energies of 1313, 1621, and 1730 MeV respectively. For a cutoff of 2 BeV the energies become 1118, 1595, and 1715 MeV respectively.

We note that both the nucleon and the $\Lambda$ appear as bound states in this model. This is because the lowest thresholds for the $I = \frac{1}{2}$, $Y = 1$ state and the $I = 0$, $Y = 0$ state are the $\pi N$ threshold (at an energy of 1077 MeV) and the $\pi\Sigma$ threshol (at an energy of 1331 MeV).

We also note that $\Sigma$ and $\equiv$ appear in this model as resonances. That is, they appear at energies above the lowest thresholds for the

I = 1, Y = 0 and the I = ½, Y = -1 states respectively. These lowest thresholds are at the $\pi\Lambda$ threshold (at an energy of 1253 MeV) and the $\pi\Xi$ threshold (at an energy of 1456 MeV).

iii) Mass Formula.

The Gellmann Okubo mass formula for the baryon octet can be written as

$$\frac{M_N + M_\Xi}{2} = \frac{3M_\Lambda + M_\Sigma}{4} . \qquad (6.13)$$

This expression is well satisfied experimentally as shown in rows 6 and 7 of table 6-2.

The values predicted by our model are given in columns 3 to 6 of table 6-2 for values of the cutoff of 1.88, 1.89, 1.9, and 2 BeV. By looking at this table we note that the Gellmann Okubo mass formula for the baryon octet seems to be satisfied in our calculations to about 12%.

2. Other ½+ Resonances.

As we have discussed in Section A, there seems to be experimental evidence for the existence of a higher ½+ resonance. This is the so-called $N^*_{\frac{1}{2}}(1400)$. In Section B we have discussed Brehm and Kane's suggestion that this resonance might be the member of a $\overline{10}$ and not 8, in disagreement with the quark model.

Our model does not predict the existence of any higher ½+ resonances. In Figure 6-15 the scattering eigenphase predicted by our model for the $P_{11}$ partial wave amplitude is shown. The

Fig. 6-15. Eigenphase for the I = ½, Y = +1, $P_{1/2}$ state. The solid curve gives the results obtained using the same coupling constants and exchanges as in Figure 6.14 with a cutoff of 2 BeV. The dotted curve gives the experimental phase shift as obtained by Roper.

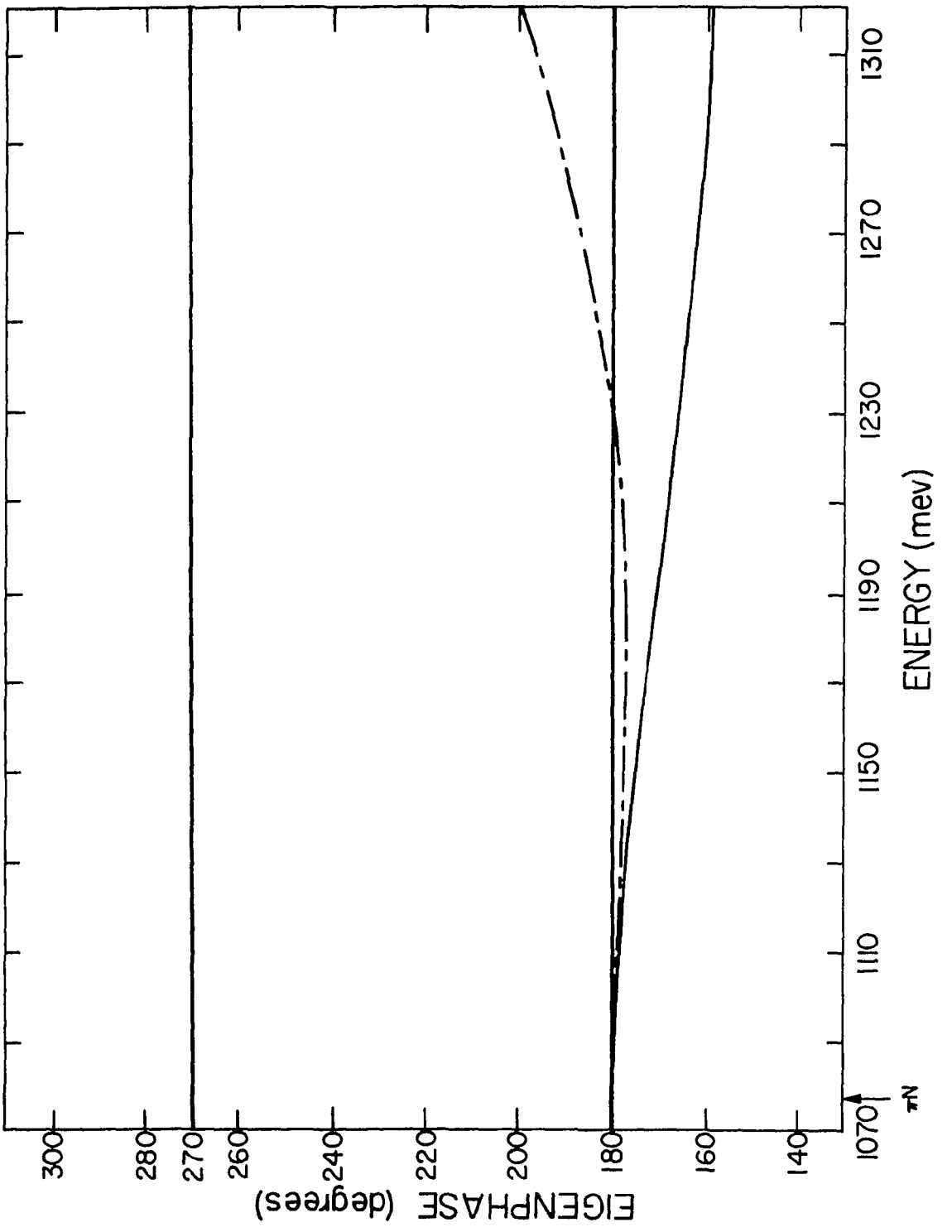
EIGENPHASE (degrees)
300
280
270
260
240
220
200
180
160
140
ENERGY (mev)
1070
1110
1150
1190
1230
1270
1310
$\pi N$

experimentally observed eigenphase is also shown in the same figure. We note that both eigenphases start at $180^{\circ}$ since there is a bound state corresponding to the nucleon. However, while the experimental eigenphase rises, the eigenphase obtained from our model falls. By increasing the cutoff to 2.5 BeV we can make the eigenphase rise and go through $90^{\circ}$, corresponding to $N^{*}_{\frac{1}{2}}(1400)$. However, the nucleon then appears as a negative energy bound state.

To further investigate the possibility of the existence of a resonating $\overline{10}$, we consider the largest hypercharge state in the $\overline{10}$ representation of SU(3). This is the I = 0, Y = 2 state. The only channel which contributes to this state is the KN channel. The eigenphase obtained for this case is shown in Figure 6-16. We see that an attractive scattering amplitude is obtained for this isospin state. However, insufficient attraction is obtained to produce a resonance, unless we further increase the cutoff. Thus we find that vector, baryon, and decuplet exchange produce attractive forces in the $\overline{10}$ irreducible representation of SU(3). However, the attraction is not sufficient to produce resonances. In this sense our results seem to agree with those given in M.W. 2.

However, these results are in disagreement with the conclusions of Brehm and Kane. They concluded that decuplet exchange alone was sufficient to produce a resonant $\overline{10}$ representation. This is not too surprising, since as we may recall all of these methods make use of different approximations. Martin and Wali made use of Bjorken's determinantal approximation to the multichannel N/D equations. Brehm

Fig. 6-16. Eigenphase for the I = 0, Y = +2, $P_{\frac{1}{2}}$ state for the same coupling constants and exchanges as in Figure 6-14, with a cutoff of 2 BeV.

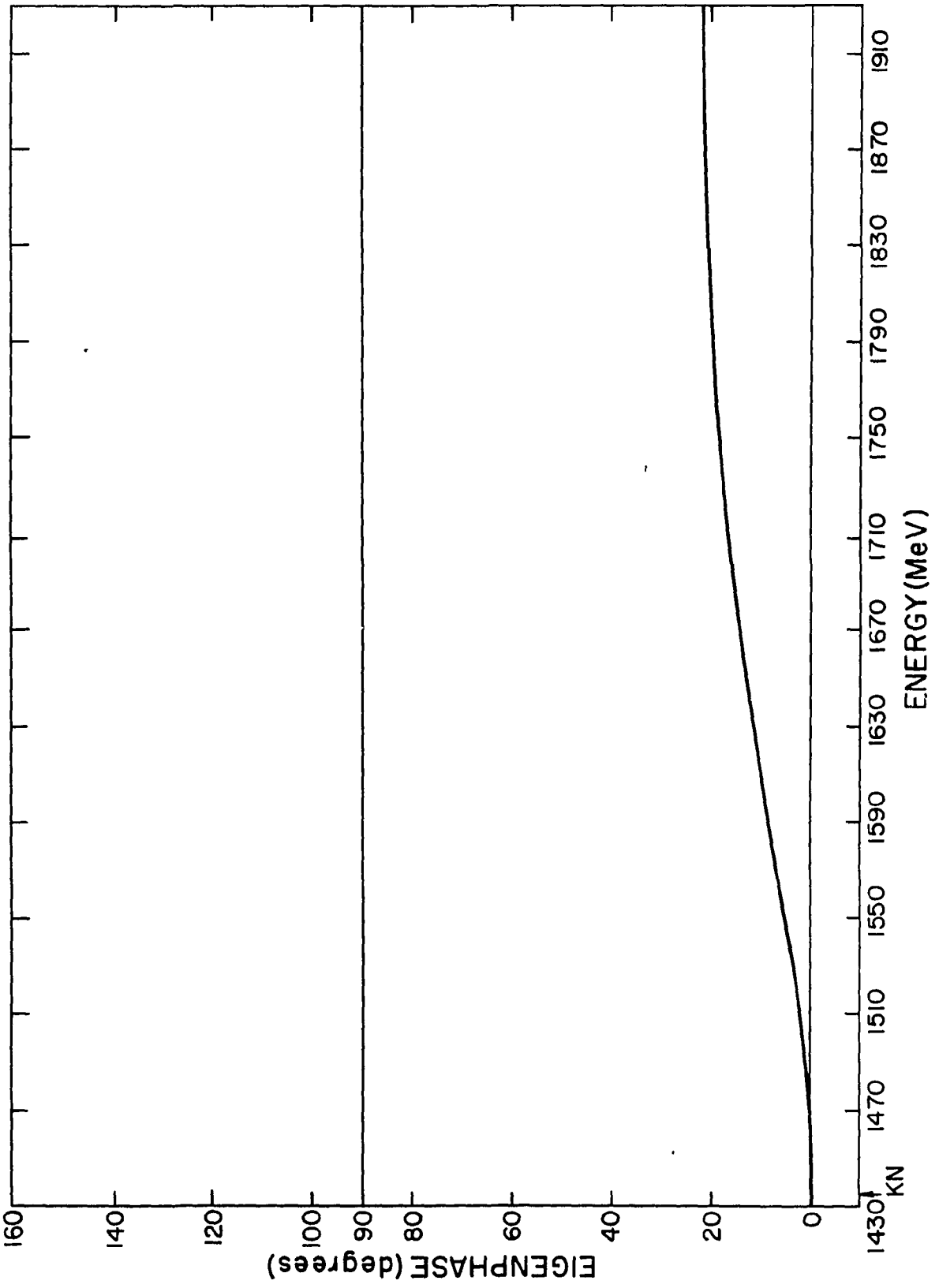
EIGENPHASE (degrees)
160
140
120
100
90
80
60
40
20
0
1430
1470
1510
1550
1590
1630
1670
1710
1750
1790
1830
1870
1910
KN
ENERGY(MeV)

and Kane solved the multichannel N/D equations using Pagel's method. We solved the multichannel relativistic Schrödinger equation.

E. Study of Nonresonant P Wave Amplitudes

In addition to predicting the observed P wave resonances, it is equally important that the model shows that there are no resonances in the remaining isospin amplitudes. We next consider them in the case of pion nucleon scattering. It will then become apparent that no resonances appear in these amplitudes, in agreement with experiment. Moreover, phase shifts for these amplitudes seem to be in qualitative agreement with experiment.

1. The $P_{31}$ Amplitude

Both baryon and vector exchange provide a strong repulsive force in this partial wave amplitude. The contribution due to decuplet exchange is strongly attractive. The net effect is a repulsive force. Both the experimentally observed phase shifts and our phase shifts are shown in Figure 6-17 for different cutoff values. We note that both the experimental and our phase shifts have the same sign and are in good qualitative agreement.

2. The $P_{13}$ Amplitude

Both vector and decuplet exchange yield attractive forces. However, baryon exchange produces a strongly repulsive force. The net effect is a repulsive force. In Figure 6-18 we compare the experimental phase shift with the phase shift predicted by our model for different values of the cutoff parameter. We note that both the experimental and also our phase shift have the same sign and are small.

Fig. 6-17. Eigenphases for the I = 3/2, Y = +1, $P_{\frac{1}{2}}$ state for the same coupling constants and exchanges as in Figure 6-14. The solid and dashed curves give the eigenphases for cutoffs of 1.88 and 2 BeV respectively. The dot-dash curve gives the experimental phase shift as given by Behrends et al.

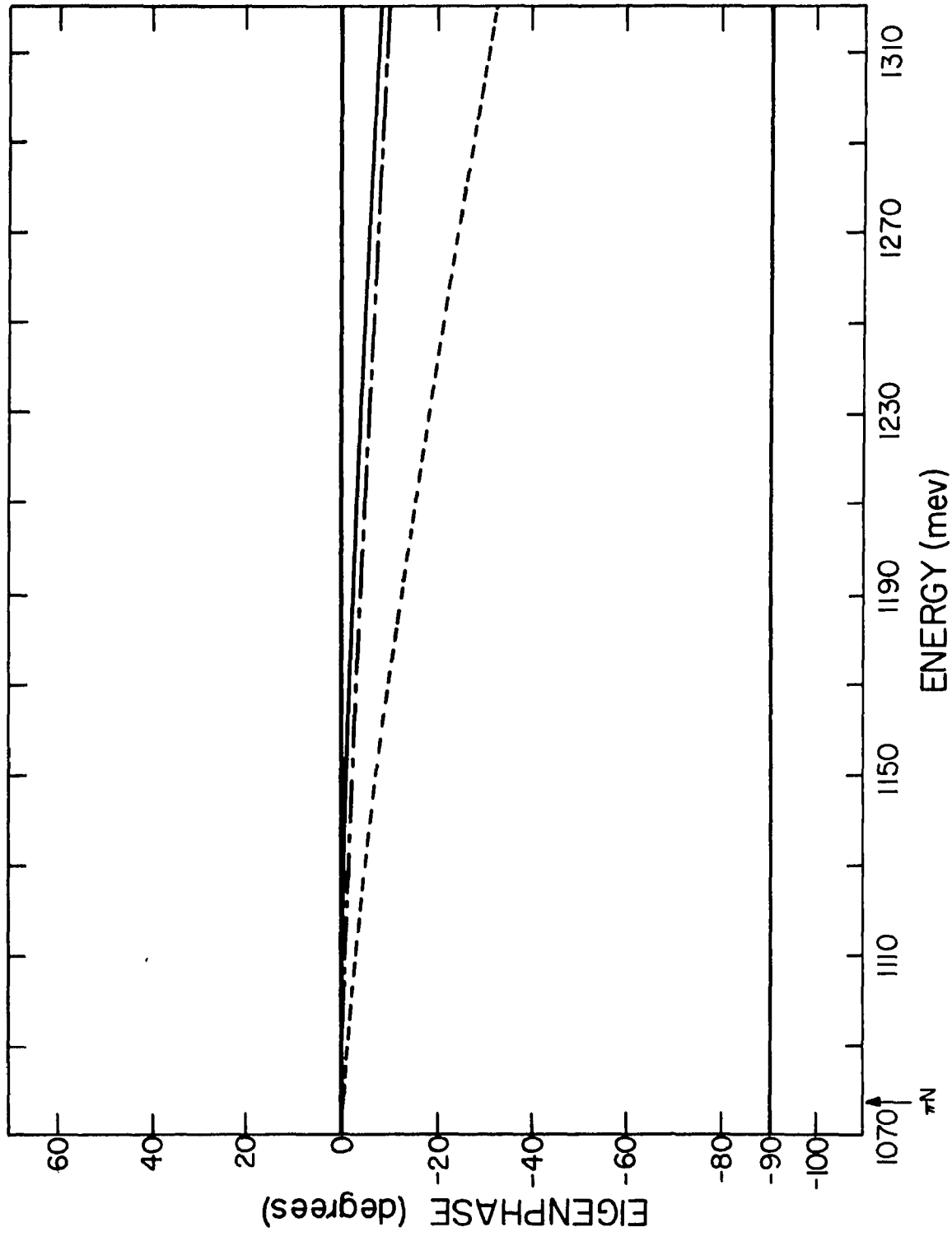
EIGENPHASE (degrees)
60
40
20
0
-20
-40
-60
-80
-90
-100
1070
$N^*$
1110
1150
1190
1230
1270
1310
ENERGY (mev)

Fig. 6-18. Eigenphases for the $I = \frac{1}{2}$, $Y = +1$, $P_{3/2}$ state for the same coupling constants and exchanges as in Figure 6-14. The solid and dashed curves give the phase shifts for cutoffs of 1.88 and 2 BeV respectively. The dot-dash curve gives the experimental phase shift as given by Behrends et al.

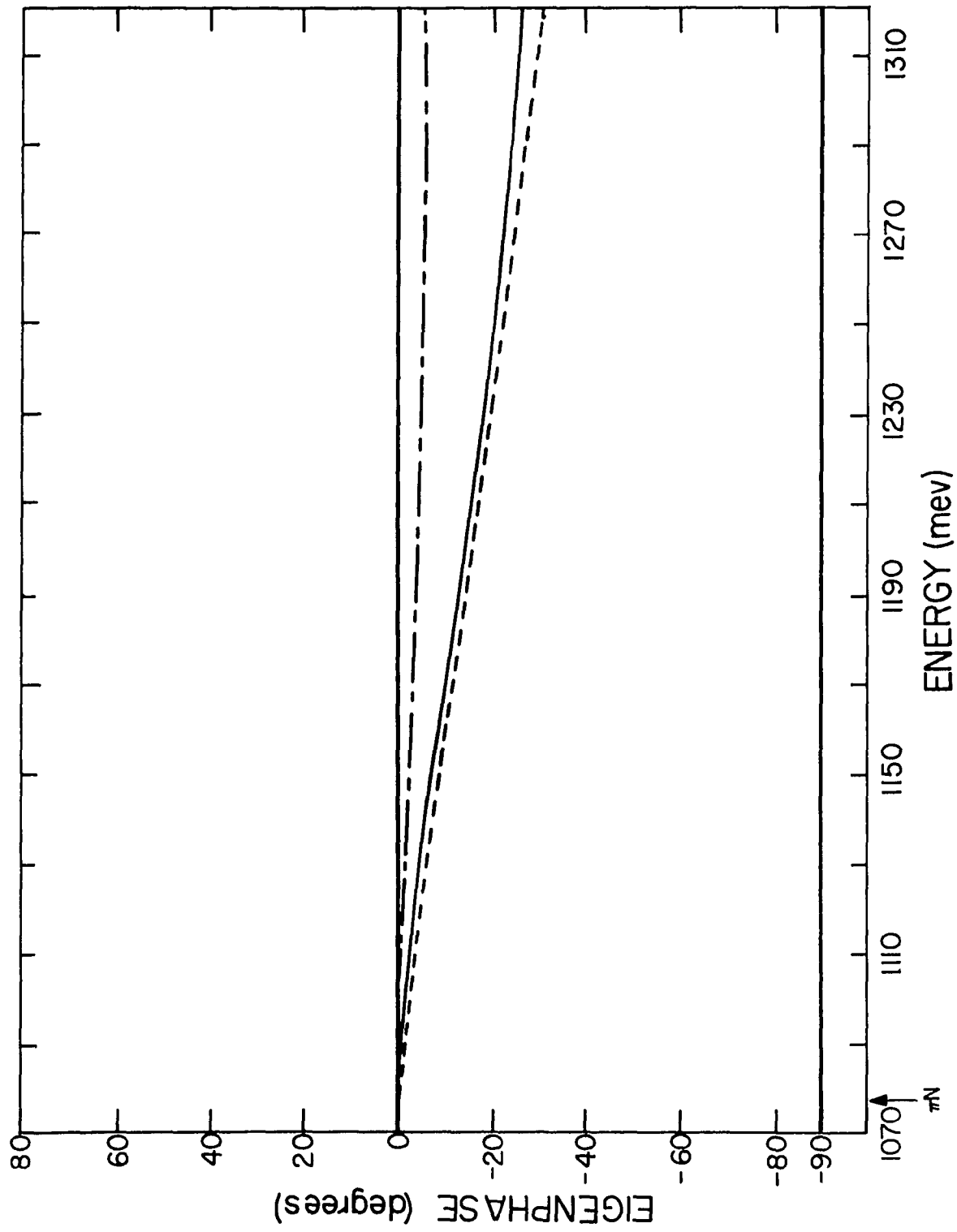
EIGENPHASE (degrees)
80
60
40
20
0
-20
-40
-60
-80
-90
1070
$\pi N$
1110
1150
1190
1230
1270
1310
ENERGY (mev)

# VII. REGGE RECURRENCES AND HIGHER WAVE RESULTS

## A. Experimental Situation

Analysis of pseudoscalar meson baryon scattering experiments seem to indicate the existence of four families (Regge trajectories) of baryon resonances. There are two vector families distinguished by the spatial character of the decuplet exchange process, which is attractive for odd $\ell$ and repulsive for even $\ell$.[1] We call these vector families because the main contribution to the force in the partial wave amplitudes to which their members belong is from the vector exchange process. The first vector family consists of the $P_{\frac{1}{2}}$ octet and the $F_{5/2}$ resonances.[2] The second vector family consists of the $D_{3/2}$ resonances. Next there is a baryon family which consists of the $P_{3/2}$ decuplet and the $F_{7/2}$ resonances. The baryon family is so designated because baryon exchange is the main contribution for $P_{3/2}$. However, both vector and baryon exchanges give important contributions for $F_{7/2}$. There is also another family of baryon resonances consisting of the $S_{\frac{1}{2}}$ and $D_{5/2}$ resonances.

The $F_{5/2}$ resonances consist of $N^*_{\frac{1}{2}}(1688)$, $Y^*_1(1910)$, $Y_0^*(1820)$, and possibly $\equiv^*(1930)$. However, there is as yet not enough experimental information about the spin and parity of $\equiv^*(1930)$. If $\equiv^*(1930)$ is found to have spin parity 5/2+, then there would be a complete octet of $F_{5/2}$ resonances. The existence of such an octet is expected on the

---

1. This is discussed in D.H.

2. We restrict our attention to the four lowest partial waves.

basis of SU(3) symmetry and the quark model. The $F_{5/2}$ resonances in the order listed above have widths of about 110, 60, 83, and 140 MeV respectively. The main decay mode of $N^*_{\frac{1}{2}}(1688)$ is the $\pi N$ channel. The corresponding branching ratio is about 65%. Other pseudoscalar meson baryon channels into which it decays are the $K\Lambda$ and $\eta N$ channels. However, the corresponding branching ratios are small. The P.B. decay modes of $Y^*_1(1910)$ are the $\Lambda\pi$, $\bar{K}N$, and $\Sigma\pi$ channels respectively.[3] The respective branching ratios for these channels are about 10%, 8%, and 3% respectively. The $Y_o^*(1820)$ main P.B. decay mode is the $\bar{K}N$ channel. The corresponding branching ratio is about 70%. Its other P.B. decay modes are the $\Sigma\pi$ and $\Lambda\eta$ channels, with branching ratios of about 11% and 1%. The P.B. decay modes of $\Xi^*(1930)$ are into the $\pi\Xi$ and $\bar{K}\Lambda$ channels. There is not enough experimental information on the branching ratios for these channels.

The only experimentally known $F_{7/2}$ resonances are $N^*_{3/2}(1920)$ and $Y^*_1(2035)$. However, since $F_{7/2}$ is the Regge recurrence of $P_{3/2}$, it seems plausible to expect the eixstence of a decuplet of $F_{7/2}$ resonances. This would also be expected on the basis of SU(3) and quark model arguments. However, there is not yet enough experimental evidence about the existence of the other members of this possible decuplet. The widths of $N^*_{3/2}(1920)$ and $Y^*_1(2035)$ are about 200 and 160 MeV. The main decay mode for $N^*_{3/2}(1920)$ is the $\pi N$ channel. The corresponding branching ratio is about 50%. Another P.B. decay mode for $N^*_{3/2}(1920)$

---

3. We use the term P.B. channel as an abbreviation for "pseudoscalar meson baryon channel."

is the $K\Sigma$ channel. However, the corresponding branching ratio is small and has not yet been measured. The $Y_1^*(2035)$ decays mainly into the $\Lambda\pi$ and $\bar{K}N$ channels with branching ratios of about 25% and 16%. This resonance has also been observed to decay into the $\Sigma\pi$ channel. However, the corresponding branching ratio has not yet been experimentally measured.

The experimentally known $D_{3/2}$ resonances consist of $N_{\frac{1}{2}}^*(1525)$, $Y_1^*(1660)$, and $Y_o^*(1520)$. Also $\Xi^*(1815$ might be a member of the set of $D_{3/2}$ resonances. However, its spin and parity have not yet been measured experimentally. On the basis of the Gellman Okubo mass formula we do not expect $Y_o^*(1520)$ to be a member of an octet of $D_{3/2}$ resonances. Therefore, SU(3) considerations indicate the existance of another I = 0, Y = 0 $D_{3/2}$ resonance which with $Y_o^*(1520)$ and the other $D_{3/2}$ resonances would then form a nonet of resonances. This other I = 0, Y = 0 resonance might be identified with $Y_o^*(1700)$.[4] However, the spin and parity of $Y_o^*(1700)$ are experimentally uncertain at present. The widths of $N_{\frac{1}{2}}^*(1525)$, $Y_1^*(1660)$, $Y_o^*(1520)$, and $\Xi^*(1815)$ are 105, 50, 16, and $16\pm8$ MeV respectively. The $N_{\frac{1}{2}}^*(1525)$ decays mainly into the $\pi N$ channel with a branching ratio of about 65%. The $Y_1^*(1660)$ decays mainly into $Y_o^*(1405)\pi$, and its P.B. decay modes are small. The main P.B. decay mode of $Y_o^*(1520)$ is the $\Sigma\pi$ channel with a branching ratio of about 51%. Its other P.B. decay mode is the $\bar{K}N$ channel with a branching ratio of about 39%.

---

4. Note that the physical particles $Y_o^*(1520)$ and $Y_o^*(1700)$ are each mixtures of a $D_{3/2}$ unitary singlet and the I = 0, Y = 0 member of a $D_{3/2}$ octet. The reason for this is the same as that in the case of $\varphi$-$\omega$ mixing.

The $\Xi^*(1815)$ decays into the $\pi\Xi$ and $\bar{K}\Lambda$ channels. However, the corresponding branching ratios have not yet been determined.

The known $D_{5/2}$ resonances consist of $N^*_{\frac{1}{2}}(1670)$ and $Y_1^*(1770)$. On the basis of SU(3) and quark model arguments, we would expect the existence of an octet of $D_{5/2}$ resonances. However other members of this possible octet are not yet experimentally known. The width of $N^*_{\frac{1}{2}}(1670)$ is about 140 MeV. The $Y_1^*(1770)$ has a width of about 89 MeV. The main decay mode of $N^*_{\frac{1}{2}}(1670)$ is the $\pi N$ channel with a branching ratio of about 40%. Its other P.B. decay modes are small. The main P.B. decay mode of $Y_1^*(1770)$ is into the $\bar{K}N$ channel with a branching ratio of about 49%. Its other P.B. decay modes are the $\Lambda\pi$, $\Sigma\eta$, and $\Sigma\pi$ channels with the corresponding branching ratios of about 17%, 2%, and 1%.

B. Results of Other Calculations

In this section we will briefly review the D and F wave results of the calculations of Coulter and Shaw, Martin and Wali, and Donnachie and Hamilton. Coulter and Shaw restricted themselves to pion nucleon partial wave amplitudes with $J \leq 3/2$. Thus the only higher waves which they considered were those corresponding to the $D_{13}$ and $D_{33}$ partial wave amplitudes. The $D_{13}$ phase shifts obtained in their model agree with the experimental phase shifts up to an energy of about 1380 MeV. Above that energy their phase shift started to decrease. This contradicted the experimental phase shift which keeps increasing and goes through $90^\circ$ at about 1518 MeV. The $D_{33}$ phase

shifts which they obtained agreed with the experimental phase shifts up to an energy of about 1160 MeV. However, the experimental phase shift then rise , while theirs became negatively decreasing.

The calculations discussed in M.W. 2 indicated the existence of a singlet $D_{3/2}$ resonance. However, no other D or F resonances were found in their model.

The calculations of D. H. indicated the existence of pion nucleon resonances in the $D_{13}$, $F_{15}$, and $F_{37}$ partial wave amplitudes. The center of mass energies at which these resonances appeared in their model were roughly 1638, 1792, and 1994 MeV respectively. The experimental energies are 1525, 1688, and 1920 MeV respectively. Their model did not account for the known pion nucleon resonance in the $D_{15}$ partial wave amplitude. Also they did not incorporate SU(3) symmetry. Therefore, they could discuss only the pion nucleon $I = \frac{1}{2}$, $Y = 1$, and $I = 3/2$, $Y = 1$ meson baryon resonances. We also mention that the low energy phase shifts obtained in their model seemed to be in good agreement with experiment. Analysis of the main contributions to these partial wave amplitudes in their model seemed to indicate that both $\rho$ and N* exchanges were the main contribution to $D_{13}$. The main contribution to $F_{15}$ was due to $\rho$ exchange. Their analysis of the $F_{37}$ amplitude showed that both $\rho$ and N exchange yielded the main contributions in this case.

C. D Wave Results

1. The 3/2⁺Resonances

Here we will consider the contributions from vector, baryon, and decuplet exchange as the input potential. We investigate the 3/2⁺resonances by solving the multichannel relativistic Schrödinger equation with this input potential. A cutoff is introduced to convert the coupled system of integral equations for the scattering amplitude into a Fredholm system. We use a cutoff value of 2 BeV. We recall this value was also used in our discussions of the P waves.

i) $I = \frac{1}{2}$, $Y = 1$ state.

The eigenphase corresponding to the $I = \frac{1}{2}$, $Y = 1$ amplitude is shown in Figure 7-1. This figure shows that the corresponding eigenphase goes through $90^{\circ}$ at an energy of about 1669 MeV, with which we compare the experimental energy of about 1518 MeV. However, $N^{*}_{\frac{1}{2}}(1525)$ appears in our model as a narrow resonance.

Analysis of the signs and strengths of the different exchanges which contribute to this state shows that both baryon and decuplet exchange are repulsive. Vector exchange yields an attractive contribution. Vector exchanges yields a strong attractive both force and decuplet. The contribution of both the baryon and decuplet exchange are of a smaller absolute value. The net result is an attractive force.

ii. Other Isospin States.

Analysis of the other isospin states shows the model predicts a nonet of $D_{3/2}$ resonances, i.e., an octet and a unitary singlet.

Fig. 7-1. Eigenphase for the $I = \frac{1}{2}$, $Y = +1$, $D_{3/2}$ state for the coupling constants $\frac{g^2_{\pi NN}}{4\pi} = 14.6$, $\frac{g_{\rho\pi\pi}\, g_{\rho NN}}{4\pi} = 1$, and $\frac{g^2_{N^*N\pi}}{4\pi} = 22.6$ $BeV^{-2}$. The contributions from vector, baryon, and decuplet exchange to the input potential are considered. A cutoff of 2 BeV is used.

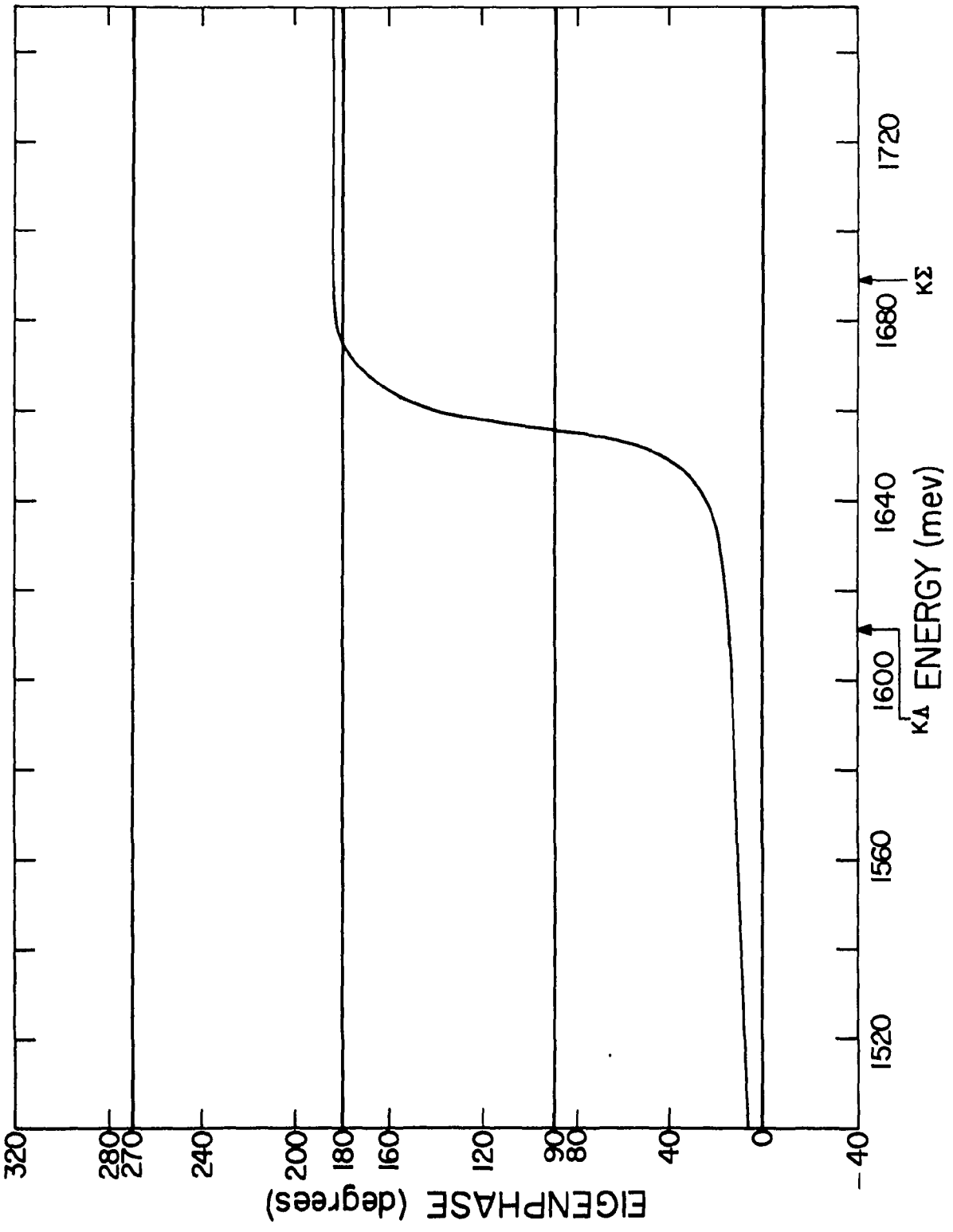
EIGENPHASE (degrees)
320
280
270
240
200
180
160
120
90
80
40
0
-40
1520
1560
1600
KΛ
1640
1680
KΣ
1720
ENERGY (mev)

The experimental values are $N^*_{\frac{1}{2}}(1525)$, $Y_1^*(1660)$, $Y_0^*(1700)$, $Y_0^*(1520)$, and $\Xi^*(1815)$. In our model they appear as narrow resonances at energies of about 1669, 1770, 1879, 1752, and 1950 MeV respectively.

iii) Mass Formula.[5]

This model predicts

$$\frac{M_{N^*} + M_{\Xi^*}}{2} = 1808 \text{ MeV} . \tag{7.1}$$

The experimental result is

$$\frac{M_{N^*} + M_{\Xi^*}}{2} = 1670 \text{ MeV}. \tag{7.2}$$

Not much can be said experimentally about the quantity $\frac{3M_{Y_1^*} + M_{Y_0^*}^{(8)}}{4}$, which on the basis of the Gellmann Okubo mass formula should have the same numerical value as that given in 7.2.[5] Such is the case because the only way to determine $M_{Y_0^*}^{(8)}$ is by equating the above quantity to the value given in 7.2 and then solving.

iv) Branching Ratios.

The $N^*_{\frac{1}{2}}(1525)$ appears in our model as a resonance which decays mainly into the $\pi N$ channel. Branching ratios for its decay into other P.B. channels are negligible.

---

5. We denote the mass of the I = 0, Y = 0 member of the $D_{3/2}$ octet by $M_{Y_0^*}^{(8)}$.

The $Y_1^*(1660)$ decays mostly into the $\pi\Lambda$ and $\pi\Sigma$ channels. The corresponding branching ratios are about equal to each other and each is about 38%. It can also decay into the $\bar{K}N$ channel. The corresponding branching ratio is about 23%. The branching ratio for its decay into the $\eta\Sigma$ channel is small (about 1%).

The $Y_0^*(1700)$ decays mainly into the $\pi\Sigma$ channel. The corresponding branching ratio is about 84%. It can also decay into the $\bar{K}N$ channel. The corresponding branching ratio is about 14%. The branching ratio for its decay into the $\eta\Lambda$ channel is about 2%. Even though its decay into the $K\Xi$ is energetically allowed, the corresponding branching ratio is almost negligible.

The $Y_0^*(1520)$ decays mainly into the $\pi\Sigma$ channel. The corresponding branching ratio is about 63%. It can also decay into the $\bar{K}N$ channel. The corresponding branching ratio is about 35%. Since in our model $Y_0^*(1520)$ appears above the $\eta\Lambda$ threshold, it can also decay into this channel. However, the corresponding branching ratio is small (about 2%).

The $\Xi^*(1815)$ appears in our model as a resonance which decays mainly into the $\pi\Xi$ channel with a branching ratio of about 95%. It can also decay into the $\bar{K}\Lambda$ channel. The corresponding branching ratio is about 5%. Branching ratios for its decay into other SU(3) channels are negligible.

2. The 5/2-Resonances

Experiments seem to indicate the existence of two $D_{5/2}$ resonances. These are $N^*_{\frac{1}{2}}(1670)$ and $Y_1^*(1770)$. On the basis of the

quark model we would expect the existence of an octet of such resonances. As of yet there is no experimental evidence for the existence of the other members of this possible octet.

The phase shift obtained in our model for the $D_{5/2}$ states do not seem to exhibit a resonant behavior. Thus these resonances do not appear in our model.

The experimental phase shift for the $D_{15}$ state is positively increasing. It reaches $3^{o}$ at an energy of about 1368 MeV. For larger values of the energy the real part of the phase shift then continues to rise, reaching $90^{o}$ at an energy of about 1512 MeV.

Our phase shift is positively increasing but small. At an energy of about 1250 MeV it reaches a value of about $3^{o}$. It then starts decreasing up to an energy of about 1350 MeV, where it becomes zero. It then increases slowly and negatively. For example, at an energy of about 1468 MeV our phase shift becomes about $-2.05^{o}$. This is contrast with the experimental phase shift, which reaches a value of $3^{o}$ at this energy.

Analysis of the signs and magnitudes of the force in this state due to the different exchanges shows that both baryon and vector exchange provide an attractive force. The decuplet contribution is repulsive and strong. The net effect is a slightly attractive force up to about 1350 MeV. It then becomes slightly repulsive.

3. Nonresonant D Wave Amplitudes

a. The $D_{35}$ Amplitude

The experimental phase shift for this state is increasing negatively. It starts at zero and becomes $-7^{o}$ at an energy of about 1368 MeV. Our phase shifts are small and negatively increasing. For example, at an energy of 1165 MeV we obtain a phase shift of $-0.3^{o}$ in comparison with the experimental one of about $-5^{o}$.

Analysis of the signs and magnitudes of the forces in this state from the different exchanges shows that both the baryon and decuplet exchange contributions are attractive. The vector exchange contribution is repulsive but larger than the baryon and decuplet exchange contributions. The net effect is a repulsive force.

b. The $D_{33}$ Amplitude

The experimental phase shift starts at zero and then increases positively. At an energy of 1368 it reaches about $7^{o}$.

Our phase shift is small and positive up to an energy of about 1208 MeV where it reaches about $0.05^{o}$. It then starts to decrease up to an energy of about 1290 MeV, where it reaches zero. At somewhat larger values of the energy, it is negative and small. For example, at an energy of about 1368 MeV our phase shift is about $-0.27^{o}$, in comparison with the experimental phase shift of about $7^{o}$.

Analysis of the signs and magnitudes of the forces in this case from the different exchanges shows that vector and decuplet exchange yield a repulsive force. The baryon exchange contribution is attractive. Baryon exchange dominates up to about 1280 MeV. At

this energy both vector and decuplet exchange dominate over the baryon exchange force. The net effect is then a slightly repulsive force.

D. F Wave Results

1. The 7/2+ Resonances

a. Electric ($\gamma_\mu$) Vector and Baryon Exchange Contributions to the Driving Force.

Here we consider as the input potential the contribution from the $\gamma_\mu$ part of the vector exchange process and the contribution from baryon exchange.[6] We then investigate the 7/2+ baryon resonances by solving the multichannel relativistic Schrödinger equation for the $F_{7/2}$ partial wave amplitudes.

A cutoff of 8.7 BeV is introduced to convert the coupled system of linear integral equations for the scattering amplitude into a Fredholm system. We recall that this was the value of the cutoff required to produce $N^*_{3/2}(1236)$ at its observed experimental energy when only the contribution from baryon exchange was considered as the input potential. We would like to note that in our present calculation a cutoff is not really necessary. The system of integral equations for the scattering amplitude can also be made Fredholm by making the replacement $a_o + b_o + c_o + d_o \to 2\sqrt{s}$ in equations D.3 and D.4. As we have discussed in Chapter V, the effect of such a replacement is to make the potential weaker. Therefore, after making such a replacement we need larger values of the coupling constants to

---

6. The calculations of D.H. showed that both $\rho$ and $N$ exchange were the main contribution to the force in the $F_{37}$ partial wave amplitude.

position a given resonance at its observed experimental energy. However, the qualitative results are the same. Thus results similar to those which we discuss in this section can be obtained without a cutoff. Note that if we introduce the $\sigma_{\mu\nu}$ term of the vector exchange process, we can no longer convert the system of integral equations into a Fredholm system by making the above replacement. This is the main reason we do not take this term into account in this part of the calculation.

1) I = 3/2, Y = 1 State.

Both the coupling constant $\frac{g_{\rho\pi\pi}\, g_{\rho NN}}{4\pi}$ and the cutoff are fixed at values of 1 and 8.7 BeV. We take the coupling constant $\frac{g^2_{\pi N}}{4\pi}$ as a variable parameter, to be fixed by requiring the corresponding eigenphase in this state to go through $90^o$ at an energy of about 1920 MeV. Such a resonance corresponds to $N^*_{3/2}(1920)$. In Figure 7-2 the corresponding eigenphases for values of the coupling constant of 24, 24.6, and 25 are shown. Analysis of that figure shows that for a value of $\frac{g^2_{\pi N}}{4\pi} = 24$, the eigenphase goes through $90^o$ at an energy of about 1978 MeV.

For coupling constants of 24.6 and 25 the $N^*_{3/2}(1920)$ appears at energies of 1913 and 1872 MeV. We note that increasing the coupling constant from 24 to 25 makes the $N^*_{3/2}(1920)$ resonance energy move down by about 5%. For coupling constants of 24, 24.6, and 25, the $N^*_{3/2}(1920)$ appears with a width of 115, 80, or 69 MeV respectively. Thus we see that increasing the coupling constant from 24 to 25 decreases the width of the resonance by about 40%.

Fig. 7-2. Eigenphases for the I = 3/2, Y = +1, $F_{7/2}$ state. Only the contribution from the $\gamma_\mu$ part of the vector exchange process and baryon exchange to the input potential are considered. The solid curve gives the results obtained for the coupling constant $\frac{g^2_{\pi NN}}{4\pi} = 25$. The dashed curve gives the results obtained for the coupling constant $\frac{g^2_{\pi NN}}{4\pi} = 24.6$. The dot-dashed curve gives the result obtained for the coupling constant $\frac{g^2_{\pi NN}}{4\pi} = 24$. We used $\frac{g_{\rho\pi\pi}\, g_{\rho NN}}{4\pi} = 1$ in these calculations.

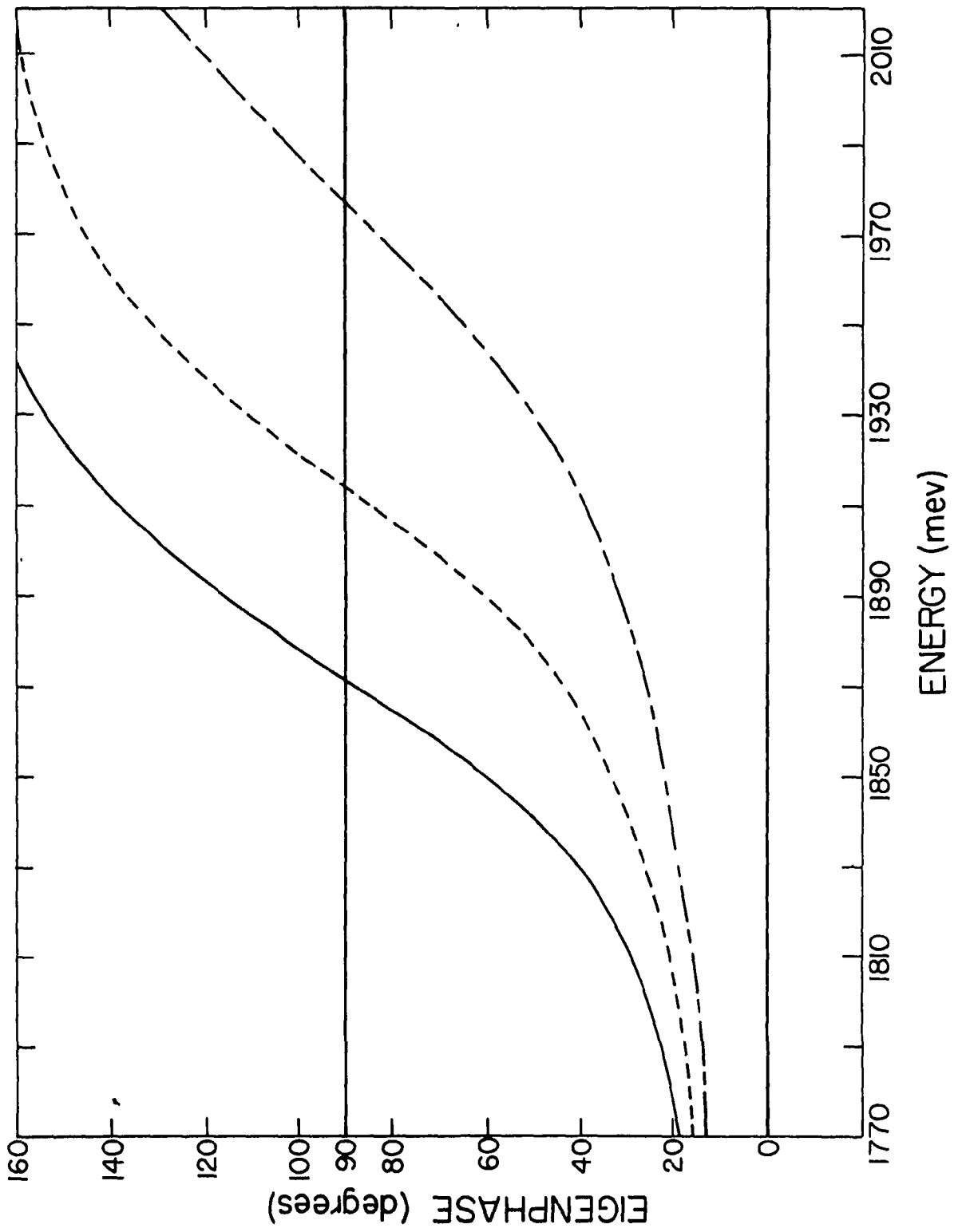
EIGENPHASE (degrees)
160
140
120
100
90
80
60
40
20
0
ENERGY (mev)
1770
1810
1850
1890
1930
1970
2010

ii) Other Isospin States.

If we next consider the other isospin states, we note for a coupling constant of 24 both $Y_1^*(2035)$ and $\Omega^-$ appear at energies of 1932 and 2444 MeV respectively. However, $\equiv^*$ does not appear for this value of the coupling constant. By increasing the coupling constant to 24.6, we then note that all the members of this possible decuplet now appear. With this coupling constant $Y_1^*(2035)$, $\equiv^*$, and $\Omega^-$ now appear at energies of 1844, 2108, and 2384 MeV respectively. With a coupling constant of 25 the energies of $Y_1^*(2035)$, $\equiv^*$, and $\Omega^-$ are now 1924, 2104, and 2360 MeV respectively. For coupling constants of 24, 24.6, or 25 the width of $Y_1^*(2035)$ is 58, 48, or 42 MeV respectively. The width of the $\equiv^*$ is about 26 or 24 MeV for coupling constants for 24.6 or 25 respectively. The $\Omega^-$ width is 79, 76, or 75 MeV for coupling constants of 24, 24.6, or 25 respectively. The main conclusion of the model discussed in this section is that both $\equiv^*$ and $\Omega^-$ seem to be predicted by the model.

iii) Equal Spacing Rule.

As we have discussed in connection with the 3/2+ decuplet, the Gellmann Okubo mass formula predicts an equal spacing rule between consecutive members of a decuplet. Since there are only two members of the possible 7/2+ decuplet which are know experimentally, not much can be deduced from experiment about such a rule in this case. The experimental energy difference between $Y_1^*(2035)$ and $N^*_{3/2}(1920)$ is about 115 MeV. Thus the equal spacing rule would predict the existence of $\equiv^*$ and $\Omega^-$ at energies of about 2150 and 2265 MeV.

Consideration of our results shows the following mass differences

$$M_{Y^*} - M_{N^*} = -70 \text{ or } \quad \text{MeV},$$
$$M_{\equiv^*} - M_{Y^*} = 264 \text{ or } 80 \text{ MeV, and} \tag{7.3}$$
$$M_{\Omega^-} - M_{\equiv^*} = 276 \text{ or } 256 \text{ MeV},$$

for coupling constants of 24.6 or 25.

Analysis of these results shows that even though $\equiv^*$, $Y^*$, and $\Omega^-$ seem to follow an equal spacing rule, $N^*$ does not. The equal spacing rule is not satisfied since the $Y^*$ resonance energy appears below the resonance energy for the $N^*$ for coupling constants of 24 or 24.6, rather than above, as the experimental results seem to indicate. For a coupling constant of 25, $Y^*$ appears above $N^*$ as it should. However, consideration of the $\equiv^*$, $Y^*$, and $\Omega^-$ does seem to indicate a rough validity of the equal spacing rule, at least for these members of the decuplet.

iv) Branching Ratios.

Here we will discuss the branching ratios predicted by this model for each of the members of the 7/2+ decuplet. The model predicts the $N^*_{3/2}(1920)$ to decay mostly into the $\pi N$ channel. The corresponding branching ratio is almost 100%. The $N^*_{3/2}(1920)$ branching ratio into the $K\Sigma$ channel is very small (less than 1%). This agrees with the experimental results, which indicate that the $\pi N$ channel is the main P.B. decay mode for this resonance. Note that the width predicted by our model for $N^*_{3/2}(1920)$ is in agreement with the experimental width since this resonance is experimentally known to decay about 50% into the $\pi N$ channel, and its width is about 200 MeV. Therefore, consideration of only the P.B. channels would yield an experimental width of about 100 MeV for this resonance, which agrees with the width predicted by our model.

Consideration of the $Y_1^*(2035)$ in our model shows that its main decay mode is the $\Lambda\pi$ channel. This agrees with experiment. For coupling constants of 24.6 and 25 we obtain branching ratios for the decay into the $\Lambda\pi$ channel of about 88% and 95%. The $Y_1^*(2035)$ decay branching ratios into the $\Sigma\pi$ and $\bar{K}N$ channels are smaller. Its decay into the $\eta\Lambda$ and $K\Xi$ channels is negligible. The $\Sigma\pi$ decay branching ratio is about 10% for a coupling constant of 24.6. For a coupling constant of 25 it decreases to about 4%. For a coupling constant of 24.6 the $\bar{K}N$ decay branching ratio is about 2%. It decreases to 1% by increasing the coupling constant to 25. Experimentally $Y_1^*(2035)$ decays mainly into the $\Lambda\pi$ channel with a branching ratio of about 25%. The corresponding branching ratio into the $\bar{K}N$ channel is about 16%. The $\Sigma\pi$ branching ratio is smaller and has not yet been measured. Other P.B. decay modes are negligible. Considering only P.B. channels, we would thus expect to obtain for the $Y_1^*(2035)$ about 50% of its experimental width. Thus considering only P.B. channels, we would expect its width to be about 80 MeV. This agrees with the width predicted by this model.

Consideration of $\Xi^*$ shows that this model predicts this state to decay mainly into the $\pi\Xi$ channel. The corresponding branching ratio is about 95% for a coupling constant of 24.6 or about 97% for a coupling constant of 25. It can also decay into the $\bar{K}\Lambda$ and $\bar{K}\Sigma$ channels, but with much smaller branching ratios. For a coupling constant of 24.6 the branching ratios into the $\bar{K}\Lambda$ and $\bar{K}\Sigma$ channels are about 2% and 1% respectively. In principle it can also decay into the $\eta\Xi$

channel, since the resonance energy for $\Xi^*$ is above the $\pi\Xi$ threshold. However, the corresponding branching ratio predicted by this model is negligible. We also note that the $\Xi^*$ predicted by this model has a P.B. width of about 26 MeV. Therefore, if $\Xi^*$ is seen experimentally, we would expect its P.B. width to be smaller than both the N* and Y* widths.

Consideration of the $\Omega^-$ shows that this model predicts this resonance to be a 100% $\bar{K}\Xi$ resonance. This is so, since this is the only P.B. channel which contributes to the I = 0, Y = -2 state. The corresponding $\Omega^-$ width is about 76 MeV. Thus on the basis of this model, we would expect the $\Omega^-$ to appear experimentally with an P.B. width larger than both the $Y_1^*(2035)$ width and the $\Xi^*$ width. However, we expect its width to be smaller than the $N^*_{3/2}(1920)$ width.

b. Vector Baryon, and Decuplet Exchange Contributions to the Driving Force

In this section we reinvestigate the 7/2+ baryon resonances by considering the contributions to the input potential due to vector, baryon, and decuplet exchanges. This discussion differs from section a in that the contribution of the $\sigma_{\mu\nu}$ part of the vector exchange process and also the 3/2+ decuplet exchange contribution are considered. We have stated these last two contributions lead to a divergent potential. Thus to solve the multichannel relativistic Schrödinger equation, we must introduce a cutoff. We choose a cutoff value of 2 BeV. The values for the coupling constants which we use are $\frac{g^2_{\pi NN}}{4\pi} = 14.6$, $\frac{g_{\rho\pi\pi}\, g_{\rho NN}}{4\pi} = 1$, and $\frac{g^2_{N^*N\pi}}{4\pi} = 22.6\ \text{BeV}^{-2}$.

i) I = 3/2, Y = +1 State.

The results for the I = 3/2 , Y = 1 amplitude are shown in Figure 7-3. We note that $N^*_{3/2}(1920)$ now appears in our model at an energy of about 1777 MeV. In addition to requiring a smaller cutoff, the introduction of the additional contributions to the potential due to the $\sigma_{\mu\nu}$ part of the vector exchange process and the 3/2+ decuplet exchange has been to decrease the resonance energies. Also the width of the decuplet members is now greatly reduced. They now appear as narrow resonances.

Analysis of the magnitudes and signs of the forces in this state from the different exchanges shows that vector and baryon exchange provide a strong attractive force. Decuplet exchange also yields an attractive force, but is somewhat smaller than the other forces.

ii) Other Isospin States.

Analysis of other isospin states shows the energy at which they appear is also reduced. For example, Y* appears an an energy of 1814 MeV. We recall that when only the $\gamma_\mu$ part of the vector exchange process and baryon exchange were considered as the input potential, Y* appeared at an energy of about 1844 MeV, when a coupling constant $\frac{g^2_{\pi N}}{4\pi}$ value of 24.6 was used. Thus we note that the effect of the additional contributions to the potential matrix has decreased the Y* resonance energy by about 30 MeV. We recall that when only the $\gamma_\mu$ contribution of the vector exchange process and the baryon exchange process are taken as the input potential, Y* appeared at a somewhat

Fig. 7-3. Eigenphase for the I = 3/2, Y = +1, $F_{7/2}$ state for coupling constants of $\frac{g^2_{\pi NN}}{4\pi} = 14.6$, $\frac{g_{\rho\pi\pi}\, g_{\rho NN}}{4\pi} = 1$, and $\frac{g^2_{N^*N\pi}}{4\pi} = 22.6$ $BeV^{-2}$. The contributions from vector, baryon, and decuplet exchange to the input potential are considered. A cutoff of 2 BeV is used.

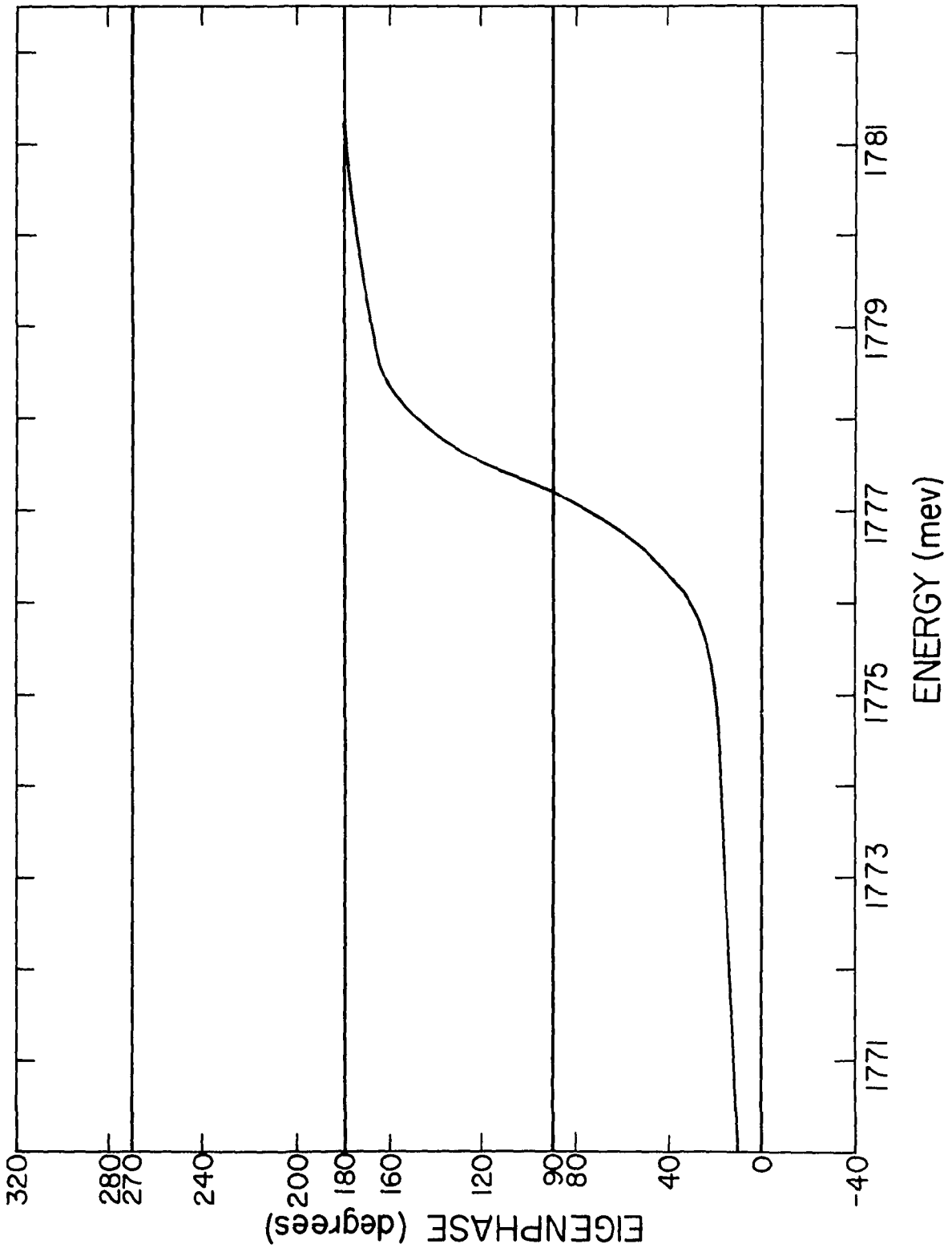
EIGENPHASE (degrees)
320
280
270
240
200
180
160
120
90
80
40
0
-40
1771
1773
1775
1777
1779
1781
ENERGY (mev)

smaller energy than $N^*_{3/2}$ for coupling constants $\frac{g^2_{\pi N}}{4\pi}$ of 24 and 24.6. However, after the $\sigma_{\mu\nu}$ part of the vector exchange process and the 3/2+ decuplet exchange contributions are added to the potential, this feature is no longer present when we fix $\frac{g^2_{\pi N}}{4\pi}$ at its experimental value. In fact, Y* now appears at an energy of 1814 MeV, which is above the energy at which $N^*_{3/2}(1920)$ appears as a resonance in this model (about 1777 MeV). Also $\equiv^*$ and $\Omega^-$ now appear at energies of about 2070 and 2285 MeV.

We note that the mass differences between members of the decuplet are now

$$\begin{aligned} M_{Y^*} - M_{N^*} &= 37 \text{ MeV}, \\ M_{\equiv^*} - M_{Y^*} &= 256 \text{ MeV}, \quad \text{and} \\ M_{\Omega^-} - M_{\equiv^*} &= 215 \text{ MeV}. \end{aligned} \tag{7.4}$$

Thus the equal spacing rule is approximately satisfied for $Y^*$, $\equiv^*$, and $\Omega^-$. However, this is not the case for N*. This is the same conclusion we had made when discussing both the $\gamma_\mu$ contribution of the vector exchange process and the baryon exchange contribution to the input potential. We note that even though Y* is now heavier than N* (in contrast to the case when only the $\gamma_\mu$ part of the vector exchange process and baryon exchange were considered and the value $\frac{g^2_{\pi N}}{4\pi}$ = 24 or 24.6 was used) the equal spacing rule is still not satisfied in this mode

Analysis of the branching ratios shows that $N^*_{3/2}(1920)$ appears as mostly a $\pi N$ resonance. The decay branching ratio into this channel is almost 100%. This is similar to our results when we considered the $\gamma_\mu$ part of the vector exchange force and the baryon

exchange contributions. It is in agreement with the experimental results.

Analysis of the other isospin states shows that Y * decays mostly into the $\Lambda\pi$ channel. The corresponding branching ratio is about 62%. It can also decay into the $\Sigma\pi$ and $\bar{K}N$ channels. The corresponding branching ratios are about 37% and 1%. The branching ratios into the $\eta\Lambda$ and $K\Xi$ channels is negligible. We note that this is the same qualitative conclusion we had reached when considering only the contribution from the $\gamma_\mu$ part of the vector exchange process and baryon exchange to the input potential.

Similarly consideration of the $\Xi^*$ shows that its main decay mode is the $\pi\Xi$ channel. It can also decay into the $\bar{K}\Lambda$ channel. However, the corresponding branching ratio is much smaller. The branching ratio for its decay into the $\bar{K}\Sigma$ channel is even smaller. Even though it can also decay into the $\eta\Xi$ channel, the corresponding branching ratio is negligible. These are the same conclusions we had reached before.

Since only one channel contributes to the $\Omega^-$ state $(\bar{K}\Xi)$, we conclude that the model predicts the $\Omega^-$ to decay 100% into the $\bar{K}\Xi$ channel.

2. The 5/2+ Resonances

a. Electric ($\gamma_\mu$) Vector Exchange Contributions to the Driving Force

Here we consider the contribution from the $\gamma_\mu$ part of the vector exchange process as the input potential.[7] We then investigate

---

7. The calculations of D.H. showed that $\rho$ exchange was the main contribution to the force in the $F_{15}$ partial wave amplitude.

the 5/2+ baryon resonances by solving the multichannel relativistic Schrödinger equation for the $F_{5/2}$ partial wave amplitudes. A cutoff of 8.7 BeV is introduced to convert the system of coupled integral equations for the scattering amplitude into a Fredholm system. We recall this was the value of the cutoff required to produce the $N_{3/2}^*(1236)$ at its observed experimental energy when only the contribution from baryon exchange was considered as the input potential. This was discussed in Chapter VI. We consider only the $\gamma_\mu$ contribution of the vector exchange process for the same reason as discussed in connection with the 7/2+ resonances.

1) $I = \frac{1}{2}$, $Y = 1$ State.

The cutoff is fixed at a value of 8.7 BeV. We take the coupling constant $\frac{g_{\rho\pi\pi}\, g_{\rho NN}}{4\pi}$ as a variable parameter. In Figure 7-4 the eigenphases for the $I = \frac{1}{2}$, $Y = 1$ state for coupling constant values of 1.0 and 2.0 are shown. We note that for a coupling constant of one, the eigenphase increases slowly. We obtain a broad resonance at a very large energy. For a coupling constant of 2.0, we obtain a resonance corresponding to $N_{\frac{1}{2}}^*(1688)$ at an energy of about 2390 MeV. By further increasing the coupling constant we can move the resonance down. However, this requires a value of $\frac{g_{\rho\pi\pi}\, g_{\rho NN}}{4\pi}$ much larger than the experimental value. Analysis of Figure 7-4 indicates the eigenphase corresponding to the $\eta N$ channel seems to resonate even for a coupling constant of 2.0. To lower the resonance position of $N_{\frac{1}{2}}^*$ (considering only the $\gamma_\mu$ part of the vector exchange process as the input potential) we must increase the attraction by a large amount.

Fig. 7-4. Eigenphases for the $I = \frac{1}{2}$, $Y = +1$, $F_{5/2}$ state. Only the contribution from the $\gamma_\mu$ part of the vector exchange process to the input potential is considered. The solid curve given the results obtained for the coupling constant $\frac{g_{\rho\pi\pi}\, g_{\rho NN}}{4\pi} = 1$. The dotted curve gives the results obtained for the coupling constant $\frac{g_{\rho\pi\pi}\, g_{\rho NN}}{4\pi} = 2$.

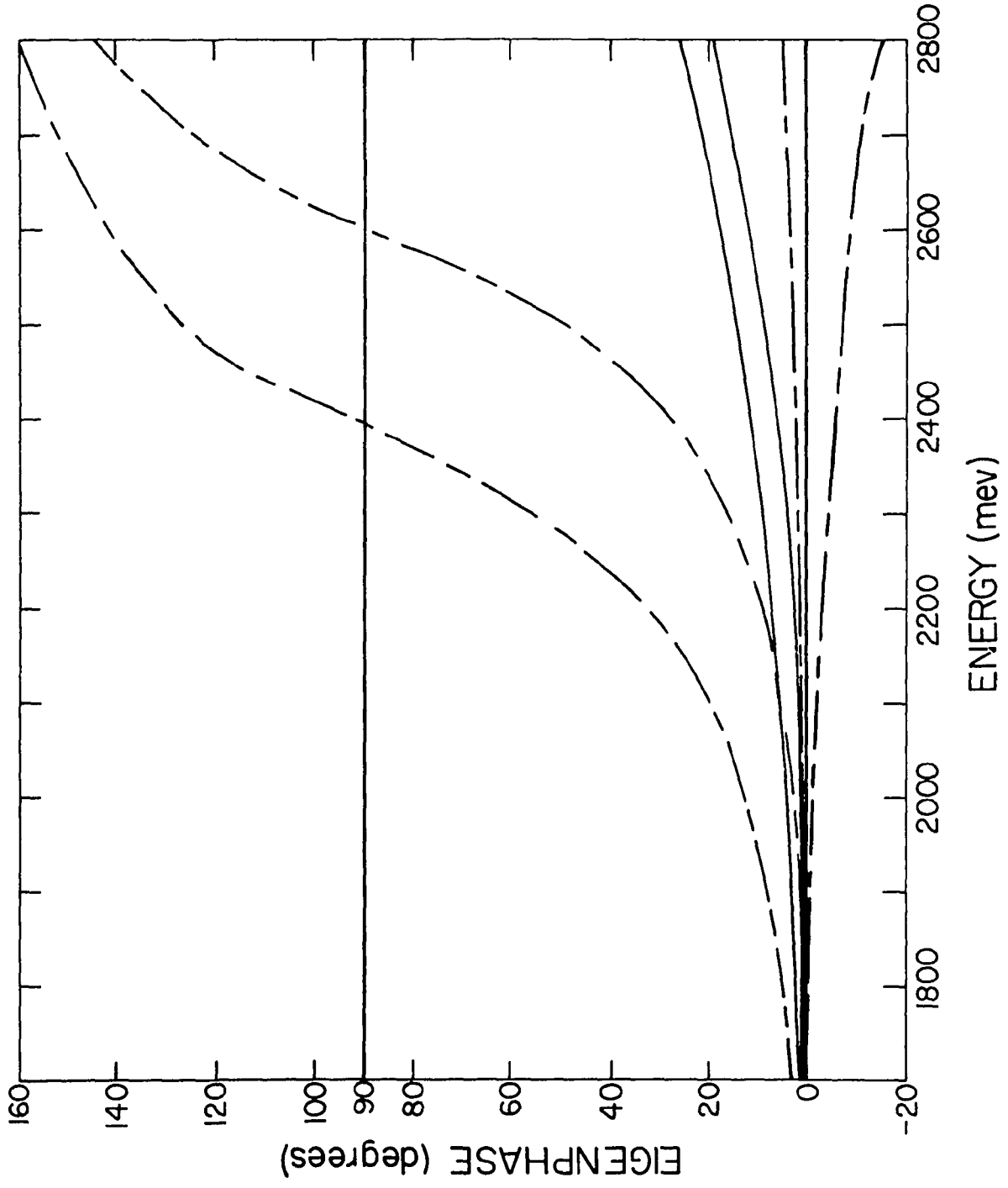
EIGENPHASE (degrees)
160
140
120
100
90
80
60
40
20
0
-20
1800
2000
2200
2400
2600
2800
ENERGY (mev)

For a coupling constant of 2.0, $N\frac{1}{2}(1688)$ appears with a width of about 333 MeV.

ii) Other Isospin States.

Analysis of the other isospin states shows that for a coupling constant of 2.0, all the members of the octet appear with energies and widths larger than the experimental values. The $Y_1^*(1910)$, $Y_o^*(1820)$, and $\Xi^*(1930)$ appear at energies of 2600, 2540, and 3064 respectively. Their corresponding widths are 309, 900, and 690 MeV. We wish to note that the mass ordering is the same as the experimental one. The width ordering is the same as the experimental one, except in the case of $Y_1^*(1910)$ and $\Xi^*(1930)$. In the model $\Xi^*(1930)$ appears with a larger width than $Y_1^*(1910)$ which is not the case experimentally.

The model predicts

$$\frac{M_{N^*} + M_{\Xi^*}}{2} = 2727 \text{ MeV and}$$

$$\frac{3M_{Y_o^*} + M_{Y_1^*}}{4} = 2555 \text{ MeV.} \qquad (7.5)$$

This is compared with experimental values of

$$\frac{M_{N^*} + M_{\Xi^*}}{2} = 1809 \text{ MeV and}$$

$$\frac{3M_{Y_o^*} + M_{Y_1^*}}{4} = 1842 \text{ MeV.} \qquad (7.6)$$

We observe that the masses obtained in this model seem to satisfy the Gellmann Okubo mass formula to about 6%.

The $N^*\frac{1}{2}(1688)$ is predicted by this model to decay mainly into the $\pi N$ channel. The corresponding branching ratio obtained with a coupling constant of 2.0 is about 94%. It can also decay into the $\eta N$, $K\Lambda$, and $K\Sigma$ channels. The corresponding branching ratios are much smaller. For a coupling constant of 2.0 these branching ratios have the numerical values of about 3%, 2%, and 1% respectively.

The $Y_1^*(1910)$ is predicted by this model to decay mainly into the $\Lambda\pi$ channel. For a coupling constant of 2.0 the corresponding branching ratio is about 68%. Another channel in which it can decay is the $\bar{K}N$ channel. The corresponding branching ratio obtained with a coupling constant of 2.0 is about 20%. The $Y_1^*(1910)$ can also decay into the $\Sigma\pi$ and $\eta\Sigma$ channels. The corresponding branching ratios obtained with the same value of the coupling constant are about 9% and 3%.

The $Y_0^*(1820)$ is predicted by this model to decay mainly into the $\pi\Sigma$ and $\bar{K}N$ channels. The corresponding branching ratios obtained with a coupling constant of 2.0 are about 59% and 33%. It can also decay into the $\eta\Lambda$ and $K\Xi$ channels. The corresponding branching ratios are smaller. For the same value of the coupling constant they have the numerical values of about 7% and 1% respectively.

The $\Xi^*(1930)$ is predicted to decay mainly into the $\pi\Xi$ channel. For a coupling constant of 2.0 the corresponding branching ratio is about 96%. It can also decay into the $\bar{K}\Lambda$ and $\bar{K}\Sigma$ channels. The corresponding branching ratios obtained with the same coupling constant

are about 3% and 1%. Even though the decay of $\Xi^*(1930)$ into the $\pi\Xi$ channel is also energetically allowed, the corresponding branching ratio is negligible.

b. Vector, Baryon, and Decuplet Exchange Contributions to the Driving Force

In this section we reinvestigate the 5/2+ resonances by considering the contributions to the input potential due to vector, baryon, and decuplet exchange . We differ from section a in that we have added the contributions from the $\sigma_{\mu\nu}$ part of the vector exchange process and baryon and decuplet exchange . We solve the multichannel relativistic Schrödinger equation with this input potential. We use a cutoff value of 2 Bev. This is the same cutoff we used when discussing the 7/2+ decuplet. The values for the coupling constants which we use are $\frac{g^2_{\pi N}}{4\pi} = 14.6$, $\frac{g_{\rho\pi\pi}g_{\rho NN}}{4\pi} = 1$, and $\frac{g^2_{N^*N\pi}}{4\pi} = 22.6 \text{ Bev}^{-2}$.

i) $I = \frac{1}{2}$, $Y = +1$ State.

The results for this case of the $I = \frac{1}{2}$, $Y = +1$ amplitude are shown in figure 6-5. We note that the $N^*_{\frac{1}{2}}(1688)$ now appears at an energy of 1665 Mev. Thus we observe that the effect of introducing the additional exchanges has been to decrease the cutoff and the energies at which the resonances appear. We recall that considering only the $\gamma_\mu$ contribution of the vector exchange process with a cutoff of 8.7 Bev, we obtained $N^*\frac{1}{2}(1688)$ at an energy of 2390 Mev. After inclusion of the additional exchanges, the cutoff moves down to 2 Bev, and the resonance energy decreases from 2390 Mev to about 1665 Mev. Also we are now using

$\frac{g_{\rho\pi\pi} g_{\rho NN}}{4\pi} = 1$, rather than 2, as we used in the previous calculation. We must also note that inclusion of the additional exchanges decreases the width considerably. The F. resonances now appear as narrow resonances.

ii) Other Isospin States.

Considering the other isospin states we observe that $Y_1^*(1910)$ and $Y_0^*(1820)$ appear in our model at energies of 1841 Mev and 1810 Mev. Also $\Xi^*$ appears at an energy of about 1970 Mev. This is compared with its experimental energy of about 1930 Mev.

iii) Mass Formula.

From this model we obtain

$$\frac{M_{N^*} + M_{\Xi^*}}{2} = 1817 \text{ Mev and}$$

$$\frac{3M_{Y_0^*} + M_{Y_1^*}}{4} = 1818 \text{ Mev.} \qquad (7.6)$$

This is compared with the experimental results of

$$\frac{M_{N^*} + M_{\Xi^*}}{2} = 1809 \text{ Mev and}$$

$$\frac{3M_{Y_0^*} + M_{Y_1^*}}{4} = 1842 \text{ Mev.} \qquad (7.7)$$

Thus we see that the Gellmann Okubo mass formula seems to be satisfied for this octet of resonances to better than 1%.

iv) Branching Ratios.

The $N^*\frac{1}{2}(1688)$ appears in this model as a resonance which decays mainly into the $\pi N$ channel. The corresponding branching ratio is

Fig. 7-5. Eigenphase for the $I = \frac{1}{2}$, $Y = +1$, $F_{5/2}$ state for the coupling constants $\frac{g^2_{\pi NN}}{4\pi} = 14.6$, $\frac{g_{\rho\pi\pi}g_{\rho NN}}{4\pi} = 1$, and $\frac{g^2_{N^*N\pi}}{4\pi} = 22.6$ Bev$^{-2}$. The contributions from vector, baryon, and decuplet exchange to the input potential are considered. A cutoff of 2 Bev is used.

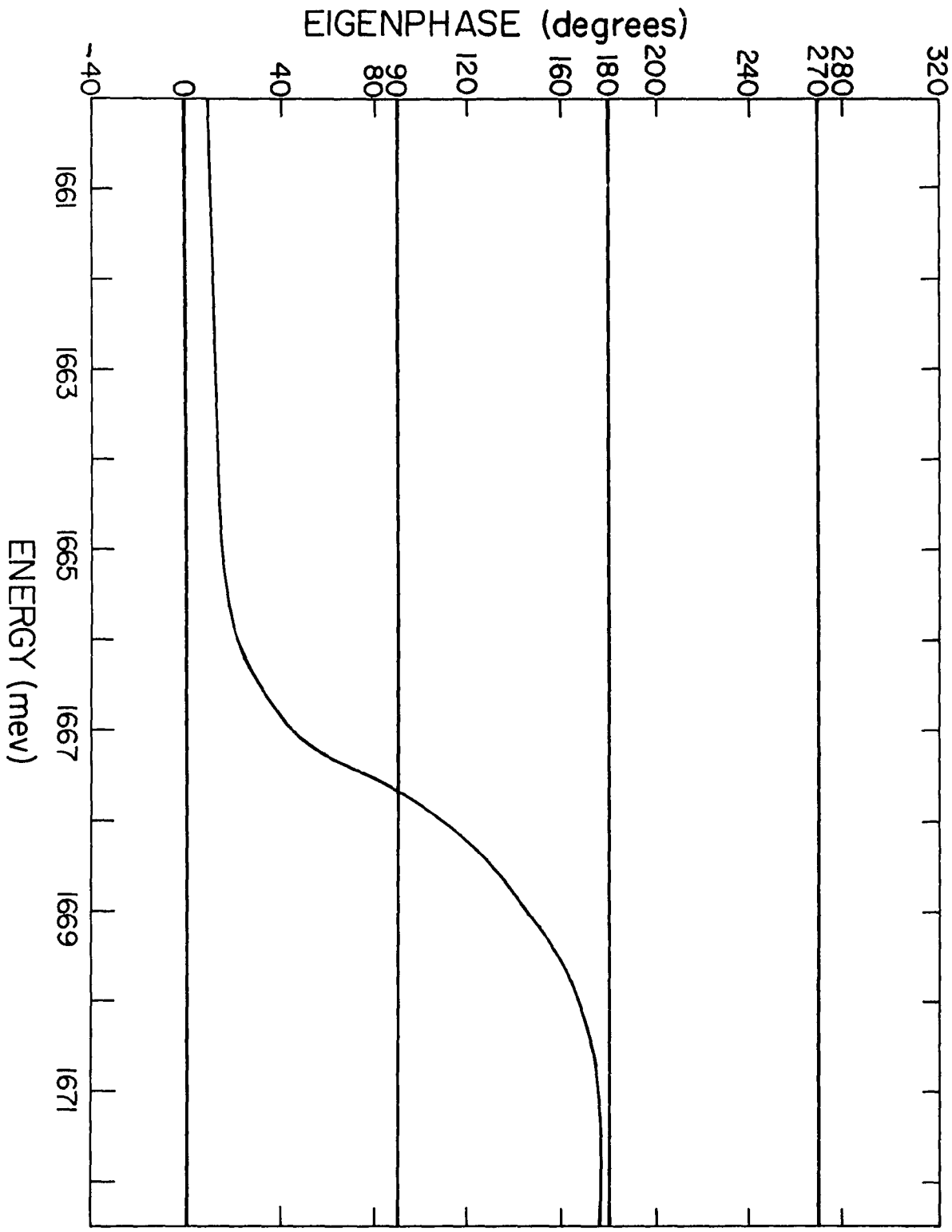
EIGENPHASE (degrees)
-40
0
40
80
90
120
160
180
200
240
270
280
320
ENERGY (mev)
1661
1663
1665
1667
1669
1671

almost 100%. The branching ratios of the other possible P.B. channels in which it can decay are negligible.

The $Y_1^*(1910)$ appears in this model as a resonance which decays mainly into the $\pi\Lambda$ channel. The corresponding branching ratio is about 68%. Another P.B. channel in which it can decay is the $\bar{K}N$ channel. The corresponding branching ratio is about 14%. It can also decay into the $\pi\Sigma$ and $\eta\Sigma$ channels. The corresponding branching ratios are about 11% and 7%.

The model predicts $Y_0^*(1820)$ to be a resonance which decays mainly into the $\bar{K}$ N channel. The corresponding branching ratio is about 99%. It can also decay into the $\pi\Sigma$ and $\eta\Lambda$channels. However, the corresponding branching ratios for each of these channels is small (about ½%). The branching ratio into the $K\Xi$ channel is negligible.

The $\Xi^*(1930)$ is predicted by the model to be a resonance which decays mainly into the $\pi\Xi$ channel. The corresponding branching ratio is large (about 98%). The branching ratios into the $\bar{K}\Lambda$, $\bar{K}\Sigma$, and $\eta\Xi$ channels are small and of the same order of magnitude (less than 1%).

3. Nonresonant F Wave Amplitudes

a. The $F_{17}$ Amplitude

The experimental phase shift for this state is small (practically zero) and positive up to an energy of about 1368 Mev. Our phase shifts are positive and small but increase slightly for larger energies. For example, at an energy of 1188 Mev our phase shift is about $0.0023^{\circ}$. At an energy of 1368 Mev our phase shift is now

slightly larger ($0.69^{o}$). Analysis of the contributions to this amplitude from the different exchanges shows that both vector and decuplet exchange give attractive forces. The baryon exchange contribution is strong and repulsive. The contributions from the vector and decuplet exchange are of the same order of magnitude. The net result is a slightly attractive force.

b. The $F_{35}$ Amplitude

The experimental phase shift start at zero and increase positively to an energy of about 1180 Mev. At this energy it reaches a maximum of about $0.08^{o}$. It then starts decreasing and reaches zero at an energy of about 1267 Mev. At energies larger than 1267 Mev the phase shift then increases negatively and slowly. At an energy of about 1368 Mev, it is about $-0.15^{o}$.

Our phase shifts are negatively increasing and small. For example, at an energy of 1368 Mev our phase shift is about $-0.20^{o}$ in comparison with the experimental phase shift of about $-0.15^{o}$.

Analysis of the contributions to this amplitude from the different exchanges shows that both vector and baryon exchange yield a repulsive contribution. The contribution from decuplet exchange is attractive. Each of these contributions is essentially of the same order of magnitude. Thus the net effect is a slightly repulsive force.

# VIII. SUMMARY AND CONCLUSIONS

We have studied a model for scattering of the pseudoscalar meson octet by the baryon octet in the four lowest partial waves. Actual physical masses of the particles were used, so that SU(3) symmetry was broken. Our model made use of the relativistic Schrödinger equation as the dynamical equation. The potential which we used in this equation was obtained by computing allowed single particle exchange processes for which the exchange particles have spin less than or equal to 3/2, following some simple rules.

Different techniques which are generally used in determining scattering amplitudes were reviewed. In this review emphasis was placed on their advantages and disadvantages. The purpose of this discussion was to note that as of yet there are no perfect calculational tools, and there is certainly a need for other techniques. The relativistic Schrödinger equation was then considered as an example of another possible technique. To justify the possible use of the relativistic Schrödinger equation to obtain scattering amplitudes a brief discussion of its properties was given. We noted that this equation obeyed two particle unitarity, relativistic invariance, and macrocausality. We then concluded that this equation was an acceptable tool to be used in determining scattering amplitudes. In fact, we indicated that it may even be a better approximation than other techniques based on the N/D method, since it includes iterations of the potential.

The Blankenbecler-Sugar equation and its relation to the relativistic Schrödinger equation was discussed. It was observed that the Blankenbecler-Sugur equation is nothing more than a relativistic Schrödinger equation with a special prescription for computing the potential and the propagator. However, we noted that such a prescription is not unique. It depends on the choice of coordinate frame. Thus no simple rule for determining the potential can be "derived" starting from two particle unitarity and the Bethe-Salpeter equation.

We should not expect simple dynamical models to predict exact locations and widths of resonances, since they are known to be sensitive to many dynamical effects which are not fully understood. We wish to emphasize our opinion that the main point to be learned from our calculations is that use of the multichannel relativistic Schrödinger equation yields results which are in qualitative agreement with those obtained using other techniques such as the N/D method. Thus the qualitative features of the results obtained in these calculations seem to be roughly independent of the technique employed in performing them.

Our results indicate that phase shifts, resonance positions, and branching ratios obtained in this model are usually in rough agreement with experiment. However, widths did not always agree with experiment. The main triumph of the model consisted in accounting for most of the experimentally known baryon resonances.

Study of the $S_{\frac{1}{2}}$ amplitudes showed the existence of a unitary singlet (the $Y_0^*(1405)$), an octet of resonances (with both the I = 1,

Y = 0, and I = 0, Y = 0 states missing) to which $N^*_{\frac{1}{2}}(1570)$ belongs, and a decuplet of resonances to which $N^*_{3/2}(1670)$ belongs.

Study of the $P_{\frac{1}{2}}$ amplitudes showed the existence of an octet of states consisting of N(939), $\Lambda(1115)$, $\Sigma(1193)$, and $\Xi(1318)$. No resonance corresponding to $N^*_{\frac{1}{2}}(1400)$ was obtained.

Study of the $P_{3/2}$ amplitudes showed the existence of a decuplet of resonances consisting of $N^*_{3/2}(1236)$, $Y_1^*(1385)$, $\Xi^*(1529)$, and $\Omega^-(1675)$.

Study of the $D_{3/2}$ amplitudes showed the existence of a nonet of resonances consisting of $N^*_{\frac{1}{2}}(1525)$, $Y_1^*(1660)$, $Y_o^*(1520)$, $Y_o^*(1700)$, and $\Xi^*(1815)$.

Study of the $D_{5/2}$ amplitudes did not show any resonant behavior.

Study of the $F_{5/2}$ amplitudes showed the existence of an octet of resonances consisting of $N^*_{\frac{1}{2}}(1688)$, $Y_o^*(1820)$, $Y_1^*(1910)$, and $\overset{*}{\Xi}(1930)$.

Study of the $F_{7/2}$ amplitudes showed the existence of a decuplet of resonances consisting of $N^*_{3/2}(1920)$, $Y_1^*(2035)$, $\Xi^*(2150)$, and $\Omega^-(2265)$.

# Appendix A. SU(2) and SU(3) Considerations

## 1. General Considerations and Notation

This appendix will give the appropriate crossing coefficients by which we must multiply the momentum dependence of the potentials given in Appendix D to obtain the complete potentials. To reiterate, we shall assume invariance under the three dimensional unitary group SU(3) insofar as to obtain relations between coupling constants, but we break the symmetry in the sense that we use physical masses for both the exchanged and the incoming and outgoing particles. The SU(3) crossing coefficients can be obtained by merely writing out the Lagrangian and multiplying the coupling constants for particles in the process in question by the appropriate isotopic spin factor.

In the case of perfect SU(3) symmetry, however, it is easier to compute the SU(3) crossing coefficients directly by expanding the SU(3) field operators in the exchange diagram into SU(3) irreducible tensors in the s channel and then taking matrix elements between physical states.

We compute our coefficients by a combination of both methods. In fact in many cases only one particle is exchanged, due to simple conservation laws like isospin, G parity and hypercharge. Thus once we compute the crossing coefficient in the limit of perfect SU(3) we already have it in the broken case.

In other cases, however, more than one particle can be exchanged. An example of this is the case of $\Lambda$ and $\Sigma$ exchange. Then we must compute the crossing coefficient directly as explained before.

We denote the baryon octet by $B^i_k$, the pseudoscalar meson octet by $P^i_k$ and the vector meson octet by $V^\mu_k$, where $\mu$, k run from 1 to 3 and $\mu$ is a Lorentz index characterizing the vector mesons. The explicit elements of each of the above are more conveniently shown in terms of the usual matrices which follow

$$B^i_k = \begin{pmatrix} \frac{\Sigma^o}{\sqrt{2}} + \frac{\Lambda}{\sqrt{6}} & \Sigma^+ & p \\ \Sigma^- & -\frac{\Sigma^o}{\sqrt{2}} + \frac{\Lambda}{\sqrt{6}} & n \\ \Xi^- & \Xi^o & -\frac{2}{\sqrt{6}}\Lambda \end{pmatrix},$$

$$P^\mu_k = \begin{pmatrix} \frac{\pi^o}{\sqrt{2}} + \frac{\eta}{\sqrt{6}} & \pi^+ & K^+ \\ \pi^- & -\frac{\pi^o}{\sqrt{2}} + \frac{\eta}{\sqrt{6}} & K^o \\ K^- & \bar{K}^o & -\frac{2}{\sqrt{6}}\eta \end{pmatrix}, \text{ and}$$

$$\tilde{V}^i_j = \begin{pmatrix} \frac{\rho^o}{\sqrt{2}} + \frac{\varphi_o}{\sqrt{6}} + \frac{\omega_o}{\sqrt{3}} & \rho^+ & K^{*+} \\ \rho^- & -\frac{\rho^o}{\sqrt{2}} + \frac{\varphi_o}{\sqrt{6}} + \frac{\omega_o}{\sqrt{3}} & K^{*o} \\ K^{*-} & \bar{K}^{*o} & -\frac{2\varphi_o}{\sqrt{6}} + \frac{\omega_o}{\sqrt{3}} \end{pmatrix}$$

In the above the symbols stand for the field operators which destroy the corresponding particles. We have denoted the vector meson matrix by $\tilde{V}^1_j$ rather than $V^i_j$ because we have introduced the singlet vector meson $\omega_o$. The octet part $V^i_j$ is obtained by merely subtracting this term divided by $\sqrt{3}$ along the diagonal.

2. $\varphi$, $\omega$ mixing.

We will now review the so-called $\varphi$, $\omega$ mixing (Sakurai, 1962). Since both $\varphi_o$ and $\omega_o$ have identical quantum numbers, one expects mixing between them. The physical states $\varphi$ and $\omega$ are related to $\varphi_o$ and $\omega_o$ by

$$\varphi = \cos\alpha\, \varphi_o + \sin\alpha\, \omega_o$$

and (A.1)

$$\omega = -\sin\alpha\, \varphi_o + \cos\alpha\, \omega_o$$

and are eigenstates of the total Hamiltonian

$$H = H_o + H_1$$

where $H_o$ is invariant under SU(3) and $H_1$ is a perturbation.

One is then led to diagonalize the mass submatrix given by

$$\begin{pmatrix} M_8^2 + \epsilon_{11} & \epsilon_{12} \\ \epsilon_{21} & M_1^2 + \epsilon_{22} \end{pmatrix}$$

where $\epsilon_{12} = \epsilon_{21} = \langle 8|H_1|1\rangle$, $\epsilon_{11} = \langle 8|H_1|8\rangle$, $\epsilon_{22} = \langle 1|M_1|1\rangle$, and where

$M_8^2$ and $M_1^2$ represent the corresponding SU(3) limit masses for the octet and the singlet respectively.

Requiring $\varphi$ and $\omega$ to be eigenstates of the above matrix we obtain

$$(\tan\alpha)^2 = \frac{m_\varphi^2 - m_8^2}{m_8^2 - m_\omega^2} \tag{A.2}$$

where $m_8^2 = m_8^2 + \epsilon_{11}$ is the value given by the mass formula for the octet

$$2m_{k^*}^2 = \frac{3}{2} m_8^2 + \frac{1}{2} m_p^2 .$$

By inserting the known values of $m_{k^*}$ and $m_\rho$ one obtains $m_8 \approx 930$ MeV. Substituting into (A.2) we obtain

$$(\tan\alpha)^2 = \frac{1020 - 930}{930 - 783} = 0.61.$$

The value obtained using the quark model with the usual assumptions is $(\tan\alpha)^2 = 0.50$. We shall, for simplicity, merely use this result.

Thus we have

$$\varphi = -\sqrt{\frac{2}{3}}\,\varphi_o + \sqrt{\frac{1}{3}}\,\omega_o$$

and (A.3)

$$\omega = \sqrt{\frac{1}{3}}\,\varphi_o + \sqrt{\frac{2}{3}}\,\omega_o .$$

Expressing $\tilde{V}^i_j$ in terms of physical particles, we then obtain

$$\tilde{V}^i_j = \begin{pmatrix} \frac{\rho^o}{\sqrt{2}} + \frac{\omega}{\sqrt{2}} & \rho^+ & K^{*+} \\ \rho^- & -\frac{\rho^o}{\sqrt{2}} + \frac{\omega}{\sqrt{2}} & K^{*o} \\ K^{*-} & \bar{K}^{*o} & \varphi \end{pmatrix} .$$

3. Direct Product of Two Octets

If we consider the direct product of two octets characterized by irreducible tensors $\Psi^i_j$ and $\varphi^k_\ell$ respectively, we obtain[1]

$$\Psi^i_j \varphi^k_\ell = T^{ik}_{j\ell} + \frac{1}{\sqrt{30}} [-2\delta^1_j \theta^k_{s\ell} - 2\delta^k_\ell \theta_{s_j}{}^1 + 3\delta^k_j \theta_{s\ell}{}^1 + 3\delta^i_\ell \theta_{sj}{}^k]$$

$$+ [\frac{1}{2\sqrt{2}} \delta^i_\ell \delta^k_j - \frac{1}{6\sqrt{2}} \delta^i_j \delta^k_\ell] S + \frac{1}{\sqrt{2}} \epsilon_{\rho j\ell} D^{\rho ik} + \frac{1}{\sqrt{2}} \epsilon^{\rho ik} \bar{D}_{\rho j\ell}$$

$$+ \frac{1}{\sqrt{6}} [\delta^k_j \theta_{a\ell}{}^1 - \delta^i_\ell \theta_{aj}{}^k], \qquad (A.4)$$

where

$$S = \frac{1}{\sqrt{8}} \Psi^\alpha_\beta \varphi^\beta_\alpha ,$$

1. This corresponds to the well-known reduction:
$8 \otimes 8 = 1 + 8_1 + 8_2 + 10 + \overline{10} + 27$.

$$\theta_{sj}^{\ i} = \sqrt{\frac{3}{10}}\ (\Psi^1_\alpha \varphi^\alpha_j + \Psi^\alpha_j \varphi^1_\alpha - \frac{2}{3}\ \delta^i_j \Psi^\alpha_\beta\ \varphi^\beta_\alpha),$$

$$\theta_{aj}^{\ i} = \sqrt{\frac{1}{6}}\ (\Psi^1_\alpha \varphi^\alpha_j - \Psi^\alpha_j \varphi^i_\alpha),$$

$$D^{1jk} = \frac{1}{6\sqrt{2}}[\epsilon^{i\alpha\beta}\ \Psi^j_\alpha \varphi^k_\beta + \epsilon^{1\alpha\beta}\ \Psi^k_\alpha \varphi^J_\beta + \epsilon^{J\alpha\beta}\ \Psi^k_\alpha \varphi^1_\beta + \epsilon^{j\alpha\beta}\ \Psi^i_\alpha \varphi^k_\beta$$

$$+ \epsilon^{k\alpha\beta}\ \Psi^1_\alpha \varphi^j_\beta + \epsilon^{k\alpha\beta}\ \Psi^J_\alpha \varphi^i_\beta\ ],$$

$$\overline{D}_{ijk} = \frac{1}{6\sqrt{2}}[\ \epsilon_{i\alpha\beta} \Psi^\alpha_j \varphi^\beta_k + \epsilon_{i\alpha\beta}\ \Psi^\alpha_k \varphi^\beta_J + \epsilon_{j\alpha\beta}\ \Psi^\alpha_k \varphi^\beta_1 + \epsilon_{j\alpha\beta}\ \Psi^\alpha_i \varphi^\beta_k$$

$$+ \epsilon_{k\alpha\beta}\ \Psi^\alpha_i\ \varphi^\beta_J + \epsilon_{k\alpha\beta}\ \Psi^\alpha_J\ \varphi^\beta_1], \quad \text{and}$$

$$T^{ik}_{j\ell} = \frac{1}{4}\ [\Psi^i_j\ \varphi^k_\ell + \Psi^k_j\ \varphi^i_\ell + \Psi^i_\ell\ \varphi^k_J + \Psi^k_\ell\ \varphi^i_J] - \frac{1}{20}\ [\delta^i_J(\Psi^k_\alpha\ \varphi^\alpha_\ell + \Psi^\alpha_\ell\ \varphi^k_\alpha)$$

$$+ \delta^k_J(\Psi^i_\alpha\ \varphi^\alpha_\ell + \Psi^\alpha_\ell\ \varphi^i_\alpha) + \delta^i_\ell(\Psi^k_\alpha\ \varphi^\alpha_j + \Psi^\alpha_J\ \varphi^k_\alpha) + \delta^k_\ell(\Psi^1_\alpha\ \varphi^\alpha_j + \Psi^\alpha_j\ \varphi^1_\alpha\ ]$$

$$+ \frac{1}{40}\ [\delta^1_j\ \delta^k_\ell + \delta^i_\ell\ \delta^k_j\ ]\Psi^\beta_\alpha\ \varphi^\alpha_\beta$$

## 4. General Expression for SU(2) Crossing Coefficients

For completeness we will discuss in this section the general expressions for SU(2) crossing coefficients in terms of Racah coefficients as given by Mandelstam et al. (1962) and Carruthers and Krisch (1965). Consider two body reactions of the type

s channel: $a + b \rightarrow c + d$,

t channel: $a + \bar{c} \rightarrow \bar{b} + d$, and

u channel: $a + \bar{d} \rightarrow c + \bar{b}$ .

This is shown in Figure A-1.

Crossing symmetry asserts that if the invariants s, t, and u are continued to the physical domain of a crossed channel, the continued amplitude describes the process in question. Explicitly that is

$$\langle cd|T_s|ab\rangle = \xi_{su} \langle c\bar{b}|T_u|a\bar{d}\rangle \tag{A.5}$$

and

$$\langle cd|T_s|ab\rangle = \xi_{st} \langle \bar{b}d|T_t|a\bar{c}\rangle, \tag{A.6}$$

where $\xi_{su}$ and $\xi_{st}$ are phases which are determined by requiring states to transform according to the Condon and Shortley phase convention so as to allow us to use the usual tables of Clebsch Gordan coefficients.

We then use isospin conservation to write

$$\langle cd|T_s|ab\rangle = \sum_{s'} T_s(s')\, C(abs';\, \alpha\beta)\, C(cds';\, \gamma\delta), \tag{A.7}$$

$$\langle c\bar{b}|T_u|a\bar{d}\rangle = \sum_{u'} T_u(u')\, C(adu';\, \alpha - \delta)\, C(cbu';\, \gamma - \beta), \tag{A.8}$$

and

$$\langle \bar{b}d|T_t|a\bar{c}\rangle = \sum_{t'} T_t(t')\, C(act';\, \alpha - \gamma)\, C(bdt';\, -\beta\delta), \tag{A.9}$$

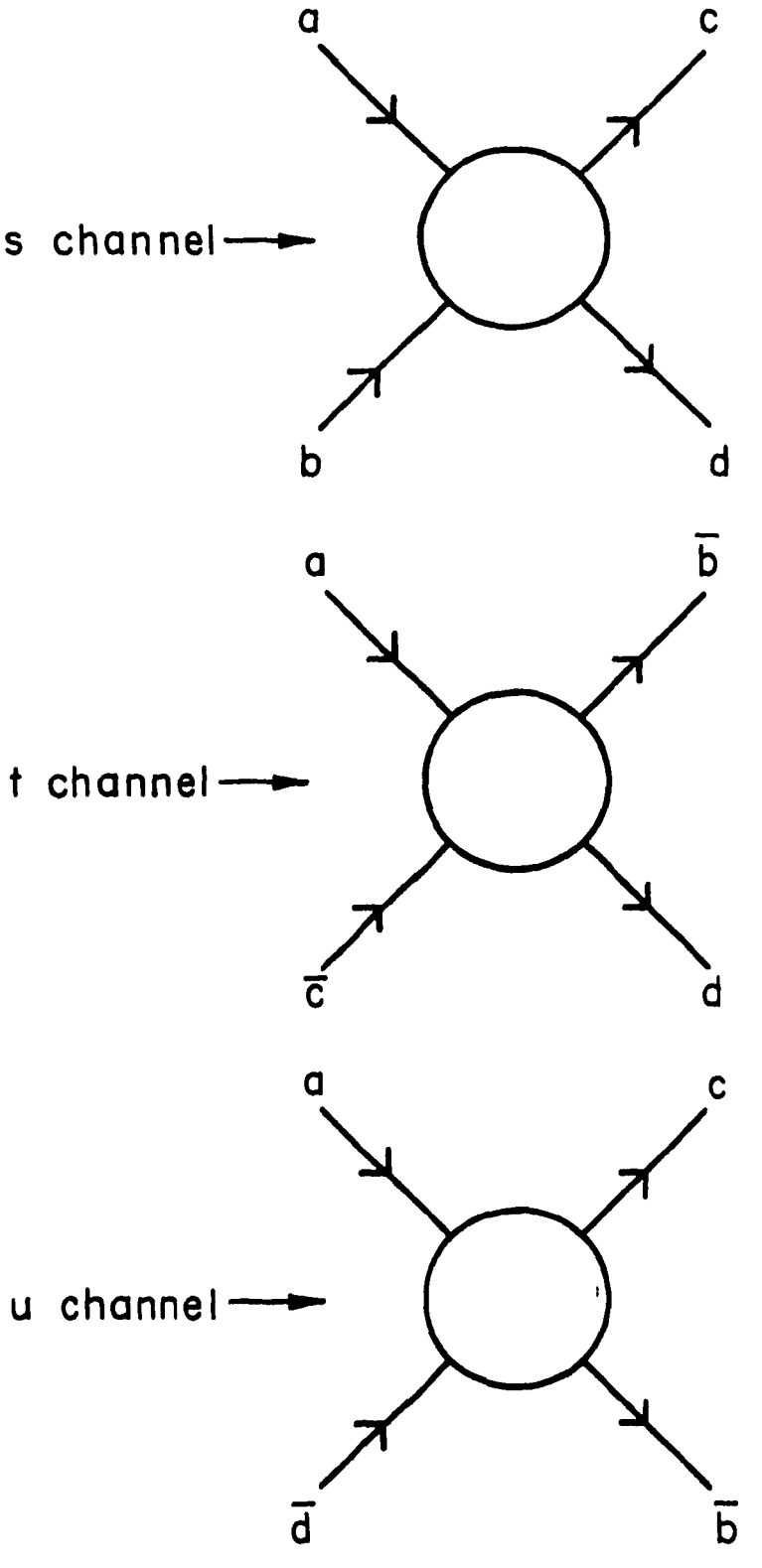


FIG. A-1 CONNECTION BETWEEN THE s, t AND u CHANNELS.

where $T_u(u')$ denotes the amplitude for scattering in isospin u' in channel u, the C's denote the Clebsch-Gordan coefficients in the notation of Rose (1957) and $\alpha$, $\beta$, $\gamma$, and $\delta$ denote the z components of isospin for particles a, b, c, and d respectively.

We then use the following standard formulas involving the Racah coefficients:

$$C(abs';\ \alpha\ )\ C(cds';\ \gamma\delta) = \sum_{u'} (2s'+1)\ (-)^{\gamma-\alpha+a-c} W(abdc;\ s'u')$$

$$\times\ C(adu';\ \alpha-\delta)\ C(cdu';\ \gamma-\beta) \quad \text{and} \tag{A.10}$$

$$C(abs';\ \alpha\beta\ )\ C(cds';\ \gamma\delta) = \sum_{t'} (2s'+1)\ (-)^{\delta-\alpha+a+d}\ W(as't'd;\ bc)$$

$$\times\ C(bdt';\ -\beta\delta)\ C(act';\ \alpha-\gamma)\ . \tag{A.11}$$

It is from this that we obtain the crossing matrices $X_{u's'}$, $X_{t's'}$ defined by

$$T_u(u') = \sum_{s'} X_{u's'}\ T_s(s') \tag{A.12}$$

and

$$T_t(t') = \sum_{s'} X_{t's'}\ T_s(s')\ . \tag{A.13}$$

Taking care of the phases $\xi$ we then obtain the corresponding crossing matrices

$$X^{I}_{us} = X^{III}_{us} = (-)^{a+b-c+d}\ (2s+1)\ W(abdc;\ su), \tag{A.14}$$

$$X^{I}_{ts} = X^{III}_{ts} = (-)^{a+b+c+d} (2\bar{s} + 1) W(astd; bc), \quad (A.15)$$

$$X^{I}_{us} = (-)^{a-b-c+d} (2\bar{s} + 1) W(abdc; su), \text{ and} \quad (A.16)$$

$$X^{II}_{ts} = (-)^{a-b+c+d} (2s + 1) W(astd; bc), \quad (A.17)$$

where I, II, and III are used to differentiate between the cases in which the crossed particles are both self conjugate, both conjugate doublets, or one is self conjugate and the other is a conjugate doublet.

There exist convenient tables of Racah coefficients so the problem of computing SU(2) crossing coefficients is reduced to the problem of looking up these coefficients. We mention Biedenharn, Blatt, and Rose (1952) as an example of these tables. They give explicit analytic expressions for most Racah coefficients for simple cases.

5. The reaction $0^{-} + \frac{1}{2}^{+} \rightarrow 0^{-} + \frac{1}{2}^{+}$.

a. Baryon exchange

We first consider baryon exchange in the u channel as shown in Figure A-2. The BPB interaction Lagrangian is given by

$$-\mathcal{L}_{int} = i \sqrt{2}\, g_{\pi N}\, \bar{B}^{i}_{j}\, \gamma_5 [(1-2f)\, B^{j}_{k}\, P^{k}_{l} + B^{k}_{i}\, P^{j}_{k}], \quad (A.18)$$

where $g_{\pi N}$ is the pion nucleon coupling constant and f, the so-called F/D ratio, is more or less known experimentally.

If we expand the above, we have

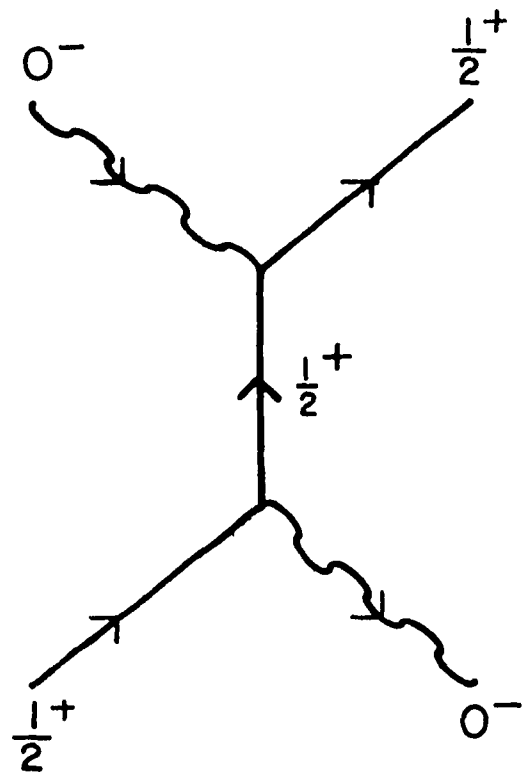


FIG. A-2 BARYON EXCHANGE IN THE u CHANNEL.

$$\mathcal{L}_{int} = [g_{\pi NN}\,\vec{\pi}\cdot\vec{N}\,\vec{\tau}\,N + g_{\Lambda\pi\Sigma}(\vec{\pi}\cdot\bar{\Lambda}\Sigma + h.c.) - ig_{\Sigma\pi\Sigma}\,\vec{\pi}\cdot(\bar{\vec{\Sigma}}\times\vec{\Sigma})$$

$$+ g_{\equiv\pi\equiv}\,\vec{\pi}\cdot\bar{\equiv}\,\vec{\tau}\,\equiv + g_{\Lambda KN}\,(\bar{N}\Lambda K + h.c.) + g_{\Sigma KN}(\bar{N}\,\vec{\tau}\cdot\vec{\Sigma}K + h.c.)$$

$$+ g_{\Lambda K\equiv}\,(\bar{\equiv}\,\Lambda K^{c} + h.c.) + g_{\Sigma K\equiv}\,(\bar{\equiv}\,\vec{\tau}\cdot\vec{\Sigma}\,K^{c} + h.c.) + g_{N\eta N}\,\bar{N}\,N\eta$$

$$g_{\Lambda\eta\Lambda}\,\eta\,\bar{\Lambda}\,\Lambda + g_{\Sigma\eta\Sigma}\,\eta\bar{\Sigma}\cdot\Sigma + g_{\equiv\eta\equiv}\eta\bar{\equiv}\equiv], \qquad (A.19)$$

where we have omitted the $i\gamma_5$, and where

$$g_{\pi NN} = g_{\pi N},$$

$$g_{\Lambda\pi\Sigma} = \frac{2}{\sqrt{3}}(1-f)\,g_{\pi N},$$

$$g_{\Sigma\pi\Sigma} = 2fg_{\pi N},$$

$$g_{\equiv\pi\equiv} = (1-2f)\,g_{\pi N},$$

$$g_{\Lambda KN} = -\frac{1}{\sqrt{3}}\,(1+2f)\,g_{\pi N},$$

$$g_{\Sigma KN} = (1-2f)\,g_{\pi N},$$

$$g_{\Lambda K\equiv} = -\frac{1}{\sqrt{3}}\,(1-4f)\,g_{\pi N},$$

$$g_{\Sigma K\equiv} = g_{\pi N},$$

$$g_{N\eta N} = -\frac{1}{\sqrt{3}}\,(1-4f)\,g_{\pi N},$$

$$g_{\Lambda\eta\Lambda} = -\frac{2}{\sqrt{3}}\,(1-f)\,g_{\pi N},$$

$$g_{\Sigma\eta\Sigma} = \frac{2}{\sqrt{3}} (1-f)\ g_{\pi N}, \text{ and}$$

$$g_{\Xi\eta\Xi} = -\frac{1}{\sqrt{3}} (1+2f)\ g_{\pi N}\ .$$

In addition we have defined

$$\bar{N}\vec{\tau}\cdot N\pi = (\bar{p}p-\bar{n}n)\pi^{o} + \sqrt{2}\ (\bar{n}p\pi^{-} + \bar{p}n\pi^{+})$$

$$\vec{\pi}\cdot\bar{\Lambda}\ \vec{\Sigma} + h.c = \bar{\Lambda}(\Sigma^{+}\pi^{-} + \Sigma^{-}\pi^{+} + \Sigma^{o}\pi^{o}) + (\bar{\Sigma}^{+}\pi^{+} + \bar{\Sigma}^{-}\pi^{-} + \bar{\Sigma}^{o}\pi^{o})\Lambda,$$

$$_{1}(\bar{\vec{\Sigma}} \times \vec{\Sigma})\cdot\vec{\pi} = (\bar{\Sigma}^{-}\Sigma^{-} - \bar{\Sigma}^{+}\Sigma^{+})\pi^{o} + (\bar{\Sigma}^{o}\Sigma^{+} - \bar{\Sigma}^{-}\Sigma^{o})\pi^{-} + (\bar{\Sigma}^{+}\Sigma^{o} - \bar{\Sigma}^{o}\Sigma^{-})\pi^{+},$$

$$\vec{\pi}\cdot\bar{\Xi}\ \vec{\tau}\ \Xi = (\bar{\Xi}^{-}\Xi^{-} - \bar{\Xi}^{o}\Xi^{o})\pi^{o} + \sqrt{2}\ (\bar{\Xi}^{-}\Xi^{o}\pi^{-} + \bar{\Xi}^{o}\Xi^{-}\pi^{+}),$$

$$\bar{N}\Lambda K + h.c. = \bar{\Lambda}(pK^{-} + n\bar{K}^{o}) + (\bar{p}K^{+} + \bar{n}K^{o})\Lambda,$$

$$\bar{N}\vec{\tau}\cdot\vec{\Sigma}\ K + h.c. = (\bar{p}K^{+} - \bar{n}K^{o})\Sigma^{o} + \sqrt{2}\ (\bar{n}K^{+}\Sigma^{-} + \bar{p}\Sigma^{+}K^{o}) + \bar{\Sigma}^{o}(pK^{-} - n\bar{K}^{o})$$

$$+ \sqrt{2}\ (\bar{\Sigma}^{-}nK^{-} + \bar{\Sigma}^{+}p\bar{K}^{o}),$$

$$\bar{\Xi}\Lambda K^{c} + h.c. = \bar{\Lambda}(\Xi^{-}K^{+} + \Xi^{o}K^{o}) + (\bar{\Xi}^{-}K^{-} + \bar{\Xi}^{o}\bar{K}^{o})\Lambda,$$

$$\bar{N}\ N\eta = (\bar{p}p + \bar{n}n)\eta,$$

$$\bar{\Lambda}\ \Lambda\eta = \bar{\Lambda}\ \Lambda\eta,$$

$$\bar{\vec{\Sigma}}\cdot\vec{\Sigma}\eta = (\bar{\Sigma}^{+}\Sigma^{+} + \bar{\Sigma}^{-}\Sigma^{-} + \bar{\Sigma}^{o}\Sigma^{o})\eta,$$

$$\bar{\Xi}\quad\Xi\eta = (\bar{\Xi}^{-}\Xi^{-} + \bar{\Xi}^{o}\Xi^{o})\eta, \text{ and}$$

$$\bar{\Xi}\vec{\tau}\cdot\vec{\Sigma}K^{c} + h.c. = -(\bar{\Xi}^{o}\bar{K}^{o} - \bar{\Xi}^{-}K^{-})\Sigma^{o} + \sqrt{2}\ (\bar{\Xi}^{-}\bar{K}^{o}\Sigma^{-} + \bar{\Xi}^{o}K^{-}\Sigma^{+}) - \bar{\Sigma}^{o}(\Xi^{o}K^{o} - \Xi^{-}K^{+})$$

$$+ \sqrt{2}\ (\bar{\Sigma}^{-}K^{o}\Xi^{-} + \bar{\Sigma}^{+}K^{+}\Xi^{o}),$$

where the symbols stand for the field operators which destroy the corresponding particles. For example, $\Sigma^+$ denotes the field operator which destroys the positively charged $\Sigma^+$. Also a bar placed over a symbol as for example $\bar{\Sigma}^+$, denotes the field operator which creates the corresponding particle. We use

$$B^i_j \bar{B}^k_\ell = (\delta^i_\ell \delta^k_j - \frac{1}{3} \delta^i_j \delta^k_\ell) \tag{A.20}$$

and

$$-\mathcal{L}_{int} = \sqrt{2}\, g_{\pi N} \bar{B}^i_j[(1-2f)\, B^j_k P^k_i + B^k_i P^j_k] = \sqrt{2}\, g_{\pi N}[(1-2f)\, \bar{B}^\ell_j P^i_\ell + \bar{B}^i_\ell P^\ell_j] B^j_i, \tag{A.21}$$

where we have dropped the $i\gamma_5$. We then obtain as the result of the contracti for the process in consideration

$$2\, g^2_{\pi N}\{[(1-2f)\, B^j_k P^{+k}_i + B^k_i P^{+j}_k][(1-2f)\, \bar{B}^\ell_j P^i_\ell + \bar{B}^i_\ell P^\ell_j] - \frac{1}{3}[(1-2f)\, B^j_k P^{+k}_j + B^k_j P^{+j}_k][(1-2f)\, \bar{B}^\ell_i P^i_\ell + \bar{B}^i_\ell P^\ell_i]\} . \tag{A.22}$$

Using relation (A.4) we obtain

$$\bar{B}^\ell_j P^{+k}_i B^j_k P^i_\ell = |T><T| - \frac{2}{3}|\theta_s><\theta_s| - \frac{1}{3}|S><S| - |D><D| + |\bar{D}><\bar{D}|, \tag{A.23}$$

where we have used the outer product notation and where $|S>$, $|\theta_s>$, $|\theta_a>$, $|D>$, $|\bar{D}>$, and $|T>$ denote the normalized scalar, symmetric octet, antisymmetric octet, 10, $\overline{10}$, and 27 states respectively.

Similarly we obtain

$$\bar{B}^{l}_{\ell}\, P^{+j}_{k}\, B^{k}_{i}\, P^{\ell}_{j} = |T><T| - \frac{2}{3}|\theta_s><\theta_s| - \frac{1}{3}|S><S| + |D><D| - |\bar{D}><\bar{D}|, \tag{A.24}$$

$$\bar{B}^{l}_{\ell}\, P^{+k}_{i}\, B^{j}_{k}\, P^{\ell}_{j} = \frac{5}{6}|\theta_s><\theta_s| - \frac{3}{2}|\theta_a><\theta_a| + \frac{8}{3}|S><S|, \tag{A.25}$$

$$\bar{B}^{\ell}_{j}\, P^{+j}_{k}\, B^{k}_{i}\, P^{l}_{\ell} = \bar{B}^{i}_{\ell}\, P^{+k}_{i}\, B^{j}_{k}\, P^{\ell}_{j}, \tag{A.26}$$

and

$$\bar{B}^{\ell}_{i}\, P^{+k}_{j}\, B^{j}_{k}\, P^{l}_{\ell} = |T><T| + |\theta_s><\theta_s| + |S><S| - |\bar{D}><\bar{D}| - |D><D| - |\theta_a><\theta_a|. \tag{A.27}$$

Substituting relations (A.21) to (A.24) into (A.22) we obtain

$$\Big\{\frac{4}{3}(4f^2 - 2f + 1)|T><T| - 2(4f^2 - 2f + 1)|\theta_s><\theta_s| + \frac{2}{3}(4f^2 + 10f - 5)|\theta_a><\theta_a| - \frac{8}{3}(2f^2 - f - 1)|D><D| + \frac{8}{3}(4f^2 - 5f + 1)|\bar{D}><\bar{D}| - \frac{4}{3}(4f^2 + 10f - 5)|S><S|\Big\}\varepsilon^2_{\pi N}. \tag{A.28}$$

The contribution to the relevant isotopic spin, hypercharge states is easily computed once we have the crossing matrix given above by using De Swart's tables (1963). Exceptions occur in those cases when we have $\Lambda$ and $\Sigma$ exchange in which we compute the crossing coefficient directly by multiplying the relevant coupling constant by the isotopic spin factor, as has been discussed in Part 3 of this appendix. In so doing we must use properly normalized field operator expressions for the isotopic spin states.

We list SU(3) crossing coefficients for each hypercharge and isotopic spin state as a matrix whose (i, j) element represents the crossing coefficient for the scattering from channel i to channel j, and where the symbol in parentheses next to each crossing coefficient represents the particles being exchanged. Due to symmetry we need only list half of the off diagonal terms. We denote the isotopic spin and hypercharge by I and Y respectively.

<u>I = 1, Y = 2</u>

$$KN\left(\frac{1}{3}(1+4f+4f^2)\overset{kN}{(\Lambda)} + (1-4f+4f^2)(\Sigma)\right) g^2_{\pi N} ,$$

<u>I = 0, Y = 2</u>

$$KN\left(-\frac{1}{3}(1+4f+4f^2)\overset{KN}{(\Lambda)} + 3(1-4f+4f^2)(\Sigma)\right) g^2_{\pi N} ,$$

<u>I = 3/2, Y = 1</u>

$$\begin{array}{c} \\ \pi N \\ K\Sigma \end{array} \begin{array}{c} \begin{array}{cc} \overset{\pi N}{} & \overset{K\Sigma}{} \end{array} \\ \begin{pmatrix} 2(N) & -\frac{2}{3}(1+f-2f^2)(\Lambda) - 2(f-2f^2)(\Sigma) \\ & 2(\equiv) \end{pmatrix} \end{array} g^2_{\pi N},$$

$\underline{I = \frac{1}{2},\ Y = 1}$

| | $\pi N$ | $\eta N$ | $K\Lambda$ | $K\Sigma$ |
|---|---|---|---|---|
| $\pi N$ | $-1\,(N)$ | $(1-4f)\,(N)$ | $-2(1-3f+2f^2)\,(\Sigma)$ | $\frac{2}{3}(1+f-2f^2)\,(\Lambda) - 2(2f-4f^2)\,(\Sigma)$ |
| $\eta N$ | | $\frac{1}{3}(1-8f+16f^2)\,(N)$ | $\frac{2}{3}(1+f-2f^2)\,(\Lambda)$ | $2(1-3f+2f^2)\,(\Sigma)$ |
| $K\Lambda$ | | | $\frac{1}{3}(1-8f+16f^2)\,(\equiv)$ | $-(1-4f)\,(\equiv)$ |
| $K\Sigma$ | | | | $-1\,(\equiv)$ |

$g^2_{\pi N}$ ,

$\underline{I = 1,\ Y = 0}$

| | $\pi\Lambda$ | $\pi\Sigma$ | $\bar{K}N$ | $\eta\Sigma$ | $K\equiv$ |
|---|---|---|---|---|---|
| $\pi\Lambda$ | $\frac{4}{3}(1-2f+f^2)\,(\Sigma)$ | $4\sqrt{\frac{2}{3}}\,(1+2f)\,(\Sigma)$ | $\sqrt{\frac{2}{3}}\,(1+2f)\,(N)$ | $-\frac{4}{3}\,(1-2f+f^2)\,(\Lambda)$ | $\sqrt{\frac{2}{3}}\,(1-6f+8f^2)\,(\equiv)$ |
| $\pi\Sigma$ | | $-\frac{4}{3}(1-2f-f^2)\,(\Lambda) + 4f^2\,(\Sigma)$ | $2(1-2f)\,(N)$ | $-4\sqrt{\frac{2}{3}}\,(f-f^2)\,(\Sigma)$ | $-2(1-2f)\,(\equiv)$ |
| $\bar{K}N$ | | | $0$ | $\sqrt{\frac{2}{3}}\,(1-6f+8f^2)\,(N)$ | $-\frac{1}{3}(1-2f-8f^2)\,(\Lambda)$ $-(1-2f)\,(\Sigma)$ |
| $\eta\Sigma$ | | | | $\frac{4}{3}\,(1-2f+f^2)\,(\Sigma)$ | $\sqrt{\frac{2}{3}}(1+2f)\,(\equiv)$ |
| $K\equiv$ | | | | | $0$ |

$g^2_{\pi N}$,

$\underline{I = 0,\ Y = 0}$

$$
\begin{array}{c}
 \\
\pi\Sigma \\
\bar{K}N \\
\eta\Lambda \\
K\Xi
\end{array}
\begin{array}{c}
\begin{array}{cccc}
\pi\Sigma & \bar{K}N & \eta\Lambda & K\Xi
\end{array} \\
\begin{pmatrix}
\frac{4}{3}(1-2f+f^2)\,(\Lambda) - 8f^2\,(\Sigma) & -\sqrt{6}(1-2f)\,(N) & 4\frac{\sqrt{3}}{3}(1-2f+f^2)\,(\Sigma) & \sqrt{6}(1-2f)\,(\Xi) \\
 & 0 & \frac{\sqrt{2}}{3}(1-2f-8f^2)\,(N) & -\frac{1}{3}(1-2f-8f^2)\,(\Lambda) - (1-2f)\,(\Sigma) \\
 & & \frac{4}{3}(1-2f+f^2)\,(\Lambda) & -\frac{\sqrt{2}}{3}(1-2f-8f^2)\,(\Xi) \\
 & & & 0
\end{pmatrix} g^2_{\pi N},
\end{array}
$$

$\underline{I = \frac{1}{2},\ Y = -1}$

$$
\begin{array}{c}
 \\
\pi\Xi \\
\bar{K}\Lambda \\
\bar{K}\Sigma \\
\eta\Xi
\end{array}
\begin{array}{c}
\begin{array}{cccc}
\pi\Xi & \bar{K}\Lambda & \bar{K}\Sigma & \eta\Xi
\end{array} \\
\begin{pmatrix}
-(1-4f+4f^2)\,(\Xi) & 2(1-f)\,(\Sigma) & \frac{2}{3}(1-5f+4f^2)\,(\Lambda) + 4f\,(\Sigma) & -(1-4f^2)\,(\Xi) \\
 & \frac{1}{3}(1+4f+4f^2)\,(N) & (1-4f^2)\,(N) & \frac{2}{3}(1-5f+4f^2)\,(\Xi) \\
 & & -(1-4f+4f^2)\,(N) & -2(1-f)\,(\Sigma) \\
 & & & \frac{1}{3}(1+4f+4f^2)\,(\Xi)
\end{pmatrix} g^2_{\pi N},
\end{array}
$$

$\underline{I = 0,\ Y = -2}$

$\bar{K}\equiv$

$\bar{K}\equiv \left(-\frac{1}{3}\,(1-8f+16f^2)(\Lambda) + 3(\Sigma)\right) g^2_{\pi N}.$

b. Decuplet Exchange

We next consider decuplet exchange in the u channel as shown in Figure A-3.

In this case, since all members of the decuplet have different hypercharge, knowledge of the crossing coefficients in the case of perfect SU(3) symmetry gives us also the crossing coefficients in broken SU(3). This is because only one particle can be exchanged for each process.

We can write for the B*BP coupling the interaction Lagrangian

$$-\mathcal{L}_{int} = g_{N*}\left[\epsilon^{\ell mk}\frac{\partial}{\partial x_\mu} B^n_\ell\, P^\alpha_m\, \bar{D}^\mu_{kn\alpha} + \epsilon_{\ell mk}\frac{\partial}{\partial x_\mu}\bar{B}^\ell_n\, P^m_\alpha\, D^{kn\alpha}_\mu\right], \qquad (A.29)$$

where $\mu$ denotes a Lorentz index, $g_{N*}$ denotes the N* $p\pi+$ coupling constant (as computed from the width of the N*) and $\epsilon_{\ell mk}$ is the antisymmetric Levi Cevita tensor given by

$$\epsilon_{\ell mk} = \begin{cases} +1 & \text{if } (\ell mk) \text{ is an even permutation of } (123), \\ -1 & \text{if } (\ell mk) \text{ is an odd permutation of } (123), \\ 0 & \text{otherwise.} \end{cases}$$

If we expand the above SU(3) Lagrangian omitting space time complications, we obtain

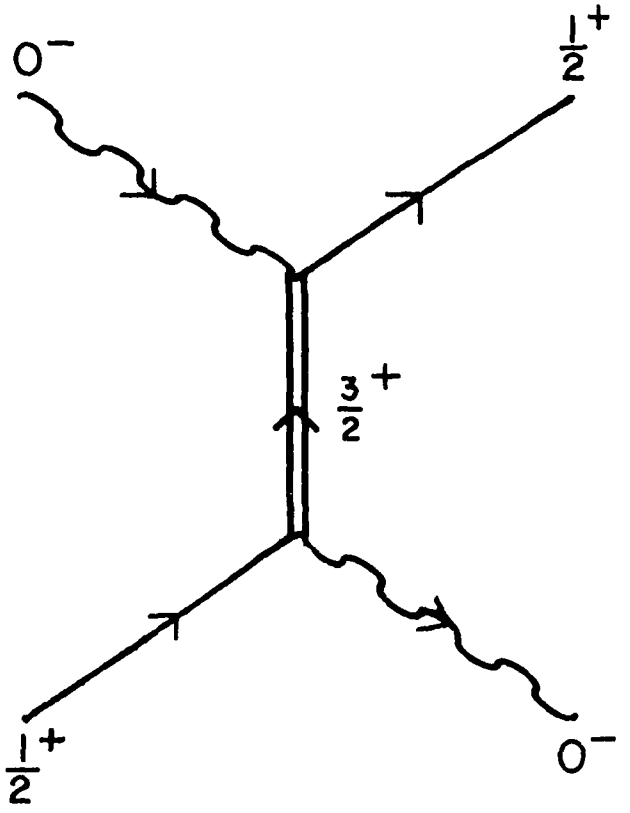


FIG. A-3 DECUPLET EXCHANGE IN THE u CHANNEL.

$$-\mathcal{L}_{int} = g_{N^*}[\sqrt{2}\ \vec{\bar{N}}^*\{(N\pi)_{3/2} - (\Sigma K)_{3/2}\} + \frac{1}{\sqrt{3}}\ \bar{Y}_1^*(\bar{K}\ \vec{\tau}\ N + K^c\ \vec{\tau} \equiv$$

$$-\imath\ \vec{\Sigma} \times \vec{\pi} - \sqrt{3}\ \Lambda\ \vec{\pi} + \sqrt{3}\ \vec{\Sigma}\ \eta) + \frac{1}{\sqrt{3}}\ \bar{\Xi}^*\ (\vec{\tau}\cdot\vec{\Sigma}\ K^c - \vec{\tau}\cdot\vec{\pi} \equiv + \sqrt{3}\ K^c\Lambda \qquad (A.30)$$

$$-\sqrt{3} \equiv \eta) + \sqrt{2}\ \bar{\Omega}^-\ \bar{K}\equiv] + h.c.,$$

where we have defined

$$N^*(N\pi)_{3/2} = \bar{N}^*_{++}\ p\pi^+ + \frac{1}{\sqrt{3}}\ \bar{N}^*_{+}(\sqrt{2}\ p\pi^o - n\pi^+) + \frac{1}{\sqrt{3}}\ \bar{N}^*_{o}(p\pi^- + \sqrt{2}\ n\pi^o) + \bar{N}^*_{-}n\pi^-,$$

with a similar expression for $N^*(\Sigma K)_{3/2}$. The rest of the terms are defined as on page 12.

For the diagram of Figure A-3 we obtain

$$g^2_{N^*}[D^{k'n'\alpha'}\bar{D}_{kn\alpha}]\ \epsilon_{\xi\beta k'}\bar{B}^{\xi}_{n'}\ P^{\beta}_{\alpha'}\ \epsilon^{\gamma\delta k}\ B^{n}_{\gamma}\ P^{+\alpha}_{\delta}\ . \qquad (A.31)$$

We then obtain for the above expression in the s channel

$$\frac{g^2_{N^*}}{6}\ [-15|S><S| + 6|\theta_s><\theta_s| - 3\sqrt{s}(|\theta_s><\theta_a| + |\theta_a><\theta_s|)$$

$$+ 3|D><D| + 3|\bar{D}><\bar{D}| + |T><T|], \qquad (A.32)$$

where the notation is as before.

We then obtain for the crossing coefficients in the different isotopic spin and hypercharge states the following results:

<u>I = 1, Y = 2</u>

$$KN\left(\frac{1}{6}\ (Y^*)\right)^{K\bar{N}}\ g^2_{N^*},$$

$\underline{I = 0,\ Y = 2}$

$$\begin{matrix} & K\Xi \\ K\Xi & \left(-\frac{1}{6}\ (Y^*)\right) \end{matrix} g^2_{N^*} \ ,$$

$\underline{I = 3/2,\ Y = 1}$

$$\begin{matrix} & \pi N & K\Sigma \\ \pi\Delta & \left(\frac{1}{3}\ (N^*) \right. & \left. -\frac{1}{6}\ (Y^*)\right) \\ K\Sigma & & \frac{1}{3}\ (\equiv^*) \end{matrix} g^2_{N^*} \ ,$$

$\underline{I = 1/2,\ Y = 1}$

$$\begin{matrix} & \pi N & \eta N & K\Lambda & K\Sigma \\ \pi N & \left(\frac{4}{3}\ (N^*)\right. & 0 & \frac{1}{2}\ (Y^*) & -\frac{1}{3}\ (Y^*) \\ \eta N & & 0 & 0 & \frac{5}{8}\ (Y^*) \\ K\Lambda & & & \frac{1}{2}\ (Y^*) & -\frac{1}{2}\ (Y^*) \\ K\Sigma & & & & \left. -\frac{1}{6}\ (Y^*)\right) \end{matrix} g^2_{N^*} \ ,$$

$\underline{I = 1,\ Y = 0}$

$$\begin{matrix} & \pi\Lambda & \pi\Sigma & \bar{K}N & \eta\Sigma & K\Xi \\ \pi\Lambda & \left(\frac{1}{2}\ (Y^*)\right. & -\frac{\sqrt{6}}{6}\ (Y^*) & 0 & 0 & \left. -\frac{\sqrt{6}}{6}\ (\equiv^*)\right) \\ \pi\Sigma & & \frac{1}{6}\ (Y^*) & \frac{2}{3}\ (N^*) & -\frac{\sqrt{6}}{6}\ (Y^*) & \frac{1}{3}\ (\equiv^*) \\ \bar{K}N & & & 0 & 0 & \frac{1}{6}\ (Y^*) \\ \eta\Sigma & & & & \frac{1}{2}\ (Y^*) & -\frac{\sqrt{6}}{6}\ (\equiv^*) \\ K\Xi & & & & & 1\ (\Omega^-) \end{matrix} g^2_{N^*} \ ,$$

$\underline{I = 0,\ Y = 0}$

$$
\begin{array}{c}
 \\
\pi\Sigma \\
\bar{K}N \\
\eta\Lambda \\
K\Xi
\end{array}
\begin{array}{c}
\begin{array}{cccc} \pi\Sigma & \bar{K}N & \eta\Lambda & K\Xi \end{array} \\
\left(\begin{array}{cccc}
-\frac{1}{3}\,(Y^*) & \frac{2\sqrt{6}}{3}\,(N^*) & \frac{\sqrt{3}}{2}\,(Y^*) & -\frac{\sqrt{6}}{6}\,(\Xi^*) \\
 & 0 & 0 & \frac{1}{2}\,(Y^*) \\
 & & 0 & \frac{\sqrt{2}}{2}\,(\Xi^*) \\
 & & & -1\,(\Omega^-)
\end{array}\right) g_{N^*}^2 ,
\end{array}
$$

$\underline{I = 1/2,\ Y = -1}$

$$
\begin{array}{c}
 \\
\pi\Xi \\
\bar{K}\Lambda \\
\bar{K}\Sigma \\
\eta\Xi
\end{array}
\begin{array}{c}
\begin{array}{cccc} \pi\Xi & \bar{K}\Lambda & \bar{K}\Sigma & \eta\Xi \end{array} \\
\left(\begin{array}{cccc}
-\frac{1}{6}\,(\Xi^*) & \frac{1}{2}\,(Y^*) & -\frac{1}{3}\,(Y^*) & -\frac{1}{2}\,(\Xi^*) \\
 & 0 & 0 & 0 \\
 & & \frac{4}{3}\,(N^*) & \frac{1}{2}\,(Y^*) \\
 & & & \frac{1}{2}\,(\Xi^*)
\end{array}\right) g_{N^*}^2 ,
\end{array}
$$

$\underline{I = 0,\ Y = -2}$

$$
\begin{array}{c}
 \\
\bar{K}\Xi
\end{array}
\begin{array}{c}
\begin{array}{c} \bar{K}\Xi \end{array} \\
\left(\begin{array}{c}
\frac{1}{2}\,(Y^*)
\end{array}\right) g_{N^*}^2 .
\end{array}
$$

c. Vector Exchange

We next consider vector meson exchange in the t channel as shown in Figure A-4. For the VPP interaction (denoting the $\rho\pi\pi$ coupling constant by $g_\rho$) we may write the following SU(3) Lagrangian:

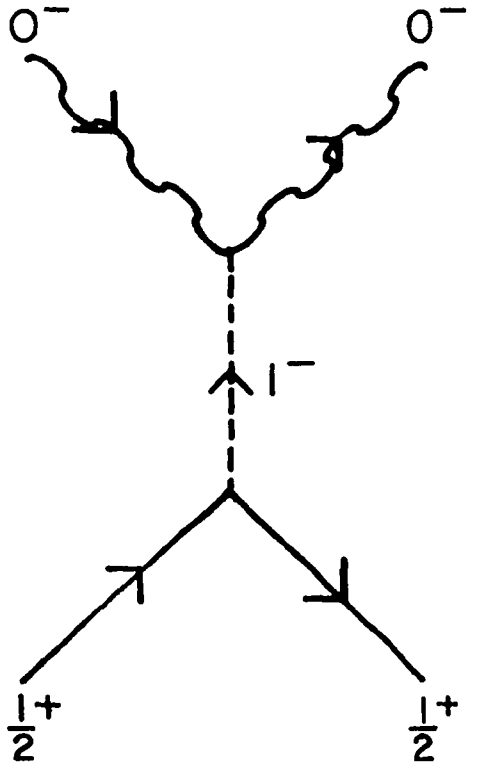


FIG. A-4 VECTOR MESON EXCHANGE IN THE $t$ CHANNEL.

$$-\mathcal{L}_{int} = \frac{ig_\rho}{\sqrt{2}} V_{\mu j}^{\ i} \left[ P_k^j \frac{\partial P_i^k}{\partial x_\mu} - P_i^k \frac{\partial P_k^l}{\partial x_\mu} \right] = -\frac{g_\rho}{\sqrt{2}} (p_{1\mu} + p_{2\mu}) V_{\mu j}^{\ i} \left[ P^{\dagger j}_k P_i^k - P^{\dagger k}_i P_k^j \right] . \tag{A.33}$$

Note that the above term is zero if we consider the singlet vector meson. Thus the singlet vector meson does not couple to two pseudoscalar mesons. We also note that the interaction is pure F type due to the assumed invariance of the Lagrangian under charge conjugation.

If we expand the above (omitting space time complications) we obtain

$$-\mathcal{L}_{int} = g_\rho [\vec{\rho} \cdot (\vec{\pi} \times \vec{\pi} + iK^\dagger \vec{\tau} K) + (iK^{*\dagger} \vec{\tau} K \cdot \vec{\pi} + h.c.)$$
$$+ \sqrt{3} (iK^{*\dagger} K\eta + h.c.) + \sqrt{3} \varphi_o iK^\dagger K], \tag{A.34}$$

where we have used the same notation as before.

For the VBB interaction, denoting the $\rho NN$ coupling constant by $g'_\rho$, we may write the following SU(3) interaction Lagrangian:

$$-\mathcal{L}_{int} = g'_\rho \sqrt{2} \{ [(1-2f_1) \bar{B}_k^l B_j^k + \bar{B}_j^k B_k^i] + \frac{\mathcal{K}}{2m} [(1-2f_2) \bar{B}_k^l B_j^k + \bar{B}_j^k B_k^i] \} V_i^j, \tag{A.35}$$

where we have dropped the $i\gamma_\mu$ in the first term and the $i\sigma_{\mu\nu} e_\nu$ in the second term.[2] In addition we have dropped the singlet exchange part since it does not couple to two pseudoscalar mesons. Assuming as usual that the 1-1 component of the traceless octet is the electromagnetic current, we obtain $f_1 = 1$. This is so since the 1-1 component of the traceless octet corresponding to the first term is

---

2. The $e_\nu$ appearing in $i\sigma_{\mu\nu} e_\nu$ denotes the $\nu$th component of momentum transfer as defined in Appendix B.

$$[(1-2f_1)\bar{B}^1_k\, B^k_1 + \bar{B}^k_1\, B^1_k - \frac{2}{3}\,(1-f_1)\bar{B}^\ell_k\, B^k_\ell]. \tag{A.36}$$

We recall that the form for the $\gamma_\mu$ part of the electromagnetic current is given by

$$J_\mu = i[\bar{B}^k_1\, \gamma_\mu\, B^1_k - \bar{B}^1_k\, \gamma_\mu\, B^k_1]. \tag{A.37}$$

Therefore, both of them agree provided $f_1 = 1$. In addition $f_2$ is determined from the ratio of the magnetic moments of the neutron and proton.

We obtain

$$\frac{\mathcal{K}_n}{\mathcal{K}_p} = -\frac{2(1-f_2)}{1+2f_2}\,. \tag{A.38}$$

Upon using $\mathcal{K}_n = -1.91$, $\mathcal{K}_p = 1.79$ in nuclear magnetons (n.m), we obtain

$$f_2 = 0.226.$$

Also since the magnetic moment of the proton is 2.79 n.m., we obtain

$$\mathcal{K}[1 - \tfrac{2}{3}(1-f_2)] = \mathcal{K}_p = 2.79 \text{ n.m.}, \tag{A.39}$$

from which we obtain

$$\mathcal{K} = 3.70 \text{ n.m.}$$

Therefore, we use for the interaction Lagrangian

$$-\mathcal{L}_{int} = g'_\rho \sqrt{2}\, [\{\bar{B}^k_j\, B^i_k - \bar{B}^i_k\, B^k_j\} + \frac{3.70}{2m}\,\{(1-2f_2)\bar{B}^i_k\, B^k_j + \bar{B}^k_j\, B^i_k\}]\, V^j_i, \tag{A.40}$$

where $f_2 = 0.226$.

We then obtain for the process in question unitary spin factors of the form

$$g_\rho g'_\rho [P^{+j}_k P^k_1 - P^{+k}_1 P^j_k][\{\bar{B}^k_j B^i_k - \bar{B}^i_k B^k_j\} + \frac{3.70}{2m}\{(1-2f_2)\bar{B}^i_k B^k_j + \bar{B}^k_j B^i_k\}]. \tag{A.41}$$

By expanding the above expression into the appropriate irreducible s channel tensors, this becomes

$$g_\rho g'_\rho [(6|S><S| + 3|\theta_s><\theta_s| + 3|\theta_a><\theta_a| - 2|T><T|)$$

$$\frac{3c}{mb+md}(6\ f_2|S><S| + 3\ f_2|\theta_s><\theta_s| + 3\ f_2|\theta_a><\theta_a| - 2f_2|T><T|$$

$$-\sqrt{5}\ (1-f_2)|\theta_s><\theta_a| - \sqrt{5}\ (1-f_2)|\theta_a><\theta_s| - 2(1-f_2)|D><D|$$

$$+ 2(1-f_2)|\bar{D}><\bar{D}|)], \tag{A.42}$$

where we have replaced 2m by mb + md in the broken SU(3) case.

We note that the second term can be written as the first term times $f_2$ plus

$$g_\rho g'_\rho [-\sqrt{5}\ (1-f_2)|\theta_s><\theta_a| - \sqrt{5}\ (1-f_2)|\theta_a><\theta_s| - 2(1-f_2)|D><D|$$

$$+ 2(1-f_2)|\bar{D}><\bar{D}|], \tag{A.43}$$

where we have omitted the common factor 3.70/(mb+md). We will, therefore, only tabulate the crossing coefficients corresponding to

$$g^2[6|S><S| + 3|\theta_s><\theta_s| + 3|\theta_a><_a| - 2|T><T|] \tag{A.44}$$

and

$$g^2[-\sqrt{5}\ (1-f_2)|\theta_s><\theta_a| - \sqrt{5}\ (1-f_2)|\theta_a><\theta_s| - 2(1-f_2)|D><D| + 2(1-f_2)|\bar{D}><\bar{D}|], \tag{A.45}$$

where $g^2$ denotes $g_\rho g'_\rho$, $\frac{g_\rho g'_\rho}{mb+md}\mathcal{K}f_2$ or $\frac{g_\rho g'_\rho}{mb+md}\mathcal{K}$. We obtain for the crossing coefficients corresponding to (A.44) the following results:

<u>I = 1, Y = 2</u>

$$\overset{KN}{KN}\left(-\tfrac{1}{2}(\rho) - \tfrac{1}{2}(\omega) - 1(\varphi)\right)g^2,$$

<u>I = 0, Y = 2</u>

no coupling,

<u>I = 3/2, Y = 1</u>

$$\begin{array}{c} \\ \pi N \\ K\Sigma \end{array}\begin{array}{c} \begin{array}{cc} \pi N & K\Sigma \end{array} \\ \begin{pmatrix} -1(\rho) & -1(K^*) \\ & -\frac{1}{2}(\rho) - \frac{1}{2}(\omega) \end{pmatrix} \end{array} g^2,$$

$\underline{I = 1/2,\ Y = 1}$

$$
\begin{array}{c}
 \\ \pi N \\ \eta N \\ K\Lambda \\ K\Sigma
\end{array}
\begin{array}{c}
\begin{array}{cccc} \pi N & \eta N & K\Lambda & K\Sigma \end{array} \\
\left(\begin{array}{cccc}
2(\rho) & 0 & \frac{3}{2}(K^*) & -\frac{1}{2}(K^*) \\
 & 0 & -\frac{3}{2}(K^*) & -\frac{3}{2}(K^*) \\
 & & 0 & 0 \\
 & & & \frac{5}{3}(\rho)+\frac{1}{3}(\omega)
\end{array}\right) g^2,
\end{array}
$$

$\underline{I = 1,\ Y = 0}$

$$
\begin{array}{c}
 \\ \pi\Lambda \\ \pi\Sigma \\ \bar{K}N \\ \eta\Sigma \\ K\equiv
\end{array}
\begin{array}{c}
\begin{array}{ccccc} \pi\Lambda & \pi\Sigma & \bar{K}N & \eta\Sigma & K\equiv \end{array} \\
\left(\begin{array}{ccccc}
0 & 0 & -\frac{\sqrt{6}}{2}(K^*) & 0 & -\frac{\sqrt{6}}{2}(K^*) \\
 & 2(\rho) & -1(K^*) & 0 & 1(K^*) \\
 & & -\frac{1}{2}(\rho)+\frac{1}{2}(\omega)+(\varphi) & -\frac{\sqrt{6}}{2}(K^*) & 0 \\
 & & & 0 & -\frac{\sqrt{6}}{2}(K^*) \\
 & & & & -\frac{1}{2}(\rho)+\frac{1}{2}(\omega)+(\varphi)
\end{array}\right) g^2,
\end{array}
$$

$\underline{I = 1/2,\ Y = -1}$

$$
\begin{array}{c}
 \\ \pi\equiv \\ \bar{K}\Lambda \\ \bar{K}\Sigma \\ \eta\equiv
\end{array}
\begin{array}{c}
\begin{array}{cccc} \pi\equiv & \bar{K}\Lambda & \bar{K}\Sigma & \eta\equiv \end{array} \\
\left(\begin{array}{cccc}
2(\rho) & \frac{3}{2}(K^*) & -\frac{1}{2}(K^*) & 0 \\
 & 0 & 0 & -\frac{3}{2}(K^*) \\
 & & \frac{5}{3}(\rho)+\frac{1}{3}(\omega) & -\frac{3}{2}(K^*) \\
 & & & 0
\end{array}\right) g^2,
\end{array}
$$

I = 0, Y = 0

$$\begin{array}{c} \\ \pi\Sigma \\ \bar{K}N \\ \eta\Lambda \\ K\Xi \end{array} \begin{array}{c} \begin{array}{cccc} \pi\Sigma & \bar{K}N & \eta\Lambda & K\Xi \end{array} \\ \begin{pmatrix} 4(\rho) & -\frac{\sqrt{6}}{2}(K^*) & 0 & \frac{\sqrt{6}}{2}(K^*) \\ & \frac{3}{2}(\rho)+\frac{1}{2}(\omega)+(\varphi) & \frac{3\sqrt{2}}{2}(K^*) & 0 \\ & & 0 & -\frac{3\sqrt{2}}{2}(K^*) \\ & & & \frac{3}{2}(\rho)+\frac{1}{2}(\omega)+(\varphi) \end{pmatrix} \end{array} g^2,$$

I = 0, Y = -2

no coupling.

For the crossing coefficients corresponding to (A.45) we obtain the following results:

I = 1, Y = 2

no coupling,

I = 0, Y = 2

$$\begin{array}{c} \\ KN \end{array} \begin{array}{c} \begin{array}{c} KN \end{array} \\ \left( 1(\rho) + 1(\varphi) \right) \end{array} g^2(1-f_2),$$

I = 3/2, Y = 1

$$\begin{array}{c} \\ \pi N \\ K\Sigma \end{array} \begin{array}{c} \begin{array}{cc} \pi N & K\Sigma \end{array} \\ \begin{pmatrix} -1(\rho) & +1(K^*) \\ & -\frac{1}{2}(\rho) - \frac{1}{2}(\omega) \end{pmatrix} \end{array} g^2(1-f_2),$$

$\underline{I = 1/2,\ Y = 1}$

$$
\begin{array}{c}
 \\ \pi N \\ \eta N \\ K\Lambda \\ K\Sigma
\end{array}
\begin{array}{c}
\begin{array}{cccc} \pi N & \eta N & K\Lambda & K\Sigma \end{array} \\
\left(\begin{array}{cccc}
2(\rho) & 0 & \frac{1}{2}(K^*) & \frac{1}{2}(K^*) \\
 & 0 & -\frac{1}{2}(K^*) & \frac{3}{2}(K^*) \\
 & & -\frac{1}{6}(\rho)-\frac{1}{6}(\omega)+\frac{4}{3}(\varphi) & -1(\varphi) \\
 & & & -\frac{1}{2}(\rho)-\frac{1}{2}(\omega)
\end{array}\right)
\end{array}
g^2(1_T f_2),
$$

$\underline{I = 1,\ Y = 0}$

$$
\begin{array}{c}
 \\ \pi\Lambda \\ \pi\Sigma \\ \bar{K}N \\ \eta\Sigma \\ K\equiv
\end{array}
\begin{array}{c}
\begin{array}{ccccc} \pi\Lambda & \pi\Sigma & \bar{K}N & \eta\Sigma & K\equiv \end{array} \\
\left(\begin{array}{ccccc}
0 & -\frac{2\sqrt{6}}{3}(\rho) & -\frac{\sqrt{6}}{6}(K^*) & 0 & \frac{\sqrt{6}}{6}(K^*) \\
 & 0 & 1(K^*) & 0 & 1(K^*) \\
 & & -1(\varphi) & \frac{\sqrt{6}}{2}(K^*) & 0 \\
 & & & 0 & -\frac{\sqrt{6}}{2}(K^*) \\
 & & & & 1(\varphi)
\end{array}\right)
\end{array}
g^2(1-f_2),
$$

$\underline{I = 0,\ Y = 0}$

$$
\begin{array}{c}
 \\ \pi\Sigma \\ \bar{K}N \\ \eta\Lambda \\ K\equiv
\end{array}
\begin{array}{c}
\begin{array}{cccc} \pi\Sigma & \bar{K}N & \eta\Lambda & K\equiv \end{array} \\
\left(\begin{array}{cccc}
0 & \frac{\sqrt{6}}{2}(K^*) & 0 & \frac{\sqrt{6}}{2}(K^*) \\
 & \frac{3}{2}(\rho)+\frac{1}{2}(\omega)-(\varphi) & \frac{\sqrt{2}}{2}(K^*) & 0 \\
 & & 0 & \frac{\sqrt{2}}{2}(K^*) \\
 & & & -\frac{3}{2}(\rho)-\frac{1}{2}(\omega)+(\varphi)
\end{array}\right)
\end{array}
g^2(1-f_2),
$$

$\underline{I = 1/2,\ Y = 1}$

$$
\begin{array}{c}
 \\
\pi\Xi \\
\bar{K}\Lambda \\
\bar{K}\Sigma \\
\eta\Xi
\end{array}
\begin{array}{c}
\begin{array}{cccc}
\pi\Xi & \bar{K}\Lambda & \bar{K}\Sigma & \eta\Xi
\end{array} \\
\begin{pmatrix}
-2(\rho) & \frac{1}{2}(K^*) & -\frac{1}{2}(K^*) & 0 \\
 & \frac{1}{6}(\rho)+\frac{1}{6}(\omega)-\frac{4}{3}(\varphi) & -1(\varphi) & -1(K^*) \\
 & & -\frac{1}{2}(\rho)-\frac{1}{2}(\omega) & \frac{3}{2}(K^*) \\
 & & & 0
\end{pmatrix}
\end{array}
g^2(1-f_2),
$$

$\underline{I = 0,\ Y = -2}$

$$
\begin{array}{c}
 \\
\bar{K}\Xi
\end{array}
\begin{array}{c}
\begin{array}{c}
\bar{K}\Xi
\end{array} \\
\begin{pmatrix}
-1(\rho) - 1(\varphi)
\end{pmatrix}
\end{array}
g^2(1-f_2).
$$

## 6. The Reaction $0^- + \frac{1}{2}^+ \rightarrow 1^- + \frac{1}{2}^+$

Here we will consider pseudoscalar meson exchange in the t channel as shown in Figure A-5. We write the SU(3) Lagrangian which we have already discussed and consider the appropriate s channel expansion. We find

$$
\begin{aligned}
k^2[&3f|\theta_s><\theta_s| + 3f|\theta_a><\theta_a| - \sqrt{5}\,(1-f)|\theta_s><\theta_a| \\
&- \sqrt{5}\,(1-f)|\theta_a><\theta_s| - 2(1-f)|D><D| + 2(1-f)|\bar{D}><\bar{D}| \\
&+ 6f|S><S| - 2f|T><T|],
\end{aligned}
\tag{A.46}
$$

where f is as we have already defined for the PBB Lagrangian and $k^2$ is the product of the $\rho\pi\pi$ coupling constant and the $\pi NN$ coupling constant. We obtain the following results:

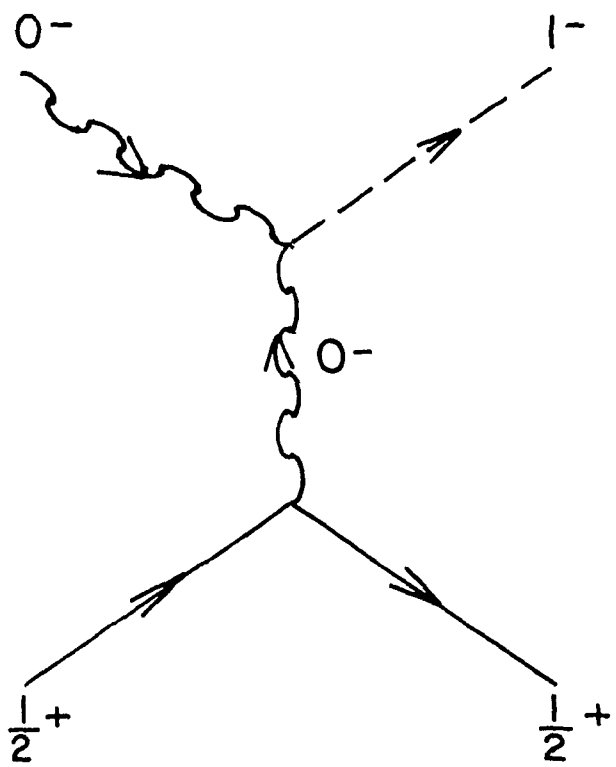


FIG. A-5 PSEUDOSCALAR MESON EXCHANGE IN THE $t$ CHANNEL.

I = 3/2, Y = 1

$$\begin{array}{c} \\ \pi N \\ K\Sigma \end{array} \begin{array}{c} \begin{array}{cc} \pi N & K\Sigma \end{array} \\ \begin{pmatrix} -1(\pi) & (1-2f)\,(K) \\ (1-2f)\,(K) & -gf(\pi)+g(f-1)\,(\eta) \end{pmatrix} \end{array} k^2,$$

I = 1/2, Y = 1

$$\begin{array}{c} \\ \pi N \\ \eta N \\ K\Lambda \\ K\Sigma \end{array} \begin{array}{c} \begin{array}{cccc} \rho N & \varphi_o N & K^*\Lambda & K^*\Sigma \end{array} \\ \begin{pmatrix} 2(\pi) & 0 & \frac{1}{2}(1+2f)\,(K) & \frac{1}{2}(1-2f)\,(K) \\ 0 & 0 & -\frac{1}{2}(1+2f)\,(K) & \frac{3}{2}(1-2f)\,(K) \\ \frac{1}{2}(1+2f)\,(K) & -\frac{1}{2}(1+2f)\,(K) & (1-f)\,(\eta) & -(1-f)\,(\pi) \\ \frac{1}{2}(1-2f)\,(K) & \frac{3}{2}(1+2f)\,(K) & -(1-f)\,(\pi) & 2f(\pi)-(1-f)\,(\eta) \end{pmatrix} \end{array} k^2,$$

$\underline{I = 1,\ Y = 0}$

$$
\begin{array}{c}
 \\
\pi\Lambda \\
\pi\Sigma \\
\bar{K}N \\
\eta\Sigma \\
K\equiv
\end{array}
\begin{array}{c}
\begin{array}{ccccc}
\rho\Lambda & \rho\Sigma & \bar{K}^{*}N & \varphi_{o}\Sigma & K^{*}\equiv
\end{array} \\
\left(\begin{array}{ccccc}
0 & -\frac{2\sqrt{6}}{3}(1-f)\,(\pi) & \frac{\sqrt{6}}{6}(1+2f)\,(K) & \frac{\sqrt{6}}{2}(1-2f)\,(K) & \frac{\sqrt{6}}{6}(1-4f)\,(K) \\
-\frac{2\sqrt{6}}{3}(1-f)\,(\pi) & 2f(\pi) & (1-2f)\,(K) & 0 & 1(K) \\
\frac{\sqrt{6}}{6}(1+2f)\,(K) & (1-2f)\,(K) & -\frac{1}{2}(\pi)-\frac{1}{2}(1-4f)\,(\eta) & 0 & 0 \\
0 & 0 & \frac{\sqrt{6}}{2}(1-2f)\,(K) & 0 & -\frac{\sqrt{6}}{2}\,(K) \\
\frac{\sqrt{6}}{6}(1-4f)\,(K) & 1(K) & 0 & -\frac{\sqrt{6}}{2}(K) & \frac{1}{2}(1-2f)\,(\pi)+\frac{1}{2}(1+2f)\,(\eta)
\end{array}\right) k^{2},
\end{array}
$$

$\underline{I = 0,\ Y = 0}$

$$
\begin{array}{c}
 \\
\pi\Sigma \\
\bar{K}N \\
\eta\Lambda \\
K\equiv
\end{array}
\begin{array}{c}
\begin{array}{cccc}
\rho\Sigma & \bar{K}^{*}N & \varphi_{o}\Lambda & K^{*}\equiv
\end{array} \\
\left(\begin{array}{cccc}
4f(\pi) & \frac{\sqrt{6}}{2}(1-2f)\,(K) & 0 & \frac{\sqrt{6}}{2}(K) \\
\frac{\sqrt{6}}{2}(1-2f)\,(K) & \frac{3}{2}(\pi)-\frac{1}{2}(1-4f)\,(\eta) & \frac{\sqrt{2}}{2}(1+2f)\,(K) & 0 \\
0 & \frac{\sqrt{2}}{2}(1+2f)\,(K) & 0 & \frac{\sqrt{2}}{2}(1-4f)\,(K) \\
\frac{\sqrt{6}}{2}(K) & 0 & \frac{\sqrt{2}}{2}(1-4f)\,(K) & -\frac{3}{2}(1-2f)\,(\pi)+\frac{1}{2}(1+2f)\,(\eta)
\end{array}\right) k^{2},
\end{array}
$$

$\underline{I = 1/2,\ Y = -1}$

$$
\begin{array}{c}
 \\
\pi\equiv \\
\bar{K}\Lambda \\
\bar{K}\Sigma \\
\eta\equiv
\end{array}
\begin{array}{c}
\begin{array}{cccc} \rho\equiv & \bar{K}^*\Sigma & \bar{K}^*\Lambda & \varphi_o\equiv \end{array} \\
\begin{pmatrix}
-2(1-2f)(\pi) & 0 & \frac{1}{2}(1-4f)(K) & -\frac{1}{2}(K) \\
\frac{1}{2}(1-4f)(K) & \frac{1}{2}(1-4f)(K) & -(1-f)(\eta) & -(1-f)(\pi) \\
-\frac{1}{2}(K) & \frac{2}{3}(K) & -(1-f)(\pi) & 2f(\pi)+(1-f)(\eta) \\
0 & 0 & \frac{1}{2}(1-4f)(K) & \frac{3}{2}(K)
\end{pmatrix} k^2.
\end{array}
$$

## 7. The Reaction $0^- + \frac{1}{2}^+ \rightarrow 0^- + 3/2^+$

Here we will consider only $1^-$ exchange as shown in Figure A-6. The SU(3) interaction Lagrangians used for this process have already been discussed. We will consider only the I = 3/2, Y = 1 case. We obtain, denoting by $h^2$ the product $g_\rho g_{N^*\rho}$, where $g_\rho$ is the $\rho\pi\pi$ coupling constant and $g_{N^*\rho}$ is the $N^*_{++}\, p\rho^+$ coupling constant, the following results:

$\underline{I = 3/2,\ Y = 1}$

$$
\begin{array}{c}
 \\
\pi N \\
K\Sigma
\end{array}
\begin{array}{c}
\begin{array}{ccc} \pi N^* & \eta N^* & K\Sigma^* \end{array} \\
\begin{pmatrix}
-\frac{1}{\sqrt{15}}(\rho) & 0 & -\frac{1}{\sqrt{6}}(K^*) \\
\frac{1}{2\sqrt{15}}(K^*) & \frac{\sqrt{3}}{2}(K^*) & \frac{1}{2\sqrt{6}}(\rho)+\frac{1}{2\sqrt{6}}(\omega)+\frac{1}{\sqrt{6}}(\varphi)
\end{pmatrix} h^2.
\end{array}
$$

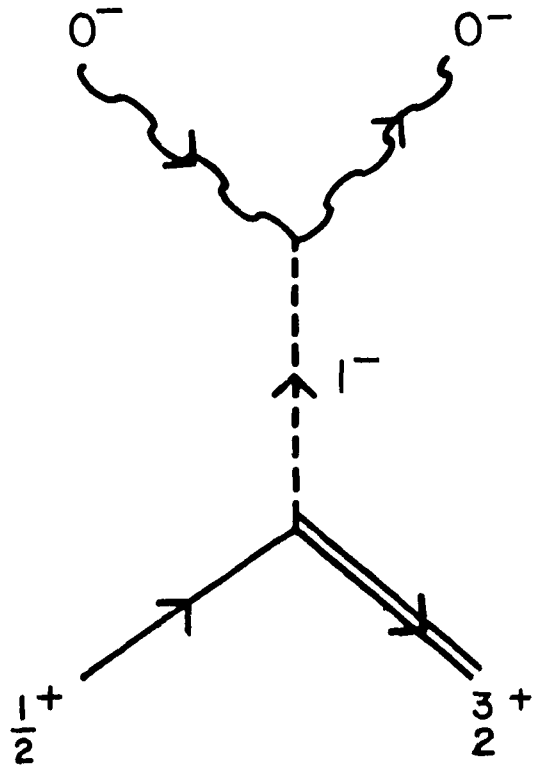


FIG. A-6 VECTOR EXCHANGE IN THE t CHANNEL.

# Appendix B. NOTATION

1.

a. For the Dirac matrices we use:

$$\gamma_k = \begin{pmatrix} 0 & -i\sigma_k \\ i\sigma_k & 0 \end{pmatrix},$$

where k = 1 to 3,

$$\gamma_4 = \begin{pmatrix} 1 & 0 \\ 0 & -1 \end{pmatrix}, \qquad \gamma_5 = \begin{pmatrix} 0 & -1 \\ -1 & 0 \end{pmatrix},$$

and

$$\sigma_{\mu\nu} = \frac{1}{2i}(\gamma_\mu \gamma_\nu - \gamma_\nu \gamma_\mu),$$

where $\mu,\nu$ = 1 to 4.

b. For the spin ½ baryons we use the Dirac spinor $u(\vec{p})$ such that

$$(i\gamma p + m)u(\vec{p}) = 0 \text{ and } \bar{u}(\vec{p})u(\vec{p}) = u^+(\vec{p})\gamma_4 u(\vec{p}) = 1. \tag{B.1}$$

The explicit form of the spinor is

$$u(\vec{p}) = \sqrt{\frac{p_o+m}{2m}} \begin{pmatrix} \chi_j \\ \dfrac{\vec{\sigma}\cdot\vec{p}}{p_o+m}\chi_j \end{pmatrix}, \tag{B.2}$$

where $\chi_j$ is a Pauli spinor.

c. The vector mesons are represented by a polarization four vector $\epsilon_\mu$ such that $\epsilon \cdot k = 0$, k being the four momentum of the vector mesons. In the rest frame of the vector particle, the $\epsilon_\mu$ corresponding to the creation of a particle with z components of spin m are

$$m = 1, -\left(\frac{\epsilon_x - i\epsilon_y}{\sqrt{2}}\right),$$

$$m = 0, \epsilon_z; \text{ and} \qquad \text{(B.3)}$$

$$m = -1, \left(\frac{\epsilon_x + i\epsilon_y}{\sqrt{2}}\right) .$$

The $\epsilon_\mu$ for other directions and frames are obtained from these by a Lorentz transformation.

d. For the spin 3/2 baryons we use the Rarita-Schwinger formalism. The particle is represented by $U_\mu(\vec{p})$ where

$$(i\gamma p + M)\ U_\mu(\vec{p}) = 0,$$

$$\gamma_\mu U_\mu(\vec{p}) = 0, \text{ and } p_\mu\ U_\mu = 0. \qquad \text{(B.4)}$$

If we define the unit polarization vectors

$$\vec{\epsilon}\pm = \mp\ (\vec{\epsilon}_1 \pm i\vec{\epsilon}_2)\ \frac{1}{\sqrt{2}}\ ,\ \vec{\epsilon}_o = \vec{\epsilon}_3,$$

the three vector parts of $U_\mu^{(i)}$ can be written as

$$\vec{U}^{(1)} = \vec{\epsilon}_+ \; u_1,$$

$$\vec{U}^{(2)} = \frac{1}{\sqrt{3}} \vec{\epsilon}_+ \; u_2 + \sqrt{\frac{2}{3}} \vec{\epsilon}_o \left(\frac{E}{M}\right) u_1,$$

$$\vec{U}^{(3)} = \frac{1}{\sqrt{3}} \vec{\epsilon}_- \; u_1 + \sqrt{\frac{2}{3}} \vec{\epsilon}_o \left(\frac{E}{M}\right) u_2, \text{ and} \tag{B.5}$$

$$\vec{U}^{(4)} = \vec{\epsilon}_- \; u_2,$$

where $u_1$ and $u_2$ denote the Dirac spinors corresponding to spin up or down, respectively. The time part is

$$U_4^{(i)} = iU_o^{(i)},$$

where

$$U_o^{(1)} = 0,$$

$$U_o^{(2)} = \sqrt{\frac{2}{3}} \; \frac{p}{M} \; u_1,$$

$$U_o^{(3)} = \sqrt{\frac{2}{3}} \; \frac{p}{M} \; u_2, \text{ and} \tag{B.6}$$

$$U_o^{(4)} = 0.$$

These equations are valid provided the z direction is taken along the direction of the particle motion. In the above we have denoted by E and M the energy and mass respectively of the spin 3/2 particle. The propagator for a spin 3/2 particle is then

$$\frac{M - i\gamma p}{i(M^2 + p^2)} \; P_{\mu\nu}, \tag{B.7}$$

where

$$P_{\mu\nu} = \left[\delta_{\mu\nu} - \frac{1}{3}\gamma_\mu\gamma_\nu + \frac{1}{3M}(\gamma_\mu p_\nu + \frac{i}{3M}(\gamma_\mu p_\nu - \gamma_\nu p_\mu) + \frac{2}{3M^2} p_\mu p_\nu\right] . \quad (B.8)$$

It seems worthwhile to point out that insofar as the spin 3/2 particle can be off shell, it is not strictly true to say that the propagator is ambiguous, because one can arbitrarily add terms that become zero at $p^2 = -M^2$. In fact to obtain the propagator, all we need is $< 0|T[\Psi_\mu(x)\ \Psi_\nu(y)]|0 >$ which can most easily be obtained from finding a matrix $C_{\mu\nu}$ such that

$$C_{\mu\lambda}\ D_{\lambda\nu} = \delta_{\lambda\nu}[\Box - M^2], \quad (B.9)$$

where $D_{\lambda\nu}\ \Psi_\nu = 0$ is the Rarita-Schwinger equation. Once we have $C_{\mu\nu}$ we obtain the propagator in momentum space merely by

$$< 0|T\ [\Psi_\mu(x)\ \Psi_\nu(y)]|0 > = -\frac{i}{(2\pi)^4}\int d^4p\ \frac{e^{ip(x-y)}}{p^2+M^2-i\epsilon}\ C_{\mu\nu}(p), \quad (B.10)$$

as discussed by Peierls (1952).

2. We consider the reaction

$a + b \rightarrow c + d$

where the particles and four momenta are represented by the letters a, b, c, and d respectively as shown in Figure B-1. The pseudoscalar meson is represented by "a", "b" represents the nucleon, "c" represents

a spin 0 or 1 meson, and "d" represents a spin ½ or 3/2 baryon. We define the momentum transfer e by e = b-d. The scalar product of two vectors a = $(a,a_o)$, b = $(b,b_o)$ is $a \cdot b = \vec{a}\cdot\vec{b} - a_o b_o$. The usual Mandelstam variables are

$$\begin{aligned} S &= -(a+b)^2 = -(c+d)^2, \\ t &= -(a-c)^2 = -(b-d)^2, \text{ and} \\ u &= -(a-d)^2 = -(b-c)^2. \end{aligned} \tag{B.11}$$

We shall in our calculations work in the center of mass frame.

3) The S matrix and the invariant amplitude $\mathcal{M}_{fi}$ are related by

$$S_{fi} = \delta_{fi} - (2\pi)^4 i\, \delta^{(4)}(P_f - P_i)\sqrt{\frac{m_b\, m_d}{4a_o b_o c_o d_o}}\, \mathcal{M}_{fi}, \tag{B.12}$$

where

$$\mathcal{M}_{fi} = \bar{u}(\vec{p}_f)\, u(\vec{p}_i) \tag{B.13}$$

If we define

$$\mathcal{M}_{fi} = -\frac{4\pi\sqrt{S}}{\sqrt{m_b\, m_d}}\, T_{fi} \tag{B.14}$$

the cross section is given by

$$\frac{d\sigma_{fi}}{d\Omega} = \frac{q_f}{q_i}\, |T_{fi}|^2. \tag{B.15}$$

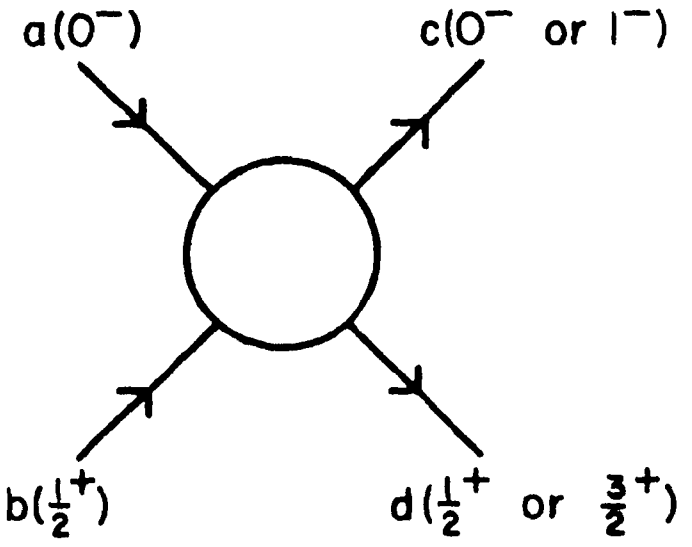


FIG. B-1 DESIGNATION OF PARTICLES.

The states i and f may be taken as helicity states, and we use

$$\langle cd;\ \lambda_c\ \lambda_d\ |T|\ ab;\ \lambda_a\ \lambda_b \rangle$$

or simply

$$T_{\lambda_c\lambda_d;\ \lambda_a\lambda_b}.$$

We shall assume $\varphi = 0$ by taking the y axis normal to the production plane.

In addition we shall define $T'_{if}$ by

$$T'_{if} = \sqrt{q_i}\ T\ \sqrt{q_f} \tag{B.16}$$

where qi and qf stand for the momenta in the incident and outgoing channels.

We now construct appropriate linear combinations of the helicity states to obtain states of definite parity and total angular momentum $\epsilon$ and J respectively. The amplitude $T'^{J}_{(if)\epsilon}$ corresponding to total angular momentum J and parity $\epsilon$ so obtained is then a linear combination of the amplitudes $T'_{if}$. The i and f in $T'^{J}_{(if)\epsilon}$ correspond to the initial and outgoing particles, helicity indices being subsumed in $J,\epsilon$. The two particle unitary condition is

$$\mathrm{Im}\, T'^{J}_{(if)\epsilon} = \sum_m T'^{J}_{(im)\epsilon}\ T'^{J}_{(mf)\epsilon}\ . \tag{B.17}$$

We shall discuss in more detail the procedure to obtain definite angular momentum and parity amplitudes in Appendix C.

# Appendix C. ANGULAR MOMENTUM DECOMPOSITION

In this appendix we shall briefly review the helicity formalism of Jacob and Wick (1959) and other related points.

## 1. Normalizations

We introduce $|\hat{p}\ \lambda a\ \lambda b>$ to denote a two particle state in which particle a is moving the direction $\hat{p}$ and particles a and b have helicities $\lambda a$ and $\lambda b$ respectively.

We also introduce $|jm\ \lambda a\ \lambda b>$ to denote a two particle state in which the two particles a and b have helicities $\lambda a$ and $\lambda b$ as before. The irreducible representation of the rotation group in the Hilbert space of physical states according to which this state transforms is denoted by j, and the states within an irreducible representation are distinguished by m. The normalization conditions are

$$<\hat{p}\ \lambda a\ \lambda b|\hat{p}'\lambda a'\ \lambda b'> = \delta_{\lambda a\lambda a'}\ \delta_{\lambda b\lambda b'}\ \delta(\hat{p}-\hat{p}'), \tag{C.1}$$

where

$$\delta(\hat{p}-\hat{p}') = \delta(\cos\theta - \cos\theta')\ \delta(\varphi - \varphi'),$$

and

$$<j'm'\ \lambda a'\lambda b'|jm\ \lambda a\lambda b> = \delta_{jj'}\ \delta_{mm'}\ \delta_{\lambda a\lambda a'}\ \delta_{\lambda b\lambda b'}. \tag{C.2}$$

## 2. Expansions and Definitions of e Functions

A state $|\hat{p}\ \lambda a\lambda b>$ can be expanded

$$|\hat{p}\ \lambda a\lambda b> = \sum_{jm} |jm\ \lambda a\lambda b>\sqrt{\frac{2j+1}{4\pi}}\ D^{j}_{m\lambda}(\varphi,\theta,0). \tag{C.3}$$

In the above $D^J_{m\lambda}(\varphi,\theta,0)$ is a Wigner D function (Wigner, 1959) corresponding to $\lambda = \lambda a - \lambda b$, and the arguments in parenthesis denote its Euler angles. We can invert relation (C.1) to obtain

$$|\, jm\ \lambda a\ \lambda b > = \sqrt{\frac{2J+1}{4\pi}} \int d\Omega\ D^{*J}_{m\lambda}\ (\varphi,\theta,0)\, |\hat{p}\ \lambda a \lambda b > \ . \tag{C.4}$$

We obtain

$$T_{\lambda c \lambda d;\ \lambda a \lambda b} = \sum_j\ (2j+1)\ T^J_{\lambda c \lambda d;\ \lambda a \lambda b}\ D^{*j}_{\lambda\mu}\ (\varphi,\theta,0) \tag{C.5}$$

making use of the rotational invariance. In the above $T^J_{\lambda c \lambda d;\ \lambda a \lambda b}$ denotes the corresponding matrix element for the transition in a definite angular momentum state j from the two particle state with helicities $\lambda a$ and $\lambda b$ into the two particle state with helicities $\lambda c$ and $\lambda d$, and where we have defined $\lambda = \lambda a - \lambda b$ and $\mu = \lambda c - \lambda d$. Choosing $\varphi = 0$, the above becomes:

$$T_{\lambda c \lambda d;\ \lambda a \lambda b} = \sum_j\ (2j+1)\ T^J_{\lambda c \lambda d;\ \lambda a \lambda b}\ d^J_{\lambda\mu}(\theta)\,, \tag{C.6}$$

where the $d^J_{\lambda\mu}(\theta)$ are given for example by Jacob and Wick. Solving for $T^J_{\lambda c \lambda d;\ \lambda a \lambda b}$ we obtain

$$T^j_{\lambda c \lambda d;\ \lambda a \lambda b} = \frac{1}{2} \int_{-1}^{1} d(\cos\theta)\ d^j_{\lambda\mu}(\theta)\ T_{\lambda c \lambda d;\ \lambda a \lambda b}. \tag{C.7}$$

An arbitrary Born amplitude calculated from a Feynman graph can be written in the form

$$T_{\lambda c \lambda d;\ \lambda a \lambda b} = (\cos\,\theta/2)^{|\lambda+\mu|}\ (\sin\,\theta/2)^{|\lambda-\mu|}\ \frac{t(\cos\theta)}{z-\cos\theta}\ , \tag{C.8}$$

where $t(\cos\theta)$ is a polynomial in $\cos\theta$ and $z$ is a function of the magnitudes of momenta and the exchanged mass. We then write

$$(\cos\theta/2)^{|\lambda+\mu|}(\sin\theta/2)^{|\lambda-\mu|}\frac{t(\cos\theta)}{z-\cos\theta} = (\cos\theta/2)^{|\lambda+\mu|}(\sin\theta/2)^{|\lambda-\mu|}\left[\frac{t(z)}{z-\cos\theta} + c(\cos\theta)\right] . \tag{C.9}$$

This we can do most easily by merely writing $\cos\theta = z-(z-\cos\theta)$.

We next define the e functions by[1]

$$\sum_{j=M}^{\infty}(2j+1)e^{j}_{\lambda\mu}(z)\ d^{j}_{\lambda\mu}(\cos\theta) = \left(\frac{1+\cos\theta}{1+z}\right)^{\frac{|\lambda+\mu|}{2}}\left(\frac{1-\cos\theta}{z-1}\right)^{\frac{|\lambda-\mu|}{2}}\frac{1}{z-\cos\theta}, \tag{C.10}$$

where $M = \max(|\lambda|,|\mu|)$ and $z > 1$. From this we obtain

$$\frac{(\cos\theta/2)^{|\lambda+\mu|}(\sin\theta/2)^{|\lambda-\mu|}}{z-\cos\theta} = \left(\frac{1+z}{2}\right)^{\frac{|\lambda+\mu|}{2}}\left(\frac{z-1}{2}\right)^{\frac{|\lambda-\mu|}{2}}\sum_{j=M}^{\infty}(2j+1)e^{j}_{\lambda\mu}(z)\ d^{j}_{\lambda\mu}(\cos\theta) \tag{C.11}$$

Also we can expand

$$(\cos\theta/2)^{|\lambda+\mu|}(\sin\theta/2)^{|\lambda-\mu|}\,c(\cos\theta) = \sum_{j=M}^{N} c^{j}_{\lambda\mu}\ d^{j}_{\lambda\mu}(\cos\theta), \tag{C.12}$$

where N-M is the degree of the polynomial $c(\cos\theta)$.

---

1. It is important to note that the e functions here defined differ from those given by Andrews and Gunson (1964) by a phase factor.

Comparing (C.6), (C.8), and (C.11) we see that

$$T^J_{\lambda c \lambda d;\, \lambda a \lambda b} = \left(\frac{1+z}{2}\right)^{\frac{|\lambda+\mu|}{2}} \left(\frac{z-1}{2}\right)^{\frac{|\lambda-\mu|}{2}} e^J_{\lambda\mu}(z)\, t(z) + \frac{1}{2J+1}\, e^j_{\lambda\mu}(z). \tag{C.13}$$

The integral representation for the e functions is, for $|\mu| < \lambda$

$$e^{\lambda\mu}_J(z) = (-)^{\lambda-\mu} \left[\frac{(J+\lambda)!\,(J-\lambda)!}{(J+\mu)!\,(J-\mu)!}\right]^{\frac{1}{2}} \left(\frac{1+z}{2}\right)^{\frac{|\lambda+\mu|}{2}} \left(\frac{z-1}{2}\right)^{\frac{|\lambda-\mu|}{2}} Q^{\lambda-\mu,\lambda+\mu}_{J-\lambda}, \tag{C.14}$$

where

$$Q^{\alpha\beta}_n(z) = 2^{-n-1}(z-1)^{-\alpha}(z+1)^{-\beta} \int_{-1}^{1} (x-\xi)^{-n-1}(1-\xi)^{n+\alpha}(1+\xi)^{n+\beta}\, d\xi. \tag{C.15}$$

In addition the e functions obey the symmetry properties

$$e^{\lambda\mu}_J(z) = (-)^{\lambda-\mu} e^{\mu\lambda}_J(z) = (-)^{\lambda-\mu} e^{-\lambda,-\mu}_J(z) = e^{-\mu,-\lambda}_J(z). \tag{C.16}$$

### 3. Parity Amplitudes

The result of the parity operator P on $|J\,m\,\lambda a \lambda b\rangle$ is

$$P\,|J\,m\,\lambda a \lambda b\rangle = \eta_a \eta_b (-)^{J - S_a - S_b}\, |J\,m\,-\lambda a\,-\lambda b\rangle, \tag{C.17}$$

where $\eta_a$ and $\eta_b$ are the intrinsic parities of particles a and b and $S_a$ and $S_b$ denote their spin.

Assuming parity conservation, we then obtain

$$\langle -\lambda c\, -\lambda d\,|\,T_J\,|\,-\lambda a\, -\lambda b\rangle = \frac{\eta_a \eta_b}{\eta_c \eta_d}\, (-)^{S_a+S_b-S_c-S_d}\, \langle \lambda c \lambda d\,|\,T_J\,|\,\lambda a \lambda b\rangle. \tag{C.18}$$

States of definite parity and angular momentum are then

$$|\epsilon_r J m|\lambda a|\,|\lambda b|> = \frac{1}{\sqrt{2}}\,[\,|J m\ \lambda a \lambda b> \pm \eta_a \eta_b (-)^{j-S_a-S_b}\ |J m-\lambda a-\lambda b>], \quad \text{(C.19)}$$

where $\epsilon$ denotes the parity eigenvalue, and where we choose the + or - sign on the right hand side of the above equation according to whether $\epsilon$ is + or -, and $r = \lambda a\ \lambda b$ enumerates the distinct possible states. We then see that

$$< |\lambda c|\,|\lambda d|r'\ |T_J|\ |\lambda a|\,|\lambda b|r> = < \lambda c \lambda d|T_J|\ \lambda a \lambda b> \pm \eta_a \eta_b (-)^{j-S_a-S_b}$$

$$< \lambda c \lambda d|T_J|\ -\lambda a-\lambda b>\ , \quad \text{(C.20)}$$

for each r and r'.

## Appendix D. MOMENTUM DEPENDENCE OF THE POTENTIALS

Here we shall consider the momentum dependence of the potentials to be used. The resultant potential used in our calculations is then obtained by multiplying the momentum dependent part (here computed using the Lagrangians discussed in Appendix A) by the corresponding crossing coefficients as given in the same appendix.

### 1. The Reaction $0^- + \frac{1}{2}^+ \rightarrow 0^- + \frac{1}{2}^+$

We write

$$\mathcal{M}_{fi} = \bar{u}(\vec{d})\left[-\alpha + i\gamma\left(\frac{a+c}{2}\right)\mathcal{B}\right]u(\vec{b}) . \tag{D.1}$$

We can rewrite the above as

$$\mathcal{M}_{fi} = \sqrt{\frac{(b_o+m_b)(d_o+m_d)}{4m_b m_d}}\ \chi^+_{\lambda d}[X + 4_{\lambda b\lambda d}\ Y]\ \chi_{\lambda b}, \tag{D.2}$$

where $\chi_{\lambda d}$ and $\chi_{\lambda a}$ denote the Pauli spinors corresponding to helicities $\lambda d$ and $\lambda a$ respectively. We have defined

$$X = \left[-\alpha - \frac{\mathcal{B}}{2}\{a_o+b_o+c_o+d_o - m_b-m_d\}\right] \tag{D.3}$$

and

$$Y = \left[\alpha - \frac{\mathcal{B}}{2}\{a_o+b_o+c_o+d_o+m_b+m_d\}\right]\sqrt{\frac{(b_o-m_b)(d_o-m_d)}{(b_o+m_b)(d_o+m_d)}} . \tag{D.4}$$

We define

$$\begin{pmatrix} X^\ell \\ Y^\ell \end{pmatrix} = \frac{1}{2}\int_{-1}^{1} dx \begin{pmatrix} X \\ Y \end{pmatrix} P_\ell(x) . \tag{D.5}$$

Denoting by $T'_{\ell+}$ and $T'_{\ell-}$ the parity amplitudes corresponding to $j = \ell + \frac{1}{2}$ and $j = \ell - \frac{1}{2}$ as already defined in Appendix B, we use

$$T'_{\ell\,\pm} = \langle \tfrac{1}{2}|T'|\tfrac{1}{2}\rangle \pm \langle \tfrac{1}{2}|T'|-\tfrac{1}{2}\rangle , \tag{D.6}$$

and

$$\cos\theta/2\; d^{j}_{\frac{1}{2},\frac{1}{2}}(\theta) = \frac{1}{2}\left[P_{\ell}(\cos\theta) + P_{\ell+1}(\cos\theta)\right], \qquad j = \ell + \tfrac{1}{2} \tag{D.7}$$

$$\sin\theta/2\; d^{j}_{-\frac{1}{2},\frac{1}{2}}(\theta) = \frac{1}{2}\left[P_{\ell}(\cos\theta) - P_{\ell+1}(\cos\theta)\right], \tag{D.8}$$

where

$$T'_{fi} = -\frac{1}{4\pi}\sqrt{m_b}\sqrt{|\vec{b}|}\;\; {}_{f1}\sqrt{|\vec{d}|}\sqrt{m'_d}\;\frac{1}{\sqrt{(a_o+b_o)(c_o+d_o)}}\,, \tag{D.9}$$

to obtain

$$T'_{\ell\,\pm} = -\frac{1}{4\pi}\sqrt{\frac{(b_o+m_b)(d_o+m_d)}{(a_o+b_o)(c_o+d_o)}}\;\sqrt{|\vec{b}||\vec{d}|}\;\left[X_{\ell} + Y_{\ell\,\pm 1}\right]. \tag{D.10}$$

Denoting the Born approximations to $\mathcal{M}$, T, $T^1$, $\mathcal{A}$, and $\mathcal{B}$ by M, V, $V^1$, A and B respectively, we then obtain the following results.

a. Baryon exchange

We will consider the process shown in Figure A-2. We obtain using the Lagrangian discussed in Appendix A

$$A = -\left[m_e - \frac{m_b+m_d}{2}\right]\frac{1}{(\vec{b}+\vec{d})^2 - \frac{1}{4}(b_o-a_o-c_o+d_o)^2 + m_e^2} \tag{D.11}$$

and

$$B = - \frac{1}{(\vec{b}+\vec{d})^2 - \frac{1}{4}(b_o - a_o - c_o + d_o)^2 + m_e^2} \quad , \tag{D.12}$$

where the mass of the baryon being exchanged is denoted by $m_e$.

Upon defining

$$Q_\ell(z) = \frac{1}{2}\int_{-1}^{1} dx \, \frac{P_\ell(x)}{z-x} \quad , \tag{D.13}$$

we obtain

$$A_\ell = \left[ m_e - \frac{m_b+m_d}{2} \right] \frac{(-)^{\ell+1}}{2|\vec{b}||\vec{d}|} \; Q_\ell(z) \tag{D.14}$$

and

$$B_\ell = \frac{(-)^{\ell+1}}{2|\vec{b}||\vec{d}|} \; Q_\ell(z) \, , \tag{D.15}$$

where

$$z = \frac{|\vec{b}|^2 + |\vec{d}|^2 - \frac{1}{4}(a_o - b_o - d_o + c_o)^2 + m_e^2}{2|\vec{b}||\vec{d}|} \tag{D.16}$$

b. Decuplet exchange

Here we will consider the process shown in Figure A-3. Using the Lagrangian discussed in Appendix A, we obtain

$$A = \left\{ b\cdot d \left[ m_e + \frac{m_b+m_d}{2} \right] + b\cdot c \left[ \frac{1}{3} m_d + \frac{7}{6} \frac{m_d^2}{m_e} - \frac{1}{6} \frac{m_b m_d}{m_e} + \frac{1}{3} \frac{m_d^3}{m_e^2} \right. \right.$$

$$+ \frac{1}{3}\frac{m_b m_d^2}{m_e^2}\Big] + a\cdot d\Big[\frac{1}{3}m_b + \frac{7}{6}\frac{m_b^2}{m_e} - \frac{1}{6}\frac{m_b m_d}{m_e} + \frac{1}{3}\frac{m_b^3}{m_e^2} + \frac{1}{3}\frac{m_b^2 m_d}{m_e^2}\Big]$$

$$+ b\cdot c\ a\cdot d\Big[\frac{4}{3}\frac{1}{m_e} + \frac{1}{3}\frac{m_d}{m_e^2} + \frac{1}{3}\frac{m_b}{m_e^2}\Big] + \Big[\frac{1}{3}m_e m_b m_d + \frac{1}{6}m_b m_d^2$$

$$+ \frac{1}{6}m_b^2 m_d + \frac{m_b^2 m_d^2}{m_e} - \frac{1}{6}\frac{m_b m_d^3}{m_e} - \frac{1}{6}\frac{m_b^3 m_d}{m_e} + \frac{1}{3}\frac{m_b^2 m_d^3}{m_e^2} + \frac{1}{3}\frac{m_b^3 m_d^2}{m_e^2}\Big]\Big\}$$

$$\Big\{\frac{1}{(\vec{b}+\vec{d})^2 - \frac{1}{4}(b_o - a_o + d_o - c_o)^2 + m_e^2}\Big\} \qquad \text{(D.17)}$$

and

$$B = \Big\{-b\cdot d + b\cdot c\Big[\frac{1}{3}\frac{m_d}{m_e} - \frac{2}{3}\frac{m_d^2}{m_e^2}\Big] + a\cdot d\Big[\frac{1}{3}\frac{m_b}{m_e} - \frac{2}{3}\frac{m_b^2}{m_e^2}\Big]$$

$$+ a\cdot d\ b\cdot c\Big[\frac{2}{3m_e^2}\Big] + \Big[-\frac{1}{3}m_b m_d - \frac{1}{3}\frac{m_b^2 m_d}{m_e} - \frac{1}{3}\frac{m_b m_d^2}{m_e} + \frac{2}{3}\frac{m_b^2 m_d^2}{m_e^2}\Big]\Big\}$$

$$\Big\{\frac{1}{(\vec{b}+\vec{d}) - \frac{1}{4}(b_o - a_o + d_o - c_o)^2 + m_e^2}\Big\}, \qquad \text{(D.18)}$$

where the mass of the particle exchanged is denoted by $m_e$. Defining

$$\alpha_1 = m_e + \frac{m_b + m_d}{2},$$

$$\alpha_2 = \frac{1}{3}m_d + \frac{7}{6}\frac{m_d^2}{m_e} - \frac{1}{6}\frac{m_b m_d}{m_e} + \frac{1}{3}\frac{m_d^3}{m_e^2} + \frac{1}{3}\frac{m_b m_d^2}{m_e^2},$$

$$\alpha_3 = \frac{1}{3}m_b + \frac{7}{6}\frac{m_b^2}{m_e} - \frac{1}{6}\frac{m_b m_d}{m_e} + \frac{1}{3}\frac{m_b^3}{m_e^2} + \frac{1}{3}\frac{m_b^2 m_d}{m_e^2},$$

$$\alpha_4 = \frac{4}{3}\frac{1}{m_e} + \frac{1}{3}\frac{m_d}{m_e^2} + \frac{1}{3}\frac{m_b}{m_e^2}\,, \tag{D.19}$$

$$\alpha_5 = \frac{1}{3}\, m_e m_b m_d + \frac{1}{6}\, m_b m_d^2 + \frac{1}{6}\, m_b^2 m_d + \frac{m_b^2 m_d^2}{m_e} - \frac{1}{6}\frac{m_b m_d^3}{m_3}$$

$$- \frac{1}{6}\frac{m_b^2 m_d}{m_e} + \frac{1}{3}\frac{m_b^2 m_d^3}{m_e^2} + \frac{1}{3}\frac{m_b^3 m_d^2}{m_e^2}\,,$$

$$\beta_1 = 1,$$

$$\beta_2 = \frac{1}{3}\frac{m_d}{m_e} - \frac{2}{3}\frac{m_d^2}{m_e^2}\,,$$

$$\beta_3 = \frac{1}{3}\frac{m_b}{m_e} - \frac{2}{3}\frac{m_b^2}{m_e^2}\,, \tag{D.20}$$

$$\beta_4 = \frac{2}{3}\frac{1}{m_e^2}\,,$$

$$\beta_5 = -\frac{1}{3}\, m_b m_d - \frac{1}{3}\frac{m_b^2 m_d}{m_e} - \frac{1}{3}\frac{m_b m_d^2}{m_e} + \frac{2}{3}\frac{m_b^2 m_d^2}{m_e^2}\,,$$

$$z = \frac{|\vec{b}|^2 + |\vec{d}|^2 - \frac{1}{4}(a_o - b_o + c_o - d_o)^2}{2|\vec{b}||\vec{d}|},$$

$$\mathcal{K}_1 = \frac{1}{2}\{\alpha_1 - \alpha_2 - \alpha_3 + (a_o d_o + b_o c_o - bdz)\alpha_4\},$$

$$\mathcal{K}_2 = \frac{1}{6}\,|\vec{b}||\vec{d}|\alpha_4,$$

$$\mathcal{K}_3 = \frac{1}{2|\vec{b}||\vec{d}|}\{\alpha_1[-|\vec{b}||\vec{d}|z - b_o d_o] + \alpha_2[|\vec{b}||\vec{d}|z - b_o c_o]$$

$$+ \alpha_3[|\vec{b}||\vec{d}|z - a_o d_o] + \alpha_4[|\vec{b}|^2 - |\vec{b}||\vec{d}|(a_o d_o + b_o c_o)z]\}, \quad (D.21)$$

$$\lambda_1 = \frac{1}{2}\{\beta_1 - \beta_2 - \beta_3 + (a_o d_o + b_o c_o - bdz)\beta_4\},$$

$$\lambda_2 = \frac{1}{6}|\vec{b}||\vec{d}|\beta_4,$$

and

$$\lambda_3 = \frac{1}{2|\vec{b}||\vec{d}|}\{\beta_1[-|\vec{b}||\vec{d}|z - b_o d_o] + \beta_2[|\vec{b}||\vec{d}|z - b_o c_o]$$

(D.22)

$$+ \beta_3[|\vec{b}||\vec{d}|z - a_o d_o] + \beta_4[|\vec{b}|^2|\vec{d}|^2 - |\vec{b}||\vec{d}|(a_o d_o + b_o c_o)z]\},$$

we obtain

$$A_\ell = \mathcal{K}_1\delta_{\ell o} + \mathcal{K}_2\delta_{\ell 1} + \mathcal{K}_3(-)^\ell Q_\ell(z) \quad (D.23)$$

and

$$B_\ell = \lambda_1\delta_{\ell o} + \lambda_2\delta_{\ell 1} + \lambda_3(-)^\ell Q_\ell(z) \quad (D.24)$$

c` Vector exchange

Here we consider the effect of the diagram shown in Figure A-4. Both the $\gamma_\mu$ (electric) and the $\sigma_\nu$ (magnetic) parts of the VBB coupling are considered. We first consider the contribution due to the $\gamma_\mu$ coupling.

i) Electric ($\gamma_\mu$) contribution

Here we obtain

$$A = \frac{1}{(\vec{b}-\vec{d})^2 - \frac{1}{4}(a_o-b_o-c_o+d_o)^2 + m_e^2} \left(\frac{m_a^2-m_c^2}{m_e^2}\right)(m_b-m_d) \tag{D.25}$$

and

$$B = -\frac{2}{(\vec{b}-\vec{d})^2 - \frac{1}{4}(a_o-b_o-c_o+d_o)^2 + m_e^2} . \tag{D.26}$$

Thus we have

$$A_\ell = \frac{1}{2|\vec{b}||\vec{d}|}\left(\frac{m_a^2-m_c^2}{m_e^2}\right)(m_b-m_d)\ Q_\ell(z) \tag{D.27}$$

and

$$B_\ell = -\frac{1}{|\vec{b}||\vec{d}|}\ Q_\ell(z)\ , \tag{D.28}$$

where

$$z = \frac{|\vec{b}|^2 + |\vec{d}|^2 + m_e^2 - \frac{1}{4}(a_o-b_o-c_o+d_o)^2}{2|\vec{b}||\vec{d}|}. \tag{D.29}$$

ii) Magnetic ($\sigma_{\mu\nu}e_\nu$) contribution

We will next consider the contribution due to the anomalous magnetic moment of the baryons ($\sigma_{\mu\nu}e_\nu$ coupling). Using the relation

$$\bar{u}(\vec{d})\sigma_{\mu\nu}e_\nu\ u(\vec{b}) = \bar{u}(\vec{d})[\gamma_\mu(m_b+m_d) + i(b+d)_\mu]\ u(\vec{b}), \tag{D.30}$$

we can reduce the $\sigma_{\mu\nu}e_\nu$ term to the sum of two terms.

The first term has the same spatial structure as the $\gamma_\mu$ term already considered. For the second term we drop the factor $1/(m_b+m_d)$ which we have included in the SU(3) considerations and obtain

$$A = - \frac{(a+c)\cdot(b+d) + \frac{(m_a^2-m_c^2)(m_d^2-m_b^2)}{m_e^2}}{(\vec{b}-\vec{d})^2 - \frac{1}{4}(a_o-b_o-c_o+d_o)^2 + m_e^2}, \tag{D.31}$$

$$B = 0. \tag{D.32}$$

By using $(a + c) \cdot (b + d) = u - s = m^2_a + m^2_b + m^2_c + m^2_d - 2s - t,$ (D.33)

$$\sqrt{s} = \frac{1}{2}(a_o+b_o+c_o+d_o), \tag{D.34}$$

and defining

$$\mathcal{K}_1 = m^2_a + m^2_b + m^2_c + m^2_d - 2s + \frac{(m^2_a-m^2_c)(m^2_d-m^2_b)}{m^2_e}, \tag{D.35}$$

$$\mathcal{K}_2 = -|\vec{b}|^2 - |\vec{d}|^2 + \frac{1}{4}(a_o-b_o-c_o+d_o)^2, \text{ and} \tag{D.36}$$

$$\mathcal{K}_3 = \mathcal{K}_1 - \mathcal{K}_2, \tag{D.37}$$

we obtain

$$A_\ell = - \frac{1}{2|\vec{b}||\vec{d}|}[\mathcal{K}_3 Q_\ell(z) - 2|\vec{b}||\vec{d}| z Q_\ell(z) + 2|\vec{b}||\vec{d}|\delta_{\ell o}], \tag{D.38}$$

where

$$z = \frac{|\vec{b}|^2 + |\vec{d}|^2 - \frac{1}{4}(a_o - b_o - c_o + d_o)^2 + m_e^2}{2|\vec{b}||\vec{d}|} \tag{D.39}$$

and $$B_\ell = 0. \tag{D.40}$$

2) The reaction $0^- + \frac{1}{2}^+ \rightarrow 1^- + \frac{1}{2}^+$

This reaction is shown in Figure A-5 with pseudoscalar meson exchange. We obtain for M:

$$M = -2i\, \bar{u}(\vec{d})\, \gamma_5\, u(\vec{b})\, \frac{1}{m_e^2 - t}\, e^{(\lambda)} \cdot a, \tag{D.41}$$

where $e^{(\lambda)}$ is the polarization vector for the vector meson. Choosing the z axis parallel to the direction of a, the y axis perpendicular to the production plane, and denoting the helicity of the vector meson by $\lambda_c$, we obtain

$$e^{(\lambda_c)} = \begin{cases} \left(-\frac{1}{\sqrt{2}}\cos\theta,\ -\frac{i}{\sqrt{2}},\ \frac{\sin\theta}{\sqrt{2}},\ 0\right) & ,\ \lambda_c = +1 \\ \left(\frac{c_o}{mc}\sin\theta,\ 0,\ \frac{c_o}{mc}\cos\theta,\ i\frac{|\vec{c}|}{mc}\right) & ,\ \lambda_c = 0 \\ \left(\frac{1}{\sqrt{2}}\cos\theta,\ 1,\ -\frac{\sin\theta}{\sqrt{2}},\ 0\right) & ,\ \lambda_c = -1. \end{cases} \tag{D.42}$$

Therefore, we obtain the following result for $e^{(\lambda_c)} \cdot a$:

$$e^{(\lambda_c)} \cdot a = \begin{cases} \dfrac{|\vec{a}| \sin\theta}{\sqrt{2}} & , \lambda_c = +1 \\ \left( \dfrac{|\vec{a}| c_o}{m_c} \cos\theta - \dfrac{|\vec{c}| a_o}{m_c} \right) & , \lambda_c = 0 \\ - \dfrac{|\vec{a}| \sin\theta}{\sqrt{2}} & , \lambda_c = -1. \end{cases} \tag{D.43}$$

We define

$$\xi_{\pm} = \sqrt{\frac{(b_o+m_b)(d_o+m_d)}{4m_b m_d}} \; (\eta_b \pm \eta_d), \tag{D.44}$$

where

$$\eta_b = \frac{|\vec{b}|}{b_o+m_b} \qquad \text{and} \quad \eta_d = \frac{|\vec{d}|}{d_o+m_d},$$

and obtain

$$\bar{u}(\vec{d}) \; \gamma_5 u(\vec{b}) = -2\lambda_b \; \xi_{-4\lambda b \lambda d}. \tag{D.45}$$

We then obtain for the different helicity amplitudes

$$M_{\lambda a \lambda b;\, \lambda c \lambda d} = 4\imath \left( \frac{1}{m_e^2 - t} \right) e^{(\lambda_c)} \cdot a \; \lambda b \; \xi_{-4\lambda b \lambda d} \; d_{\lambda b \lambda d}(\theta). \tag{D.46}$$

By using the relations discussed in Appendix C for the case $J = \frac{1}{2}$, we obtain (defining $z = \dfrac{|\vec{b}|^2 + |\vec{d}|^2 - \frac{1}{4}(a_o - b_o + c_o - d_o)^2 + m_e^2}{2bd}$)

$$M^{J=\frac{1}{2}}_{0\frac{1}{2};\,0\frac{1}{2}} = \xi_{-1}\,\frac{i}{|\vec{b}||\vec{d}|}\left\{\left(\frac{1+z}{2}\right)^{\frac{1}{2}}\left[-\frac{|\vec{b}|c_o}{m_c}z + \frac{|\vec{d}|a_o}{m_c}\right]e^{\frac{1}{2}}_{-\frac{1}{2},-\frac{1}{2}}(z) + \frac{|\vec{b}|c_o}{2m_c}\right\}, \tag{D.47}$$

$$M^{J=\frac{1}{2}}_{0-\frac{1}{2};\,0\frac{1}{2}} = \xi_{+1}\,\frac{i}{|\vec{b}||\vec{d}|}\left\{\left(\frac{z-1}{2}\right)^{\frac{1}{2}}\left[\frac{|\vec{b}|c_o}{m_c}z - \frac{|\vec{d}|a_o}{m_c}\right]e^{\frac{1}{2}}_{\frac{1}{2},-\frac{1}{2}}(z) + \frac{|\vec{b}|c_o}{2m_c}\right\}, \tag{D.48}$$

$$M^{J=\frac{1}{2}}_{0-\frac{1}{2};\,1\frac{1}{2}} = \frac{\xi_{+1}}{\sqrt{2}}\,\frac{i}{|\vec{b}||\vec{d}|}\left\{\left(\frac{z+1}{2}\right)^{\frac{1}{2}}(1-z)[|\vec{b}|]\,e^{\frac{1}{2},\frac{1}{2}}_{\frac{1}{2}}(z) + \frac{|\vec{b}|}{2}\right\}, \tag{D.49}$$

and

$$M^{J=\frac{1}{2}}_{0\frac{1}{2};\,1\frac{1}{2}} = \frac{\xi_{-1}}{\sqrt{2}}\,\frac{i}{|\vec{b}||\vec{d}|}\left\{-\left(\frac{z-1}{2}\right)^{\frac{1}{2}}(1+z)[|\vec{b}|]e^{\frac{1}{2}}_{-\frac{1}{2},\frac{1}{2}}(z) + \frac{|\vec{b}|}{2}\right\}. \tag{D.50}$$

For completeness we give $e^{\frac{1}{2}}_{\frac{1}{2},\frac{1}{2}}(z)$ and $e^{\frac{1}{2}}_{\frac{1}{2},-\frac{1}{2}}(z)$ as obtained using the relations discussed in Appendix C:

$$e^{\frac{1}{2}}_{\frac{1}{2},\frac{1}{2}}(z) = -\left(\frac{1+z}{2}\right)^{\frac{1}{2}}\frac{1}{2(1+z)}\left[\log\left|\frac{1-z}{1+z}\right| + z\log\left|\frac{1-z}{1+z}\right| + 2\right] \tag{D.51}$$

and

$$e^{\frac{1}{2}}_{\frac{1}{2},-\frac{1}{2}}(z) = -\left(\frac{z-1}{2}\right)^{\frac{1}{2}}\frac{1}{2(1-z)}\left[-\log\left|\frac{1-z}{1+z}\right| + 2 + z\log\left|\frac{1-z}{1+z}\right|\right]. \tag{D.52}$$

Using the symmetry relations satisfied by $e^{j}_{\lambda\mu}$ as discussed in Appendix C we then obtain

$$e^{\frac{1}{2}}_{-\frac{1}{2},-\frac{1}{2}}(z) = e^{\frac{1}{2}}_{\frac{1}{2},\frac{1}{2}}(z) \tag{D.53}$$

and

$$e^{\frac{1}{2}}_{-\frac{1}{2},+\frac{1}{2}}(z) = -e^{\frac{1}{2}}_{+\frac{1}{2},-\frac{1}{2}}(z) \ . \tag{D.54}$$

For $J = \frac{1}{2}$ we have two independent parity amplitudes for each $\epsilon$. This corresponds to the fact that if the meson baryon system is in an S wave state, the vector baryon system can be in an S or D wave state, due to angular momentum and parity conservation, which we assume to hold. The two independent parity amplitudes are

$$M_1^{J=\frac{1}{2},\,\epsilon} = M^{J=\frac{1}{2}}_{o\frac{1}{2};\ 1\frac{1}{2}} - \epsilon\, M^{J=\frac{1}{2}}_{o-\frac{1}{2};\ 1\frac{1}{2}} \tag{D.55}$$

and

$$M_2^{J=\frac{1}{2},\epsilon} = M^{J=\frac{1}{2}}_{o\frac{1}{2};\ o\frac{1}{2}} - \epsilon\, M^{J=\frac{1}{2}}_{o-\frac{1}{2};\ o\frac{1}{2}} \ . \tag{D.56}$$

We define

$$V^{i\,(i)}_{J,\epsilon} = -\frac{1}{4\pi}\sqrt{\frac{m_b|\vec{b}|}{a_o+b_o}}\ M_i^{J,\epsilon}\ \sqrt{\frac{m_d|\vec{d}|}{c_o+d_o}} \ . \tag{D.57}$$

We then obtain

$$V'^{(1)}_{J=\frac{1}{2},\epsilon} = -\frac{1}{4\pi}\sqrt{\frac{m_b}{a_o+b_o}}\;\frac{1}{|\vec{d}|}\;\frac{1}{\sqrt{2}}\Big[\xi_{-1}\Big\{\frac{1}{2}-\Big(\frac{z-1}{2}\Big)^{\frac{1}{2}}(1+z)\;e^{\frac{1}{2}}_{\frac{1}{2},-\frac{1}{2}}(z)\Big\}$$

$$-\epsilon\,\xi_{+1}\Big\{\Big(\frac{1+z}{2}\Big)^{\frac{1}{2}}(1-z)\;e^{\frac{1}{2}}_{\frac{1}{2},\frac{1}{2}}(z)+\tfrac{1}{2}\Big\}\Big]\sqrt{\frac{m_d}{c_o+d_o}}\sqrt{|\vec{b}||\vec{d}|} \qquad (D.58)$$

and

$$V'^{(2)}_{J=\frac{1}{2},\epsilon} = -\frac{1}{4\pi}\sqrt{\frac{m_b}{a_o+b_o}}\;\frac{1}{|\vec{b}||\vec{d}|}\;\frac{1}{m_c}\Big[\xi_{-1}\Big\{\Big(\frac{1+z}{2}\Big)^{\frac{1}{2}}(-|\vec{b}|c_o z+|\vec{d}|a_o)\,e^{\frac{1}{2}}_{-\frac{1}{2},-\frac{1}{2}}(z)$$

$$+\tfrac{1}{2}|\vec{b}|c_o\Big\}-\epsilon\,\xi_{+1}\Big\{\Big(\frac{z-1}{2}\Big)^{\frac{1}{2}}(|\vec{b}|\,c_o z-|\vec{d}|a_o)\,e^{\frac{1}{2}}_{-\frac{1}{2},\frac{1}{2}}(z)+\tfrac{1}{2}|\vec{b}|c_o\Big\}\Big]$$

$$\sqrt{\frac{m_d}{c_o+d_o}}\;\sqrt{|\vec{b}||\vec{d}|}\;, \qquad (D.59)$$

where the superscripts (1) and (2) denote the two independent total angular momentum, parity amplitudes. In addition, we have multiplied our answers by i in order to make V real.

3) The reaction $0^- + \frac{1}{2}^- \rightarrow 0^- + 3/2^+$

The process shown in Figure A-6 will be examined here. We will consider only the contribution due to vector change. For the PVP coupling we use the interaction Lagrangian discussed in Appendix A. We have assumed for our treatment of the BVB* coupling the so-called Stodolski Sakurai Lagrangian (Stodolski and Sakurai, 1963). For the space part of this interaction Lagrangian we may write

$$-\mathcal{L}_{int} = \Big[\bar{\varphi}_\mu\,\gamma_5\,\Psi V_\mu + \frac{1}{m_b+m_d}\,\bar{\varphi}_\mu\,\gamma_\nu\gamma_5\,\Psi\,\partial_\mu V_\nu\Big] + \text{h.c.} \qquad (D.60)$$

where $\varphi_\mu$, $\Psi$, and $V_\mu$ denote the Rarita Schwinger spin $3/2^+$ field, spin $\frac{1}{2}^+$ field, and spin $1^-$ field, respectively.

For the process in consideration we obtain

$$M = -\bar{U}_\mu(\vec{d})\left[\delta_{\mu\nu} + \frac{ie_\mu\gamma_\nu}{m_b+m_d}\right]\gamma_5\left[\delta_{\nu\lambda} + \frac{\bar{e}_\lambda e_\nu}{m_e^2}\right](a+c)_\lambda\, u(\vec{b})\ \frac{1}{m_e^2-t}\ . \quad (D.61)$$

We may write

$$U_\mu^{\lambda d}(\vec{d}) = \sum_\lambda C_{\lambda d,\lambda}\, u_\lambda(d)\epsilon_\mu^{\lambda d-\lambda}\ , \quad (D.62)$$

where $C_{\lambda d,\lambda}$ denotes the Clebsch Gordan coefficient for coupling the two angular momenta 1 and $\frac{1}{2}$ with z components $\lambda d-\lambda$ and $\lambda$ respectively to yield total angular momentum 3/2 with z component $\lambda d$. These coefficients have been tabulated in Appendix B.

We must compute

$$\bar{U}_\mu^{\lambda d}(\vec{d})\,(a+c)_\mu\ \gamma_5\ u_{\lambda b}(\vec{b}) = \sum_\lambda (C_{\lambda d,\lambda}\bar{u}_\lambda(\vec{d})\gamma_5 u_{\lambda b}\ \epsilon^{\lambda d-\lambda}\cdot(a+c) \quad (D.63)$$

and

$$\bar{U}_\mu^{\lambda d}(\vec{d})\ e_\mu\gamma\cdot(a+c)\gamma_5 u_\lambda(\vec{b}) = -\sum_\lambda (C_{\lambda d,\lambda}\bar{u}_\lambda(\vec{d})\gamma\cdot(a+c)\gamma_5 u_{\lambda b}\epsilon^{\lambda d-\lambda}\cdot b, \quad (D.64)$$

where we have used $U_\mu^{\lambda d}(\vec{d})\, d_\mu = 0$.

Also we must compute

$$\bar{U}_\mu^{\lambda d}(\vec{d})\ e_\mu\ \gamma_5 u_{\lambda b}(\vec{b}) = -\Sigma\ C_{\lambda d,\lambda}\,\bar{u}_\lambda(\vec{d})\gamma_5 u_{\lambda b}(\vec{b})\ \epsilon^{\lambda d-\lambda}\cdot b \quad (D.65)$$

and

$$\bar{U}_{\mu}^{\lambda d}(\vec{d})\, e_{\mu}\gamma\cdot e\gamma_5\, u_{\lambda b}(\vec{b}) = -\sum_{\lambda} C_{\lambda d,\lambda}\, \bar{u}_{\lambda}(\vec{d})\gamma\cdot e\gamma_5 u_{\lambda b}(\vec{b})\epsilon^{\lambda d-\lambda}\cdot b. \tag{D.66}$$

By using Dirac's equation and energy momentum relations and defining $\xi_{\pm}$, $\eta_b$ and $\eta_d$ as before, we obtain

$$\bar{U}_{\mu}^{\lambda d}(a+c)_{\mu}\gamma_5\, u_{\lambda b}(\vec{b}) = -2\lambda b \sum_{\lambda} \xi_{-2\lambda b\lambda} d^{\frac{1}{2}}_{\lambda a\lambda}(\theta)\; C_{\lambda d,\lambda}\epsilon^{\lambda d-\lambda}\cdot(a+c) \tag{D.67}$$

and

$$\bar{U}_{\mu}^{\lambda d} e_{\mu}\gamma\cdot(a+c)\gamma_5 u_{\lambda b}(\vec{b}) = i\lambda_b \sum_{\lambda} C_{\lambda d,\lambda}\, d^{\frac{1}{2}}_{\lambda a\lambda}(\theta)\left[(a_o+b_o+c_o+d_o)\xi_{2\lambda b\lambda}\right.$$

$$\left. + (m_b-m_d)\,\xi_{-2\lambda b\cdot\lambda}\right]\epsilon^{\lambda d-\lambda}\cdot b \tag{D.68}$$

as well as

$$\bar{U}_{\mu}^{\lambda d}(\vec{d})\, e_{\mu}\gamma_5 u_{\lambda b}(\vec{b}) = \lambda_b \sum_{\lambda} \xi_{-2\lambda b\lambda} d^{\frac{1}{2}}_{\lambda b\lambda}(\theta)\; \epsilon^{\lambda d-\lambda}\cdot C_{\lambda d,\lambda}, \tag{D.69}$$

and

$$\bar{U}_{\mu}^{\lambda d}\, e_{\mu}\gamma\cdot e\gamma_5\, u_{\lambda b}(\vec{b}) = i\lambda_b(m_b-m_d) \sum_{\lambda} \xi_{-2\lambda b\lambda} C_{\lambda d,\lambda} d^{\frac{1}{2}}_{\lambda b\lambda}(\theta)\; \epsilon^{\lambda d-\lambda}\cdot b\,. \tag{D.70}$$

Therefore, we obtain for this process

$$M_{\lambda a\lambda b;\,\lambda c\lambda d} = -\left(\frac{1}{m_e^2-t}\right) \sum_{\lambda} C_{\lambda d,\lambda} d^{\frac{1}{2}}_{\lambda b\lambda}(\theta)\; \epsilon^{\lambda d-\lambda}\cdot\Big\{-\lambda b(a+c)\xi_{-2\lambda b\lambda}$$

$$-\left(\frac{\lambda_b}{m_b+m_d}\right) b\left[(a_o+b_o+c_o+d_o)\xi_{2\lambda b\lambda} + (m_b-m_d)\,\xi_{-2\lambda b\lambda}\right]$$

$$+\left(\frac{m_c^2-m_a^2}{m_e^2}\right)\lambda_b\, b\xi_{-2\lambda b\lambda} - \left(\frac{m_c^2-m_a^2}{m_e^2}\right)\lambda_b(m_b-m_d)\, b\xi_{-2\lambda b\lambda}\Big\}. \tag{D.71}$$

Using the relations of Appendix C and the same coordinate system as we have used in the preceding reaction in this appendix, we obtain (with the same definition of z) for the case J = ½:

$$M^{J=\frac{1}{2}}_{o\frac{1}{2};\, o\frac{1}{2}} = -\frac{1}{2|\vec{b}||\vec{d}|}\sqrt{\frac{(b_o+m_b)(d_o+m_b)}{4m_b m_d}}\left[\left(\frac{1+z}{2}\right)^{\frac{1}{2}} e^{\frac{1}{2}}_{\frac{1}{2},\frac{1}{2}}(z)\left\{-\sqrt{\frac{2}{3}}(\eta_d-\eta_b)\right.\right.$$

$$\left(\frac{|\vec{d}| + |\vec{b}| z\, d_o}{m_d}\right) + \frac{|\vec{b}|(1-z)}{\sqrt{6}}(\eta_b-\eta_d) - \left(\frac{1}{m_b+m_d}\right)\sqrt{\frac{2}{3}}\left[(a_o+b_o+c_o+d_o)\right.$$

$$(\eta_b+\eta_d) + (m_b-m_d)(\eta_b-\eta_d)\left]\left[\frac{d_o}{m_d} z - \frac{|\vec{d}|}{m_d} b_o\right]\right. + \left(\frac{1}{m_b+m_d}\right)\frac{|\vec{b}|(1-z)}{\sqrt{6}}$$

$$\left[(a_o+b_o+c_o+d_o)(\eta_b-\eta_d) + (m_b-m_d)(\eta_b+\eta_d)\right] + \left(\frac{m_c^2-m_a^2}{m_e^2}\right)\sqrt{\frac{2}{3}}\left[\frac{d_o}{m_d} z\right.$$

$$\left. - \frac{|\vec{d}|}{m_d} b_o\right] - \left(\frac{m_c^2-m_a^2}{m_e^2}\right)\frac{|\vec{b}|(1-z)}{\sqrt{6}}(\eta_b+\eta_d) - \left(\frac{m_c^2-m_a^2}{m_e^2}\right)(m_b-m_d)\sqrt{\frac{2}{3}}$$

$$\left[\frac{d_o}{m_d} z - \frac{|\vec{d}| b_o}{m_d}\right] + \left(\frac{m_c^2-m_a^2}{m_e^2}\right)(m_b-m_d)\frac{|\vec{b}|(1-z)}{\sqrt{6}}(\eta_b+\eta_d)\Big\} +$$

$$\frac{1}{2}\left\{\sqrt{\frac{2}{3}}(\eta_b-\eta_d)\frac{d_o|\vec{d}|}{m_d} + (\eta_b-\eta_d)\frac{|\vec{b}|}{\sqrt{6}} + \sqrt{\frac{2}{3}}\frac{d_o}{m_d}\frac{1}{(m_b+m_d)}\left[(a_o+b_o+c_o+d_o)\right.\right.$$

$$\left.(\eta_b+\eta_d) + (m_b-m_d)(\eta_b-\eta_d)\right] + \frac{|\vec{b}|}{(m_b+m_d)\sqrt{6}}\left[(a_o+b_o+c_o+d_o)(\eta_b-\eta_d)\right.$$

$$+ (m_b - m_d)(\eta_b + \eta_d)\Big] - \left(\frac{m_c^2 - m_a^2}{m_e^2}\right)\sqrt{\frac{2}{3}}\,(\eta_b - \eta_d)\,\frac{d_o}{m_d} - \left(\frac{m_c^2 - m_a^2}{m_e^2}\right)\frac{|\vec{b}|\,(\eta_b + \eta_d)}{\sqrt{6}}$$

$$+ \left(\frac{m_c^2 - m_a^2}{m_e^2}\right)(m_b - m_d)\sqrt{\frac{2}{3}}\,(\eta_b - \eta_d)\,\frac{d_o}{m_d} - \left(\frac{m_c^2 - m_a^2}{m_e^2}\right)(m_b - m_d)\,\frac{|\vec{b}|\,(\eta_b + \eta_d)}{\sqrt{6}}\Big\}\Big]\,. \tag{D.72}$$

Similarly we may also obtain the result:

$$M^{J=\frac{1}{2}}_{o\frac{1}{2};\,o-\frac{1}{2}} = -\frac{1}{2|\vec{b}|\,|\vec{d}|}\sqrt{\frac{(b_o+m_b)(d_o+m_d)}{4m_b m_d}}\Big[\left(\frac{z-1}{2}\right)^{\frac{1}{2}} e^{\frac{1}{2},-\frac{1}{2}}(z)\Big\{-\frac{|\vec{b}|\,(1+z)}{\sqrt{2}}$$

$$(\eta_b - \eta_d) - \sqrt{\frac{2}{3}}\,(\eta_b + \eta_d)\left[\frac{d_o}{m_d}(|\vec{b}|\,z + |\vec{d}|) + \frac{|\vec{d}|\,(a_o + c_o)}{m_d}\right]$$

$$+ \frac{|\vec{b}|\,(1+z)}{\sqrt{6}\,(m_b+m_d)}\left[(a_o+b_o+c_o+d_o)(\eta_b+\eta_d) + (m_b-m_d)(\eta_b-\eta_d) + \sqrt{\frac{2}{3}}\left(\frac{1}{m_b+m_d}\right)\right.$$

$$\left.[(\eta_b-\eta_d)(a_o+b_o+c_o+d_o) + (m_b-m_d)(\eta_b+\eta_d)]\left[\frac{d_o}{m_d}\,z - \frac{|\vec{d}|\,b_o}{m_d}\right] + \left(\frac{m_c^2-m_a^2}{m_e^2}\right)\right.$$

$$\frac{|\vec{b}|\,(1+z)}{\sqrt{6}}\,(\eta_b-\eta_d) - \left(\frac{m_c^2-m_a^2}{m_e^2}\right)\sqrt{\frac{2}{3}}\,(\eta_b+\eta_d)\left[\frac{d_o}{m_d}\,z - \frac{|\vec{d}|\,b_o}{m_d}\right] + \left(\frac{m_c^2-m_a^2}{m_e^2}\right)$$

$$(m_b-m_d)(\eta_b-\eta_d)\,\frac{|\vec{b}|\,(1+z)}{\sqrt{6}} + \left(\frac{m_c^2-m_a^2}{m_e^2}\right)(m_b-m_d)\sqrt{\frac{2}{3}}\,(\eta_b+\eta_d)\left(\frac{d_o}{m_d}\,z - \frac{|\vec{d}|\,b_o}{m_d}\right)\Big\}$$

$$+ \frac{1}{2}\Big\{(\eta_b-\eta_d)\,\frac{|\vec{b}|}{\sqrt{6}} - \frac{|\vec{b}|}{m_b}\,d_o\sqrt{\frac{2}{3}}\,(\eta_b+\eta_d) + \frac{|\vec{b}|}{\sqrt{6}}\left(\frac{1}{m_b+m_d}\right)[(\eta_b+\eta_d)$$

$$(a_o+b_o+c_o+d_o) + (m_b-m_d)(\eta_b-\eta_d)] + \sqrt{\frac{2}{3}} \left(\frac{1}{m_b+m_d}\right) [(\eta_b-\eta_d)(a_o+b_o+c_o+d_o)$$

$$+ (m_b-m_d)(\eta_b+\eta_d)] \frac{\dot{d}_o}{m_d} - \left(\frac{m_c^2-m_a^2}{m_e^2}\right)(\eta_b-\eta_d) \frac{|\vec{b}|}{\sqrt{6}} - \left(\frac{m_c^2-m_a^2}{m_e^2}\right)\sqrt{\frac{2}{3}}$$

$$(\eta_b+\eta_d) \frac{d_o}{m_d} + \left(\frac{m_c^2-m_a^2}{m_e^2}\right)(m_b-m_d) \frac{|\vec{b}|}{\sqrt{6}}(\eta_b-\eta_d) + \sqrt{\frac{2}{3}} (\eta_b+\eta_d) \left(\frac{m_c^2-m_a^2}{m_e^2}\right)$$

$$(m_b-m_d) \frac{d_o}{m_d}\Big\}\Big]. \qquad \text{(D.73)}$$

We then obtain for the amplitudes corresponding to definite parity states as discussed in Appendix C the result:

$$V'_{J=\frac{1}{2},\epsilon} = -\frac{1}{4\pi}\sqrt{\frac{m_b|\vec{b}|}{a_o+b_o}}\; M^{J=\frac{1}{2},\epsilon}\sqrt{\frac{m_d|\vec{d}|}{c_o+d_o}}\,, \qquad \text{(D.74)}$$

where

$$M^{J=\frac{1}{2},\epsilon} = M^{J=\frac{1}{2}}_{o\frac{1}{2};\, o\frac{1}{2}} + \epsilon\, M^{J=\frac{1}{2}}_{o\frac{1}{2};\, o-\frac{1}{2}}\,, \qquad \text{(D.75)}$$

and $M^{J=\frac{1}{2}}_{\lambda a\lambda b;\, \lambda c\lambda d}$ is as given above.

LIST OF REFERENCES

E. Abers and C. Zemach, Phys. Rev. 131, 2305 (1963).

M. Andrews and J. Gunson, J. Math. Phys. 5, 1391 (1964).

B. Bakamjian and L. H. Thomas, Phys. Rev. 92, 1300 (1953).

L. A. P. Balazs, Phys. Rev. 137, B1510 (1964).

J. S. Ball and D. Y. Wong, Phys. Rev. 133, B179 (1964).

M. Bander, P. Coulter, and G. Shaw, Phys. Rev. Letters 14, 207 (1965).

P. Bareyre, C. Brickman, A. V. Stirling, and G. Villet, Phys. Letters 18, 342 (1965).

F. A. Behrends, A. Donnachie, and D. L. Weaver, "Photoproduction and Electroproduction of Pions: I. Dispersion Relation Theory and II. Photoproduction Below 500 Mev," CERN preprint to be published (1967).

L. C. Biedenham, J. M. Blatt, and M. E. Rose, Phys. Rev. 24, 249 (1952).

J. D. Bjorken, Phys. Rev. Letters 4, 473 (1960).

R. Blankenbecler, M. L. Goldberger, N. N. Khuri, and S. B. Treiman, Ann. Phys. (N. Y.) 10, 62 (1960).

R. Blankenbecler and R. Sugar, Phys. Rev. 142, 1051 (1966).

R. N. Bransden, P. J. Donnell, and R. G. Moorhouse, Phys. Rev. 134, B1566 (1965).

J. J. Brehm, "Vector Exchange and S. Wave Pion Nucleon Scattering," preprint to be published (1967).

J. J. Brehm and G. L. Kane, Phys. Rev. Letters 17, 764 (1966).

W. Brenigg and R. Haag, Fortschritte der Physik 7, 183 (1959).

P. Carruthers and J. P. Krisch, Ann. Phys. (N. Y.) 33, 1 (1965).

L. Castillejo, R. H. Dalitz, and F. J. Dyson, Phys. Rev. 101, 453 (1956).

G. M. Charap and S. P. Fubini, Nuevo Cimento 14, 540 (1959); Nuevo Cimento 15, 73 (1960).

G. F. Chew, Phys. Rev. 129, 2363 (1963).

G. F. Chew and F. E. Low, Phys. Rev. 101, 1571 (1956).

F. Coester, Helvetica Physica Acta 38, 7 (1965).

L. F. Cook and B. W. Lee, Phys. Rev. 127, 283 (1962).

P. W. Coulter and G. L. Shaw, Phys. Rev. 141, 1419 (1966).

R. E. Cutkosky, J. Math. Phys. 1,.429 (1960).

R. H. Dalitz, Ann. Rev. Nucl. Sci. 13, 339 (1963).

R. Dalitz and S. F. Tuan, Ann. of Phys. 3, 307 (1960).

J. J. De Swart, Rev. Mod. Phys. 35, 916 (1963).

A. Donnachie, J. Hamilton and A. T. Lea, Phys. Rev. 135, B515 (1964).

A. Donnachie and J. Hamilton, Ann. of Phys. (N.Y.) 31, 410 (1965).

A. Donnachie, A. T. Lea, and C. Lovelace, Phys. Letters 19, 146 (1965).

J. Finkelstein, Phys. Rev. 145, 1185 (1966).

R. Fong and J. Sucher, J. Math. Phys. 5, 456 (1963).

S. C. Frautschi and J. D. Walecka, Phys. Rev. 120, 1486 (1960).

G. Frye and R. Warnock, Phys. Rev. 130, 478 (1963).

M. Gellmann, Phys. Rev. 125, 1067 (1967).

J. B. Hartle and J. R. Taylor, J. of Math. Phys. 8, 651 (1967).

F. B. Hildebrand, "Introduction to Numerical Analysis," McGraw-Hill, New York (1956).

M. Jacob and G. C. Wick, Ann. of Phys. 7, 404 (1959).

C. E. Jones, Nuovo Cimento 40, 761 (1965).

T. Kato, University of California Technical Report 21, unpublished (1963).

Z. Kopal, "Numerical Analysis," Chapman and Hall Ltd., London (1961).

S. T. Kuroda, J. Math. Soc. Japan 11, 247 (1959); Nuovo Cimento 12, 431 (1959).

L. D. Landau, Nuc. Phys. 13, 181 (1959).

M. Luming Phys. Rev. 136, B1120 (1964).

S. Mandelstam, J. E. Paton, R. F. Peierls and A. Q. Sarker, Ann. Phys. 18, 198 (1962).

A. W. Martin and K. C. Wali, Phys. Rev. 130, 2455 (1963); Nuovo Cimento 31, 1324 (1967).

S. Okubo, Prog. Theor. Phys. (Kyoto) 27, 949 (1962).

H. Pagels, Phys. Rev. 140, B1599 (1965).

R. Peierls, Proc. Roy. Soc. London A214, 143 (1952).

C. E. Rickart, "General Theory of Banach Algebras," D. Van Nostrand Company, Princeton, New Jersey (1960).

F. Riesz and B. Sz-Nagy, "Functional Analysis," Ungar, New York, (1955).

L. Roper, Phys. Rev. Letters 12, 340 (1964); L. Roper and R. Wright, Phys. Rev. 138, B921 (1965).

M. E. Rose, "Elementary Theory of Angular Momentum," John Wiley, New York (1957).

J. J. Sakurai, Phys. Rev. Letters 9, 472 (1962).

J. J. Sakurai, Phys. Rev. Letters 17, 1021 (1966).

E. E. Salpeter and H. H. Bethe, Phys. Rev. 84, 1232 (1951).

L. Stodolsky and J. J. Sakurai, Phys. Rev. Letters 11, 90 (1963).

E. N. Wichmann and J. H. Chrichton, Phys. Rev. 132, 2788 (1963).

E. P. Wigner, Phys. Rev. 98, 145 (1955).

E. P. Wigner, "Group Theory and its Application to the Quantum Mechanics of Atomic Spectra," Academic Press, New York (1959).

H. W. Wyld, Jr., Phys. Rev. 155, 1649 (1967).

# VITA

Jose Katz-Masson, son of David Lipa Katz and Victoria Masson, was born in Havana, Cuba on June 6, 1944. He graduated from Candler College High School in June 1960. In February 1961 he enrolled at the University of Illinois and received his Bachelor of Science degree (with high honors) in Engineering Physics in June 1963. He continued his studies at the same university and received his Master of Science in Physics degree in June 1964. As a graduate student he has held teaching and research assistantships as well as university fellowships. He is a member of the American Physical Society, Tau Beta Pi, Pi Mu Epsilon, Sigma Tau, and Phi Kappa Phi.